

**Mode-of-Action Studies on Cytostatic Compounds
from Myxobacteria:**

Antimitotic Pretubulysins and Actin-Targeting Chondramides

Dissertation

zur Erlangung des Grades

des Doktors der Naturwissenschaften

der Naturwissenschaftlich-Technischen Fakultät III

Chemie, Pharmazie, Bio- und Werkstoffwissenschaften

der Universität des Saarlandes

von

Jennifer Herrmann

Saarbrücken

2012

Tag des Kolloquiums: 12. November 2012
Dekan: Prof. Dr. Volkhard Helms
Berichterstatter: Prof. Dr. Rolf Müller
Prof. Dr. Uli Kazmaier
Vorsitz: Prof. Dr. Manfred J. Schmitt
Akad. Mitarbeiter: Dr. Britta Diesel

Diese Arbeit entstand unter Anleitung von Prof. Dr. Rolf Müller in der Fachrichtung 8.2 Pharmazeutische Biotechnologie der Naturwissenschaftlich-Technischen Fakultät III der Universität des Saarlandes von Dezember 2007 bis September 2012.

meinen Eltern

ZUSAMMENFASSUNG

Myxobakterien haben sich als sehr nützliche Naturstoffproduzenten erwiesen, da sie eine Vielzahl von Sekundärmetaboliten mit einzigartigen Strukturen liefern. Diese Naturstoffe besitzen darüber hinaus häufig biologische Aktivität und weisen neuartige Wirkmechanismen auf.

Diese Arbeit vermittelt erste Einblicke in den Wirkmechanismus des myxobakteriellen Metabolits Prätubulysin. Synthetisches Prätubulysin und einige Derivate davon sind in größeren Mengen verfügbar und wurden im Zuge dieser Arbeit charakterisiert. Durch diese Bioaktivitätsstudien konnte eindeutig gezeigt werden, dass Prätubulysine zu einer Depolymerisation von Mikrotubuli führen und im Weiteren einen mitotischen Arrest und Apoptose in kultivierten Säugerzellen induzieren. Durch vergleichende Studien mit mehreren synthetischen Analoga konnten darüber hinaus wichtige Struktur-Aktivitäts-Beziehungen hergeleitet werden.

Ein weiteres Thema dieser Arbeit war die Implementierung von *High-Content-Screening* für die bioaktivitätsgeleitete Aufreinigung von Sekundärmetaboliten aus Myxobakterien. Im Laufe der Untersuchungen wurden so über 30 neue Chondramid-Derivate in Extrakten von *Chondromyces sp.* gefunden und zum Teil isoliert. Die biologische Evaluierung der Reinstoffe, die eine Polymerisation von G-Aktin induzieren, erbrachte wichtige Struktur-Aktivitäts-Beziehungen. Außerdem lieferten zellbasierte und *in vitro*-Studien im Falle von bromierten Analoga Hinweise auf ein vermeintliches zweites zelluläres Target.

ABSTRACT

Myxobacteria have proven to be highly valuable as sources of natural products since they produce a variety of secondary metabolites with unique structures. These natural products often exhibit astonishing biological activities with a new mode-of-action.

This thesis provides new insights into the mode-of-action of the myxobacterial metabolite pretubulysin. Synthetic pretubulysin and some of its derivatives, which are available in gram-scale quantities, were characterized and bioactivity studies clearly showed the compounds' ability to depolymerize microtubules. Pretubulysin treatment consequently leads to mitotic arrest and the induction of apoptosis in cultured mammalian cells. Furthermore, important structure-activity relationships were elucidated by comparing several synthetic analogs.

Another topic of this thesis was the implementation of high-content screening for bioactivity-guided isolation of secondary metabolites from myxobacteria. For this purpose, *Chondromyces sp.* extracts were subjected to several in-depth cell-based assays, which resulted in the discovery of over 30 new chondramide derivatives. Compounds of this class are described to target actin filaments with a phalloidin-like binding mode. In addition to structure-activity relationship insights, the biological evaluation of purified compounds provided evidence for a putative second target for some brominated analogs of this exciting class of natural products.

TABLE OF CONTENTS

ZUSAMMENFASSUNG	VII
ABSTRACT	VIII
INTRODUCTION	1
1.1 NATURAL PRODUCTS	1
1.1.1 NATURAL PRODUCTS AND PHARMACEUTICAL INDUSTRIES	1
1.1.2 MICROBIAL PRODUCERS	4
1.1.3 ROLE OF MYXOBACTERIA	6
1.2 NEW LEAD STRUCTURES FROM MICROBIAL SOURCES	11
1.2.1 SCREENING PROCESS	13
1.2.2 MICROBIAL NATURAL PRODUCTS AND THERAPEUTIC APPLICATIONS	15
1.3 NATURAL PRODUCTS AND CANCER THERAPY	16
1.3.1 THERAPEUTIC TARGETS	17
1.3.2 THE EUKARYOTIC CYTOSKELETON	19
1.3.3 MYXOBACTERIAL METABOLITES	22
1.4 SCOPE OF THE WORK	25
MATERIALS AND METHODS	27
2.1 MATERIALS	27
2.1.1 COMPOUNDS	27
2.1.2 CHEMICALS	27
2.1.3 CELL LINES AND PRIMARY CELLS	27
2.1.4 CELL CULTURE MEDIA AND REAGENTS	29
2.1.5 BUFFERS	31
2.1.6 ANTIBODIES	32
2.1.7 STAINING DYES	33
2.1.8 CYTOSKELETAL PROTEINS	33
2.1.9 TECHNICAL EQUIPMENT AND CONSUMABLES	33
2.2 METHODS	35
2.2.1 SUBCULTIVATION OF CELLS	35
2.2.2 CRYOPRESERVATION	35
2.2.3 PRIMARY CULTURES	36
2.2.4 VIABILITY ASSAY (MTT)	36
2.2.5 GIEMSA STAINING	37
2.2.6 CLONOGENIC SURVIVAL	37

Table of Contents

2.2.7	APOPTOSIS MEASUREMENT	37
2.2.8	CELL CYCLE STUDIES	37
2.2.9	IMMUNOBLOTTING	38
2.2.10	IMMUNOFLUORESCENCE	38
2.2.11	ACTIN LABELING (PHALLOIDIN PROBE)	39
2.2.12	TMRM STAINING	39
2.2.13	ACRIDINE ORANGE STAINING	39
2.2.14	HCS STUDIES	40
2.2.15	DETECTION OF DNA LADDERING	40
2.2.16	TUBULIN ISOLATION	41
2.2.17	<i>IN VITRO</i> TUBULIN POLYMERIZATION STUDIES	41
2.2.18	TRANSMISSION ELECTRON MICROSCOPY	41
2.2.19	<i>IN VITRO</i> ACTIN POLYMERIZATION STUDIES	42
2.2.20	CULTIVATION OF <i>CHONDRAMYCES SP. SBCM007</i>	42
2.2.21	EXTRACT PREPARATION AND PRE-FRACTIONATION	42
2.2.22	SEMI-PREPARATIVE HPLC	43
RESULTS		45
3.1 BIOLOGICAL CHARACTERIZATION OF PRETUBULYSINS		45
3.1.1	DETERMINATION OF GI ₅₀ VALUES	45
3.1.2	LONG-TERM SURVIVAL OF CANCER CELLS	50
3.1.3	TRIAZOLE-PRETUBULYSIN TOOL COMPOUND	51
3.1.4	MITOTIC ARREST	54
3.1.5	APOPTOSIS INDUCTION	59
3.1.6	HCS STUDIES	63
3.1.7	<i>IN VITRO</i> POLYMERIZATION STUDIES	68
3.2 DISCOVERY OF NEW CHONDRAMIDES AND INITIAL SAR STUDIES		71
3.2.1	CYTOSTATIC ACTIVITY OF SBCM007 CRUDE EXTRACT	71
3.2.2	TARGET-SPECIFIC ACTIVITY IN THE CRUDE EXTRACT	73
3.2.3	HCS ON LYSOSOMAL INTEGRITY	76
3.2.4	BIOACTIVITY-GUIDED ISOLATION OF NEW CHONDRAMIDES	79
3.2.5	DETERMINATION OF GI ₅₀ VALUES OF CHONDRAMIDES	82
3.2.5	<i>IN VITRO</i> ACTIN POLYMERIZATION	84

DISCUSSION	89
4.1 PRETUBULYSIN AS POTENTIAL NOVEL LEAD STRUCTURE	89
4.1.1 STRUCTURE-ACTIVITY RELATIONSHIP OF TUBULYSINS AND PRETUBULYSINS	89
4.1.2 PRETUBULYSIN LEADS TO MITOTIC ARREST AND APOPTOSIS INDUCTION	96
4.1.3 SMALL PRECURSOR MOLECULES DESTABILIZE MICROTUBULES	102
4.1.4 PRETUBULYSINS AS MOLECULAR PROBES	105
4.2 NEW CHONDRAMIDES WITH ALTERED ACTIVITY PROFILE	108
4.2.1 HIGH-CONTENT SCREENING IS APPLICABLE FOR CRUDE EXTRACTS	108
4.2.2 STRUCTURE-ACTIVITY RELATIONSHIP OF CHONDRAMIDES	111
4.2.3 BIOLOGICAL AND BIOCHEMICAL DATA SUGGEST A PUTATIVE OFF-TARGET	116
4.2.4 DIVERSITY OF NATURAL PRODUCT SCAFFOLDS	118
SUMMARY AND CONCLUSIONS	121
5.1 PRETUBULYSINS	121
5.2 CHONDRAMIDES	122
BIBLIOGRAPHY	125
APPENDIX	147
7.1 ABBREVIATIONS	147
7.2 PUBLICATIONS	150
7.2.1 ORIGINAL PUBLICATIONS	150
7.2.2 CONFERENCE CONTRIBUTIONS	151
7.3 DANKSAGUNG	153
7.4 CURRICULUM VITAE	154

INTRODUCTION

1.1 NATURAL PRODUCTS

Traditionally, the main sources of natural products (NPs) are soil bacteria, fungi, and higher plants. In the last decades, cyanobacteria and marine organisms were additional resources of particular interest.^[1] The term natural product is thereby commonly defined as a compound derived from natural sources, which mostly exhibits some biological activities.^[2] The definition is not clear-cut and ‘natural product’ is most often referred to as secondary metabolite, thus, describing naturally produced compounds that have no direct role in growth, development, and reproduction of the host. Secondary metabolites are rather involved in for instance, signaling, defense, cellular communication, differentiation, and sporulation. By this, the survival rate of the producer is improved in competition with other co-existing species.^[3] A prominent example is *Pseudomonas aeruginosa*, the major pathogen in the lung of cystic fibrosis (CF) patients. Due to its ability to form biofilms and excrete toxic metabolites the Gram-negative bacterium has a competitive advantage against other colonizing bacteria.^[4] In addition, it has been shown that instead of only creating a niche, *P. aeruginosa* interacts with other human-associated pathogens, like *Candida albicans*, via homoserine lactone, one of its quorum sensing molecules.^[5, 6, 7]

Contrary to the categorization of NPs as survival factors, the enormous structural diversity of natural product scaffolds and the high number of seemingly inactive metabolites (such which did not show activity in the assays performed) found with some producers, may be explained by the ‘Screening Hypothesis’. Fundamentally, this model is based on the assumption that any potent biological activity is a rare feature for any molecule to possess.^[8, 9] Any organism that is able to produce its own chemically diverse ‘screening library’ at low cost, and by this, enhance the chance to produce metabolites with useful and potent biological activity, would be evolutionary favored.^[9]

1.1.1 NATURAL PRODUCTS AND PHARMACEUTICAL INDUSTRIES

NPs have been used for millennia by humans to meet medical needs. For instance, in Traditional Chinese Medicine (TCM), which is an integral part of the Chinese culture, drugs are derived from natural sources, like herbal medicines, which are administered as complex mixture customized to each patient.^[10] However, in Western pharmaceutical industry drug formulations of purified compounds have become more typical in the last century, and research on NPs as novel therapeutics reached its peak in the period 1970-1980.^[2, 11]

Especially for the treatment of infections caused by bacterial pathogens, NP or NP-derived drugs were regarded as the ‘magic bullets’, but with the advancement of high-throughput screening (HTS) pharmaceutical companies de-emphasized NPs and instead, used chemical libraries in their screening campaigns where tens of thousands of small molecules are screened per week.^[2] This reflects one of the major drawbacks when it comes to NPs: low production yields and issues with continuous supply.^[12, 13] The classic case for the ‘supply issue’ is taxol (or paclitaxel), which was first isolated in 1969 from *Taxus brevifolia* (Pacific yew) bark (Figure 1-1).^[14] Taxol acts by promoting tubulin polymerization and stabilizing microtubules, and its clinical activity against ovarian cancer was first reported in 1989.^[15, 16] By that time, the NP was only available from the bark of the Pacific yew, which was subject of the ‘taxol supply crisis’.^[17, 18] Despite the initiation of large bark collection programs, semisynthetic approaches were developed and Bristol-Myers Squibb is now producing this blockbuster drug by plant tissue culture.^[19]

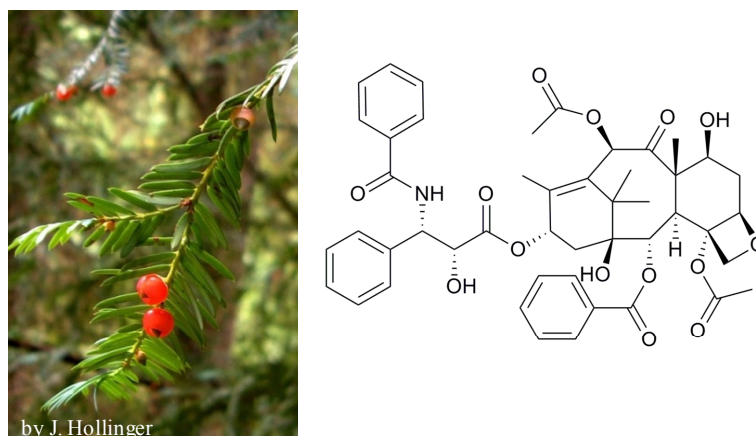


Figure 1-1: *Taxus brevifolia* leaves and chemical structure of taxol (paclitaxel).

In addition to the supply issue from biological sources, synthetic routes towards NP scaffolds are often very complex and far from being economical, as again seen in the case of taxol.^[20, 21] Ideally, chemical synthesis creates a rapid access to NPs with reasonable yields in only a few practical synthetic steps.^[22]

Despite these apparent drawbacks, NPs still play a significant role in the field of drug discovery and development of novel pharmaceuticals, particularly as anticancer and anti-infective agents, but also as immunosuppressive, cholesterol-lowering, and other drugs. As reviewed by Newman and Cragg recently, over 25% of all drugs approved between 1981 and 2010 are NPs or directly NP-derived. If one would also take into account the large

number of totally synthetic NP mimics or drugs with a NP pharmacophore, the total proportion of NP-like drugs would be >50% (Figure 1-2).^[23]

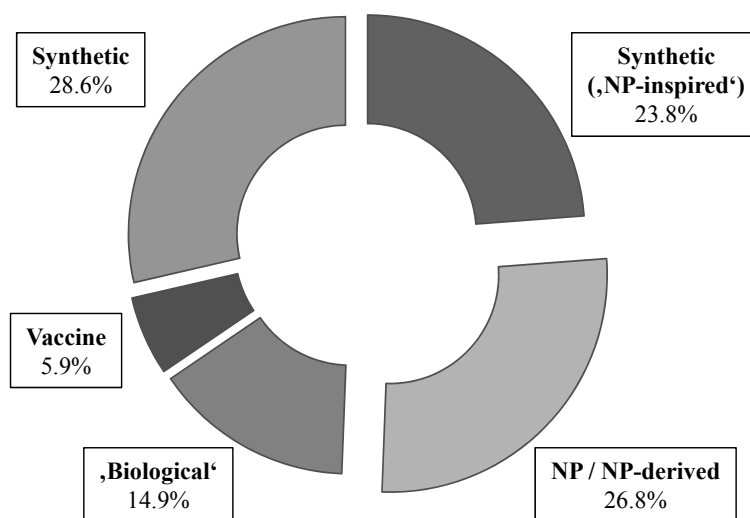


Figure 1-2: Sources of all new drugs approved between 1981 and 2010.

In total, 1355 new chemical entities (NCE) were approved in the period 1981 to 2010. NP: natural product; NP-derived: mostly semisynthetic NP variant; Biological: large peptides or proteins; Vaccine: biological preparation to improve immunity to certain diseases; Synthetic: totally synthetic drug; NP-inspired: NP mimics and totally synthetic with NP pharmacophore (adapted from ref. [23]).

Although the process of drug discovery with NPs requires more patience and is generally slower than with pure synthetic libraries, hits derived from NP libraries or from bioactivity-guided isolation approaches, are often higher quality leads.^[2] Mainly the advantages of chemical diversity and numerous biological activities (NP scaffolds are seen as ‘privileged structures’) countervails against the issues mentioned above, especially as much higher hit rates can be expected.^[11, 12, 13] It is also noticeable that out of thirteen natural product-related drugs approved between 2005 and 2007, five represent new classes of pharmaceuticals, which reflects the chemical diversity of natural products, and is a positive indicator that NPs still provide a good value to human medicine.^[24] In addition to chemical diversity *per se*, NPs are optimized in terms of possible protein interactions. In general, protein families belong to a finite number of structural elements (folds), and similar folds can even be found in proteins that are apparently different in their amino acid sequences. Due to their biosynthetic origin, NPs are optimized to interact with these common recognition elements within the protein structural arrangements.^[25, 26] In virtue of three-dimensional structure similarities of proteins, even of proteins from different pharmacological classes, NPs are able to interact with a

variety of biological target molecules and often modulate multiple signal transduction pathways.^[26, 27]

Nevertheless, major pharmaceutical companies mostly abandoned R&D programs on natural products over the last 20-30 years, and it seems unlikely that ‘Big Pharma’ will return to its former NP programs soon, as required investments are large. R&D is expected to rather be undertaken by smaller biotechnology companies or academia. This movement was mainly driven by business objectives, since it seemed more feasible to generate hits from large HTS libraries at much lower costs than with tedious NP discovery campaigns.^[2, 28] However, this paradigm shift did not meet expectations and the overall success rates of compounds in phase I clinical trials were rather low.^[29] This finding may partly be explained by the fact that many effective and successful drugs do not act on single molecules but interact with multiple receptors or enzymes, like kinase inhibitors in anticancer therapy. These drugs can target multiple pathways by inhibition of several key kinases and in turn, interact with major signaling pathways involved in cancer cell progression.^[28, 30, 31]

Typical HTS screening libraries do not appear to be the optimal strategy when it comes to assays that cover a broader range of biological interactions (phenotypic screening). Instead, privileged structures of NPs, like natural non-ribosomal peptides (NRPs) and polyketides (PKs)^[32], seem preferred for these purposes, not only due to their inherent multiple binding domains. In order to compromise between efficient screening strategies using NP scaffolds and the aim of low costs, work has mainly been focussed on biological evaluation of pre-fractionated simplified mixtures of crude extracts.^[33] Major hurdles in the context of screening these mixtures have been overcome. Thus, lead generation from NPs is strongly accelerated in terms of technological advances in detection and structural elucidation, novel robust screening assays, as well as fermentation and process development.^[28, 34]

1.1.2 MICROBIAL PRODUCERS

Mixtures of plant ingredients have widely been used in ancient medicine, but the isolation of morphine from opium produced by *Papaver somniferum* was one of the most important discoveries in medicine of the 19th century.^[35, 36] Since then, isolation of single active ingredients from plant sources was commonly accomplished, enabling the administration of precise dosages. By now, ca. 100,000 bioactive metabolites have been described from higher plants.^[37] Regarding microbial producers, the serendipitous discovery of penicillin from *Penicillium* fungi in 1929 by Fleming^[38] initiated the era of antibiotics (with the period

1950 to 1960 entitled the ‘Golden Era’ in antibiotics discovery) and, in turn, a tremendous screening of microorganisms for new bioactive compounds.^[1, 39]

From a retrospective point of view, filamentous actinomycetales species (especially *Streptomyces sp.*) are the most productive source among the microbial producers. Actinomycetes are extensively studied and produce numerous bioactive secondary metabolites, with over 10,000 reported compounds, that make up approximately 45% of all bioactive microbial metabolites.^[37] Nevertheless, success rates of discovering novel chemical entities from these microorganisms with potent biological activity decreased with time.^[40] Furthermore, the fact that for instance the aminoglycoside antibiotic streptomycin, which was discovered in the 1940s, is produced by about 1% of soil actinomycetes, significantly hampers bioactivity-guided isolation of new antibiotics. Bioactivities of NCEs (new chemical entities) might be masked by the presence of known metabolites.^[41] However, current attempts focus on the development of smart screening techniques, innovative enrichment methods of soil and marine sediments, more feasible fermentation strategies, genome mining for the discovery of novel chemotypes from ‘cryptic’ gene clusters, and combinatorial biosynthesis.^[41, 42] Complementary to these efforts, actinomycetes from so far underexplored sources in terms of microbial diversity, like the marine environment, have been actively investigated in recent decades. For instance, members of the genus *Marinispora* or *Salinispora* have proven to be a promising source of new antibiotics, as e.g. the proteasome inhibitor salinosporamide, which is currently in phase I clinical trials as anticancer agent, is produced by *Salinispora tropica*.^[43, 44, 45, 46]

Besides *Streptomyces sp.* and rare actinomycetes (non-*Streptomyces* actinomycetales species), fungal species, in particular ascomycetes, several other filamentous fungi, and endophytes, are the second rich source of bioactive secondary metabolites, which include toxins as well as antibiotics.^[37] Fungal secondary metabolite classes comprise mainly NRPs, PKs, or mixed NRP/PKs; less abundant compared to plant metabolites are terpenes and alkaloids.^[47] With the availability of fungal genomes many efforts have been made to characterize fungal gene clusters in terms of regulation, activate silent clusters, and more generally, apply genome mining approaches for the discovery of new NPs.^[47, 48] The total diversity of fungal species is estimated to be 1.5-1.6 million, based on a global extrapolation of sampled fungal communities in and around plant and soil ecosystems from Western Europe. Nevertheless, the total number of species is probably even much higher when taking into account that many unknown species of fungi from unusual habitats, like the marine environment, were not covered.^[49, 50, 51] Amongst fungal species, endophytes have been extensively investigated in

the last years as to NP isolation, and the balanced antagonism between fungal virulence and plant defence has been proposed to be one reason for a rich secondary metabolism.^[52] After transmission of the fungus to the host plant, which occurs either horizontally (via airborne spores) or vertically (via seeds), microorganisms reside in internal plant tissues in a quiescent state without causing apparent disease symptoms.^[53] Growth in this habitat involves continuous metabolic interaction, thus, endophytic fungi reveal a great potential as sources of new biologically active NPs.^[54] Interestingly, it was also found that endophytic fungi are capable of producing NPs originally known from plants, a fact which might be explained either by direct supply of the metabolites from the fungus to the plant or gene transfer from plant to microbe or vice versa.^[55]

The third group of microbial NP producers, which accounts for ca. 17% of all microbial secondary metabolites, are unicellular bacteria, with *Bacillus* and *Pseudomonas* species as the most frequent producers. In recent decades, also cyanobacteria, myxobacteria, and marine organisms are increasingly recognized.^[1, 37]

1.1.3 ROLE OF MYXOBACTERIA

Myxobacteria were initially recognized because of their unusual growth characteristics, cooperative social behaviour, and unique developmental life cycle. The soil-dwelling δ -proteobacteria of the order Myxococcales can be found in various habitats, preferentially in places that are rich in microbial life and organic matter. Several dozen genera of myxobacteria have been isolated worldwide mainly from terrestrial soils, but also from marine sediments^[56], freshwater/saltwater, tree bark, animal dung, and anaerobic^[57] and hypothermic^[58] habitats. Particularly numerous isolates originate from subtropical and tropical zones with moderate to warm temperatures (Figure 1-3).^[59, 60, 61, 62]

Myxobacteria are distinguished from other bacteria mainly by two features: they move by gliding on solid surfaces in swarm-like patterns, and upon starvation conditions they form so-called fruiting bodies containing resting cells.^[63] Many species, like *Myxococcus xanthus*^[64], live prey other microorganisms (Figure 1-4). This cooperative feeding is facilitated by the gliding movement across solid surfaces, where individual cells organize in waves which travel in a rippling-like motion^[65]. The movement is thereby generated by two genetically distinct motility systems^[66]; the social (S) motility system is characterized by type IV pili that interact with components of the *M. xanthus* exopolysaccharide (EPS) matrix^[67], and the adventurous (A) motility system allows movement of individual cells although usually

employed in the swarm context.^[68, 69] During cooperative feeding (‘wolf-pack’ behaviour^[64]) other microbial species are degraded as prey by secretion of antibiotics and exoenzymes.^[62, 70] As swarming cells collide under starvation conditions they aggregate in mounds culminating in the formation of fruiting bodies that typically harbor 10^4 to 10^6 individual cells. Vegetative cells that are usually rod-shaped (4-12 μm long and 0.7-1.2 μm wide) undergo a cellular morphogenesis within the fruiting body resulting in shortened and fattened stress-resistant myxospores. A new life cycle is started from these resting cells once nutrients are available and myxospores germinate to develop new swarms (Figure 1-5). This process is regulated by sophisticated extra- and intracellular signaling mechanisms.^[61, 63, 70]



Figure 1-3: Global distribution of myxobacteria.

White spots mark sampling sites of soils that were used for the isolation of myxobacterial strains (adapted from ref. [60]).

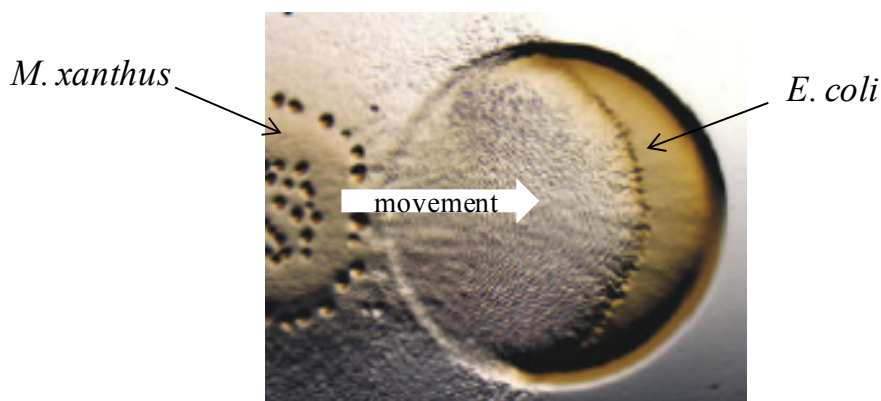


Figure 1-4: Cooperative feeding of *Myxococcus xanthus*.

A swarm of *M. xanthus* cells (left) consumes a colony of *E. coli* (right) by gliding in a swarm-like pattern and degradation of the prey organism (image by J. Berleman and J. Kirby, taken from ref. [62]).

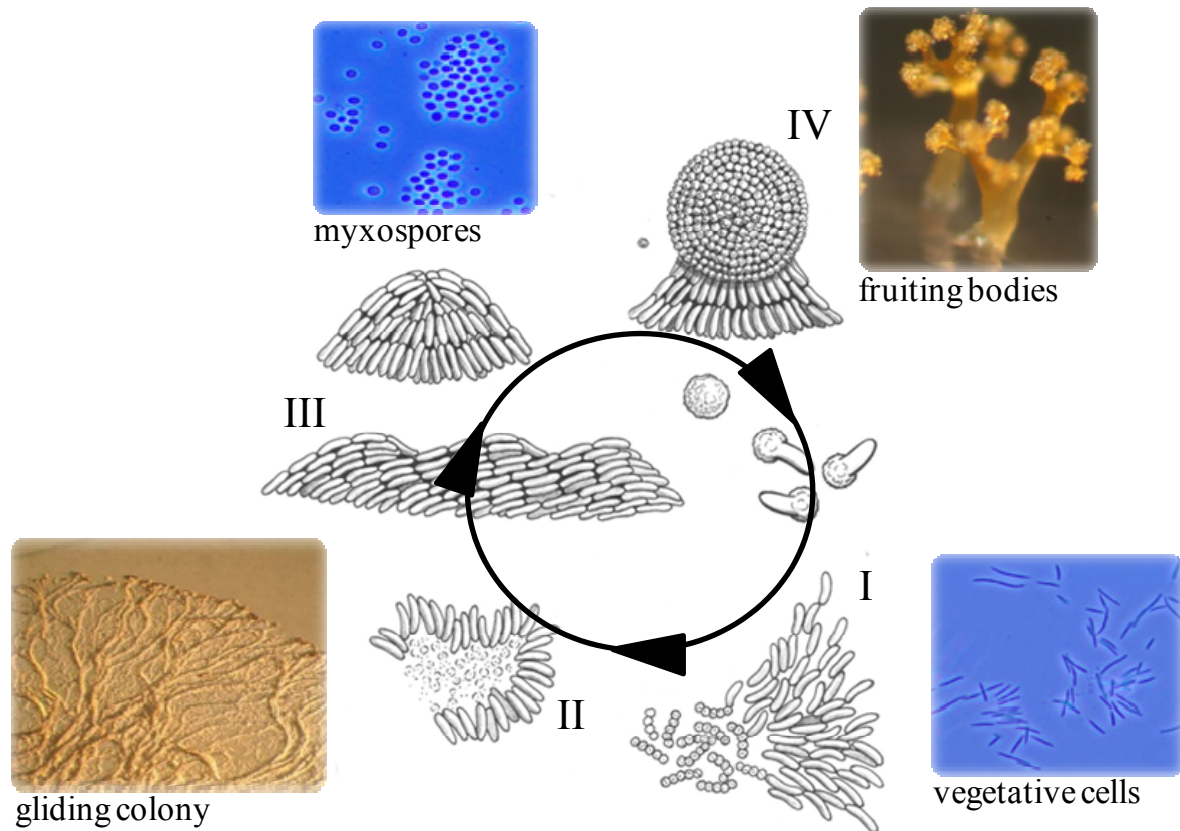


Figure 1-5: Schematic myxobacterial life cycle.

Vegetative cells move by gliding, form a swarm and some species (suborder Cystobacterineae) act as predatory collective on other microbes (I) by surrounding the prey, degradation, and consumption of the prey bacteria (II). Nutrient poor conditions trigger a changed cell movement, i.e. formation of waves and aggregation to moulds (III). This finally culminates in the formation of fruiting bodies (IV), which typically measure 20-1000 μm in height. These contain stress-resistant myxospores that germinate when nutrients are present (graphics are adapted from ref. [71]; images by Dr. R. O. Garcia).

One class of secondary metabolites that accounts to some extent for the developmental life cycle of myxobacteria, particularly *M. xanthus*, are the yellow DKxanthenes. The physiological role of these pigments in sporulation was found in the mid 90s^[72, 73] and genome-sequencing of *M. xanthus* strain DK1622 finally enabled, amongst others, the identification of the DKxanthene biosynthetic gene cluster. Targeted inactivation of the corresponding PKS and NRPS genes then indeed provided evidence that DKxanthenes are required for spore germination of *M. xanthus* (Figure 1-6).^[74]

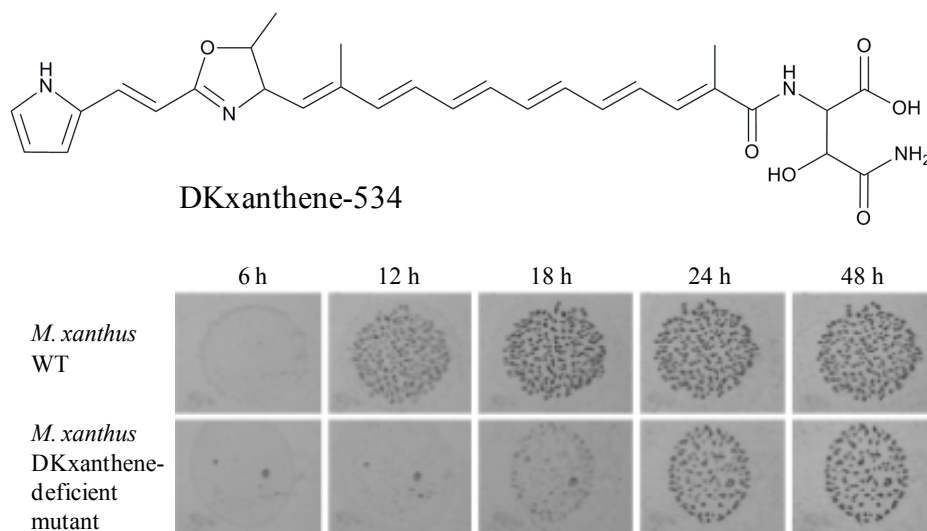


Figure 1-6: Influence of DKxanthene on fruiting body formation of *M. xanthus*.

The chemical structure of a DKxanthene derivative, a common secondary metabolite found in almost all *Myxococcus xanthus* strains, is displayed in the upper panel. Upon targeted gene inactivation in strain DK1050, fruiting body formation was found to be delayed (lower panel). In addition, the efficiency of sporulation could be restored in the deficient mutant to ca. 25% of wildtype level by supplementation with DKxanthene-534 (not shown).^[74]

Besides these fascinating ecological and developmental aspects, myxobacteria have gained increasing attention also with respect to biotechnological application as multi-producers of NPs.^[75] Within the last three decades, the proteobacteria have become an outstanding source of NPs with unique structures, broad spectrum of activities, and mostly complete novel mechanisms of action (Figure 1-7). Reported activities, in turn, include antifungal, antibacterial, cytotoxic, but also antiviral, immunosuppressive, antiplasmodial/antimalarial activities, plus some others.^[76, 77] A continuous research programme at the HZI (Helmholtz Centre for Infectious Research, Braunschweig, Germany; formerly German Research Centre for Biotechnology GBF) revealed that strains of the genus *Sorangium*, *Myxococcus*, and *Chondromyces* are the most frequent producers within the collection that comprises several thousand strains. *Nannocystis* and *Corallocooccus* were found to be rather poor producers of bioactive secondary metabolites.^[78]

So far, myxobacterial strains have yielded at least 70 core structures reported in literature and some 500 derivatives. These are mainly PKs, NRPs, PK/NRP hybrids, terpenoids, alkaloids, and phenyl-propanoids.^[76, 79, 80] With regards to reported biological activities, antibacterial (29%) and antifungal (54%) activities are predominant, most likely explained by the competitive pressure in the natural habitat. However, cellular targets and mechanisms of action are rather unusual compared to NPs from other sources.^[61, 77]

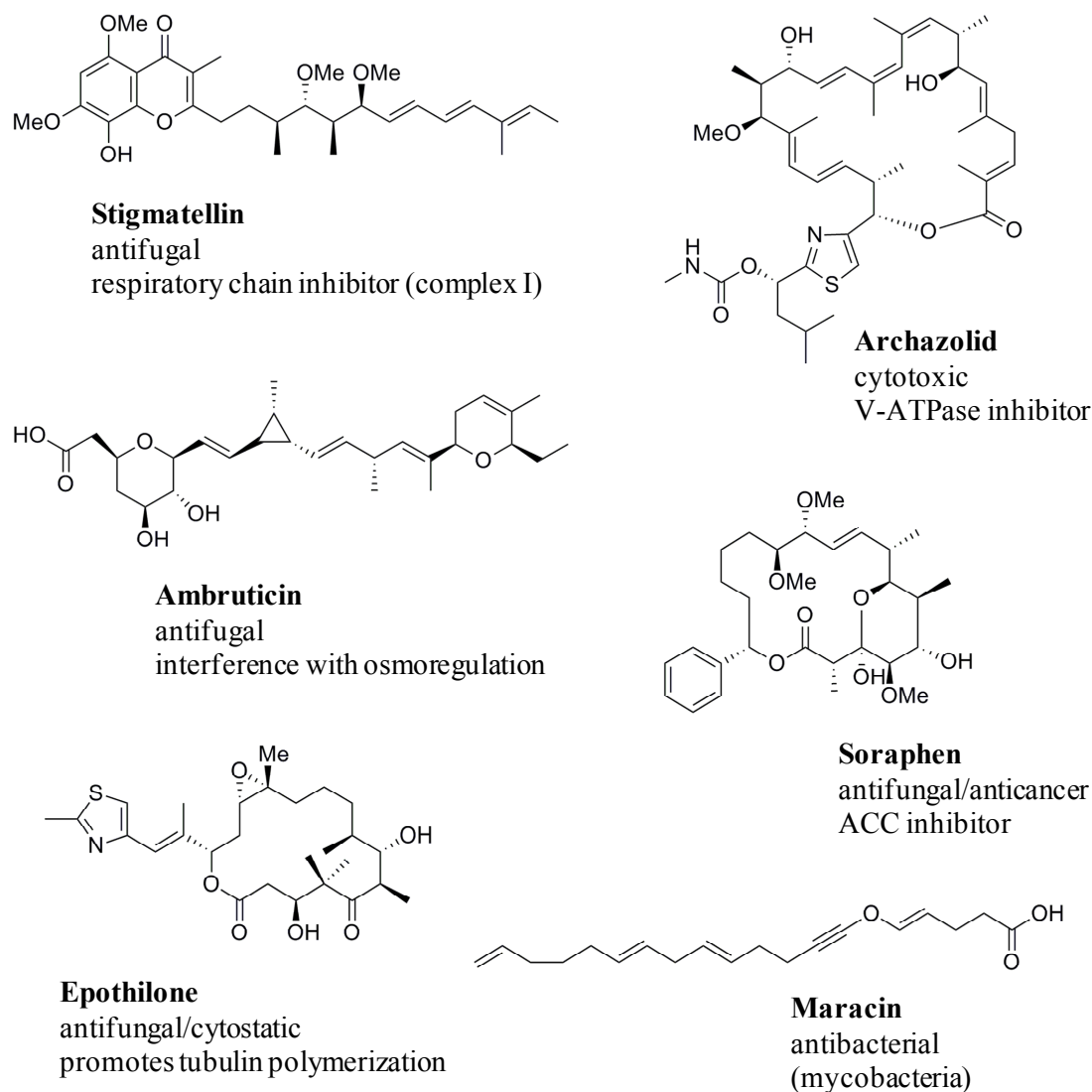


Figure 1-7: Selected antibiotic secondary metabolites isolated from myxobacteria.

Stigmatellin is produced by *Stigmatella aurantiaca* Sg a15 and was found to be active on fungi and some selected Gram-positive bacteria by inhibiting complex bc_1 of the respiratory chain.^[81, 82] The highly cytotoxic archazolids were isolated from *Archangium gephyra* Ar 3548 and *Cystobacter sp.* and were shown to be specific inhibitors of V-ATPase, an increasingly recognized putative novel target in cancer therapy.^[83, 84, 85, 86] The broad-spectrum antifungal agent ambruticin produced by *Polyangium cellulorum* subsp. *fulvum* interferes with osmoregulation by targeting the HOG pathway.^[87, 88, 89] Soraphens were initially isolated from *Sorangium cellulorum* strain So ce10 because of their strong antifungal activity by inhibiting the anticancer target acetyl CoA carboxylase (ACC).^[90, 91, 92, 93] Epothilones from *Sorangium cellulorum* So ce90 are microtubule stabilizers that act in a similar manner as taxanes. The latter compounds represent one of the highlights in myxobacterial natural product research, as epothilone B's semisynthetic analogue ixabepilone was approved in 2007 for clinical treatment of advanced breast cancer in the United States.^[94, 95, 96] Maracin and its α -chlorinated alkene analog maracen were also isolated from *S. cellulorum* strains because of their strong and specific activity on mycobacteria.^[97]

The further establishment of myxobacteria as prolific NP suppliers and the exploitation of their biosynthetic potential are currently being pursued using a panel of chemical, biological and genomics-based methods.^[78, 98] Especially the increasing availability of genome data of several myxobacterial strains has facilitated efforts towards the isolation of novel NPs. Myxobacterial genomes are very large, comprising 9-13 Mb, and have a high average GC content of approximately 70%. The model strain *Sorangium cellulosum* So ce56 has so far the largest bacterial genome, with a size of 13.0 Mb. In addition, usually around 8-10% of the sequence information is dedicated to genes encoding enzymes that are involved in secondary metabolism.^[99, 100] By this, the biosynthetic potential of myxobacteria at least equals that of sequenced streptomycetes, such as the model organism *Streptomyces coelicolor*.^[101, 102] Several biosynthetic gene clusters have already been identified from myxobacteria, whereas attempts towards NP isolation focus on heterologous expression and manipulation of the underlying megasynthetase systems, elucidation of their regulation, and activation of silent gene clusters.^[101, 103] For instance, the model organism in myxobacterial research on developmental and ecological aspects, *Myxococcus xanthus* DK1622, was regarded as a rather poor secondary metabolite producer. Complete genome sequencing then revealed in total at least 18 biosynthetic gene clusters encoding PKS, NRPS, and PKS/NRPS hybrid systems. Detailed efforts in the last seven years have revealed this species to produce at least eight different families of NPs.^[71, 77, 104]

1.2 NEW LEAD STRUCTURES FROM MICROBIAL SOURCES

In the past few decades, the process of identifying and purifying NPs from microbial sources has not changed significantly. Basically, crude extracts are prepared from microbial fermentations followed by bioactivity-guided fractionation, either employing whole cell - or *in vitro* protein assays, and *de novo* structural elucidation. In the outcome, NPs are the source of a large fraction of the current pharmaceuticals available against human disease.^[2] However, rapid identification of novelty in structure to find new leads (dereplication) in general remains one of the major issues when it comes to the discovery of NCEs. One criticism about NP screening campaigns is the high rate of repeated rediscovery of already known compounds arising from limitations in analytical techniques but more considerably from bias in screening programs themselves. Screening campaigns for antibiotics were focused only on a limited set of microbial sources, with *Streptomyces* as the best studied genus and, as a consequence, most frequent producer. Compounds isolated from streptomycetes historically play a very

prominent role in NP research since more than 50% of antibiotics available were isolated from *Streptomyces sp.* in the ‘Golden Era’.^[11, 77, 105, 106]

Besides the continuous improvement of analytical methods, engineered biosynthesis, and metabolome mining approaches, a partial shift from highly abundant and readily culturable microorganisms to unusual taxonomic groups of bacteria and more exotic species from extreme and/or underexplored natural environments took place in the last decades. Recent examples are novel bioactive NPs isolated from extremophiles^[107], fungal endophytes^[108], or organisms from the deep sea^[109] (Figure 1-8). However, existing microbial collections are also considered as a rich source of new NCEs when employing genomics approaches for the activation of silent gene clusters or production enhancement.^[2, 110, 111] In addition, extremophiles are not expected to be a rich source for secondary metabolites as competition in their habitats is usually limited. We have therefore focused our approaches on bacterial producers from highly diverse samples.^[79]

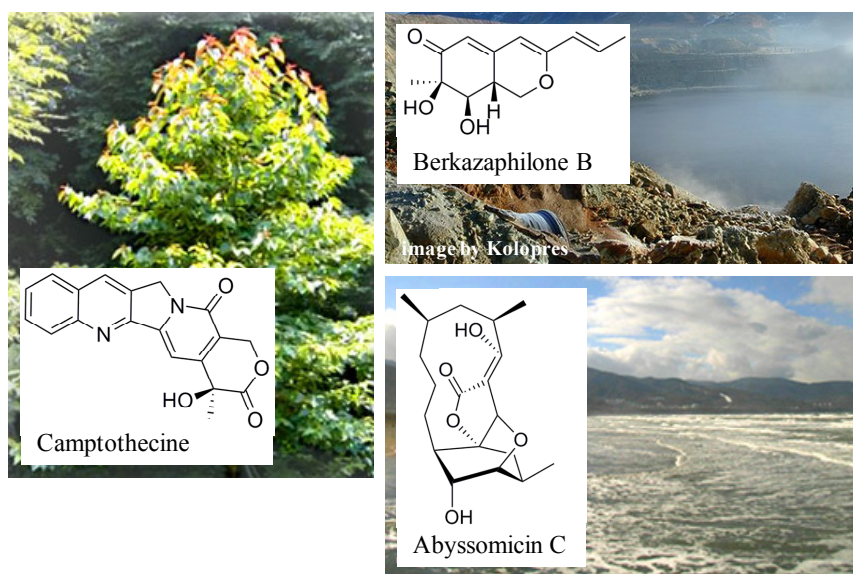


Figure 1-8: Examples of microbial NPs derived from diverse natural habitats.

Cytotoxic berkazaphilones were isolated from a *Penicillium* species that was collected from a depth of 270 m in the Berkley Pit Lake, a former mine, filled with acidic, metal-sulfate contaminated water.^[112] The antimicrobial (activity against MRSA and Mtb) abyssomicin is produced by a rare actinomycete (*Verrucosispora sp.*) collected from the deep sea of Japan.^[113, 114] The potent antineoplastic agent camptothecin that interferes with DNA topoisomerase I was isolated from the plant *Camptotheca acuminata* and later on, also found to be produced by an endophytic fungus.^[115]

1.2.1 SCREENING PROCESS

In the traditional workflow of NP isolation from microbial sources (Figure 1-9) crude extracts are prepared from small-scale cultivation batches. These extracts are then subjected to MS screening and the primary biological screening on e.g. antimicrobial, cytotoxic, or antiviral properties. Upon dereplication, extracts with unknown NPs are fractionated by chromatographic techniques and those fractions are again tested on their biological activity. Once the active target compounds are defined, the microorganism is production-optimized for the target compound and fermented in larger scale for subsequent NP purification, *de novo* structure elucidation, further activity tests, and mode-of-action (MoA) studies.^[116] For industrial use this process is regarded as too time-consuming and expensive. To overcome these hurdles, HTS may be applied for both, primary and secondary activity screening of crude extracts and fractions, respectively. In primary testing, the main issue is the complexity of extracts that often contain fluorescent or colored contaminants, which interfere with the assay read-out. Furthermore, samples might be insoluble in aqueous solution, be unstable as a mixture, or individual concentrations of active constituents are too low to be detected in HTS. Even if a robust screen yields hits in first instance reproduction of the results and access and examination of the biological resource are critical.^[1] It is believed that a better flexibility, higher quality, and tailor-made lead-finding strategies in HTS may circumvent some of these obstacles.^[117]

Mainly two different approaches evolved over the last years: the use of targeted smart screens and automated pre-fractionation with online chemical profiling of crude samples. The former strategy was successfully applied e.g. in the discovery of novel broad-spectrum antimicrobial agents that target conserved and essential enzymes of the fatty acid synthesis. In a differential-sensitivity whole cell two-plate agar diffusion assay over 250,000 microbial crude extracts were screened against a WT *S. aureus* strain and a hypersensitive mutant bearing a plasmid that produces antisense RNA to target fatty acid synthesis enzymes. The overall hit rate was exceptionally high (0.1%) and finally led to the discovery of platensimycin A and platencin.^[118, 119, 120]

Even more efficient, with regards to accelerating the screening and purification process, are methods that employ sophisticated pre-fractionation techniques. The construction of such large fraction libraries has the advantage of reduced complexity of the test material and often also accounts already for a physicochemical characterization prior to the application of bioassays.^[11, 121, 122, 123, 124]

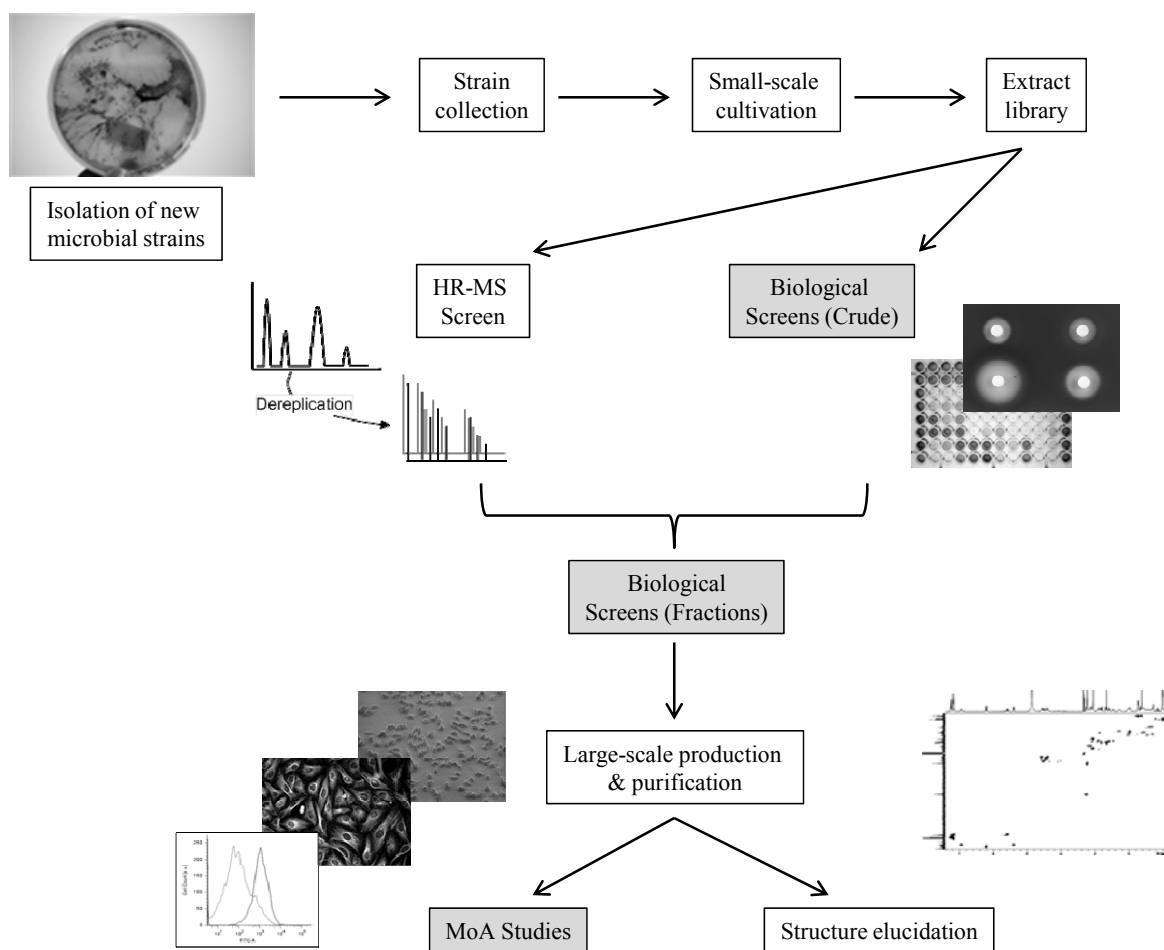


Figure 1-9: Schematic workflow of bioactivity-guided isolation of NPs from microbial sources.

Crude extracts from microbial sources are tested on biological activity either in *in vitro* or whole cell screens. In parallel, the chemical profile is determined for exclusion of already known NPs, ideally by dereplication against existing databases. This is followed by several cycles of fractionation and repeated activity testing. Finally, novel NPs are purified and structurally elucidated.

Due to significant improvements in analytics (detection, separation, structure elucidation) crude extracts from natural sources now seem to be accessible by HTS technologies. In addition, nearly all biochemical and cell-based assays can be translated to a high-throughput format. The most important recent technology, which might affect evolution of HTS campaigns, is HCS (high-content screening). Using HCS it is expected to achieve hits with greater physiological relevance and by this, determine higher quality leads. Currently, HCS is mostly applied in secondary screens, structure-activity relationship (SAR) -, target validation -, hit-to-lead optimization -, and mode-of-action studies, although it is expected that this methodology might move at least to some extent to primary compound screening. This trend is thereby accompanied by a shift from steadily increasing library sizes to smaller, more focused, and target-specific libraries.^[125, 126, 127, 128]

In contrast to HTS, the HCS technology is based on automated fluorescence imaging technology and provides spatial and temporal information on a single cell basis within a population in the context of structural and functional integrity. A wide variety of assays can be developed, such as signal transduction ^{-[129]}, GPCR (G-protein-coupled receptor) ^{-[130]}, organelle function ^{-[131]}, RNAi ^{-[132]}, or toxicity ^[133] screens. By this, HCS can be integrated into workflows typical for a broad range of research fields and is applied for instance in oncology ^{-[134]}, cardiovascular ^{-[135]}, and stem cell^[136] research using either endpoint (fixed cells) or live cell imaging techniques. More recently, HCS has also found its way into early drug discovery, such as cellular assays on antiviral replication^[137] or *in vivo* toxicity studies on zebrafish^[138].

However, most HCS applications rely on multiplexing several probes within one assay. As a result, these multiparametric screens produce scientifically complex data, which is highly beneficial for in-depth research on small molecule effectors and their impact on cellular processes. Early in the hit development process, either from NPs or synthetic compounds, it is possible to gain detailed information of a compound's MoA and to facilitate SAR studies. Nevertheless, in NP crude extract screening it is assumed that HCS may be unsuitable because of the added complexity during deconvolution of various observations, which might be caused by different compounds in an extract or even result from synergistic effects.^[2] Significant achievements in HCS small molecule library screens nevertheless encouraged researchers to apply robust HC screens for the characterization of crude extracts. Current examples are the development of a rapid HCS assay on cell cycle inhibition induced by treatment with crude extracts from myxobacterial origin^[139] or HC live cell imaging of marine-derived extracts for the discovery of new antimalarials^[140].

1.2.2 MICROBIAL NATURAL PRODUCTS AND THERAPEUTIC APPLICATIONS

In general, microbial NPs are either employed as molecular probes to study cellular functions of key proteins or further developed as lead structures in almost every therapeutic area of human disease. Over 16,500 microbial metabolites are reported to exhibit antibiotic activity.^[37] Presumably due to their origin, microbial NPs are particularly successful for the treatment of infectious disease as antibacterial and antifungal agents. Amongst NCEs that were reported in the period 1981 to 2010, nearly 55% of in total 147 compounds were either NPs or directly NP-derived, whereas a major part is from microbial sources.^[23] Although NP research in large pharmaceutical companies declined, emerging resistance, as seen with

Mycobacterium tuberculosis (MDR-TB and XDR-TB), again fosters the development of drugs with novel targets from natural sources or to engineer existing scaffolds.^[141]

The second large group of drugs developed from microbial NPs is cytostatic compounds used in cancer chemotherapy. Remarkably, over 60% of anticancer drugs in the last 30 years have originated from NPs.^[23] These comprise mainly agents that interfere with eukaryotic cell division and proliferation by targeting e.g. topoisomerases, kinases, microtubules, or DNA.^[142] The search for novel agents for cancer therapy is thereby, amongst others, motivated by the apparent heterogeneity of cancer cells, which in general complicates effective treatment strategies. Furthermore, some tumors acquire chemo-resistance, whereas for instance overexpression of classical MDR (multidrug resistant) proteins, such as P-gp (P-glycoprotein) or MRP (Multidrug Resistance Protein), is strongly correlated to resistance.^[143] Current therapeutic applications of NPs have expanded into immunosuppressive (e.g. rapamycin, isolated from *Streptomyces sp.*, inhibits mTOR^[144]), cholesterol-lowering (e.g. the fungal metabolite lovastatin inhibits HMG-CoA reductase^[145]), anthelmintic/antiparasitic (e.g. ivermectin from *Streptomyces sp.* blocks glutamate-gated anion channels^[146]), and antidiabetic agents (e.g. exendin-4, a hormone found in the saliva of *Heloderma suspectum*, acts as a GLP-1 agonist^[147]).

Other therapeutic areas, where NPs or NP-derived drugs are part of the pharmacopoeia, are inflammation, neurological diseases, cardiovascular diseases and endocrinology, and some others.^[2]

1.3 NATURAL PRODUCTS AND CANCER THERAPY

As reviewed by Newman and Cragg in 2012^[23], over 60% of anticancer drugs in the last 30 years have originated from natural products. Particularly NPs from plant sources have been exceptionally successful as anticancer agents. Since the *Vinca* alkaloids vinblastine and vincristine entered the market in early 1960s, numerous other chemotherapeutics derived from plant secondary metabolites have been launched for the treatment of various cancerous diseases.^[148] This may partly be attributed to a long history of use of relevant plants in traditional medicine. For example podophyllotoxin, isolated from a resin (podophyllin) produced by species of the genus *Podophyllum*, has been used in folk medicine for centuries and amongst other indications was found to be topically effective for skin cancers. Its semisynthetic derivative etoposide was later on developed as an anticancer agent and acts by inhibiting topoisomerase II activity (Figure 1-10).^[149, 150]

Besides plants as sources of novel anticancer agents, mainly compounds from terrestrial microorganisms and marine-derived NPs made their way into clinics. In the period 2005-2007, 23 lead compounds from plant origin, 17 from microbial sources, and 9 isolated from marine organisms were in oncology clinical trials.^[24]

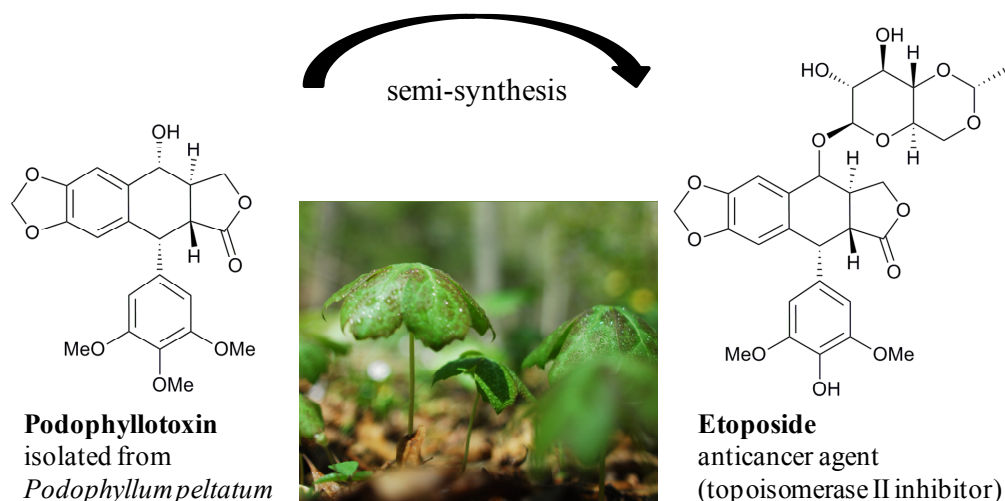


Figure 1-10: The plant-derived anticancer agent etoposide.

Podophyllotoxin is a lignan produced by several *Podophyllum spp.* and has a long history in traditional medicine. The semi-synthetic derivative etoposide was developed for clinical use as a topoisomerase II inhibitor for the treatment of cancer.

1.3.1 THERAPEUTIC TARGETS

At the outset of modern NP research, novel bioactive compounds were basically isolated following rather unspecific broad-spectrum bioactivity screens. This resulted in a significant number of new NPs, which are applied in treatment of various diseases. However, second generation cancer chemotherapeutics are more likely to be discovered in robust and particularly specific screens by which the limited use of non-selective toxic agents is circumvented. Recently, novel functional genomics approaches provide increasingly sophisticated knowledge of biological processes that underlie the malignant transformation of normal cells. By this, tumors can be classified according to their key abnormal pathways and novel ‘druggable’ targets within these networks can be identified and in turn, by using tailor-made, target-specific screens, highly selective sets of lead structures can be established.^[151]

The main targets of current anticancer drugs are DNA, key effector kinases, and tubulin. Chemotherapeutics of the first class either directly interfere with DNA or target proteins that play a role in DNA repair mechanisms, such as topoisomerases. By reducing the enhanced

capacity of many cancer cells to repair critical lesions, e.g. DSBs (DNA double-strand breaks), enhanced chemoresistance observed with such tumors can be countervailed. Novel strategies to combat drug resistance may rely on using chemosensitizers, such as PARP [poly(ADP-ribose) polymerase] inhibitors, in combination with already established topoisomerase inhibitors, DNA-alkylating agents, or radiation therapy. These combinations can cause severe genomic instability in tumor cells ultimately resulting in cell death.^[152, 153, 154]

Many signaling cascades have been identified that are to some extent dysregulated in cancer tissue and the development of selective kinase inhibitors, such as small molecule inhibitors of cell cycle regulating cyclin-dependent kinases (CDKs), is one of the prime targets in anticancer research. Nevertheless, highly selective blocking of single kinases has been associated with only limited responses in clinical trials. Thus, simultaneous inhibition of several receptor tyrosine kinases (RTKs) and/or downstream serine/threonine kinases may improve overall clinical success rates. This can be either be achieved by combination therapies of selective inhibitors or novel therapeutics that target multiple key signaling pathways, such as the multikinase inhibitor sorafenib.^[30, 155, 156]

Among the aforementioned decisive cellular targets, microtubules have played a major role, especially since the first *Vinca* alkaloids entered the market 50 years ago. Moreover, chemotherapeutics belonging to this compound class continue to be highly valuable as part of the pharmacopoeia for cancer treatment.^[24, 148] In mammalian cells, microtubules are crucial for trafficking, signaling, migration, and proliferation. Most importantly, the suppression of these dynamics by small molecules ultimately results in mitotic arrest and, in turn, the inhibition of cell proliferation and the induction of apoptosis. The search for novel microtubule-interacting compounds is primarily motivated by the need to overcome the typical resistance acquired to these drugs and the neurotoxicity of these compounds.^[157]

Other therapeutic targets include for instance proteasome inhibition^[158], antiangiogenic therapies^[159], modulation of hypoxia-inducible factor 1 (HIF-1)^[160], and V-ATPase inhibition^[86].

In addition to extensive research efforts in the elucidation of novel molecular cancer targets, the development of antibody-drug conjugates (ADCs) represents a growing research field. This approach might be of special interest when it comes to NPs or NP-derived drugs since these molecules are often not optimized to bind to one specific target but interact with different cellular targets. This intrinsic feature is often beneficial in multi-targeted therapy but may also lead to unwanted off-target effects. Coupling of rather unspecific, yet potent

cytotoxic agents ('payload') to specific antibodies greatly contributes to the reduction of collateral damage to surrounding tissue and may foster a renaissance of NPs in cancer therapy.^[28, 161] Generally, lead optimization includes the design of suitable linkers and the selection of antibodies, as in the case of the highly potent antineoplastic agent monomethylauristatin E (synthetic dolastatin analog) that has been approved as an ADC in 2011. The active component was coupled to antibodies either directed against CD30 antigen or a glycoprotein overexpressed in cancer cells via a valine-citrulline peptide linker. After receptor-mediated cellular uptake of the ADC, the linker is cleaved by lysosomal proteases and the active agent thus triggers apoptosis induction through G₂/M cell cycle arrest.^[162, 163]

1.3.2 THE EUKARYOTIC CYTOSKELETON

The eukaryotic cytoskeleton plays a crucial role during mitosis and cell division, controls intracellular transport mechanisms of organelles and cell movement, and accounts for mechanical stability of the cell. The main components are actin microfilaments, intermediate filaments, and microtubules (Figure 1-11), whereas each of these classes has a large dedicated set of accessory proteins.^[164]

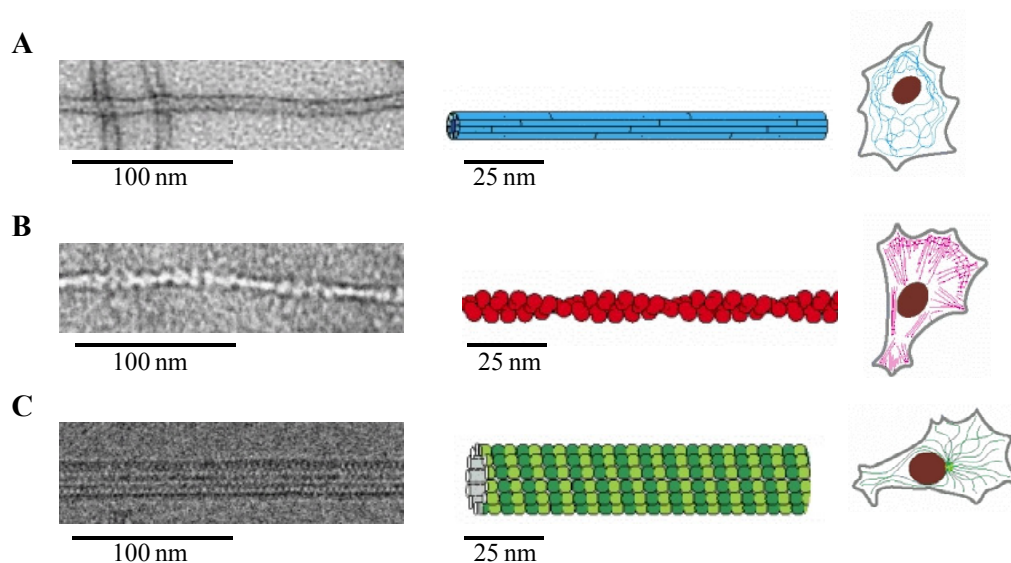


Figure 1-11: Components of the eukaryotic cytoskeleton.

A) Intermediate filaments. B) Actin microfilaments. C) Microtubules. (Micrographs: courtesy of R. Craig (A), R. Wade (B), and R. Quinlan (C); all images and graphics were taken from ref. [164]).

Among these three major systems, **intermediate filaments** (IFs) are probably the least studied with respect to their function and structure. These rope-like fibers are made of IF proteins and have a diameter of around 10 nm. The IF proteins differ largely in amino acid

sequence and are encoded by approximately 75 genes, which in turn, are regulated in a cell- and tissue-specific fashion. This results in an enormous diversity of IFs although they share common structural motives. α -Helical domains build coiled-coil dimers, which then form staggered tetramers; eight of these tetramers are packed together into rope-like filaments, which form the IF consisting of in total 32 α -helical domains. Due to this three-dimensional arrangement, IFs are especially resistant to bending or stretching forces. Although IFs were initially considered as rather static cytoskeletal elements with only little subunit exchange, current studies provide evidence that association and turnover of IFs are mainly regulated by rapid phosphorylation events. By this, IFs do not only account for mechanical resistance of cells but play also a specific role in locomotion. Based on the protein composition, four major types of IFs are distinguished: nuclear lamins, vimentin-like proteins, keratins, and neuronal IFs.^[164, 165, 166]

The other two major cytoskeletal components, actin filaments and microtubules, are involved in signaling and are critical for cell motility, maintenance of cell shape, transport mechanisms, cytokinesis, and mitosis. For the treatment of cancer, particularly antimetabolic agents directly targeting microtubules are well established chemotherapeutics.^[167] However, no actin-targeting drug is currently in clinical use, although both, tubulin and actin, have been thought to be valid anticancer targets.^[168, 169]

The dynamic **microtubule structures** are composed of α,β -tubulin heterodimers that are constantly assembled and disassembled as the microtubules oscillate between growing and shortening phases. While α - and β -tubulin are regular building blocks of microtubules, γ -tubulin has a more specific role as it associates with other proteins to form the γ -TuRC (tubulin ring complex) within the MTOC (microtubule organizing center) at the centrosome where single tubulin heterodimers are constantly assembled. By this, microtubules are polarized, with the minus-end capped by the γ -TuRC and anchored at the MTOC and the plus-end localized at the periphery of the cell. The polar protofilaments form together a bundle-like, hollow cylinder structure with a diameter of approximately 25 nm, which is composed of 13 protofilaments. One of the most important properties of microtubules is their dynamic instability^[170]. When microtubule subunits polymerize, tubulin dimers with bound GTP are added at the plus-end of the growing polymer, followed by hydrolysis of β -tubulin bound GTP to GDP. Since this hydrolysis is delayed with respect to further subunit addition, a GTP-tubulin cap is formed. Upon loss of this cap ('catastrophe') by e.g. slowed down subunit addition, a rapid depolymerization of the microtubule is induced. At some time later, the microtubule might regain its GTP-tubulin cap ('rescue') and begin to grow again. These

rapid dynamics are crucial for instance in cell division processes, such as chromosomal movements in anaphase^[171]. However, destabilization and stabilization are extrinsically regulated mostly by MAPs (microtubule-associated proteins) that bind to microtubules. One such is XMAP215^[172, 173] that stabilizes the growing end of a microtubule and suppresses the frequency of catastrophes. It has been proposed that XMAP215 acts as a template for head-to-tail oligomerization of multiple tubulin dimers and by this, facilitates the delivery of those preassembled protofilaments to the microtubule plus-end (tubulin shuttle model). However, current research also provides evidence for non-templating but tip tracking mechanisms, which might either occur via treadmilling or surfing. In contrast, proteins of the kinesin superfamily, such as MCAK^[174], oppose this action by removing the GTP-tubulin cap from growing microtubules. In a ‘diffuse and capture’ mechanism, the depolymerase MCAK couples ATP hydrolysis to the removal of GTP and triggers catastrophes at both microtubule ends.^[175, 176, 177]

Actin microfilaments determine the cell shape and polarity and are necessary for locomotive processes. The filaments are constituted of single subunits of actin, a protein which is highly conserved and the most abundant in most eukaryotic cells. In total, three main isoforms are known, including α -actin of cardiac, skeletal, and smooth muscle cells, and β - and γ -actin of nonmuscle and muscle cells. Similar to tubulin, actin permanently alternates between monomeric or globular (G-actin) and filamentous (F-actin) states. Actin subunits thereby bind ATP and assemble head-to-tail to form polarized protofilaments, whereby two of these filaments twist around each other two build up a right-handed 7-9 nm diameter helix.^[164] These actin filaments are relatively flexible but are cross-linked and bundled within the cells by various accessory proteins, such as α -actinin and filamin, that both enhance the stiffness of F-actin networks.^[178] *De novo* nucleation of actin filaments primarily occurs at the plasma membrane and is catalyzed by a number of proteins, including actin-related proteins (ARPs). Especially the Arp2/3 complex plays a central role in the regulation of actin assembly, dynamics and cross-linking. The initial association of G-actin molecules to form dimers and trimers (nucleation centers), followed by the conversion of ATP to ADP, is energetically less favorable than the elongation of already existing filaments. Similar to γ -TuRC in the MTOC, the Arp2/3 complex forms a pseudo ‘barbed end’ (minus-end), which mimics an actin trimer, and by this allows rapid elongation at the ‘pointed end’ (plus-end). Furthermore, it is possible that the bound Arp complex attaches to another actin filament resulting in a branched network with new filaments growing at a 70° angle relative to the initial filament.^[179, 180] As a consequence of permanent ATP hydrolysis and differences in the free energy of subunit

association and dissociation reactions, a phenomenon referred to as ‘treadmilling’ is observed with actin filaments. In steady-state, filament growth at the pointed end is exactly balanced with filament shrinkage at the barbed end, leading to rapid cycles of subunits between the cytosol (G-actin) and the filaments (F-actin), while the overall length of filaments remains constant.^[164] As with microtubules, complex assembly of actin microfilaments is not only determined by inherent characteristics of actin polymerization but is tightly regulated by a large set of actin-binding proteins (ABPs). The most abundant ABP is thymosin β_4 which binds to soluble G-actin and by this prevents polymerization resulting in a reservoir of unassembled monomeric actin in the cytoplasm. Upon de-sequestration by for instance profilin, which competes with thymosin β_4 in actin-binding, polymerization is promoted again. Additionally, the filament elongation is facilitated due to configurational changes of the actin subunit upon profilin-binding that delivers polymerization-competent actin to the growing filament.^[181, 182, 183] However, certain severing and capping proteins, such as gelsolin, can negatively impact the growth of actin microfilaments. Gelsolin^[184] is regulated by Ca^{2+} and PIP_2 and binds to actin filaments rapidly prior to severing. The actin conformation within the protofilament is changed and filaments are broken by gelsolin. Once an actin filament has been severed, gelsolin remains attached to the barbed end and acts as an effective capping protein, which prevents further filament growth.^[164, 175, 185]

1.3.3 MYXOBACTERIAL METABOLITES

In a comprehensive review on myxobacterial secondary metabolites by Weissman and Müller in 2010^[76], the authors list in total 67 compound families that have been published at that time. Out of those, 31 NP classes have a cytotoxic activity towards mammalian cells. Although some of the underlying cellular mechanisms remain undiscovered, for most compounds (given in brackets) targets have been identified and include V-ATPase (apicularen and archazolid^[84]), mitochondrial $\text{F}_1\text{-ATPase}$ (cruentaren^[186]), DNA (saframycin Mx1^[187]), protein synthesis (gephyronic acid^[188]), proteasome (argyrin^[189]), and nuclear export complex formation (ratjadon^[190]). Notably, six distinct compound classes that are produced by myxobacteria have been found to directly interfere with the eukaryotic cytoskeleton (Figure 1-12) by either stabilizing or destabilizing microtubules (epothilone^[95], disorazol^[191], and tubulysin^[192]) or actin filaments (chivosazol^[193], chondramide^[194], and rhizopodin^[195]). Especially the microtubule-targeting drugs have been the subject of concerted efforts to elucidate their biosynthesis, total synthesis, and semi-synthesis in order to improve their pharmacological properties and yields.^[196, 197]

As mentioned above, a semisynthetic analog of the microtubule-stabilizer epothilone B (ixabepilone) has already been approved by the FDA in 2007 for the clinical treatment of advanced breast cancer in the United States.^[96] Although having a similar binding pattern as taxane, cross-resistance with epothilone is not observed.^[198] It is the first example of an NP exclusively produced by myxobacteria, which has been developed for clinical use. In addition, other modified epothilones and epothilone B are currently progressing clinical trials.^[24]

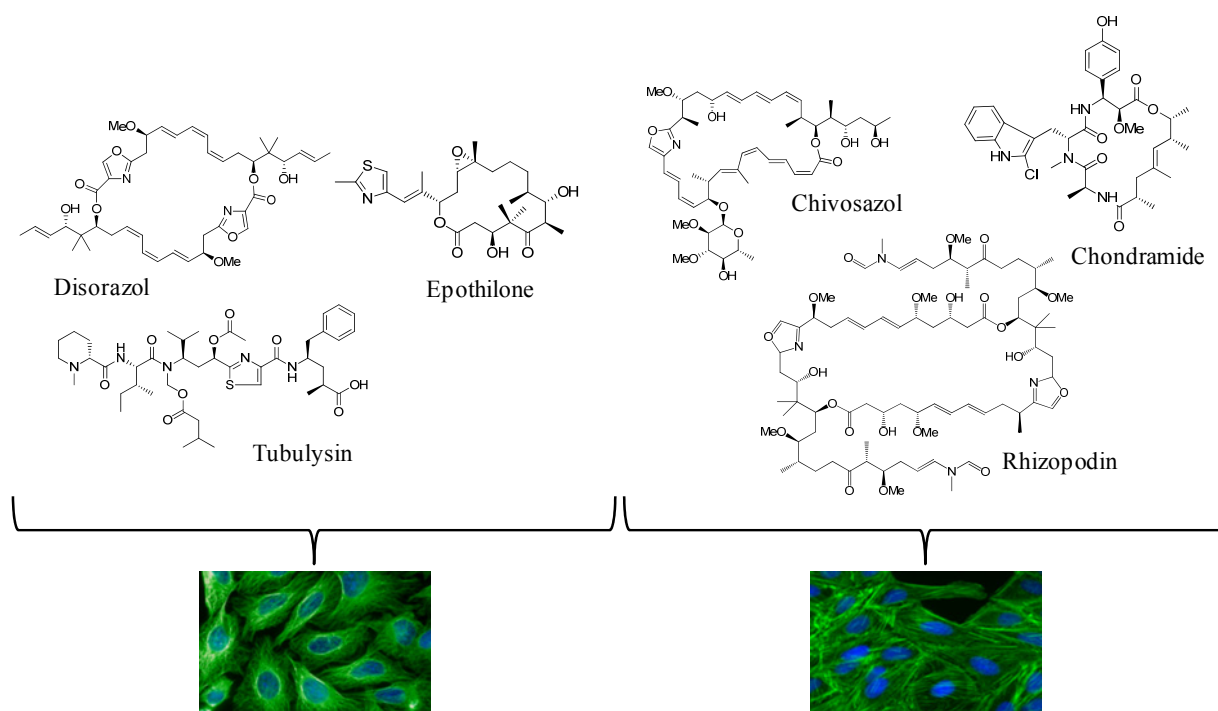


Figure 1-12: Myxobacterial secondary metabolites acting on the eukaryotic cytoskeleton.

Tubulysins, epothilones, and disorazols act on microtubules and chondramides, rhizopodin, and chivosazols act on actin filaments. The compounds can be classified either as stabilizers (epothilones and chondramides) or destabilizers (all others) of their respective target structures. Images show cytoskeletal structures in green (left: microtubules; right: actin microfilaments) and nuclei in blue.

Despite the encouraging pre-clinical evaluation of tubulysin A^[199], which acts by destabilizing microtubules, a major hurdle for the further development of this compound class is its supply. Fermentation yields only several mg per L and downstream-processing includes multiple chromatographic steps. Also total synthesis cannot be achieved so far on a reasonable and thus, economic scale.^[200, 201] With the discovery of one of its biosynthetic precursor molecules, referred to as ‘pretubulysin’ (Figure 1-13), and successful total synthesis of this NP, the supply issue can now be circumvented due to a practical chemical synthesis that yields the product in multigram quantities. Pretubulysin lacks the *N,O*-acetal and acetoxy functionalities of the amino acid tubuvalin in the original NP.^[202] Nevertheless, it could be

shown that these moieties are not crucial for biological activity and first reports demonstrate that pretubulysin might be developed, instead of tubulysins themselves, as an effective antineoplastic and antiangiogenic drug.^[203, 204]

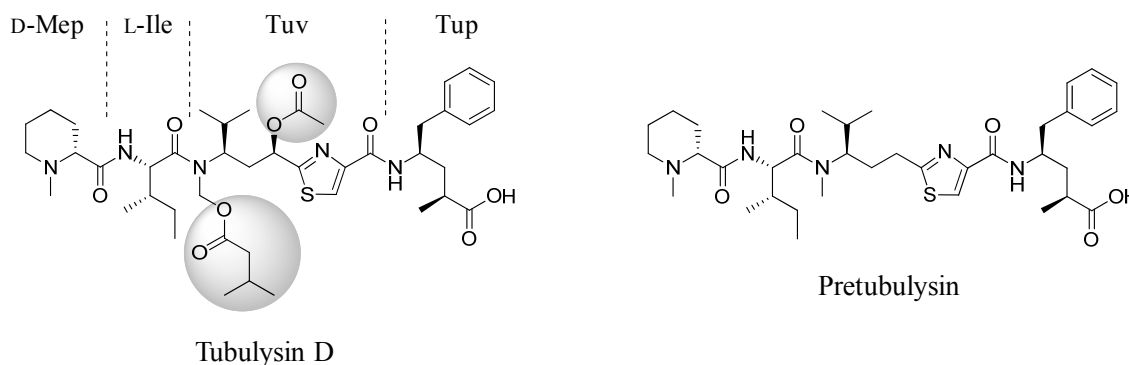


Figure 1-13: Chemical structures of tubulysin D and pretubulysin.

Biosynthesis studies revealed the presence of a precursor molecule (pretubulysin) that is released from the PKS/NRPS assembly line and undergoes post-assembly acylation and oxidation reactions to form tubulysins. Due to the lacking *N,O*-acetal and acetoxy moieties, pretubulysin can be synthesized in multigram quantities and currently undergoes pre-clinical studies. (Mep: *N*-methylpipecolic acid; Ile: isoleucine; Tuv: tubovaline; Tup: tubuphenylalanine).

Disorazols act like tubulysins by destabilizing microtubules and show extraordinary high activity (picomolar range) against a variety of cancer cell lines.^[197] Studies on the specific targeting of disorazoles to cancer cells are currently ongoing, as for instance applied for disorazol Z. The NP was coupled to an LHRH (luteinizing hormone-releasing hormone) agonist peptide that binds to the respective receptors mainly expressed on cancer cells. Upon binding and internalization of the conjugate, the linker is cleaved spontaneously and the payload (disorazol Z) is released. First *in vivo* results were encouraging and demonstrated that using this approach disorazol's tumor suppression activity can be further increased.^[205]

Research on myxobacterial NPs targeting the actin cytoskeleton has been mainly focused on unraveling their biosynthetic origin and total synthesis. Although migration of cancer cells, which might also be inhibited by actin-targeting cytostatic drugs, has become an extensively studied target in the last years, NPs of this class are rather believed to be suitable as molecular probes and their medicinal potential remains uncertain.^[168]

Especially the chondramides are believed to be suitable as effective probes for studying actin dynamics. These cyclodepsipeptides were originally isolated from terrestrial strains of *Chondromyces crocatus* and interestingly, showed high structural similarity to jasplakinolide/jasplamide isolated from marine sponges.^[194, 206, 207] Members of both

compound families are able to induce actin polymerization and share a common binding site on F-actin, similar to that of the mushroom toxin phalloidin.^[208, 209, 210] However, total synthesis of chondramides enabled researchers to further develop them as valuable fluorescent tools to study actin dynamics. In contrast to commonly applied phalloidin probes, chondramides are cell permeable and thus, can be applied in non-permeabilized cells.^[211, 212]

1.4 SCOPE OF THE WORK

The aim of this thesis was the biological characterization of pretubulysin as a novel putative lead structure in cancer therapy and in addition, the development of smart screening techniques for myxobacterial crude extracts or compounds.

In the first part of this work, pretubulysin, a synthetically accessible precursor of the tubulysin compound family was biologically characterized. A variety of cell-based and *in vitro* studies was applied to compare its antimitotic potency with that of the parent compounds tubulysins A and D. Additionally, other synthetic derivatives and precursor molecules were examined, which enabled structure-activity relationship insights. The presented study aimed to provide an initial characterization of pretubulysin and build the basis for upcoming in-depth pre-clinical studies on pretubulysin as a novel antineoplastic agent.

The second part of the work was intended to deal with the activity-guided isolation of novel chondramide derivatives. In routine screening of new myxobacterial isolates, it was found that *Chondromyces sp.* SBCm007 extracts show exceptionally high cytotoxicity against mammalian cell lines. Desirably, not only high-abundance molecules should be isolated, but also less frequently produced natural products with interesting novel activity profiles. In order to account for this, high-content screening techniques were adjusted to be suitable for crude extract and fraction screening. Coupling fermentation strategies directly to the process of bioactivity-guided isolation via HCS it was possible to isolate a number of novel chondramide derivatives. These were further characterized and compared to already known derivatives in some biological assays.

MATERIALS AND METHODS

2.1 MATERIALS

2.1.1 COMPOUNDS

The reference compounds epothilone B, disorazol A, tubulysins A and D, and chondramides A~D were kindly provided by the Microbial Drugs research group (MWIS) at the Helmholtz Centre for Infection Research (HZI, Braunschweig, Germany).

Pretubulysin and its derivatives were synthesized and kindly provided by Dr. J. L. Burkhart, Dr. A. Ullrich, and Dr. Mengxia Xue (group of Prof. Dr. U. Kazmaier at Saarland University, Institute for Organic Chemistry).

Chondramide derivatives produced by *Chondromyces sp.* SBCm007 were purified by S. Hüttel in our research group in the course of this study.

2.1.2 CHEMICALS

All chemicals were of reagent grade quality and were obtained from commercial sources and used without further purification unless otherwise noted.

2.1.3 CELL LINES AND PRIMARY CELLS

The L3.6pl cell line was kindly provided by Prof. Dr. C. J. Bruns (Department of Surgery, Clinic Großhadern, LMU Munich, Germany).^[213] Other cell lines were obtained from the American Type Culture Collection (ATCC) and the German Collection of Microorganisms and Cell Cultures (Deutsche Sammlung für Mikroorganismen und Zellkulturen, DSMZ). All cell lines were cultured under the conditions recommended by the respective depositor and are listed in Table 2-1. For L3.6pl cells cultureware was coated with collagen G (0.001% collagen/PBS).

Primary HUVEC (human umbilical vein endothelial cells; single donor) were purchased from PromoCell and cultured in Endothelial Cell Growth Medium (PromoCell) containing the following supplements: 2% FCS, 0.4% ECGS, 0.1 ng/ml EGF, 1 ng/ml bFGF, 90 µg/ml heparin, 1 µg/ml hydrocortisone.

Table 2-1: Cell lines and culture media.

Cell Line	Species	Type	Medium	Supplements
A431	human	epidermoid carcinoma	MEM	10 % FBS 1% NEAA
A549	human	lung carcinoma	DMEM	10% FBS
CHO-K1	Chinese hamster	ovary	F12	10% FBS
COS-7	African green monkey	kidney	DMEM	10% FBS
HCT-116	human	colon carcinoma	McCoy's 5A (modified)	10% FBS
HEK293T/17	human	embryonal kidney	DMEM	10% FBS
HepG2	human	hepatocellular carcinoma	DMEM	10% FBS
HL-60	human	acute myeloid leukemia	RPMI-1640	10% FBS
K562	human	chronic myeloid leukemia in blast crisis	RPMI-1640	10% FBS
KB-3.1	human	cervix carcinoma	DMEM	10% FBS
KB-V.1	human	cervix carcinoma (MDR)	MEM	15% FBS 1% NEAA
L3.6pl	human	pancreatic cancer (established in nude mice; pancreas to liver)	RPMI-1640	10% FBS 1 % pyruvate 1% NEAA
L-929	murine (mouse)	connective tissue fibroblast	RPMI-1640	10% FBS
MRC5	human	lung fibroblast	DMEM	10% FBS
NIH/3T3	murine (mouse, Swiss mouse)	embryo	DMEM	10% NCS
Ptk-2	<i>Potorous tridactylis</i>	kidney	MEM	10% FBS 1% NEAA
SH-SY5Y	human	neuroblastoma	DMEM	20% FBS
SW480	human	colon adenocarcinoma	RPMI-1640	5% FBS
U-2 OS	human	osteosarcoma	McCoy's 5A (modified)	10% FBS
U937	human	histiocytic lymphoma	RPMI-1640	10% FBS

2.1.4 CELL CULTURE MEDIA AND REAGENTS

Table 2-2: Cell culture media and supplements.

Reagent	Description	Manufacturer
DMEM	high glucose medium, contains glutamine and sodium bicarbonate	Sigma-Aldrich, Taufkirchen, Germany
Endothelial Cell Growth Medium F12	Endothelial Cell Basal Medium and Supplement Mix contains glutamine, sodium pyruvate, and sodium bicarbonate, Gibco®	PromoCell, Heidelberg, Germany Invitrogen, Karlsruhe, Germany
MEM	contains glutamine and sodium bicarbonate	Sigma-Aldrich, Taufkirchen, Germany
McCoy's 5A (modified)	high glucose medium, contains glutamine and bacto-peptone, Gibco®	Invitrogen, Karlsruhe, Germany
RPMI-1640	contains glutamine and sodium bicarbonate	Sigma-Aldrich, Taufkirchen, Germany
FBS	defined FBS, heat inactivated, EU approved (FBS 'GOLD')	PAA, Pasching, Austria
NCS	heat inactivated	PAA, Pasching, Austria
NEAA	100x solution	Sigma-Aldrich, Taufkirchen, Germany
sodium pyruvate	100 mM solution, sterile-filtered	Sigma-Aldrich, Taufkirchen, Germany

Table 2-3: Other reagents.

Reagent	Description	Manufacturer
Accutase		PromoCell, Heidelberg, Germany
Cell freezing medium	DMSO 1x	Sigma-Aldrich, Taufkirchen, Germany
Cryo-SFM	freezing medium HUVEC	PromoCell, Heidelberg, Germany
DMSO	Hybri-Max™, sterile-filtered	Sigma-Aldrich, Taufkirchen, Germany
hydroxyurea		Sigma-Aldrich, Taufkirchen, Germany
2-mercaptoethanol		Sigma-Aldrich, Taufkirchen, Germany
MTT	thiazolyl blue tetrazolium bromide	Sigma-Aldrich, Taufkirchen, Germany
PBS	pH 7.4, without Ca ²⁺ /Mg ²⁺	Sigma-Aldrich, Taufkirchen, Germany
paraformaldehyde		Sigma-Aldrich, Taufkirchen, Germany
Proteinase K from <i>Tritirachium album</i>	≥ 30 U/mg	Sigma-Aldrich, Taufkirchen, Germany
Ribonuclease A	~ 90 U/mg	Carl Roth GmbH, Karlsruhe, Germany
trypsin-EDTA	10x solution	Sigma-Aldrich, Taufkirchen, Germany

2.1.5 BUFFERS

Actin buffer (non-polymerizing; pH 8.0)

Tris	5 mM
CaCl ₂	0.2 mM
ATP	0.2 mM
DTT	1 mM

The pH was adjusted with HCl.

6x DNA loading dye

bromophenol blue	0.25% (w/v)
xylene cyanol blue	0.25% (w/v)
87% glycerol	10% (v/v)
EDTA	10 nM

PBS (pH 7.45)

sodium phosphates	10 mM
KCl	2.68 mM
NaCl	140 nM

The buffer was prepared by dissolving one solid PBS tablet (Gibco®, Invitrogen) in 500 ml distilled water. The buffer was autoclaved and stored at room temperature.

PCB (pH 7.8)

Na ₂ HPO ₄	192 mM
citric acid	4 mM

Solutions of 0.2 M Na₂HPO₄ and 0.1 M citric acid were prepared separately and mixed prior to use (192 parts Na₂HPO₄ and 8 parts citric acid).

PEM (pH 6.6)

PIPES	100 mM
EGTA	1 mM
MgSO ₄ • 7 H ₂ O	1 mM

The pH was adjusted with KOH and the buffer was stored at 4°C. For tubulin isolation, ATP and GTP were added directly prior to use as assigned in the Methods section.

50x TBE (pH 8.0)

Tris	0.89 M
boric acid	5.5% (w/v)
EDTA	0.93% (w/v)

The pH was adjusted with HCl. For electrophoresis 50x TBE was diluted with H₂O_{dd}.

TMRM assay buffer (pH 7.35)

NaCl	135 mM
KCl	5.4 mM
MgCl ₂	2 mM
Glucose	10 mM
CaCl ₂	2 mM
HEPES	10 mM

The pH was adjusted with 10 N NaOH and the buffer was stored at 4°C.

2.1.6 ANTIBODIES

All antibodies were diluted in PBS containing 10% FBS.

Table 2-4: Primary and secondary antibodies.

Antibody	Description	Dilution	Manufacturer
anti-β-actin	rabbit monoclonal (clone: EP1123Y), IgG	1:2000	Merck Millipore, Darmstadt, Germany
anti-phospho-Histone H2A.X (Ser139)	mouse monoclonal (clone: JBW301), IgG1	1:400	Merck Millipore, Darmstadt, Germany
anti-α-tubulin	mouse monoclonal (clone: DM1A), IgG1	1:2000	Sigma-Aldrich, Taufkirchen, Germany
Alexa Fluor® 488 goat anti-mouse	IgG (H + L), Molecular Probes®	1:1000	Invitrogen, Karlsruhe, Germany
Alexa Fluor® 488 goat anti-rabbit	IgG (H + L), Molecular Probes®	1:1000	Invitrogen, Karlsruhe, Germany
Alexa Fluor® 555 goat anti-rabbit	IgG (H + L), Molecular Probes®	1:1000	Invitrogen, Karlsruhe, Germany

2.1.7 STAINING DYES

Stock solutions of listed dyes (Table 2.5) were prepared and stored according to the manufacturer's recommendations.

Table 2-5: Staining dyes.

Stain	Manufacturer
Acridine orange (hydrochloride hydrate)	Sigma-Aldrich, Taufkirchen, Germany
Acti-stain™ 555 phalloidin	Cytoskeleton Inc., Denver, USA
Giemsa stain	Sigma-Aldrich, Taufkirchen, Germany
HCS CellMask™ Green	Molecular Probes®, Invitrogen, Karlsruhe, Germany
HCS CellMask™ Red	Molecular Probes®, Invitrogen, Karlsruhe, Germany
Hoechst33342	Molecular Probes®, Invitrogen, Karlsruhe, Germany
ethidium bromide	Sigma-Aldrich, Taufkirchen, Germany
propidium iodide	Carl Roth GmbH, Karlsruhe, Germany

2.1.8 CYTOSKELETAL PROTEINS

Pyrene muscle actin from rabbit muscle and MAP-rich tubulin from porcine brain were purchased from Cytoskeleton Inc., Denver, USA.

2.1.9 TECHNICAL EQUIPMENT AND CONSUMABLES

Table 2-6: Equipment.

Description	Type	Manufacturer
balances	Acculab Vicon	Sartorius AG, Göttingen, Germany
	Precisa XB220A	Gravimetrics AG, Dietikon, Switzerland
centrifuges	Heraeus Fresco 17	Thermo Fisher Scientific, Schwerte, Germany
	5180R (rotor A-4-62)	Eppendorf, Hamburg, Germany
	Sorvall (rotor GSA)	Thermo Fisher Scientific, Schwerte, Germany
	Sorvall (rotor SS-34)	Thermo Fisher Scientific, Schwerte, Germany
CO ₂ incubator	Innova CO-170	New Brunswick Scientific, Edison, USA

flow cytometer	GUAVA® EasyCyte™ Plus	Merck Millipore, Darmstadt, Germany
freezing container	Nalgene 5100 Cryo 1°C, 'Mr. Frosty'	Thermo Fisher Scientific, Schwerte, Germany
gel documentation system	Gel Doc 2000	Bio-Rad Laboratories GmbH, München, Germany
hemocytometer	Neubauer-improved (0.1 mm depth)	Paul Marienfeld GmbH & Co., Lauda- Köngshofen, Germany
liquid nitrogen tank	MVE TEC 3000	Broser, Frankenthal, Germany
microscope (automated)	Pathway 855	BD Biosciences, Heidelberg, Germany
microscope (optical)	ECLIPSE TS100	Nikon, Düsseldorf, Germany
pipettors	Pipetus®	Hirschmann Laborgeräte, Eberstadt, Germany
plate readers	SpectraMax M5 ^e EL808	Molecular Devices, Biberach, Germany Bio-Tek Instruments Inc., Winooski, USA
power supply	Standard power pack P25	Biometra GmbH, Göttingen, Germany
rotor mixer	Blender GT 800	Rotor Lips Ltd., Uetendorf, Switzerland
spectrophotometer	DU7500	Beckmann Coulter, Fullerton, USA
vacuum pump	VACUSAFE comfort	IBS Integra Biosciences, Fernwald, Germany

Table 2-7: Consumables.

Description	Type	Manufacturer
6-well plates	Costar® 6 Well, clear, flat bottom, sterile	Corning Life Sciences Inc., Lowell, MA, USA
	Corning® CellBIND® 6 Well, clear, flat bottom, sterile	Corning Life Sciences Inc., Lowell, MA, USA
96-well plates	Corning® CellBIND® 96 Well, clear, flat bottom, sterile	Corning Life Sciences Inc., Lowell, MA, USA
	96 Well, clear, flat bottom, sterile	Sarstedt AG & Co., Nümbrecht, Germany
	96 Well imaging plates, black, clear bottom, flat bottom, sterile	BD Biosciences, Heidelberg, Germany

384-well plates	Corning® 384 Well, black, NBS™ surface, flat bottom	Corning Life Sciences Inc., Lowell, MA, USA
cell scraper	24 cm, sterile	TPP, Trasadingen, Switzerland
culture flasks	25cm ² (T-25), filter cap	Sarstedt AG & Co., Nümbrecht, Germany
	75cm ² (T-75), filter cap	Sarstedt AG & Co., Nümbrecht, Germany
serological pipettes	Corning® Costar® Stripette (2 ml, 5 ml, 10 ml, 25 ml, 50 ml)	Corning Life Sciences Inc., Lowell, MA, USA

2.2 METHODS

Methods marked with an asterisk (*) were applied by collaborators and are described in brief.

2.2.1 SUBCULTIVATION OF CELLS

All cell culture experiments were performed under sterile conditions and cells were cultured in a gas-controlled incubator in a water vapor saturated atmosphere at 5% CO₂ and 37°C.

Frozen aliquots of cells were stored in liquid nitrogen. For plating, the respective full growth medium was pre-warmed to 37°C, cryovials were quickly defrosted, sterilized with 70% EtOH and cells were suspended in 10 ml growth medium. Suspension cells were washed once in complete medium, centrifuged for 5 min at 1,000 rpm (Eppendorf 5180R), resuspended in 10 ml complete medium and plated in T-25 culture flasks. The day after seeding of adherent growing cultures in T-25 flasks, medium was discarded and replaced by 10 ml fresh complete culture medium. For subcultivation, confluent cultures of adherent cells were either scrapped off or detached after washing with PBS by trypsin/EDTA and the reaction was stopped by adding the 10-fold volume of FBS-containing medium. Suspended cells were split in ratios of 1:3 to 1:20 according to the depositor's recommendations. Suspension cultures were directly diluted in fresh complete medium and cell densities were maintained at about 1x10⁵-2x10⁶ viable cells/ml.

2.2.2 CRYOPRESERVATION

The cells were seeded in T-25 flasks and grown to ca. 70% confluency (adherent cultures) and approximately 5x10⁵ viable cells/ml (suspension cultures), respectively. After detaching adherent cells as described in section 2.2.1, cells were collected by centrifugation for 5 min at room temperature at 1,200 rpm (Eppendorf 5180R), washed once with PBS and the cell pellet was resuspended in 500 µl freezing medium to achieve a final concentration of about

10^6 cells/ml. Cryoampules were cooled down at a constant rate of $-1^\circ\text{C}/\text{min}$ in a -80°C freezer (freezing container ‘Mr. Frosty’) and subsequently transferred for long-term vapor phase storage in a liquid nitrogen tank.

2.2.3 PRIMARY CULTURES

Single donor HUVEC were subcultivated once the cells reached 70-90% confluency in T-25 culture vessels. HUVEC were washed with a small volume of PBS and 3 ml accutase solution was added. The culture vessel was placed back in a CO_2 incubator for ca. 15 min and once HUVEC completely detached, cells were collected by centrifugation for 3 min at 1,000 rpm (Eppendorf 5180R). The pellet was resuspended in endothelial cell growth medium and cells were split in a ratio of 1:2 - 1:3. For cryopreservation, HUVEC were resuspended in Cryo-SFM freezing medium at 10^6 cells/ml and cryoampules were cooled down at a constant rate of $-1^\circ\text{C}/\text{min}$ in a -80°C freezer (freezing container ‘Mr. Frosty’) and subsequently transferred for long-term vapor phase storage in a liquid nitrogen tank.

2.2.4 VIABILITY ASSAY (MTT)

Cells from actively growing cultures were harvested and seeded at 6×10^3 cells per well of 96-well plates (CellBIND®surface) in 180 μl complete medium and treated after 2 h equilibration in a CO_2 incubator with compounds in serial dilution. Each compound or extract was tested in duplicate as well as the internal MeOH control. After 5 d incubation, 20 μl of 5 mg/ml MTT (thiazolyl blue tetrazolium bromide) in PBS was added per well and it was further incubated for 1-3 h (depending on the cell type) at 37°C .^[214] The medium was then discarded and cells were washed with 100 μl PBS before adding 100 μl 2-propanol/10 N HCl (250:1) in order to dissolve formazan granules. The absorbance at 570 nm was measured using a microplate reader (EL808, Bio-Tek Instruments Inc.), and cell viability was expressed as percentage relative to the respective MeOH control. IC_{50} (or GI_{50}) values were determined by sigmoidal curve fitting.

For cytotoxicity testing of fractions derived from extract purification, cells were seeded at a higher density (1.2×10^4 cells per well) and treated with the samples dissolved in MeOH at concentrations that were adjusted according to the initially detected potency of the parent sample. MTT was added already after 2-3 d and plates were processed as described above. Toxicity was expressed relative to the respective MeOH control, which was set to 0% toxicity.

2.2.5 GIEMSA STAINING

CHO-K1 cells from actively growing cultures were harvested and seeded at 2×10^4 cells per well of 96-well imaging plates in 100 μ l complete medium and directly treated with extract fractions. Following 48 h treatment, cells were gently washed with PBS, then with PBS/MeOH (1:1.5), and finally incubated for 10 min at room temperature with 200 μ l MeOH per well. For staining, MeOH was removed and replaced by 50 μ l Giemsa staining solution. After 2 min incubation at room temperature excess dye was washed off with tap water. Images were acquired in 200-fold magnification in the transmitted channel (BD Pathway 855).

2.2.6 CLONOGENIC SURVIVAL

*L3.6pl cells at 70% confluence were treated for 4 h with compounds at the assigned concentrations. After the treatment, the cells were trypsinized and 10^4 cells/well were seeded in a 6-well plate. The freshly seeded cells were allowed to grow for 6 d, followed by crystal violet staining (0.5% crystal violet, 20% MeOH, 80% H₂O) for 10 min at room temperature. After washing with tap water, cells were dried and pictures of the wells were taken. Crystal violet was redissolved with sodium citrate solution (50 mM sodium citrate, 50% EtOH, 50% H₂O) to measure the absorption at 550 nm in a SpectraFluor PlusTM (Tecan, Männedorf, Austria). For statistical analysis, the percentage of viable cells of the untreated control was set to 100%.

2.2.7 APOPTOSIS MEASUREMENT

*Apoptotic cell death was measured as described by Nicoletti *et al.*^[215]. Briefly, L3.6pl cells were treated for 48 h with compounds in various concentrations as assigned. To assess caspase-independent apoptosis induction, 10 μ M Q-VD-Oph (R&D Systems Inc.) was added 2 h prior to compound addition. After treatment, cells were permeabilized with a Triton-containing buffer and stained o/n with 50 μ g/ml propidium iodide (PI) at 4°C. The cells were analyzed by flow cytometry and cells with hypoploid DNA (sub-G₁ peaks) were considered as dead and quantified relative to the whole cell population.

2.2.8 CELL CYCLE STUDIES

Cells from actively growing cultures were harvested and seeded in 6-well plates in 5 ml of complete medium and, after an o/n equilibration, were treated with the compounds dissolved in MeOH at the appropriate concentrations and for the indicated time periods. Approximately

10^6 cells were harvested by centrifugation, washed twice with PBS (phosphate-buffered saline, pH 7.4) and fixed in cold (-20°C) 80% MeOH. After an o/n fixation at -20°C , the cells were washed with PBS and further permeabilized with 0.1% saponin in PBS. For DNA labeling, the cells were resuspended in staining solution containing 20 $\mu\text{g}/\text{ml}$ propidium iodide (PI) and 100 $\mu\text{g}/\text{ml}$ ribonuclease A (RNase A) in PBS. The cells were stained for 30 min at 37°C and analyzed on a GUAVA EasyCyte Plus flow cytometer. In total, 10^4 events, excluding cell debris, were measured, and the data were processed using FlowJo v7.6.5 software (Tree Star Inc.). For cell cycle analysis and quantification of G_1 , S, and G_2/M cell populations, the Dean-Jett-Fox algorithm was used.

2.2.9 IMMUNOBLOTTING

*L3.6pl cells were treated with compounds for the indicated time points and proteins were prepared from total cell lysates. Proteins were separated by SDS-PAGE^[216] and transferred to nitrocellulose membranes via tank blotting. Nitrocellulose membranes were incubated with antibodies raised against Bcl-2 (Calbiochem), PARP (Calbiochem) or actin (Millipore). To detect the protein levels, the ECLTM detection system (Amersham Pharmacia Biotech, Little Chalfont, UK) or the Odyssey Infrared Imaging system version 2.1 (LI-COR Biosciences, Lincoln, NE, USA) was used.

2.2.10 IMMUNOFLUORESCENCE

Human U-2 OS osteosarcoma cells were seeded at 5×10^3 cells per well in 96-well imaging plates (BD Falcon). After an o/n equilibration, the cells were treated with extracts, fractions, or compounds at the appropriate concentrations and treatment periods indicated for each experiment. The cells were fixed with cold (-20°C) acetone/MeOH (1:1) for 10 min. After washing with PBS, the cells were permeabilized with 0.01% Triton-X 100 in PBS. The following primary antibodies were used: α -tubulin mAb (Sigma), β -actin mAb (Millipore), and anti-phospho-Histone H2A.X mAb (Millipore). For labeling, cells were incubated with primary antibody for 45 min at 37°C , followed by incubation with the secondary antibody (Alexa Fluor[®] 488 goat anti-mouse or anti-rabbit, and Alexa Fluor[®] 555 goat anti-rabbit; Molecular Probes) under the same conditions. After washing with PBS, a staining solution was applied for 10 min at room temperature that contained the nuclear stain Hoechst33342 (5 $\mu\text{g}/\text{ml}$) and a whole cell stain (1 $\mu\text{g}/\text{ml}$ HCS CellMaskTM Red or Green). The samples were imaged on an automated microscope (BD Pathway 855) suitable for high-content screening with appropriate filter sets for Alexa 488, TRITC, and Hoechst fluorescence.

2.2.11 ACTIN LABELING (PHALLOIDIN PROBE)

Human U-2 OS osteosarcoma cells were seeded at 5×10^3 cells per well in 96-well imaging plates (BD Falcon). After 2 d equilibration, the cells were treated with compounds at the appropriate concentrations. After 4 h treatment, cells were washed with pre-warmed PBS (37°C) and fixed with cold (-20 °C) acetone/MeOH (1:1) for 10 min at room temperature. After washing with PBS, the cells were permeabilized with 0.01% Triton-X 100 in PBS. Actin microfilaments were then probed by adding 50 µl of an Acti-stain phalloidin working solution (100 nM, diluted with PBS). After 30 min incubation, the cells were washed with PBS and the nuclear stain Hoechst 33342 (5 µg/ml in PBS) was added for 10 min at room temperature. The samples were washed again with PBS and cells were imaged on an automated microscope (BD Pathway 855) with appropriate filter sets for TRITC and Hoechst fluorescence.

2.2.12 TMRM STAINING

U-2 OS cells from actively growing cultures were harvested and seeded at 8×10^3 cells/well in 96-well imaging plates (BD Falcon) and after 1 d, cells reached approximately 60% confluency. Reference compounds dissolved in DMSO (10 mM) were added to the cells to achieve a final concentration of 200 nM. Following 12 h treatment, the cells were washed twice with PBS and 100 µl of a staining solution (50 nM TMRM and 5 µg/ml Hoechst33342 in assay buffer) was added. The cells were stained for 30 min at 37°C and after washing with assay buffer the samples were examined on an automated microscope (BD Pathway 855) in 200-fold magnification with appropriate filter sets for rhodamine and Hoechst.

2.2.13 ACRIDINE ORANGE STAINING

U-2 OS cells from actively growing cultures were harvested and seeded at 5×10^3 cells/well in 96-well imaging plates (BD Falcon; 'culture plate') and after 2 d, cells reached approximately 80% confluency. Extracts and fractions were dissolved in MeOH and a 96-well 'sample plate' (Sarstedt) was prepared by evaporation of appropriate amounts of the samples. Dried extracts and fractions were re-dissolved in 120 µl pre-warmed McCoy's 5A complete medium and the medium of the culture plate was replaced by 100 µl of the sample plate. Following 4 h treatment, the cells were washed with PBS and 75 µl of a staining solution (5 µg/ml AO and 10 µg/ml Hoechst33342 in PBS) was added for 15 min. After staining at 37°C, cells were washed with PBS and imaged on an automated microscope (BD Pathway 855) in 200-fold magnification with appropriate filter sets for green/red fluorescence and Hoechst.

2.2.14 HCS STUDIES

All analyses were performed in AttoVision v1.6.2. The presented values were generated on a single cell basis and averaged over the complete sample (well). For the analysis of microtubules and actin filaments, a dual mask (Cyto-Nuc-Dual) for the cytoplasm and nuclei was used in the HCS CellMaskTM and Hoechst channels, respectively, and the assigned parameters were calculated in either one of these ROIs (regions-of-interest) as indicated. In an unbiased but supervised approach, an experimental test set was generated for both, tubulin- and actin-disrupting effects, and it was found that the standard deviation of fluorescence of either cytoskeletal protein is among the most optimal parameters to describe induced effects. For the DSB analyses, a polygon nuclear mask was used in the Hoechst channel, and γ H2A.X fluorescence was calculated within this ROI. In HCS experiments using either AO or TMRM as a probe, a dual mask (Cyto-Nuc-Ring) was applied. The first segment (nuclei) was generated in the Hoechst channel and as a second segment ('cytoplasm') a ring was generated around the former nuclear segment. Intensity parameters for AO and TMRM were calculated within this ring around nuclei.

2.2.15 DETECTION OF DNA LADDERING

Human HL-60 leukemia cells were seeded at a concentration of 10^5 or 2×10^5 cells/ml in 6-well plates (5 ml per well). After 2 d, compounds dissolved in MeOH were added at the indicated concentrations and cells were treated for either 24 or 48 h. DNA fragments were extracted from apoptotic HL-60 cells in phosphate-citrate buffer (PCB, pH 7.8) as described by Gong *et al.*^[217] Cells were harvested by centrifugation (1,200 rpm, 4°C, 10 min; Eppendorf 5180R), the cell pellet was resuspended in 1 ml cold PBS, and the cell suspension was transferred drop wise into 10 ml 70% EtOH (-20°C). After o/n fixation at -20°C, cells were again harvested (1,200 rpm, 4°C, 10 min; Eppendorf 5180R) and EtOH was removed thoroughly. The extraction was performed by resuspension in 40 μ l PCB buffer (pH 7.8) and 30 min incubation at room temperature. After centrifugation (2,500 rpm, 5 min; Eppendorf 5180R), the supernatant was treated with 3 μ l 0.25% Nonidet NP-40 and 3 μ l of 1 mg/ml RNase A in H₂O_{dd}. Following 30 min incubation at 37°C, 3 μ l of 1 mg/ml proteinase K in H₂O_{dd} was added and samples were further incubated for 30 min at 37°C. The extracted DNA was loaded onto an agarose gel (1.7%) and separated by 4 h of electrophoresis at 4 V/cm using 0.5x TBE buffer. The resulting bands were stained with ethidium bromide and detected under UV light.

2.2.16 TUBULIN ISOLATION

Microtubule proteins were isolated from porcine brain tissue as described previously.^[218] All works were performed at 4°C except for the polymerization phases. Blood vessels and fat rich compartments of brains (approximately 600 g initial weight) were removed and the tissue was homogenized (Blender GT 800) in 900 ml PEM buffer containing 63 µl mercaptoethanol. After centrifugation at 13,000 rpm for 90 min at 4°C (Sorvall GSA) 0.1 mM GTP and 2.5 mM ATP was added to the supernatant. The solution was pre-warmed for 30 min at 37°C and a 10% saccharose solution (37°C) was added as the bottom layer. Following centrifugation at 13,000 rpm for 45 min at 37°C (Sorvall GSA), the resulting pellet was resuspended in 75 ml ice-cooled PEM buffer containing 1 mM GTP and the tubulin pellet was homogenized. For complete depolymerization, the solution was incubated for 30 min on ice and subsequently, debris was removed by centrifugation at 18,000 rpm for 30 min at 4°C (Sorvall SS-34). The supernatant was incubated for 15 min at 37°C and tubulin pellets were collected by centrifugation at 18,000 rpm for 30 min at 37°C (Sorvall SS-34). Purified tubulin (including MAPs) was either stored at -80°C or directly used in turbidimetric assays.

2.2.17 *IN VITRO* TUBULIN POLYMERIZATION STUDIES

Tubulin polymerization was analyzed in a turbidimetric assay.^[219] The samples (200 µl, 10 µM tubulin) in PEM polymerization buffer containing 1 mM GTP were filled into ice-cooled cuvettes. These cuvettes were then placed in a water-jacketed cuvette holder in a diode array photometer (Beckman spectrophotometer DU7500) and rapidly warmed to 37°C. The absorbance at 350 nm in the presence and absence of drugs is proportional to the degree of tubulin polymerization.

2.2.18 TRANSMISSION ELECTRON MICROSCOPY

MAP-enriched tubulin from porcine brain tissue (70% tubulin, 30% microtubule-associated proteins; Cytoskeleton, Inc.) was adjusted to 12 µM tubulin with PEM buffer containing 1 mM GTP and polymerized for 30 min at 37°C in the presence or absence of drugs. *For negative staining, thin carbon support films were prepared by indirect sublimation of carbon on freshly cleaved mica. Samples were then absorbed to the carbon film and negatively stained with 2% (w/v) aqueous uranyl acetate (pH 4.5). After air drying, samples were examined in a Zeiss TEM 910 at an acceleration voltage of 80 kV and at calibrated magnifications using a line grid replica. Images were recorded digitally with a Slow-Scan

CCD-Camera (ProScan, 1024x1024, Scheuring, Germany) with ITEM-Software (Olympus Soft Imaging Solutions, Münster, Germany).

2.2.19 *IN VITRO* ACTIN POLYMERIZATION STUDIES

Fluorescence-based actin polymerization assays were performed using pyrene muscle actin (Cytoskeleton, Inc.) according to the supplier's protocol with minor modifications. Test compounds were dissolved in non-polymerizing buffer (5 mM Tris-HCl pH 8.0, 0.2 mM CaCl₂, 0.2 mM ATP, 1 mM DTT) and mixed with pyrene actin diluted in the same buffer to give a final concentration of 20 μM chondramide and 5 μM actin. Samples were prepared in black, low-volume 384-well plates (Corning, NBSTM surface). The fluorescence at 405 nm (excitation at 360 nm) was scanned every 30 s for 85 min at 37°C on a microplate reader (Spectramax M5[°], Molecular Devices). Experiments were performed in duplicates and the average relative fluorescence of polymerizing pyrene actin is given. Slopes were calculated in the linear range of kinetic measurements.

2.2.20 CULTIVATION OF *CHONDRAMYCES SP.* SBCM007

*Strain SBCm007 was cultivated in VY/2 Media (5 g/L Baker's Yeast, 1 g/L CaCl₂). A fed-batch cultivation was carried out in a 13 L bioreactor (filled with 8 L VY/2 and inoculated with 500 ml shake flask culture. For maintenance of pH a 0.2 M KOH and a 0.1 M H₂SO₄ solution was used. The feed solution consisted of 100 g/L Baker's Yeast and 1 g/L CaCl₂. After depletion of the batch media 200 ml of a XAD/water solution was added and a constant feeding rate of about 0.15 ml/min was adjusted. To replace chlorine by bromine the CaCl₂ was substituted by the same amount of KBr.

2.2.21 EXTRACT PREPARATION AND PRE-FRACTIONATION

*For crude extract preparations cells and XAD were extracted separately with MeOH. For activity testing a pre-fractionation with silica gel 60 (Merck KGaA Darmstadt, Germany) was applied. The column was filled with a hexane/silica gel slurry loaded with methanolic raw extract on kieselguhr and subsequently eluted with 2 column volumes hexane, CHCl₃ and then stepwise increasing (10%) CHCl₃/MeOH fractions up to 100% MeOH. For purification of compounds a pre-fractionation with Sephadex LH-20 (Amersham Biosciences Uppsala, Sweden) was carried out with a column volume of 500 ml. Approximately 200 mg methanolic crude extract were loaded and subsequently eluted with MeOH; fractions of 8 ml were collected and used for semi-preparative HPLC purification.

2.2.22 SEMI-PREPARATIVE HPLC

*Measurements were conducted on a Dionex HPLC system (Famos autosampler, P680 pump, TCC100 thermostat, and PDA100 detector), equipped with a Phenomenex Luna C18, 250x4.6 mm, 5 μ m dp column. Separation was achieved by variable linear gradients using (A) H₂O and (B) ACN at a flow rate of 2.5 ml/min and 25°C. The gradient started at 5-60 % B with a 0.5 min hold and increased to 100% B in a variable time frame. UV data was acquired at 220 and 280 nm. The sample was injected by μ l-pick-up technology with a H₂O/ACN (50:50 v/v) mixture as supporting solvent. A maximum of 75 μ l sample was injected before manual fraction collection.

RESULTS

3.1 BIOLOGICAL CHARACTERIZATION OF PRETUBULYSINS

Pretubulyisin and its derivatives were synthesized and provided by the group of Prof. Kazmaier (Institute for Organic Chemistry, Saarland University).

3.1.1 DETERMINATION OF GI₅₀ VALUES

Initially, the biological activity of pretubulyisin and its direct precursor molecules from total synthesis were compared to the natural parent compounds tubulyisins A and D. The growth inhibitory potential was assessed in tetrazolium salt-based assays (MTT) after 5 d treatment of cells with the compounds in serial dilution (Figure 3-1 and Table 3-1a).

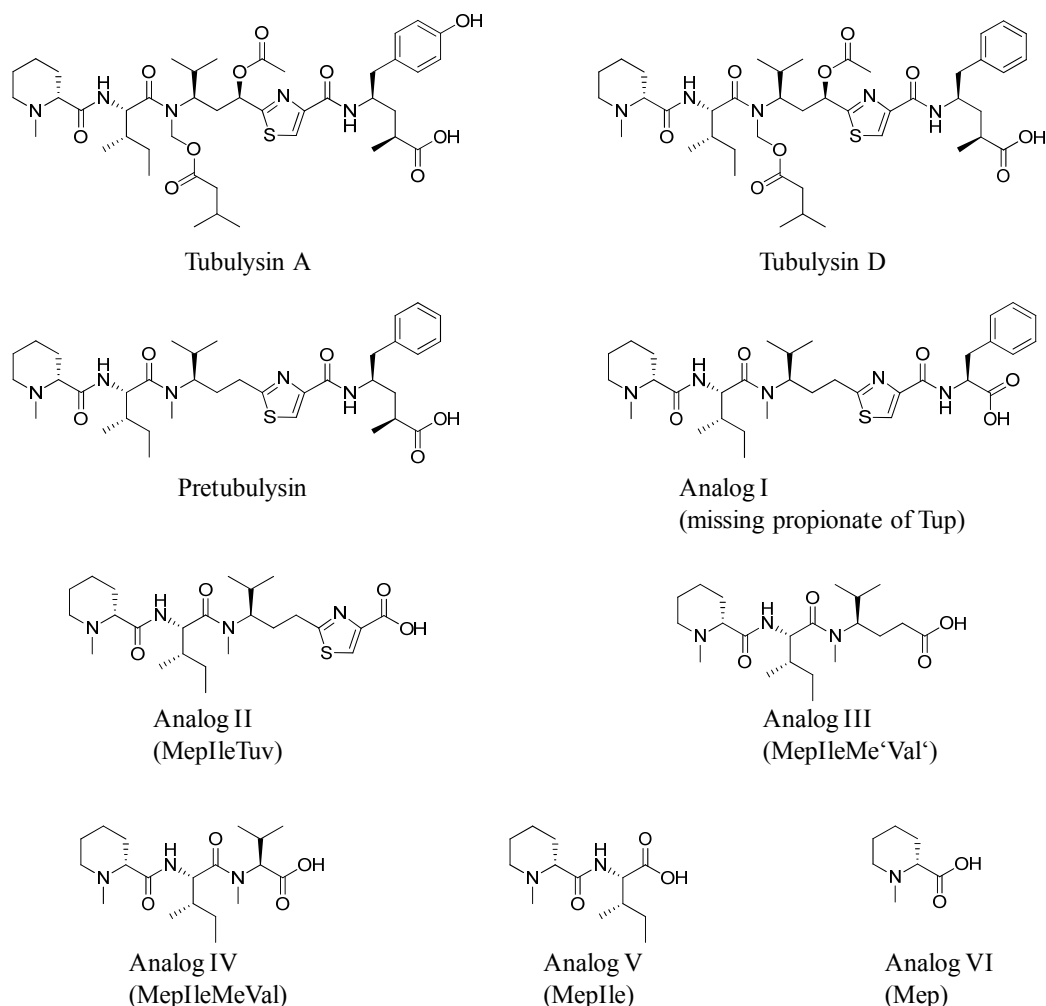


Figure 3-1: Chemical structures of tubulyisins A and D, pretubulyisin, and precursors.

The amino acid composition of shorter pretubulyisin precursors (analog I-VI) is given in brackets.

Table 3-1a: GI₅₀ values of natural tubulysins, synthetic pretubulysin, and its precursors.

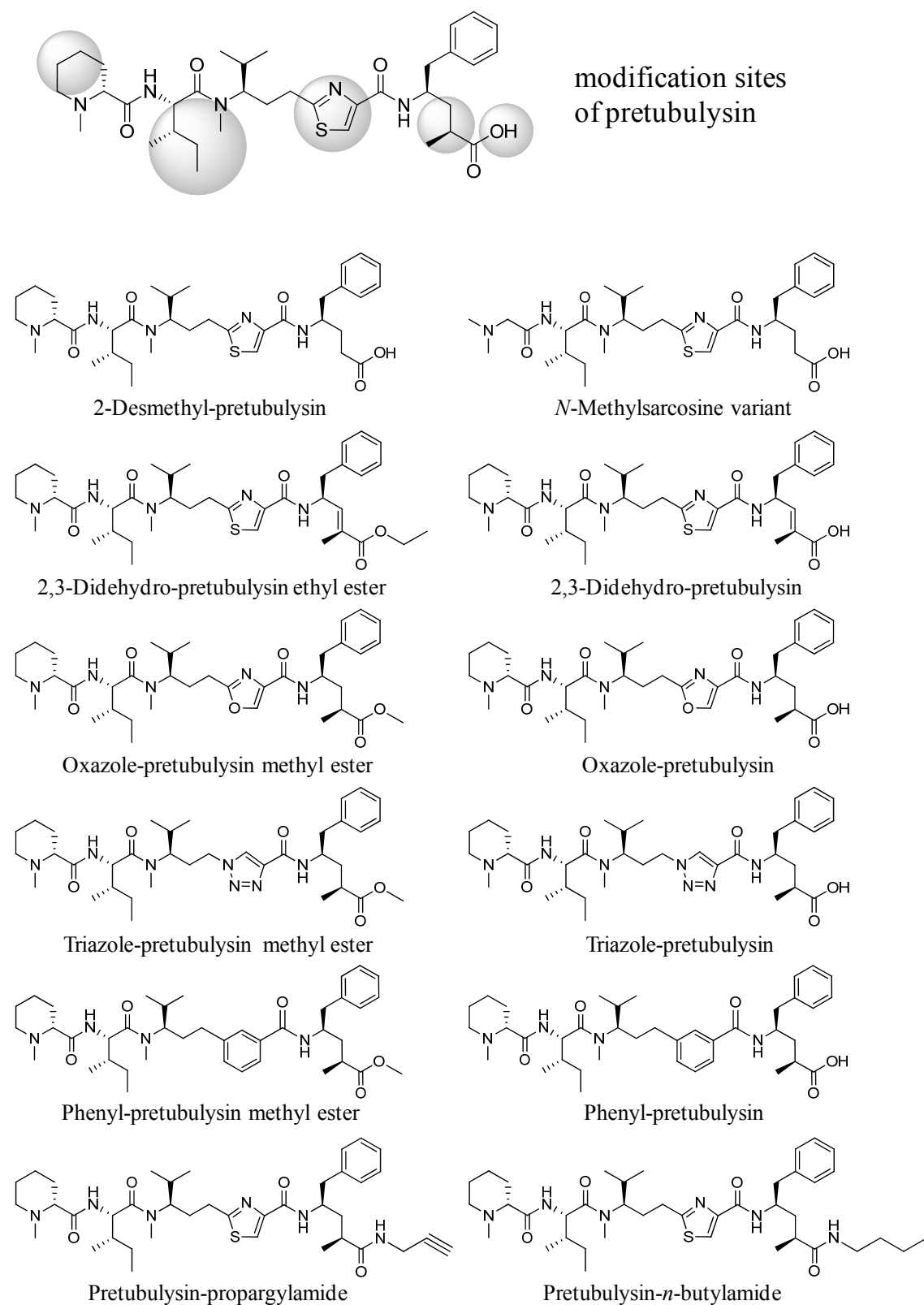
Compound ^[a]	GI ₅₀ value ^[b] [nM]
Tubulysin A	0.23
Tubulysin D	0.02
Pretubulysin	5.81
Analog I	9600
Analog II	14200
Analog III	6500
Analog IV	> 25000
Analog V	> 25000
Analog VI	> 25000

Table 3-1b: GI₅₀ values of natural tubulysins, synthetic pretubulysin, and pretubulysin derivatives.

Compound ^[a]	GI ₅₀ value ^[c] [nM]
Tubulysin A	0.23
Tubulysin D	0.04
Pretubulysin	0.84
2-Desmethyl-pretubulylsin	4.93
<i>N</i> -Methylsarcosine variant	4700
2,3-Didehydro-pretubulysin ethyl ester	487
2,3-Didehydro-pretubulysin	240
Oxazole-pretubulysin methyl ester	10.03
Oxazole-pretubulysin	1.55
Triazole-pretubulysin methyl ester	>1500
Triazole-pretubulysin	644
Phenyl-pretubulysin methyl ester	420
Phenyl-pretubulysin	119
Pretubulysin- <i>n</i> -butylamide	40.48
Pretubulysin-propargylamide	87.78
Methylproline variant	164
Pipecolic acid variant	1073
'Tuv' Variant I	1.48
'Tuv' Variant II	0.86
'Ile' Variant I	46.16
'Ile' Variant II	5.06
'Ile' Variant III	121
'Ile' Variant IV	>5000

[a] For chemical structures see Figure 3-1 and 3-2. [b]/[c] Compounds were tested in serial dilution for 5 d on ^[b]L-929 cells (mouse subcutaneous connective tissue) or ^[c]human U-2 OS cells (osteosarcoma). Viability was assessed in an MTT assay. GI₅₀ values were determined by sigmoidal curve fitting and calculated as the average of two independent measurements.

Other structural modifications of the pretubulysin core structure are displayed in Figure 3-2 and corresponding GI₅₀ values are given in Table 3-1b.



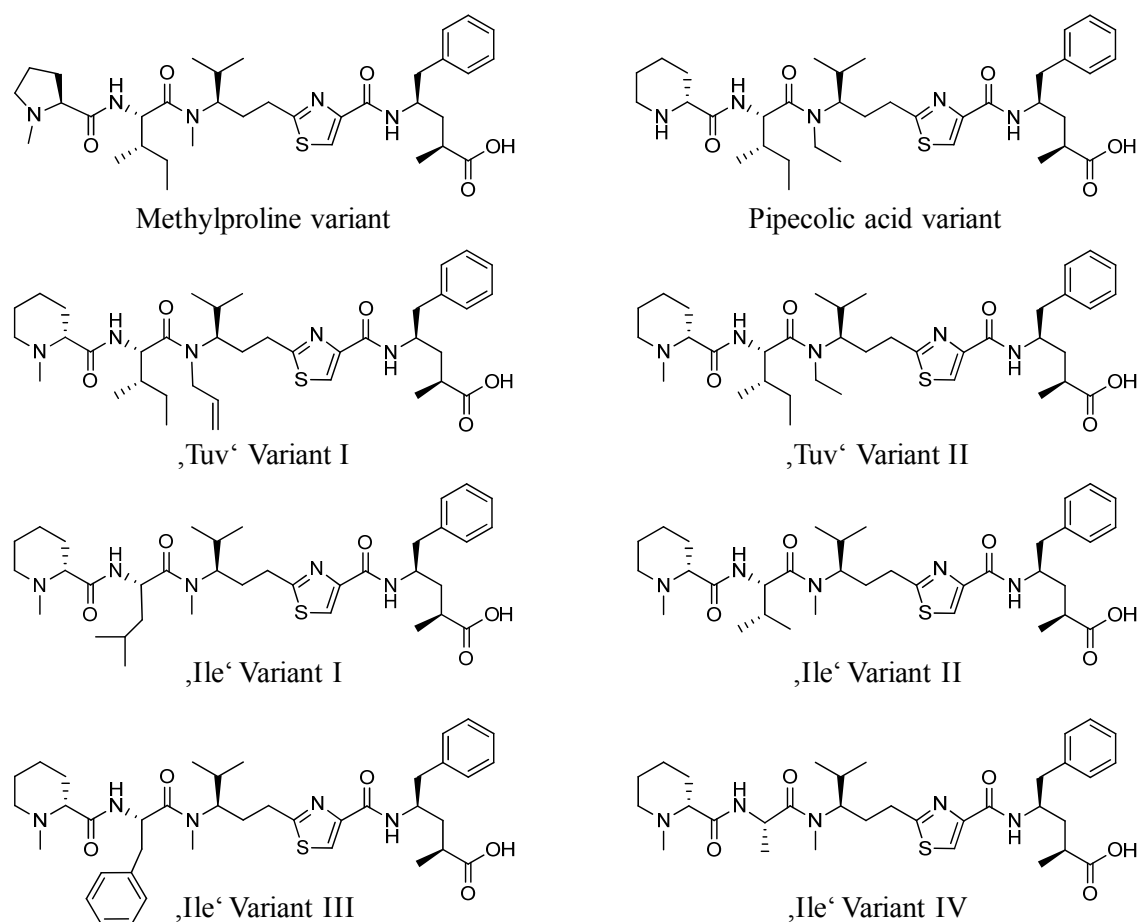


Figure 3-2: Chemical structures of pretubulysin derivatives.

Chemical variations of the pretubulysin core structure (highlighted in grey) were realized at *N*-terminal Mep, *C*-terminal Tup, the thiazole heterocycle of Tuv, and additionally, alkylation patterns of Ile and Tuv were varied.

GI₅₀ values for tubulysins A and D are in accordance with previous reports, and were determined to be in a mid picomolar to low nanomolar range.^[192] The activity of pretubulysin was comparable to that of the parent compounds tubulysins A and D (low nanomolar range). However, with shorter chain analogs bioactivity was nearly abolished, and for single MepIleMeVal, MepIle, and Mep building blocks (Analog IV-VI in Figure 3-1) GI₅₀ values were not determinable in the assay's concentration range. Interestingly, analog III, that lacks already the thiazole ring of Tuv, still shows a reasonable growth inhibitory activity (GI₅₀ of 6.5 μM), which is even higher than determined for the MepIleTuv building block (analog II; GI₅₀ of 14.2 μM).

The 2-desmethyl derivative was approximately by factor 6 less potent than pretubulysin, and the 2,3-didehydro variants, either as free carboxylic acid or ethyl ester, by factor 600 and 300,

respectively. When the *C*-terminal carboxylic acid group was replaced by an *n*-butylamide or propargylamide functional group, GI_{50} values were in the mid nanomolar range and hence, by factor 50 and 100, respectively, higher than the value for pretubulysin itself. However, variations of the *N*-terminal Mep are much less tolerated. By replacing *N*-Mep with methylproline, pipercolic acid (in variant where *N*-methyl in Tuv is replaced by an *N*-ethyl group), or methylsarcosine potency decreased approximately by factor 200, 1300 and 5600, respectively, compared to pretubulysin.

In general, potency of derivatives, where the thiazole heterocycle was substituted by either a phenyl or triazole group, was strongly diminished resulting in GI_{50} values in the high nanomolar range, and the same compounds as methyl esters were at least by factor 3 less active than the free acid analogs. Solely oxazole derivatives exhibited GI_{50} values in the low nanomolar range; 1.55 nM for the free acid and 10.03 nM for the respective methyl ester.

Different alkylation patterns at the *N*-terminus of Tuv ('Tuv' variants) do not seem to have a major impact on the bioactivity of pretubulysin, whereas in 'Ile' variants replacement of the *sec*-butyl group in L-Ile by a methyl group ($GI_{50} > 5 \mu\text{M}$) or a bulky phenyl group ('Ile' variant III; $GI_{50} = 121 \text{ nM}$) leads to significantly reduced potency. Substitution of the *sec*-butyl functional group by *iso*-butyl ($GI_{50} = 46.2 \text{ nM}$) or *iso*-propyl ($GI_{50} = 5.1 \text{ nM}$) was less relevant with regards to bioactivity. Nevertheless, potency compared to pretubulysin was reduced by factor 50 and 6, respectively.

The parent compounds tubulysins A and D, pretubulysin, and some selected pretubulysin derivatives were tested in a larger panel of various cancer and non-cancerous cell lines (Table 3-2). No certain specificity towards type of tissue or organism was observed, although fast-dividing human leukemia cell lines appear to be more sensitive towards tubulysin and pretubulysin treatment. On average, pretubulysin is by factor 10 and 100 less potent than tubulysins A and D, respectively, and exhibits throughout the panel GI_{50} values in the low nanomolar range. Furthermore, pretubulysin is active on an MDR cancer cell line (KB-V.1; $GI_{50} = 40.8 \text{ nM}$). The same is true for oxazole-pretubulysin ($GI_{50} = 52.1 \text{ nM}$), which in general, exhibits a ca. 3-fold reduced potency compared to pretubulysin. With the 2-desmethyl derivative potency is further reduced approximately by factor 10. 'Tuv' variants and 'Ile' variant II, however, are comparable active to pretubulysin itself, with 2- to 3-fold increased average activity for 'Tuv' variants and 2-fold decreased activity for the 'Ile' variant II. As mentioned earlier, the pretubulysin analog III (MepIleMe'Val') lacking the thiazole ring of Tuv, still has a reasonable activity on the three tested cell lines with GI_{50} values of around 8 μM .

Table 3-2: GI₅₀ values of selected derivatives^[c] on several cell lines.

Cell line ^[a]	GI ₅₀ values ^[b] [nM]								
	Tub. A	Tub. D	Pretub.	Desm.-pretub.	Analog III	Oxaz.-pretub.	'Tuv' Var. I	'Tuv' Var. II	'Ile' Var. II
A431	0.12	0.014	1.85	0.52	n.d.	n.d.	n.d.	n.d.	n.d.
A549	0.11	0.007	6.49	47.57	n.d.	18.11	n.d.	n.d.	n.d.
CHO-K1	1.13	0.11	n.d.	n.d.	5030	n.d.	n.d.	n.d.	n.d.
COS-7	0.095	0.041	1.69	14.68	n.d.	30.80	n.d.	n.d.	n.d.
HCT-116	0.32	0.036	2.27	n.d.	n.d.	n.d.	0.55	0.21	2.62
HEK293T	0.059	0.012	0.34	2.56	n.d.	0.67	n.d.	n.d.	n.d.
HepG2	0.14	0.008	0.96	13.34	2400	2.55	n.d.	n.d.	n.d.
HL-60	0.012	0.007	0.045	0.60	1250	0.049	n.d.	n.d.	n.d.
K562	0.47	0.027	0.52	3.81	n.d.	0.37	n.d.	n.d.	n.d.
KB-3.1	0.19	0.022	3.46	40.10	n.d.	5.37	n.d.	n.d.	n.d.
KB-V.1	n.d.	n.d.	40.83	n.d.	n.d.	52.06	n.d.	n.d.	n.d.
L-929	0.23	0.020	5.81	61.01	6500	11.17	n.d.	n.d.	n.d.
NIH/3T3	n.d.	n.d.	11.78	n.d.	n.d.	11.33	n.d.	n.d.	n.d.
SH-SY5Y	0.25	0.013	0.91	4.42	n.d.	n.d.	n.d.	n.d.	n.d.
SW480	0.024	0.005	0.31	4.82	n.d.	1.50	n.d.	n.d.	n.d.
U-2 OS	0.23	0.041	0.84	4.93	12600	1.55	1.48	0.86	5.06
U937	0.004	0.001	0.12	0.63	n.d.	0.52	n.d.	n.d.	n.d.

[a] Compounds were tested in serial dilution for 5 d on various cancer and non-cancerous cell lines. A431: human epithelial carcinoma; A549: human lung carcinoma; CHO-K1: Chinese hamster ovary; COS-7: African green monkey kidney; HCT-116: human colon carcinoma; HEK293T: human kidney; HepG2: human hepatocellular carcinoma; HL-60: human acute promyelocytic leukemia; K562: human chronic myelogenous leukemia; KB-3.1: human cervical carcinoma; KB-V.1: KB-3.1 derivative (MDR); L-929: mouse subcutaneous connective tissue; NIH/3T3: mouse embryonic fibroblasts; SH-SY5Y: human neuroblastoma; SW480: human colon adenocarcinoma; U-2 OS: human osteosarcoma; U937: human histiocytic lymphoma. [b] Viability was assessed in an MTT assay and GI₅₀ values were determined by sigmoidal curve fitting and calculated as the average of two independent measurements; n.d.: not determined. [c] For chemical structures see Figure 3-1 and 3-2. Tub.: Tubulysin; Pretub.: Pretubulysin; Desm.: 2-Desmethyl; Oxaz.: Oxazole; Var.: Variant.

3.1.2 LONG-TERM SURVIVAL OF CANCER CELLS

The following experiment was done by our collaboration partner at LMU Munich (Prof. Vollmar; Pharmaceutical Biology). Highly metastatic human L3.6pl pancreatic cancer cells were pre-treated with either tubulysin A or pretubulysin at different concentrations for 4 h. Cells were washed, detached, seeded, and further incubated for 6 d. The relative number of colonies formed by the cells was assessed by crystal violet staining and expressed as percentage clonogenic survival relative to the control, which was set to 100% (Figure 3-3).

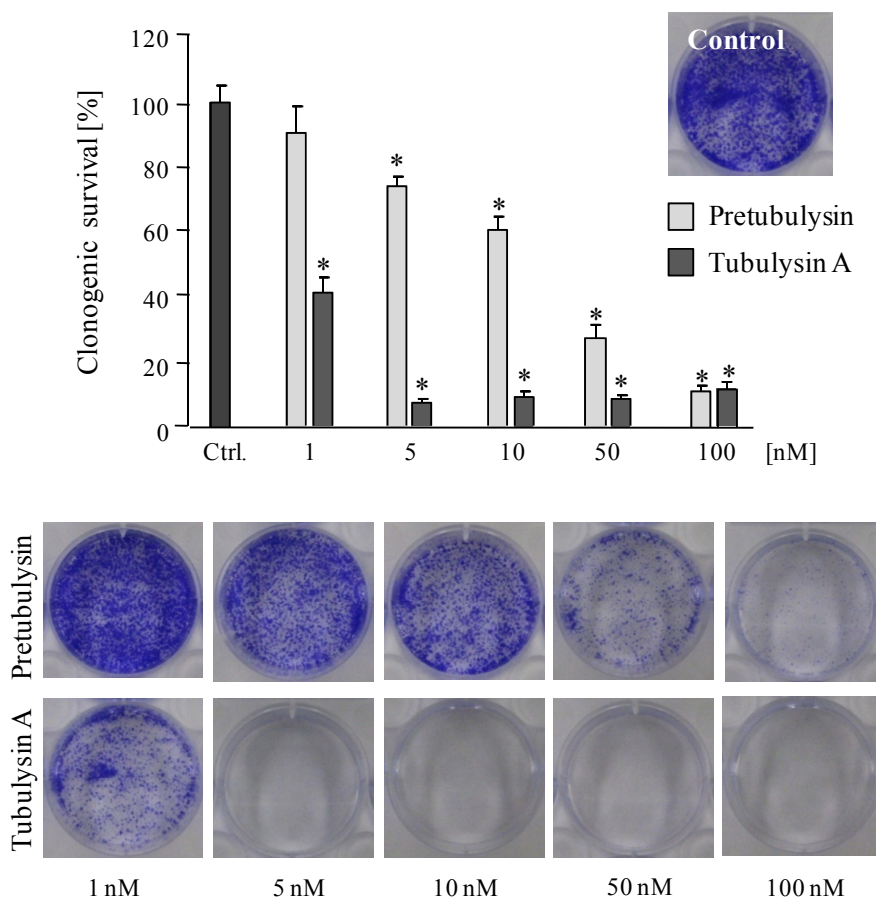


Figure 3-3: Inhibition of clonogenic survival by tubulysin A and pretubulysin.

L3.6pl cells were stimulated for 4 h and then seeded at low confluence. After 6 d, cells were stained with crystal violet, and absorbance was measured at 550 nm ($n = 3$; $*p \leq 0.05$ Anova/Dunnett).

Over the 6 d treatment period, both compounds inhibited the clonogenic survival of L3.6pl cells. Tubulysin A reduced the relative number of colonies to approximately 40% at a concentration of 1 nM and at higher concentrations the number was further reduced to ca. 10%. However, higher concentrations of pretubulysin were needed to observe this effect to the same extent. Pre-treatment with 50 nM pretubulysin reduced the number of L3.6pl colonies to approximately 30%.

3.1.3 TRIAZOLE-PRETUBULYSIN TOOL COMPOUND

In the course of chemical syntheses, a triazole-pretubulysin derivative was prepared that lacks the Tup moiety. Instead, coumarin 460 (or coumarin 1, coumarin 47) is coupled via an alkyl linker directly to the triazole heterocycle (Figure 3-4).

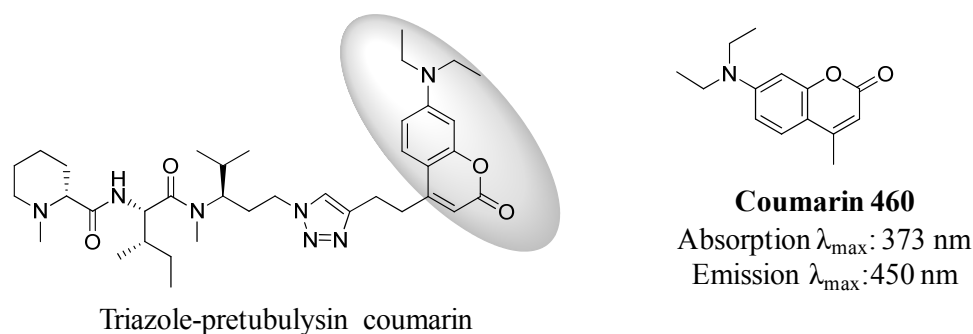


Figure 3-4: Chemical structure of the triazole-pretubulysin tool compound.

A triazole-pretubulysin derivative was prepared that bears a coumarin 460 functional group. Given absorption and emission maxima refer to ethanolic solution. The fluorescent probe was used in live cell studies.

Prior to the use in live cell imaging studies, GI_{50} values of triazole-pretubulysin coumarin were determined in an MTT assay. Human HCT-116 colon carcinoma and human U-2 OS osteosarcoma cells were treated with the compound in serial dilution for 5 d resulting in GI_{50} values of 0.45 μM and 0.53 μM , respectively. Although these values are by three orders of magnitude higher than those determined for pretubulysin, activity is still good enough so that the tool compound could be applied in live cell studies. Since tubulysins target microtubules and lead to their depolymerization, the biological functionality of the fluorescent probe was first tested in immunofluorescence (IF) experiments (Figure 3-5).



Figure 3-5: Microtubule depolymerization in U-2 OS cells by triazole-pretubulysin coumarin.

Human U-2 OS osteosarcoma cells were either left untreated (left image) or treated for 48 h with 10 $\mu\text{g/ml}$ of the tool compound (right image). Microtubules are displayed in green (IF on α -tubulin) and Hoechst-stained nuclei in blue.

Triazole-pretubulysin coumarin clearly leads to the fragmentation of nuclei, enlargement of cells, and the depolymerization of microtubules and hence, was expected to be a valuable tool in live cell imaging studies on microtubule dynamics.

Ptk-2 potoroo kidney cells were plated in 96-well imaging plates and grown until 80% confluence. The cells were loaded with 1 $\mu\text{g/ml}$ triazole-pretubulysin coumarin and directly imaged on an automated microscope in the Hoechst channel for 12 h every 30 min. Cellular uptake of the probe was seen as early as 30 min after treatment. Since only a small portion of the tool compound accumulated in cells by that time, residual compound in the culture medium led to strong background fluorescence. After 1 h, small vesicles became visible, that were present in all cells and after prolonged incubation (images are shown after 6 h, 9 h, and 12 h) these vesicles were more pronounced and somewhat accumulated mainly around the nuclei. After 12 h, the time-lapse experiment was stopped and cells were fixed and permeabilized. By probing α -tubulin in IF experiments it was observed that Ptk-2 cells were strongly affected by the treatment with triazole-pretubulysin coumarin. Compared to control cells microtubules were not yet completely depolymerized, but an enlargement of cell bodies and a higher density of microtubules around the nuclear periphery was seen, both effects being typically observed prior to complete microtubule depolymerization (Figure 3-6).

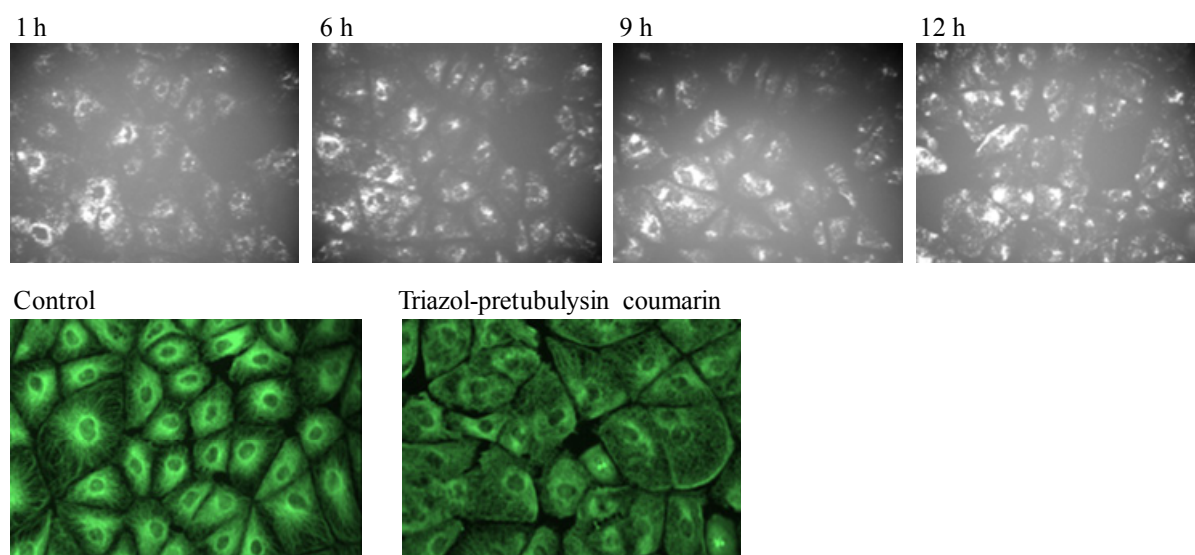


Figure 3-6: Live cell imaging study in Ptk-2 cells with triazole-pretubulysin coumarin.

80% confluent Ptk-2 potoroo kidney cells were loaded with 1 $\mu\text{g/ml}$ of the tool compound and imaged over a 12 h treatment period in Hoechst channel (upper panel). After 12 h, the cells were fixed. Images of the lower panel show IF images of microtubules either of the untreated control or triazole-pretubulysin coumarin treated Ptk-2 cells.

Interestingly, a microtubular localization of triazole-pretubulysin coumarin was not observed at any time point. Among cellular compartments, vesicles observed upon tool compound treatment most resembled lysosomes. Thus, Ptk-2 cells were treated for 12 h with the probe,

washed, and counterstained with acridine orange (AO). The dye specifically accumulates in acidic compartments (mainly lysosomes) and consequently exhibits a strong red fluorescence. An overlay of coumarin and AO fluorescence images confirmed a co-localization of the tool compound and lysosomes of Ptk-2 cells (Figure 3-7).

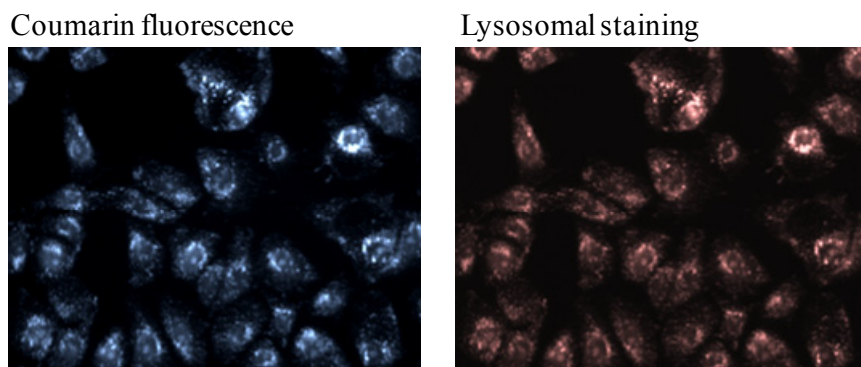


Figure 3-7: Localization of triazole-pretubulysin coumarin in lysosomes.

Ptk-2 cells were incubated with 1 $\mu\text{g/ml}$ tool compound for 12 h. Lysosomes were stained with acridine orange and images were recorded in the Hoechst and red fluorescence channel. Displayed are identical image sections of a sample dual-stained with the tool compound (left) and acridine orange (right).

3.1.4 MITOTIC ARREST

As for other tubulin-targeting drugs, antimitotic tubulysins induce a G_2/M cell cycle arrest. In an initial experiment with mouse L-929 subcutaneous connective tissue cells, pretubulysin and tubulysin A were tested (Figure 3-8). The cells were treated at approximately 60% confluency with the compounds at concentrations near their respective GI_{90} values and further incubated for 24 h. Cells were collected by centrifugation, fixed and permeabilized, and DNA was labeled with propidium iodide (PI) as described in the Methods section. The DNA content was determined by flow cytometric measurements (FCM) on a Guava EasyCyte Plus system. Data was processed in FlowJo v7.6.5 software and cell cycle histograms were analyzed according to Dean-Jett-Fox algorithm (Table 3-3).

As expected, both compounds are able to halt cells in the G_2/M phase already after 24 h treatment. Similarly to results from growth inhibition experiments (GI_{50} value determination), pretubulysin is ca. 10-fold less potent than the reference compound tubulysin A. Approximately 26% of control cells are in G_2/M and 40% in G_1 phase of the cell cycle. Upon treatment with tubulysin A the G_2/M population steadily increases with higher concentrations and at finally 12 nM tubulysin A 45% of cells accumulate in G_2/M , whereas the G_1 population decreases to ca. 27%. For a similar effect (31% in G_1 and 47% in G_2/M) L-929 cells were

treated with pretubulysin at a final concentration of 150 nM. However, a less pronounced antimitotic effect (29% in G₂/M) could already be observed at a concentration of 30 nM.

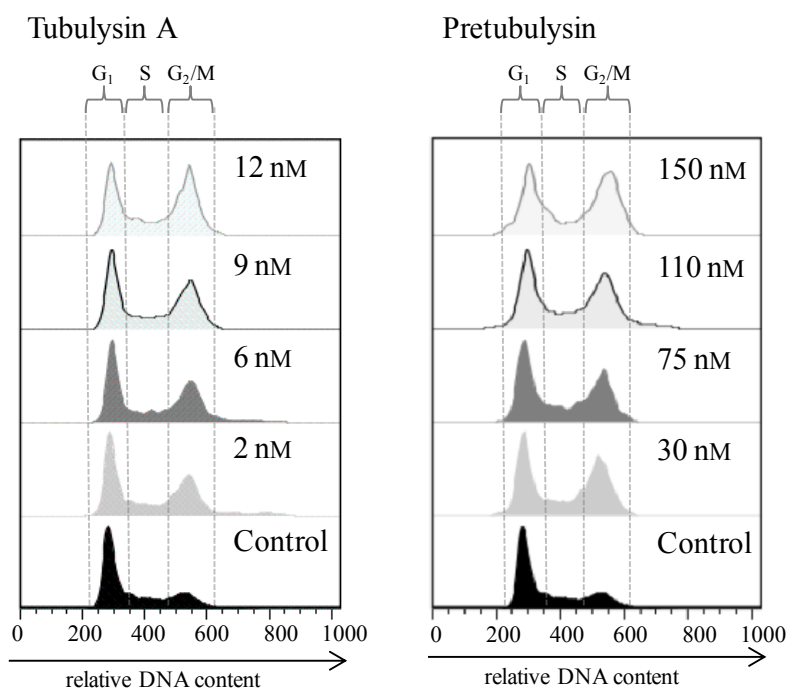


Figure 3-8: G₂/M cell cycle arrest in L-929 cells treated with tubulysin A or pretubulysin.

L-929 cells were either left untreated (control) or treated for 24 h with tubulysin A and pretubulysin at the assigned concentrations. Cells were analyzed after PI staining by FCM. Histograms of gated populations (excluding debris) were obtained by Dean-Jett-Fox algorithm in FlowJo v7.6.5 software.

Table 3-3: Calculated percentage of L-929 cells in G₁, S, and G₂/M phase of the cell cycle.^[a]

% Cells	Control	Tubulysin A ^[b]				Pretubulysin ^[b]			
	-	2 nM	6 nM	9 nM	12 nM	30 nM	75 nM	110 nM	150 nM
G ₁	40.5	39.1	32.8	35.2	26.7	41.2	38.1	32.2	30.7
S	31.2	20.2	22.9	20.8	27.1	21.7	25.2	25.1	21.0
G ₂ /M	26.3	39.5	39.8	43.2	45.4	29.4	30.6	36.9	46.6

[a] Corresponding histograms are displayed in Figure 3-8. Percentages were calculated in FlowJo v7.6.5 software. [b] L-929 cells were treated for 24 h with compounds at the assigned assay concentrations.

Growth inhibition experiments revealed that some shorter chain pretubulysin analogs exhibit GI₅₀ values in the low to mid micromolar range (analog I-III in Figure 3-1). The MepIleMe'Val' analog (III), although lacking the thiazole heterocycle, still shows a significant effect on several cell lines, with human HL-60 acute promyelocytic leukemia cells being the most sensitive (GI₅₀ = 1.25 μM) towards pretubulysin analog III treatment. The

potency of analog III was even higher than that of the MepIleTuv analog (II). However, it was not clear whether the effect is cytostatic (antimitotic) or rather due to unspecific cytotoxicity. For this reason, HL-60 cells were treated with analog III at its approximate GI_{90} concentration (10 μ M) for 48 h and cell cycle histograms were determined (Figure 3-9).

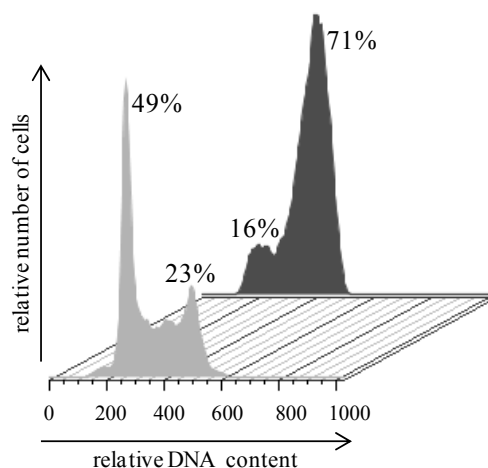


Figure 3-9: G₂/M cell cycle arrest in HL-60 cells treated with pretubulysin analog III.

Cell cycle histograms of control cells (light grey) and HL-60 cells treated for 48 h with 10 μ M pretubulysin analog III (dark grey) as determined by PI staining and FCM. Percentages of cells in G₁ and G₂/M phase of the cell cycle are given and were determined by Dean-Jett-Fox algorithm in FlowJo v7.6.5 software.

In control HL-60 cells, approximately 50% of cells were in G₁ and 23% in G₂/M phase. Following treatment with the small precursor molecule led to a significant increase of cells in G₂/M phase (70%) and in parallel, to a decrease of the G₁ population (23%). These results suggest that also the MepIleMe'Val' analog is able to destabilize microtubules and in turn, leads to an antimitotic (G₂/M cell cycle arrest) effect.

The effects of tubulysin A, pretubulysin, and pretubulysin analog III were also directly compared in cell cycle studies. Human HepG2 hepatocellular carcinoma cells were treated with the compounds for 24 h (Figure 3-10 and Table 3-4).

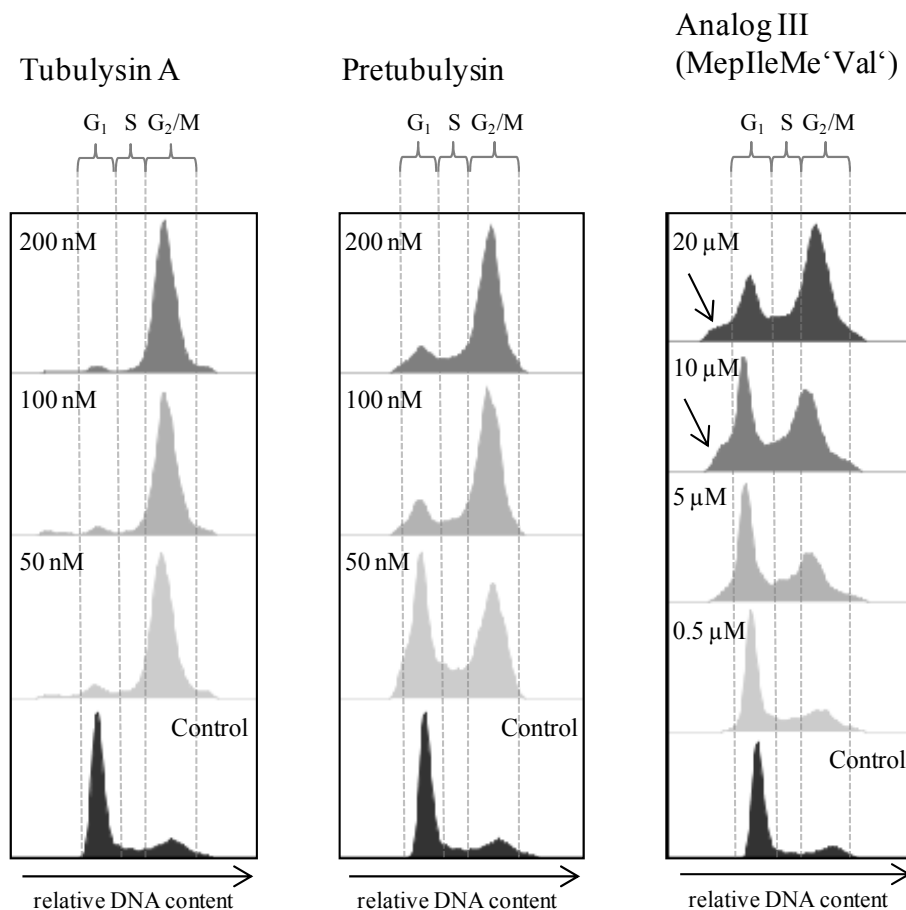


Figure 3-10: G₂/M cell cycle arrest in HepG2 cells treated with tubulysin A, pretubulysin, or pretubulysin analog III.

HepG2 cells were treated for 24 h with compounds at varying concentrations as indicated. Cells were analyzed after PI staining in FCM and histograms of gated populations (excluding debris) were prepared in FlowJo v7.6.5 using Dean-Jett-Fox algorithm. Arrows in cell cycle histograms of analog III-treated cells indicate sub-G₁ populations.

All three compounds are able to halt HepG2 cells in the G₂/M phase after 24 h of treatment. Similar to the results from the initial growth inhibition experiments with HepG2 cells, the antimitotic activity of pretubulysin is comparable to that of the reference compound tubulysin A (GI₅₀ = 0.14 nM and 0.96 nM for tubulysin A and pretubulysin, respectively). The results are also in accordance with data generated from L-929 cells (Figure 3-8).

Table 3-4: Calculated percentage of HepG2 cells in G₁, S, and G₂/M phase of the cell cycle.^[a]

% Cells	Ctrl.	Tubulysin A ^[b]			Pretubulysin ^[b]			Analog III (MepIleMe'Val') ^[b]			
	-	50 nM	100 nM	200 nM	50 nM	100 nM	200 nM	0.5 μM	5 μM	10 μM	20 μM
G ₁	53.3	9.0	4.8	3.5	41.8	15.4	16.2	47.4	49.2	35.6	23.5
S	21.9	11.9	10.0	8.8	12.5	14.5	10.9	23.9	6.8	13.8	8.6
G ₂ /M	21.7	72.6	77.7	81.6	44.0	68.4	70.2	26.4	37.4	41.1	58.9

[a] Corresponding histograms are displayed in Figure 3-10. Percentages were calculated in FlowJo v7.6.5 software. [b] HepG2 cells were treated for 24 h with compounds at the assigned concentrations.

Approximately 22% of the control HepG2 cells are in G₂/M phase and 53% in G₁ phase. The G₂/M population increases to approximately 70% or 82% after 24 h treatment with 200 nM pretubulysin or tubulysin A, respectively. However, nearly full cell cycle inhibition was already achieved in cells treated with 50 nM tubulysin A (73% in G₂/M), whereas with pretubulysin a concentration-dependent effect was observed (44-70% in G₂/M at different concentrations). Simultaneous to increasing G₂/M populations, the G₁ population decreases from 53% to 4% or 16% of the total number of measured cells treated with either 200 nM tubulysin A or pretubulysin, respectively. Similar to results with HL-60 cells (Figure 3-9) an induction of G₂/M cell cycle arrest was observed in HepG2 cells treated with the pretubulysin precursor compound (analog III). At a final concentration of 5 μM, nearly 40% of all viable cells accumulated in G₂/M phase. However, at higher drug concentrations (10 and 20 μM), the percentage of viable cells in G₂/M further increased to up to 60% in parallel with an emerging sub-G₁ population, which most likely reflects late apoptotic cells in which the DNA has already been degraded (Table 3-4 and Figure 3-10).

Complementary to FCM results, typical cellular events induced by antimetabolic drugs were observed in human U-2 OS osteosarcoma and potoroo Ptk-2 kidney cells. Treatment of cells with 25 nM pretubulysin for 24 h resulted in an abnormal accumulation of microtubules around the periphery of nuclei. At higher concentrations (50 nM) microtubules were completely depolymerized and most of the cells showed fragmented nuclei. In addition, normal mitotic cells, which were present in the control population, were no longer observed. Instead, cells with abnormal multipolar spindle pole structures were present (Figure 3-11). However, these effects account for a pronounced G₂/M cell cycle arrest as cells are not able to divide anymore.

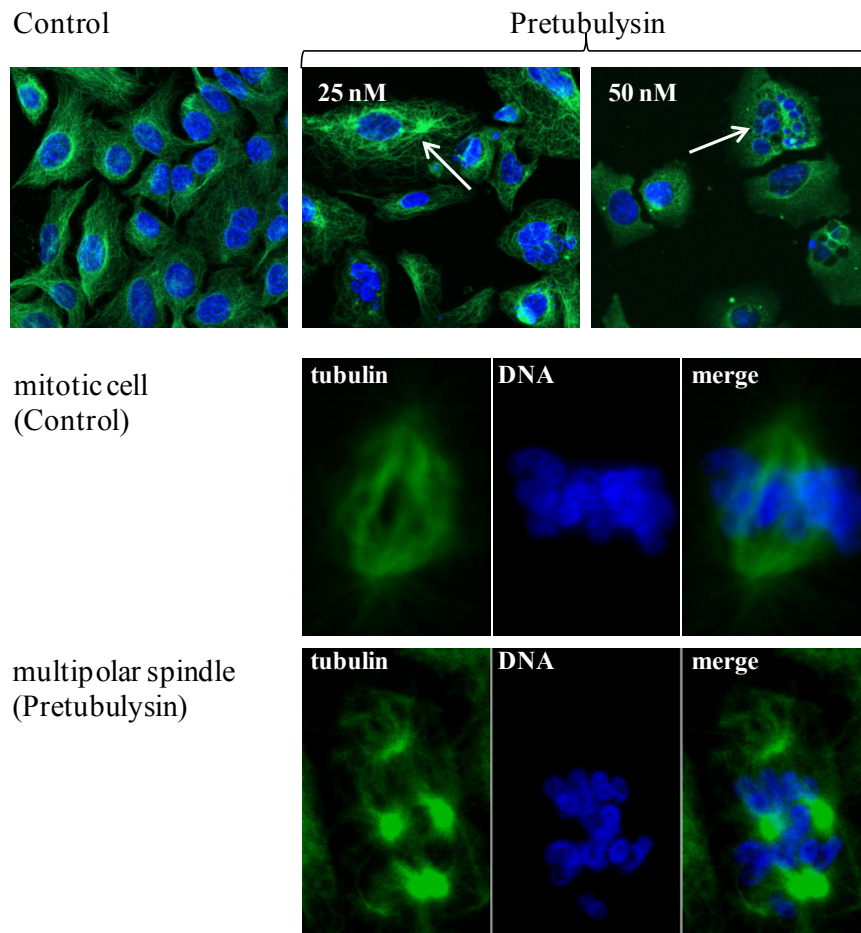


Figure 3-11: Typical cellular events upon pretubulysin treatment.

Human U-2 OS osteosarcoma cells (upper panel) were treated for 24 h with pretubulysin at the assigned concentrations. Microtubules were visualized by IF staining of α -tubulin (pseudocolor green) and nuclei were stained with Hoechst33342 (pseudocolor blue). Arrows indicate the abnormal accumulation of microtubules (25 nM) and cells with completely depolymerized microtubules and fragmented nuclei (50 nM). Images of dividing potoroo Ptk-2 kidney cells (middle and lower panel) were prepared likewise by IF. Cells were either left untreated or treated with 50 nM pretubulysin for 24 h.

3.1.5 APOPTOSIS INDUCTION

The late apoptosis measurements and immunoblot analyses mentioned in this paragraph were done by our collaboration partner at LMU Munich (Prof. Vollmar; Pharmaceutical Biology).

According to a modified protocol described by Nicoletti *et al.*^[215], apoptosis induction by tubulysin A and pretubulysin in human L3.6pl pancreatic cancer cells was assessed by PI staining of cells and subsequent FCM. In brief, treated cells are permeabilized with Triton-X 100 containing buffer and DNA is stained with PI. In late apoptotic cells, a so-called DNA laddering can be observed due to caspase-3 activated DNase. Small DNA fragments can

then diffuse through the nuclear membrane and in FCM analysis a sub-G₁ population (DNA content < 2n) is observed. This population is quantified and serves as a measure for apoptotic cells with fragmented DNA. Here, L3.6pl cells were treated with tubulysin A and pretubulysin and apoptotic cells were quantified after 48 h (Figure 3-12).

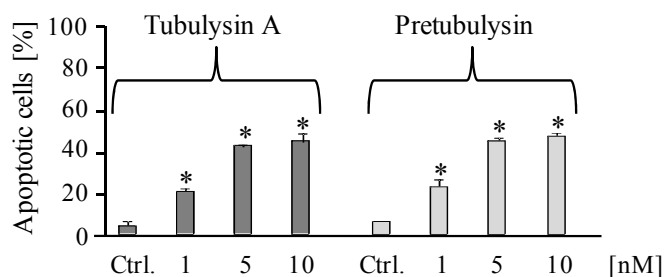


Figure 3-12: Induction of apoptosis in L3.6pl cells (Nicoletti assay).

Human pancreatic cancer cells were treated for 48 h with varying concentrations of tubulysin A or pretubulysin. The percentage of apoptotic cells in the whole cell population was determined by PI staining (n = 2; *p ≤ 0.05 Anova/Dunnett).

Both compounds already induced apoptosis at a concentration of 1 nM (ca. 20%) and at higher concentrations the percentage of apoptotic cells in the whole cell population increased to approximately 50% with either compound.

It was already reported that treatment of KB-3.1 cells with tubulysin A leads to DNA laddering^[220] and the same effect could be clearly confirmed for pretubulysin and one of its derivatives, 2-desmethyl pretubulysin. Complementary to the Nicoletti assay, human HL-60 acute promyelocytic leukemia cells were treated for 24 and 48 h with pretubulysins and extracted chromosomal DNA was separated by agarose gel electrophoresis. Resulting DNA bands were stained with ethidium bromide and detected under UV light (Figure 3-13). Cleavage of chromosomal DNA in distinct fragment, as a hallmark of apoptosis, was induced with either compound after 24 h and 48 h treatment. At the same concentrations (30 nM and 75 nM), DNA laddering caused by pretubulysin treatment was more pronounced compared to analogous 2-desmethyl pretubulysin samples.

In an additional experiment it was found that the induction of apoptosis, as demonstrated by DNA laddering and emerging sub-G₁ populations, is partly caspase-dependent. L3.6pl cells were treated with pretubulysin and tubulysin A for 48 h and the percentage of apoptotic cells was again assessed after PI staining in FCM. The broad spectrum caspase inhibitor Q-VD-OPh reduced drug-induced apoptosis from approximately 46% to 26% and from 39% to 27% for tubulysin A and pretubulysin, respectively (Figure 3-14).

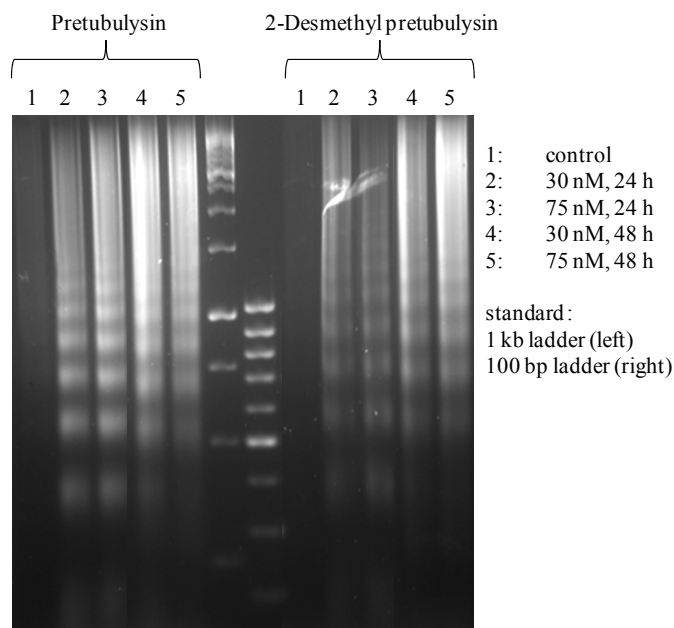


Figure 3-13: DNA laddering in HL-60 cells treated with pretubulysins.

HL-60 cells were either left untreated or treated with pretubulysin and 2-desmethyl pretubulysin at the assigned concentrations and time period. Chromosomal DNA was extracted and typical fragments (DNA laddering) were separated by agarose gel electrophoresis.

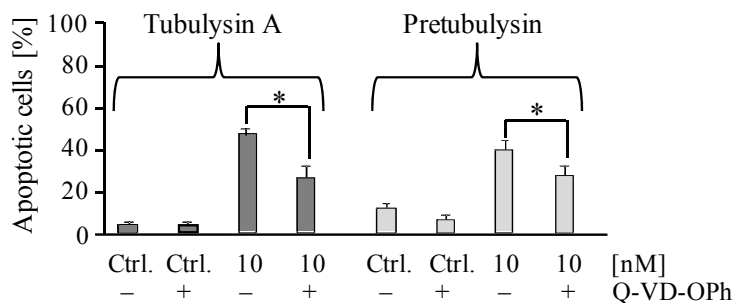


Figure 3-14: Caspase-dependent induction of apoptosis in L3.6pl cells (Nicoletti assay).

Human pancreatic cancer cells were treated for 48 h with 10 nM tubulysin A or pretubulysin in conjunction with 10 mM caspase inhibitor Q-VD-OPh. The percentage of apoptotic cells in the whole cell population was determined by PI staining ($n = 3$; $*p \leq 0.05$ Anova/Dunnett).

Molecular mechanisms of mitotic arrest mentioned in section 3.1.4, are often found to trigger signaling towards the mitochondrial apoptosis pathway. For instance, routine screening of a myxobacterial compound library revealed all microtubule-destabilizers that were included in the library (disorazol and tubulysin derivatives) as effective modulators of the mitochondrial membrane potential (Figure 3-15).

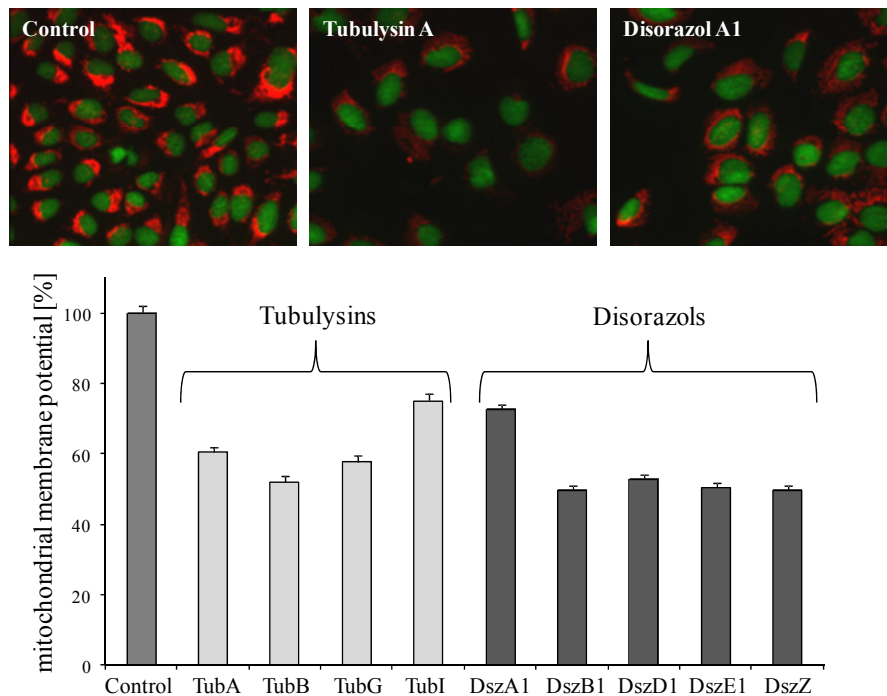


Figure 3-15: Mitochondrial membrane potential (MMP) in U-2 OS cells treated with antimicrobials.

In routine HCS, 90% confluent U-2 OS cells were treated with myxobacterial compounds at a final concentration of 200 nM for 12 h. Mitochondria were labeled with TMRM (pseudocolor red) and nuclei with Hoechst33342 (pseudocolor green). Images were acquired on a BD Pathway855 automated microscope and subsequently processed in AttoVision v1.6.2. Images show representative results from control cells and cells treated with tubulysin A or disorazol A. The relative MMP was calculated based on TMRM fluorescence intensity in the cytoplasmic segment. Bars represent the mean \pm SEM of all cellular segments within a well.

The reduction of MMP, as depicted by diminished TMRM fluorescence of mitochondria, is generally considered as an initial and irreversible step towards apoptosis. All microtubule-destabilizing compounds in the library significantly reduced the MMP in U-2 OS cells after 12 h treatment at a final concentration of 200 nM to approximately 50-70% of the control.

One of the key players in mitochondrial apoptosis is the proto-oncoprotein Bcl-2 (B cell lymphoma 2) because its phosphorylation status is linked to cellular redox status, cell growth and particularly, regulation of apoptosis. Immunoblot analyses demonstrated that antiapoptotic Bcl-2 is inactivated, i.e. phosphorylated, upon treatment with tubulysin A and pretubulysin (Figure 3-16A). Human L3.6pl pancreatic cancer cells were treated with 10 nM of either compound, which resulted in transiently enhanced levels of phosphorylated Bcl-2 (pBcl-2) after 8 and 24 h treatment. Highest pBcl-2 levels were detected after either 24 h tubulysin A treatment or 8 h of pretubulysin treatment.

In addition, treatment of L3.6pl cells with tubulysin A or pretubulysin leads to cleavage of poly(adenosine diphosphateribose) polymerase (PARP), which is a substrate of caspase-3 and

functions in DNA repair (Figure 3-16B). PARP cleavage was detectable after 24 h treatment with both compounds and the effect was even more pronounced after 48 h.

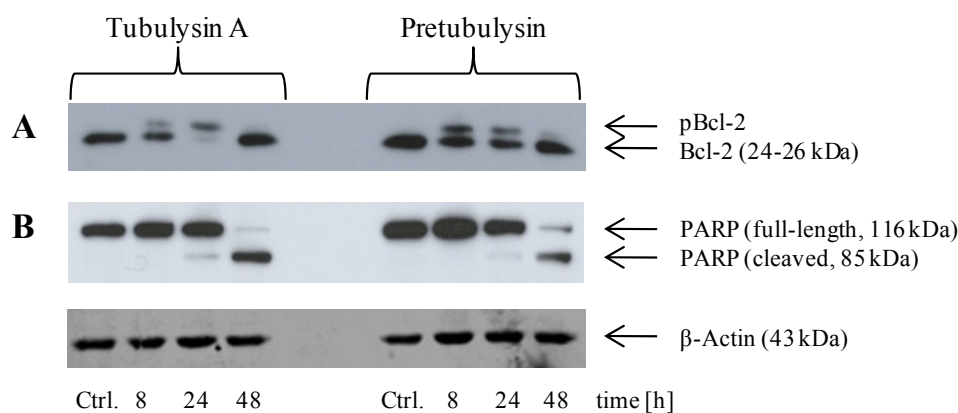


Figure 3-16: Immunoblot analysis of L3.6pl cells treated with tubulysin A and pretubulysin.

Human pancreatic cancer cells were treated for the indicated time points with 10 nM tubulysin or 10 nM pretubulysin. Lysates were immunoblotted for A) Bcl-2 and pBcl-2 or B) for PARP; β -actin served as a reference for the quantification of protein levels.

3.1.6 HCS STUDIES

For comparative high-content screening (HCS) studies the following compounds were selected: tubulysins A and D, pretubulysin, pretubulysin analog III, disorazol A, and epothilone B. Human U-2 OS cells were treated with the compounds for 24 h or 48 h at final concentrations that were adjusted according to respective GI_{50} values.

In order to assess microtubule disruption and apoptotic events, α -tubulin was probed by immunofluorescence, nuclei were stained with Hoechst33342, and the whole cell stain HCS CellMaskTM Red was added to facilitate subsequent segmentation of the cytoplasmic region. Most apparently, enlargement of cells, fragmentation of nuclei, and rearrangements of the microtubule structures were found. For quantification, a cytoplasm-nuclei dual mask was applied to generate the respective segments for every cell within all wells (Figure 3-17). Analyses were performed on a single cell basis and averaged over the complete sample. Throughout all HCS experiments the SEM increased with increasing concentrations of the compounds, which was due to a larger portion of apoptotic cells and therefore more heterogeneous cell populations mainly with regards to cell size.

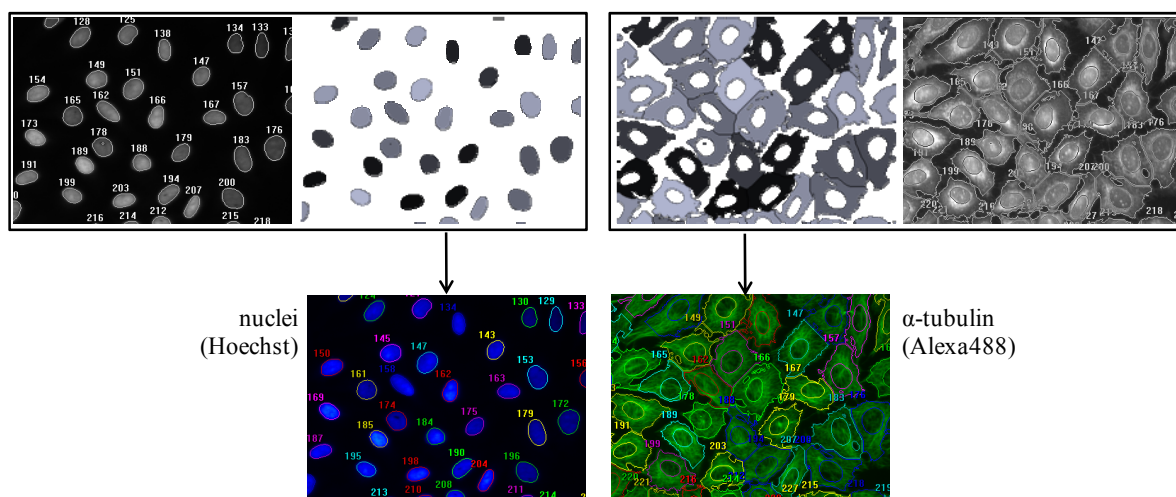


Figure 3-17: Schematic segmentation process of HCS image data.

Nuclear segments are based on Hoechst33342 fluorescence (left upper panel) and cytoplasmic segments are generated around each nucleus based on HCS CellMask™ Red fluorescence (right upper panel). The obtained masks are then overlaid in the respective fluorescence channel for analysis (lower panel; nuclear mask in Hoechst33342 channel and cytoplasmic mask in Alexa488 channel).

The enlargement of cells and fragmentation of nuclei were determined in AttoVision v1.6.2 by calculating the area of cytoplasmic and nuclear segments, respectively. In accordance with growth inhibition induced by all of the tested compounds, the cell bodies (cytoplasmic area, Figure 3-18) were significantly enlarged in a concentration-dependent manner as a result of the compounds' cytostatic activity. Epothilone B, the only microtubule stabilizer in the test panel, yielded the same macroscopic effects as the other microtubule destabilizers. Treatment with increasing concentrations of tubulysin A and pretubulysin led to a steady increase of average cell size. However, also upon treatment with tubulysin D, disorazol A, and epothilone B, cells enlarged but a slight drop was observed at the highest concentrations tested. Image data dereplication revealed a relatively large number of rounded-up, late apoptotic cells in these samples. Interestingly, treatment with 50 μ M pretubulysin analog III also induces the enlargement of cells.

The average size of nuclei (Figure 3-19) determined in the same experiment is in accordance with the results from cytoplasmic area calculations. Not only nuclear size increased with increasing concentrations of the antimetotics but also the relative number of fragmented nuclei. Since these could not be resolved as single fragments by image segmentation, fragmented nuclei also contributed to higher average values of the nuclear area. In late apoptotic cells (at highest concentrations of tubulysin D, disorazol A, and epothilone B),

chromatin condensation was observed which resulted in very high values for average nuclear fluorescence intensity (data not shown) and decreased nuclear area.

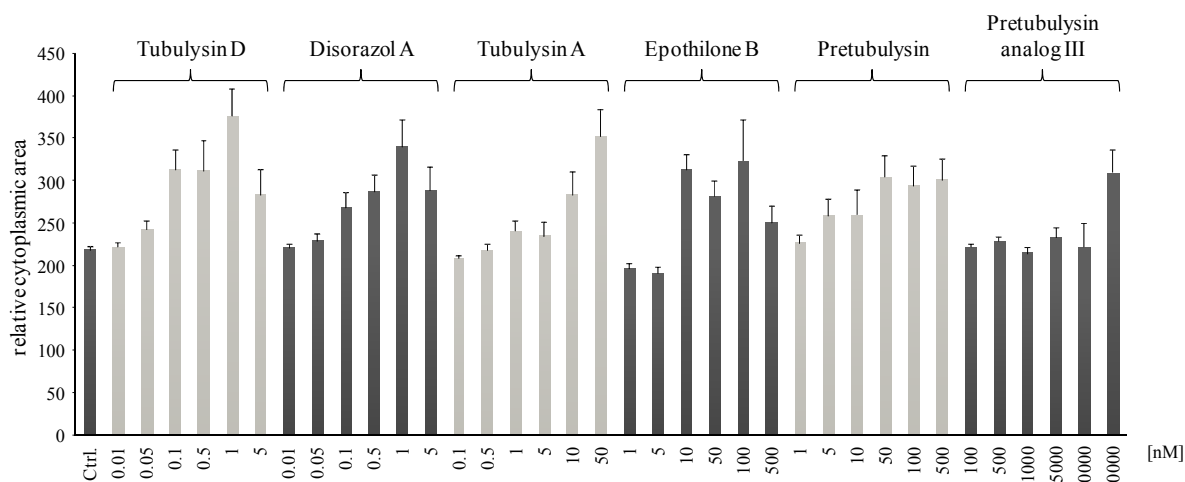


Figure 3-18: Cytoplasmic area of U-2 OS cells treated with antimitotic compounds.

Human U-2 OS osteosarcoma cells were treated for 24 h with the compounds at assigned concentrations. Cells were fixed, probed on α -tubulin, and stained with Hoechst33342 and HCS CellMaskTM Red. Bars represent the mean cytoplasmic area \pm SEM of all cellular segments within a well as determined in AttoVision v1.6.2.

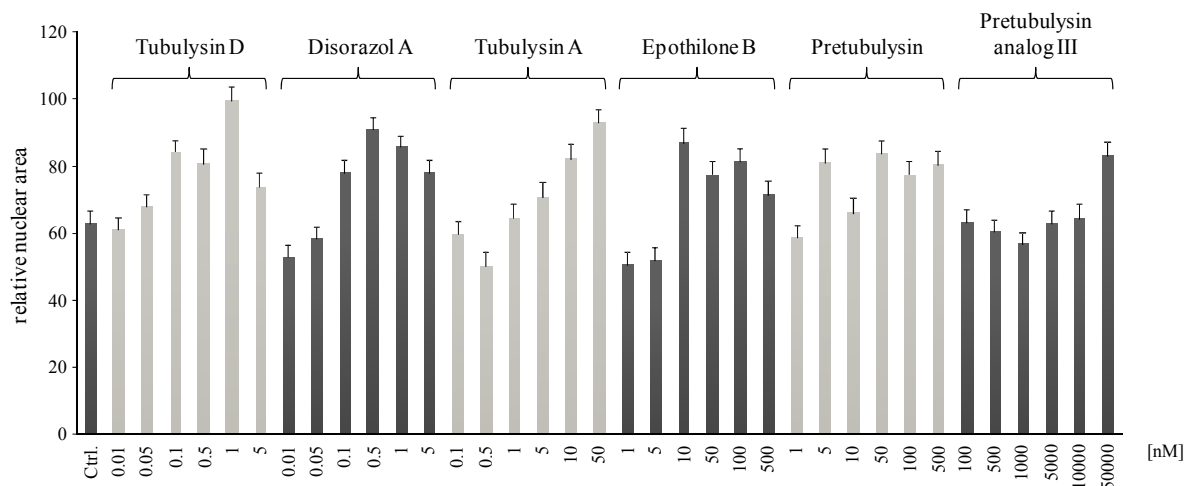


Figure 3-19: Nuclear area of U-2 OS cells treated with antimitotic compounds.

Cells were treated and analyzed as in the experiment on cytoplasmic area (Figure 3-18). Bars represent the mean nuclear area \pm SEM of all cellular segments within a well as determined in AttoVision v1.6.2.

For the analysis of microtubule disruption by HCS several parameters were determined using statistical methods that are most suitable to describe antimitotic phenomena based on

microtubule fluorescence (data not shown). Among these parameters, the standard deviation (SD) of tubulin fluorescence in the cytoplasmic segments seemed to be the most robust parameter and was therefore calculated as a measure for microtubule disruption (Figure 3-20).

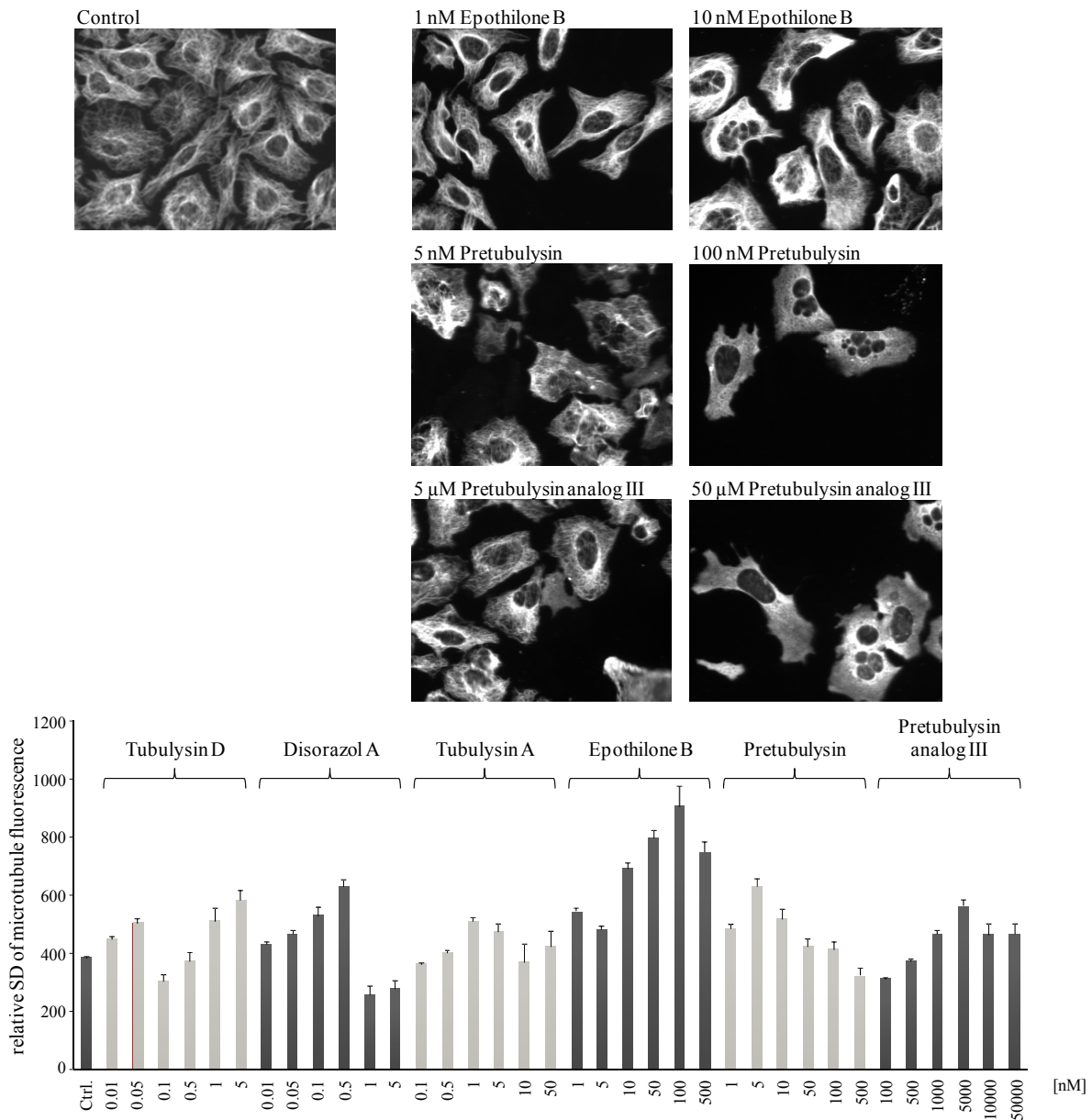


Figure 3-20: Microtubule disruption in U-2 OS cell treated with antimetabolic compounds.

Representative images of human U-2 OS osteosarcoma cells treated with epothilone B, pretubulysin, or its small precursor (upper panel). Cells were treated and analyzed as in the experiment on cytoplasmic area (Figure 3-18). Bars represent the mean SD of tubulin fluorescence in the cytoplasmic segment \pm SEM of all cellular segments within a well as determined in AttoVision v1.6.2 (lower panel).

The more uniform tubulin appears in the cells, the lower the SD is, i.e., lowest SD values were observed for cells with completely depolymerized microtubules. For all microtubule destabilizing compounds, the SD of tubulin fluorescence peaks at intermediate concentrations used in the HC assay. This first maximum value is followed by a decline at higher concentrations, and for tubulysins A and D a second peak was observed. Upon image data dereplication it was apparent that an increase in tubulin fluorescence SD was linked to initial microtubule depolymerizing effects that are characterized by a greater number of mitotic cells with abnormal spindle pole structures and a higher density of interphase microtubules around the nuclear periphery in most cells. Increasing concentrations led to complete microtubule depolymerization (decline in SD) and a second peak of tubulin fluorescence SD at highest concentrations, as for tubulysins A and D, was caused by cell debris. For the microtubule stabilizer epothilone B, a continuous increase of fluorescence SD was observed. At a final concentration of 500 nM the SD slightly falls off, which is most likely due to the very pronounced microtubule stabilizing effect.

In a study on DNA double-strand breaks (DSBs), human U-2 OS osteosarcoma cells were treated as in the aforementioned assays but for 48 h instead of 24 h. Cells were probed on phosphorylated histone H2A.X (γ H2A.X), which is a marker for DSBs, by immunostaining, and nuclei were stained with Hoechst33342. The fluorescence intensity of γ H2A.X was determined within the nuclear segments and averaged over the respective samples (Figure 3-21). All tested antimetabolites led to large γ H2A.X foci that were exclusively associated with already fragmented nuclei or cells with condensed chromatin as exemplarily shown for epothilone B treated U-2 OS cells. For all samples, fluorescence intensity of γ H2A.X basically increased with increasing concentrations, although a decline in intensity was observed for tubulysins A and D, and pretubulysin. As a positive control, cells were treated for 4 h with hydroxyurea (HU), which starves the DNA polymerase at the replication forks for dNTPs and thus, induces DSBs. HU-induced DSBs appeared to be evenly distributed in the nuclear region as small γ H2A.X foci in a concentration-dependent manner.

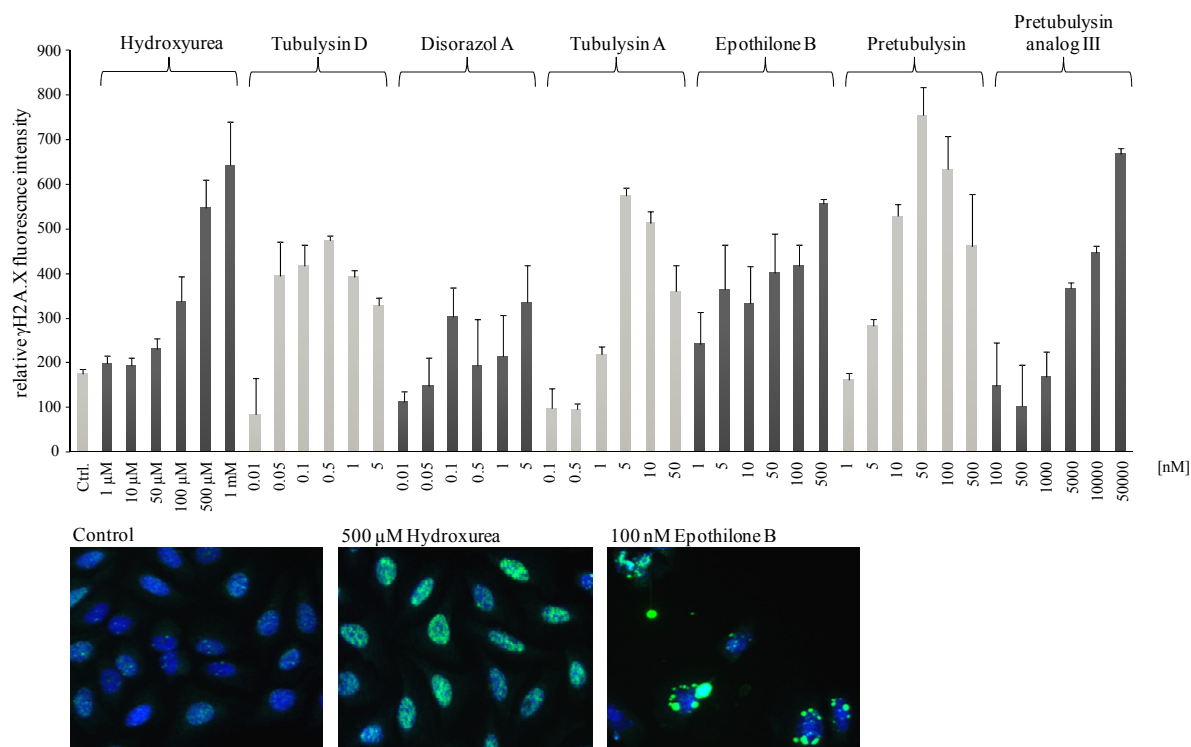


Figure 3-21: Histone H2A.X phosphorylation in U-2 OS cell treated with antimitotic compounds.

Human U-2 OS osteosarcoma cells were treated for 48 h with the compounds at assigned concentrations. Cells were fixed, probed on γ H2A.X, and nuclei were stained with Hoechst33342. Bars represent the mean intensity of γ H2A.X within the nuclear segment \pm SEM as determined in AttoVision v1.6.2 (upper panel). Representative images of human U-2 OS osteosarcoma cells treated for 48 h with 0.5 mM hydroxyurea or 100 nM etoposide B (pseudocolor blue: DNA; pseudocolor green: γ H2A.X; lower panel).

3.1.7 *IN VITRO* POLYMERIZATION STUDIES

Electron micrographs displayed in this section were prepared by our collaboration partner at HZI Braunschweig (Prof. Rohde, group: Molecular Mechanisms of Streptococci).

Previous experiments revealed that potency of pretubulysin is reduced approximately by factor 10 compared to the parent compound tubulysin A. GI_{50} values of pretubulysin analog III, which also acts by destabilizing microtubule structures, are at least one order of magnitude higher (low micromolar range) than those of pretubulysin itself. Cell-free *in vitro* experiments were performed in order to assess whether tubulysin A and synthetic pretubulysins exhibit similar tubulin-binding potencies without the cell membrane acting as a natural barrier. As a reference, the absorbance at 350 nm of 10 μ M microtubule protein in polymerization buffer with and without 1 μ M tubulysin A was recorded over time

(Figure 3-22). The addition of the antimitotic drug led to an approximately 50% reduction of built-up microtubules. Electron micrographs, which were prepared in parallel, revealed perfect tubular structures and rather long microtubules in the untreated control. However, upon pre-treatment with 1 μM tubulysin A a smaller number of shorter and disrupted microtubules were observed. The residual microtubules were either fragmented and/or the tubular structure was broken up as indicated by arrows in electron micrographs of Figure 3-22.

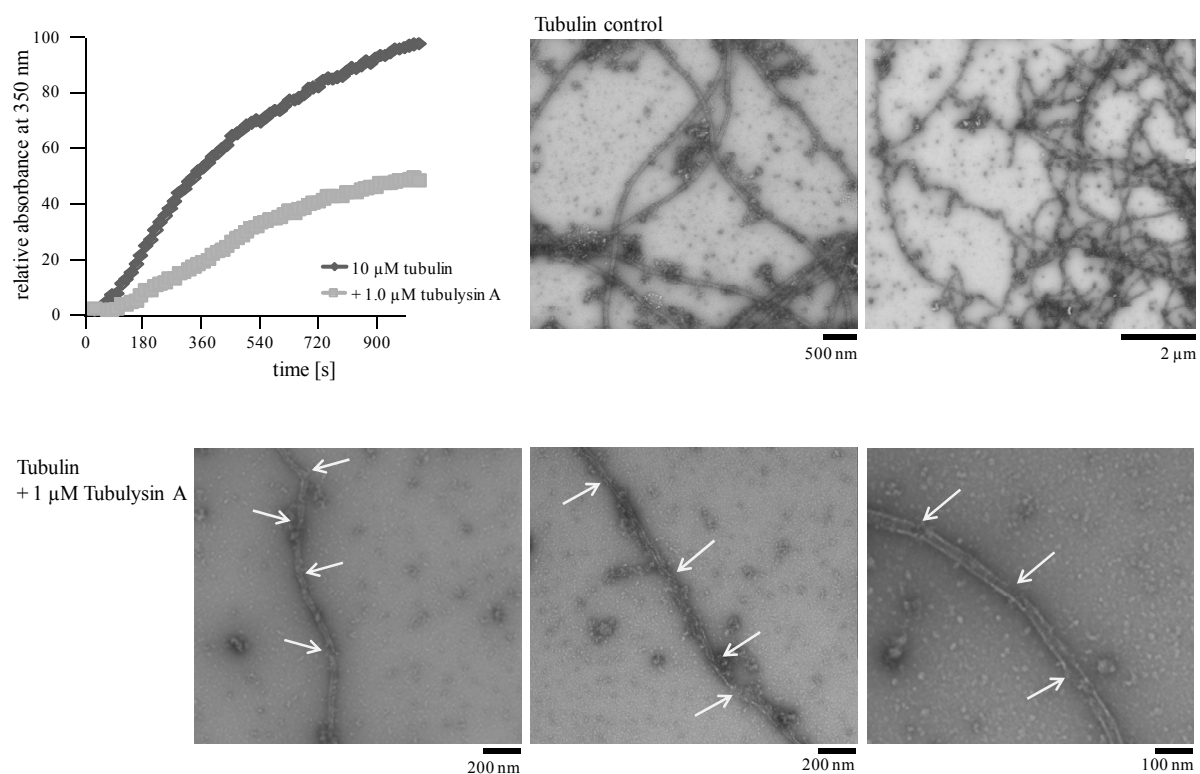


Figure 3-22: *In vitro* inhibition of tubulin polymerization by tubulysin A.

Tubulysin A (1 μM) was added to a preparation of 10 μM tubulin protein, and the absorbance was measured over time at 350 nm. The maximum value of the untreated control was set to 100% (upper left panel). Corresponding electron micrographs of the control (upper right panel) and the sample co-incubated with tubulysin A (lower panel) are given. Arrows indicate fragmented and/or broken up microtubular structures.

The results are in accordance with previous reports on tubulysin A.^[220] Furthermore, it was shown that pretubulysin can inhibit microtubule formation *in vitro* in a dose-dependent manner and can also depolymerize already assembled microtubules (Figure 3-23). Addition of 1 μM pretubulysin to the tubulin protein preparation (pre-assembly) led to an approximate 50% reduction in microtubule formation. The polymerization was further reduced with higher pretubulysin concentrations. As revealed by electron microscopy, treatment with 5 μM

pretubulysin led to completely destroyed microtubules as only single protein blocks were found. When pretubulysin was added post-assembly, higher concentrations were needed to reduce the number of already built-up microtubules to the same extent than in the pre-assembly experiment. Approximately 2 μM pretubulysin was needed to reduce the amount of microtubules by ca. 50%. At higher concentrations no further depolymerization could be observed in time course experiments. In addition, the electron micrograph recorded of a sample treated with 5 μM pretubulysin post-assembly revealed that microtubules are significantly disrupted but still not fully depolymerized.

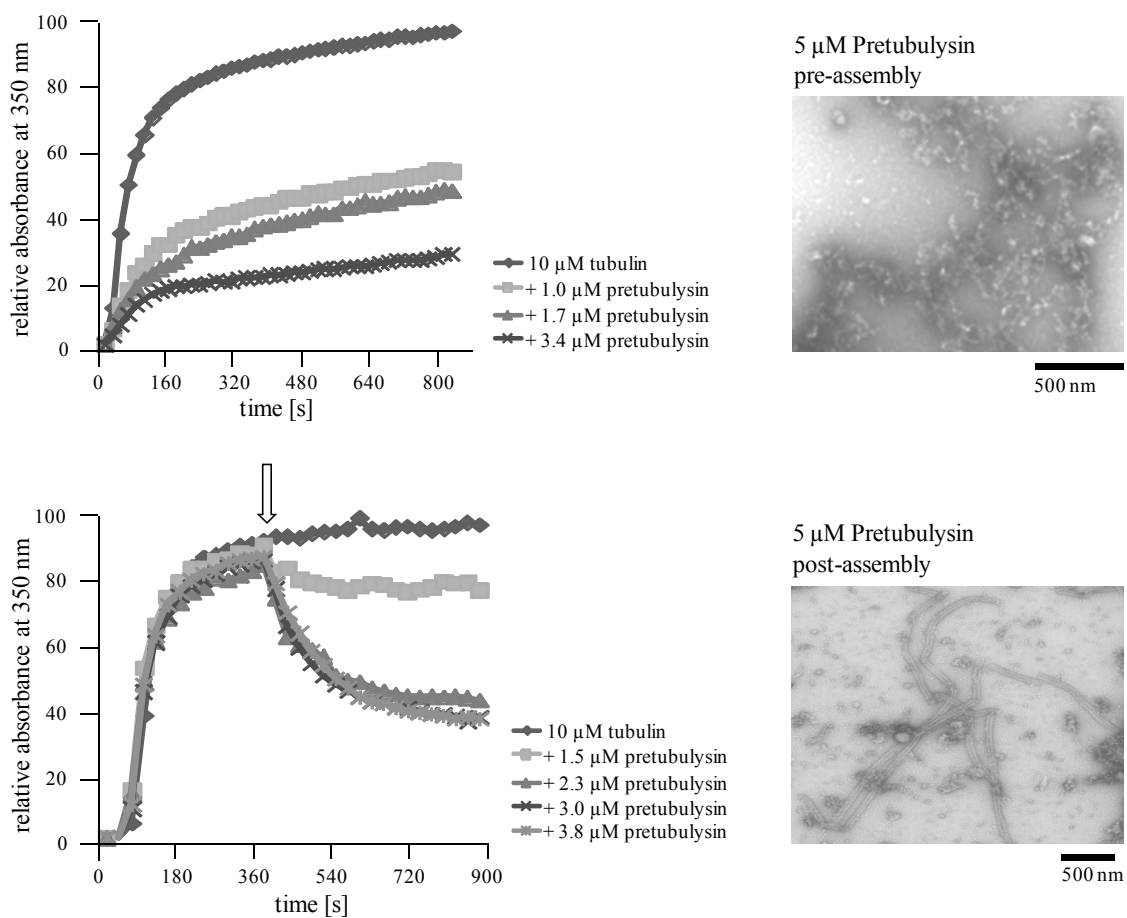


Figure 3-23: *In vitro* inhibition of tubulin polymerization by pretubulysin.

Varying concentrations of pretubulysin were added to a preparation of 10 μM tubulin protein either pre-assembly (upper panel) or after microtubule assembly (lower panel; the arrow indicates the time point of drug addition) and the absorbance was measured over time at 350 nm. The maximum values of the untreated controls were set to 100%. Electron micrographs of tubulin treated pre- or post-assembly with 5 μM pretubulysin are given.

The small precursor molecule (pretubulysin analog III) was also able to inhibit *in vitro* microtubule formation (Figure 3-24). Compared to pretubulysin its activity is approximately 10-fold reduced; either 20 μM of analog III or 2 μM of pretubulysin were needed to inhibit polymerization by about 60-70%. Furthermore, electron micrographs revealed that treatment with either 2 μM pretubulysin or 25 μM pretubulysin yields similar results with respect to microtubule disruption, as depicted by the shortened microtubules and the perturbed tubular structure relative to the control.

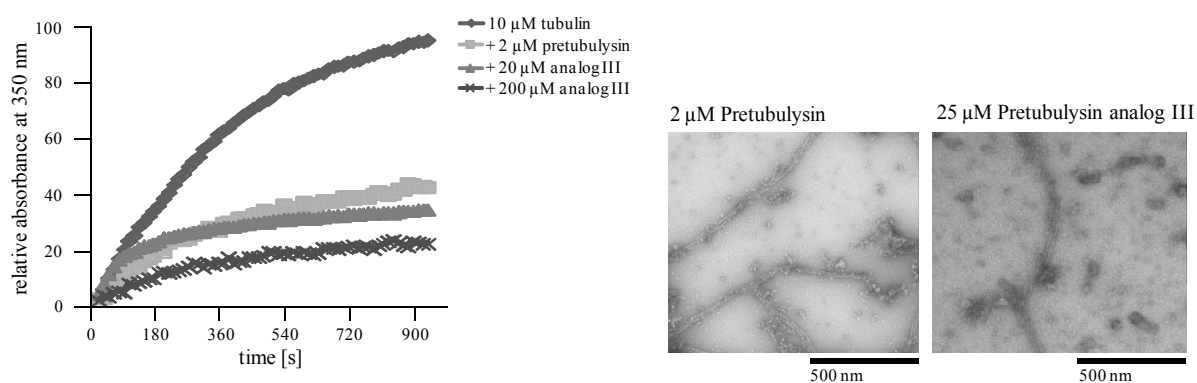


Figure 3-24: *In vitro* inhibition of tubulin polymerization by pretubulysin analog III.

Pretubulysin (2 μM) and its analog III (20 and 200 μM) were added pre-assembly to a preparation of 10 μM tubulin protein and the absorbance was measured over time at 350 nm. The maximum value of the untreated control was set to 100%. Electron micrographs of tubulin treated with 2 μM pretubulysin or 25 μM pretubulysin precursor are given.

3.2 DISCOVERY OF NEW CHONDRAMIDES AND INITIAL SAR STUDIES

Fermentation and extract preparation, chromatographic steps, purification of chondramides and their structural elucidation mentioned in this section were performed by S. Hüttel in our research group.

3.2.1 CYTOSTATIC ACTIVITY OF SBCM007 CRUDE EXTRACT

In routine screening of methanolic crude extracts from shake flask cultivations of the newly discovered *Chondromyces sp.* strain SBCM007, no significant antibacterial or antifungal activity was discovered. However, the extract exhibited a potent activity against a human leukemia cell line with an IC_{50} value of 0.54 $\mu\text{g}/\text{ml}$ (Figure 3-25).

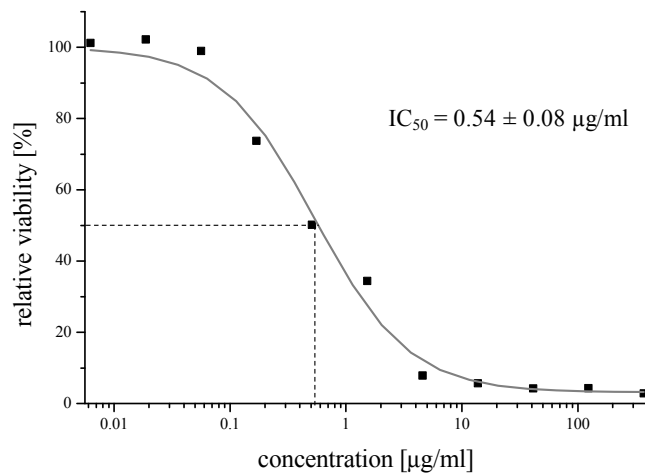


Figure 3-25: Inhibition of HL-60 cells by SBCm007 crude extract.

Human HL-60 promyelocytic leukemia cells were treated with *Chondromyces sp.* SBCm007 crude extract in serial dilution and incubated for 3 d. Viability was assessed in an MTT assay and was calculated relative to the internal control. The IC_{50} value was determined by sigmoidal curve fitting as average of two independent measurements.

In order to elucidate whether this result comes from rather acute cytotoxic effects or is caused by cytostatic compounds present in the crude extract cells were screened on typical morphological alterations. Apparently, at concentrations around the determined IC_{50} value, cells enlarged, which can already be regarded as a growth inhibitory (cytostatic effect). Nevertheless, Chinese hamster ovary CHO-K1 cells were treated with the crude extract at its IC_{50} and 10-fold IC_{50} concentration for 48 h, and for better visualization cells were stained with Giemsa (Figure 3-26).

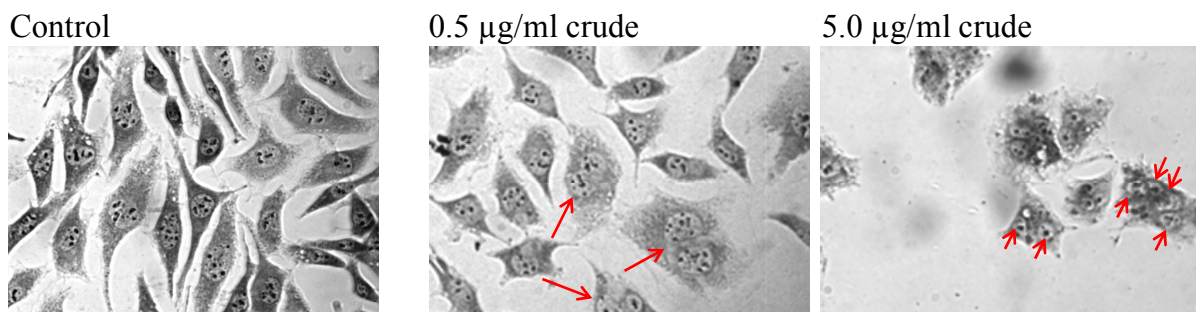


Figure 3-26: Inhibition of cytokinesis after treatment with SBCm007 crude extract.

CHO-K1 cells were treated for 48 h with the crude extract of *Chondromyces sp.* SBCm007 at assigned concentrations. Images of Giemsa-stained cells were obtained by transmitted light microscopy. Red arrows indicate multinucleated cells.

Interestingly, a quite unique phenotype characterized by bi- or even multinucleated cells was observed. At a concentration of 0.5 $\mu\text{g/ml}$ most of the CHO-K1 cells appeared to be intact but some cells were binucleated. At 10-fold higher concentrations, the cell membrane was significantly affected and even multinucleated cells (up to four nuclei) were observed.

3.2.2 TARGET-SPECIFIC ACTIVITY IN THE CRUDE EXTRACT

Strains of the genus *Chondromyces* are described as producers of various secondary metabolites with partly cytostatic activity^[221], and dereplication of LC-MS data against our in-house database revealed the presence of chondramides A~D in SBCm007 crude extracts (Figure 3-27).

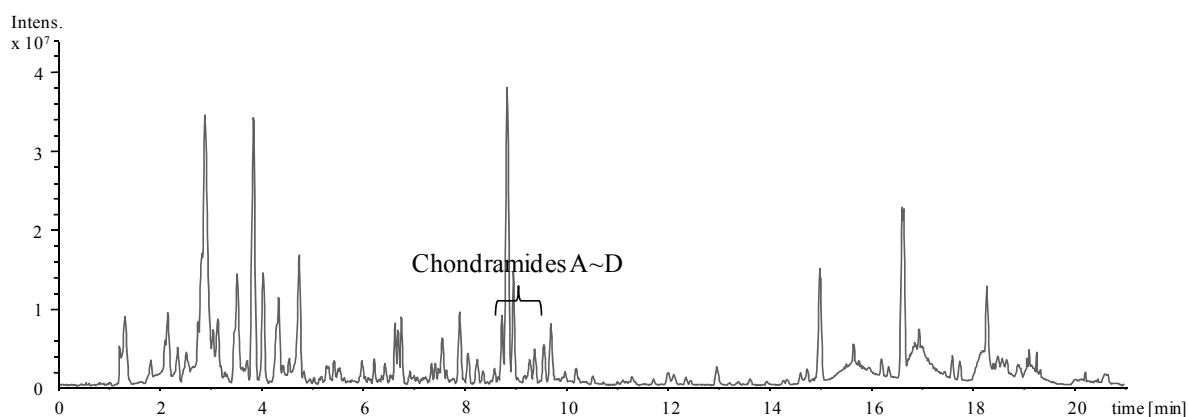


Figure 3-27: Strain SBCm007 produces chondramides.

Base peak chromatogram (BPC) of the crude methanolic extract (from adsorber resin Amberlite™ XAD™ 16) of *Chondromyces* sp. SBCm007 as analyzed by HPLC-MS in positive ionization mode.

Chondramides A~D were found to be quite abundant in the extract and eluted at a retention time of approximately 9 min in the presented chromatogram. These metabolites are usually active in the mid-nanomolar range on cultured mammalian cells and exhibit moderate activity against yeast.^[194] Still, it was surprising that IC_{50} values of the crude extract on leukemia cells were only by 2-3 orders of magnitude higher than GI_{50} values reported for pure compounds. In addition to general bioactivity studies, crude extract-treated cells were probed on other, more specific, determinants of cytotoxicity. Since it was already reported for chondramides that these NPs act by stabilizing actin filaments^[209], CHO-K1 cells were treated and subsequently analyzed by fluorescence microscopy using IF labeling on β -actin (Figure 3-28).

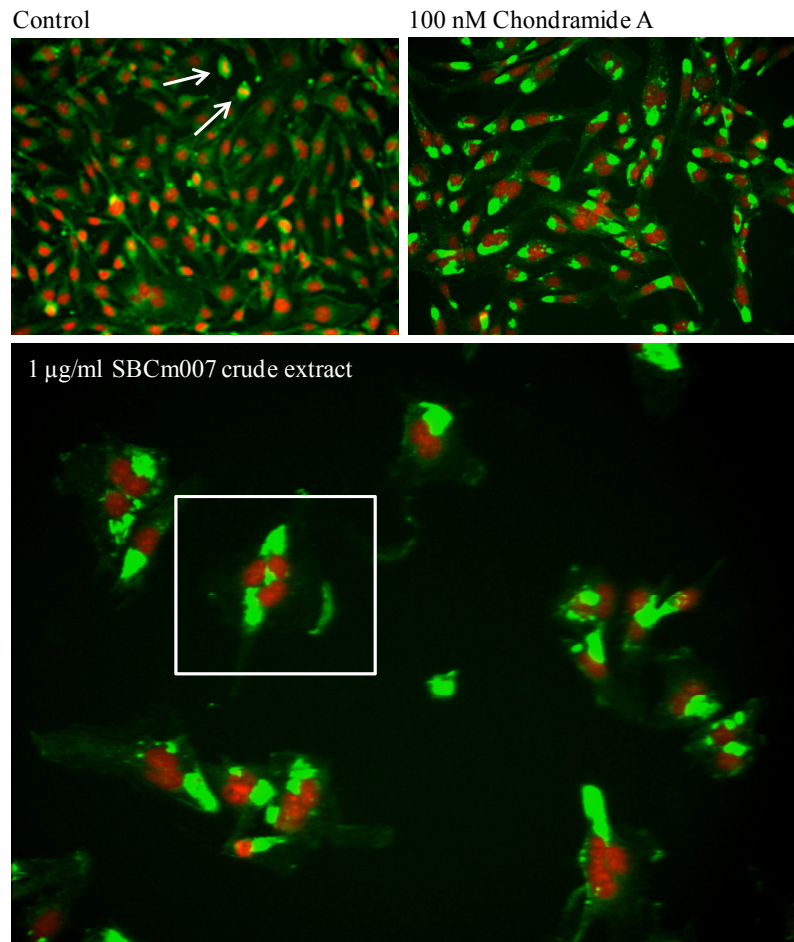


Figure 3-28: Actin condensation in CHO-K1 cells.

CHO-K1 cells were either left untreated or treated for 24 h with chondramide A as a reference or SBCm007 crude extract. Nuclei were stained with Hoechst33342 (pseudocolor red) and actin was visualized by IF on β -actin (pseudocolor green). Arrows indicate dividing cells in the control population and the box marks a representative multinucleated cell with actin lumps of the crude extract-treated sample.

Although the expected actin pattern (condensed filaments) and multinucleated cells were observed in CHO-K1 cells that were treated with SBCm007 crude extract slight differences, which mainly manifested in the overall shape of the cells, were found compared to cells that were treated with chondramide A as a reference. Thus, human U-2 OS osteosarcoma cells were used in subsequent studies since these rather large cells have an epithelial adherent morphology and have been shown to be excellently suited for a wide variety of microscopy-based assays, in particular, HCS applications. It was found that, besides influences on overall cell shape, actin lumps, nuclear condensation, and multinucleation, also lysosomal integrity was disturbed, as displayed by a less acidic lysosomal pH (Figure 3-29).

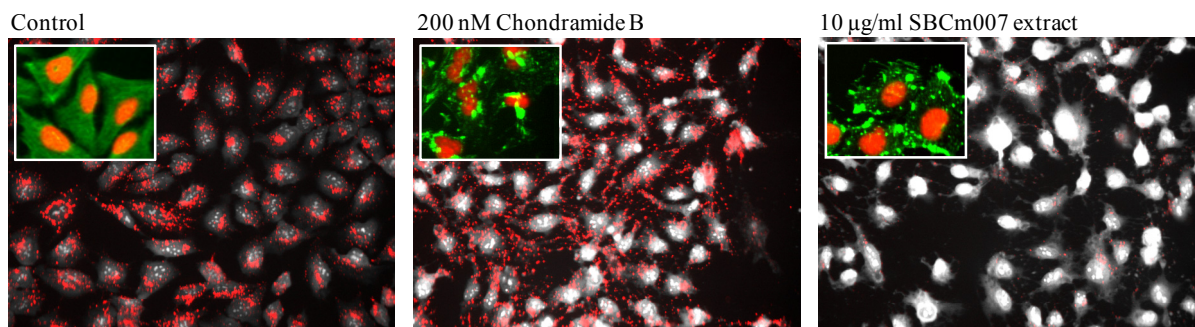


Figure 3-29: Increased lysosomal pH in U-2 OS cells.

U-2 OS cells were either left untreated or treated for 4 h with chondramide B or SBCm007 crude extract. Acidic lysosomes (pseudocolor red) were stained with acridine orange and green fluorescence of this dye is observed in the cytosol (displayed in grey). The small insert images display corresponding effects on the actin filaments as determined by IF on β -actin (pseudocolor green); nuclei were stained with Hoechst33342 (pseudocolor red).

Lysosomal membrane permeabilization (LMP) is induced by a plethora of intra- and extracellular stimuli and is the key step in the lysosomal death pathway. Upon LMP, cathepsins and other hydrolases are released from the lysosomes in the cytosol, which in turn, trigger the mitochondrial pathway of apoptosis. Additionally, release of these hydrolases may also directly lead to cell death due to digestion of proteins in the cytosol.^[222] The metachromatic fluorophor acridine orange (AO) is a lysosomotropic weak base and thus, accumulates preferentially in acidic compartments, i.e. lysosomes, where it exhibits a bright red to orange fluorescence. However, lower intracellular concentrations of AO (nuclear and cytosolic) are characterized by a green fluorescence, whereas the fluorescence intensity may increase upon lysosomal disruption, in parallel to a decrease in granular red fluorescence.^[223] Here, it could be demonstrated that upon 4 h treatment of U-2 OS cells with SBCm007 crude extract, the lysosomal pH was significantly increased (induction of LMP) as indicated by an increase in green nuclear and cytosolic AO fluorescence and a decrease in red lysosomal AO fluorescence. This effect could not be attributed to chondramide-related cellular events. In the same experiment, chondramide B was used as a reference compound and although the cellular shape and actin condensation resemble effects observed with crude extract-treated cells no direct influence on the lysosomal pH was determined.

3.2.3 HCS ON LYSOSOMAL INTEGRITY

Since the induction of LMP observed in crude-extract treated cells could not be explained by the presence of any known compound, the extract was fractionated by size-exclusion chromatography (SEC) and resulting fractions were tested in an HCS assay on lysosomal integrity (Figure 3-30). As determined by HPLC-MS, chondramides A~D were mainly present in SEC fractions 23-28 and strongest LMP induction was found with samples 20-22.

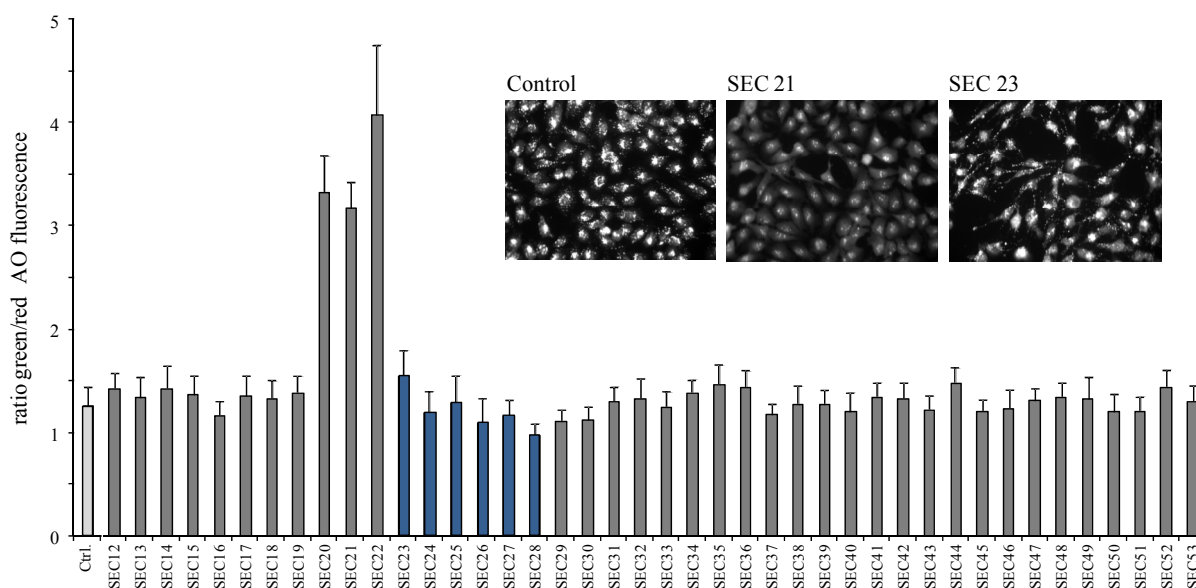


Figure 3-30: Induction of LMP in U-2 OS by SBCm007 fractions obtained by SEC.

U-2 OS cells were either left untreated or treated for 4 h with SBCm007 crude extract or fractions derived from SEC. Cells were stained with AO and Hoechst33342 and analyzed by HCS. The AO fluorescence ratio green/red is calculated based on average values from all cells within a well. Error bars display \pm SD of green fluorescence within the cytoplasmic segment. Main chondramide fractions are marked in dark blue. Exemplary images recorded in red fluorescence channel are given for the untreated control and cells treated with either SEC fraction 21 or 23.

These results again demonstrated a chondramide-independent effect on LMP. Solely in SEC fraction 23 an overlap of both effects, disruption of cellular shape as induced by chondramides and a slight increase in lysosomal pH as induced by unknown metabolites, was observed.

In addition, the crude extract of *Chondromyces sp.* SBCm007 was fractionated by column chromatography (silica gel) and samples were likewise subjected to HCS assays on lysosomal pH (Figure 3-31). Here, chondramides A~D were mainly found in silica gel fractions C and D and interestingly, also strongest effects with respect to LMP induction were observed in these

fractions. However, silica fraction E did not contain considerable amounts of chondramides but was also active in the HCS assay.

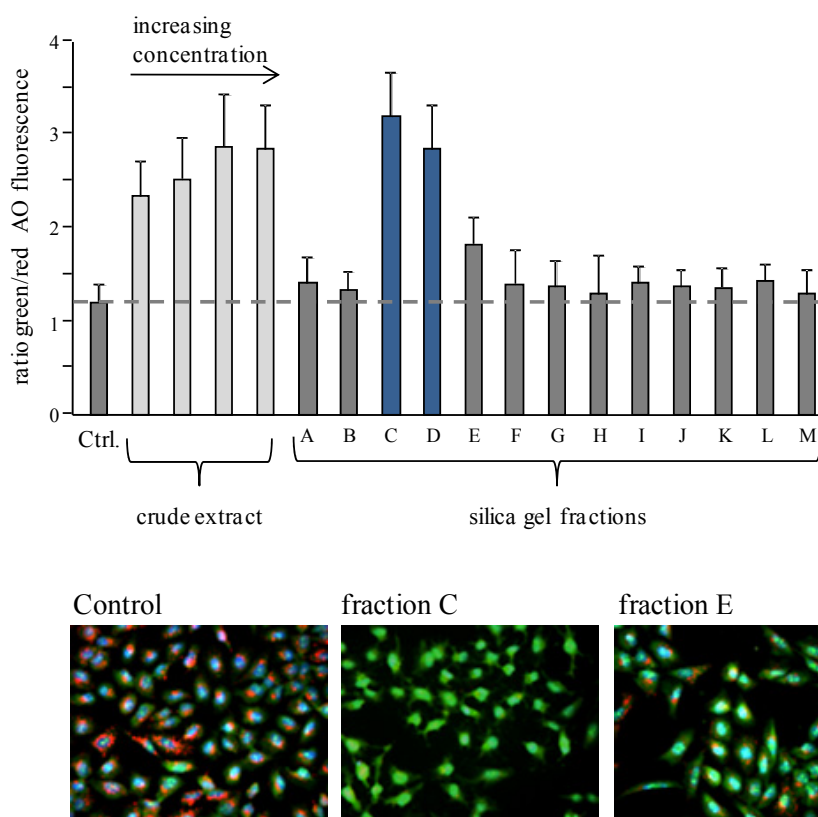


Figure 3-31: Induction of LMP in U-2 OS cells by SBCm007 silica gel fractions.

U-2 OS cells were either left untreated or treated for 4 h with SBCm007 crude extract or silica gel fractions derived thereof at a final concentration of 50 $\mu\text{g/ml}$. Cells were stained with AO (pseudocolors green/red) and Hoechst33342 (pseudocolor blue) and analyzed by HCS. The AO fluorescence ratio green/red is calculated based on average values from all cells within a well. The dashed line indicates the value of the control. Error bars display \pm SD of green fluorescence within the cytoplasmic segment. Main chondramide fractions are marked in dark blue.

For secondary purification via RP-HPLC the most active primary fractions determined in HCS assay were chosen, i.e. SEC fraction 22 and silica gel fraction C. Although the latter contains significant amounts of cytostatic chondramides, deconvolution of differential effects was considered to be practicable using HCS (Figure 3-32).

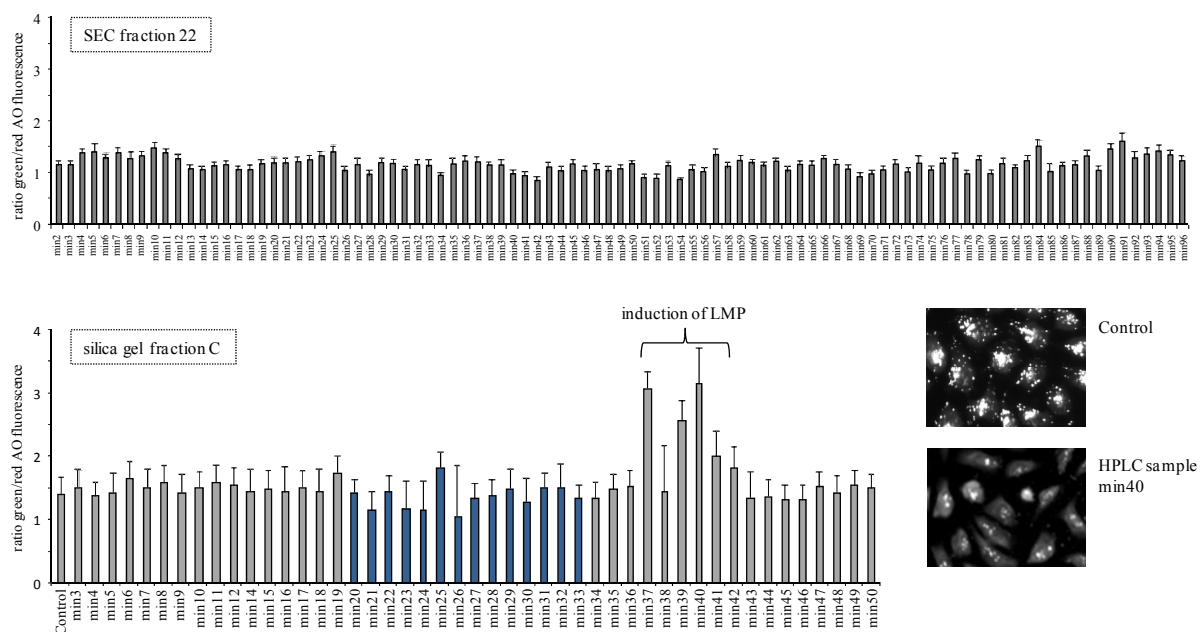


Figure 3-32: HCS on LMP with RP-HPLC fractions of SEC fraction 22 and silica gel fraction C.

Assigned primary fractions were further separated by RP-HPLC and samples were collected in 1 min intervals. Obtained RP-HPLC fractions were tested using U-2 OS cells that were stained with AO and Hoechst33342 after 4 h treatment. The AO fluorescence ratio green/red is calculated based on average values from all cells within a well. Error bars display \pm SD of green fluorescence within the cytoplasmic segment. Chondramide-containing fractions are marked in dark blue. Exemplary images recorded in red fluorescence channel are given for the untreated control and cells treated with HPLC sample min40 derived from silica gel fraction C.

Unfortunately, the bioactivity with respect to LMP induction found in SEC fraction 22 could not be tracked down to a further purified RP-HPLC fraction. None of the samples showed a significant effect on the lysosomal pH. Nevertheless, with HPLC fractions of silica gel fraction C, actin-polymerizing effects, as determined in an analogous HCS experiment on actin filaments, and LMP induction could be clearly separated. Despite this success, compounds responsible for the de-acidification of lysosomes could not be isolated in the course of this study. This shortcoming may be explained by the very low abundance of the respective metabolites in the crude extract, which also did not allow for a precise definition of target masses.

3.2.4 BIOACTIVITY-GUIDED ISOLATION OF NEW CHONDRAIMIDES

In addition to HCS on lysosomal integrity, primary fractions derived from column chromatography (silica gel) of *Chondromyces sp.* SBCm007 crude extract were generally evaluated for cytotoxic effects in a tetrazolium salt-based viability assay (Figure 3-33).

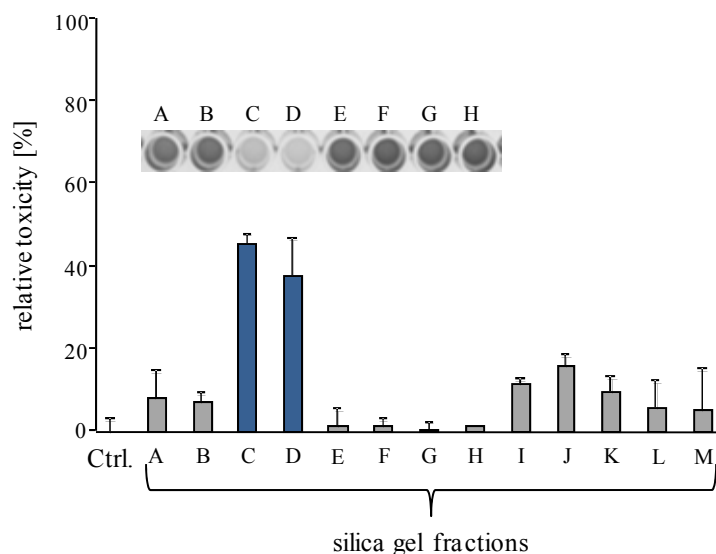


Figure 3-33: Relative toxicity of primary silica gel fractions on U-2 OS cells.

Human U-2 OS osteosarcoma cells were either left untreated or treated for 48 h with SBcm007 silica gel fractions at a final concentration of 50 $\mu\text{g/ml}$. Viability was assessed in an MTT assay and the value of the control was set to 0% toxicity. Error bars display \pm SD of three independent measurements. Main chondramide fractions are marked in dark blue. The insert image displays the assay read-out for fractions A-H; the darker the wells the more MTT was reduced and the more viable cells are.

The presence of known chondramides A~D, as analyzed by HPLC-MS, could be clearly confirmed in fractions C and D and in addition, a modest toxicity (<20%) was found in silica fractions A and B, and I-M. The activity in fractions A/B might be explained by the insufficient separation of chondramides by column chromatography and thus, minute amounts of chondramides might also be present in these fractions. However, this cannot explain the toxicity found with fractions I-M. Therefore, silica gel fractions were subjected to additional HCS studies. In first instance, it was of interest whether toxicity of fractions A/B in fact comes from known chondramides and thus, alterations of cellular and nuclear shape and actin filaments were assessed (Figure 3-34). Surprisingly, actin polymerizing effects were found in all silica gel fractions, although viability assays based on tetrazolium salt reduction (Figure 3-33) and MS analysis confirmed the presence of known chondramides only in fractions C and D. The HCS images were segmented and analyzed as described for assays on microtubules

(see section 3.1.6) and again, the standard deviation of cytoskeletal fluorescence in the cytoplasmic segment turned out to be most suitable for the characterization of actin polymerization.

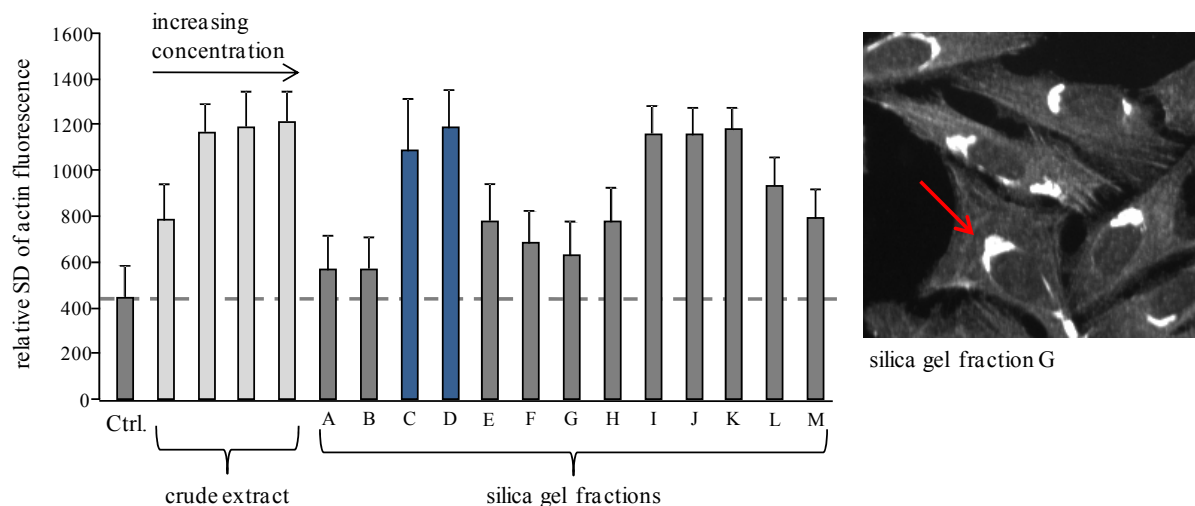


Figure 3-34: Actin polymerization in U-2 OS cells treated with SBCm007 silica gel fractions.

U-2 OS cells were either left untreated or treated for 24 h with SBCm007 crude extract or silica gel fractions derived thereof at a final concentration of 25 $\mu\text{g}/\text{ml}$. Cells were immunostained on β -actin and nuclei were stained with Hoechst33342. Cytoplasmic actin fluorescence standard deviation was analyzed on a single cell basis as average value per well. The dashed line indicates the value of the control. Error bars display \pm SD of actin fluorescence standard deviation. Fractions containing chondramides A~D are marked in dark blue. The image shows actin lumps (indicated by a red arrow) upon treatment with fraction G.

Initially, some of the silica fractions were further fractionated by RP-HPLC and subjected to HC screening. Indeed, in all cases the active HPLC fractions could be defined (as exemplarily shown for fractionated silica fraction G, Figure 3-35) and narrowed down to an elution time frame of 4-5 min within a total run length of 54 min. This in turn, enabled the definition of target masses and the subsequent purification of these metabolites. Candidate compounds were subjected to full structural elucidation using MS and NMR techniques and were thereby identified as novel chondramide derivatives, exhibiting some structural features, which are not described for members of the chondramide family so far. In total, 14 new structures were identified by NMR and the amounts of 11 new chondramides were sufficient enabling the biological characterization of these derivatives (Figure 3-36 and Table 3-5).

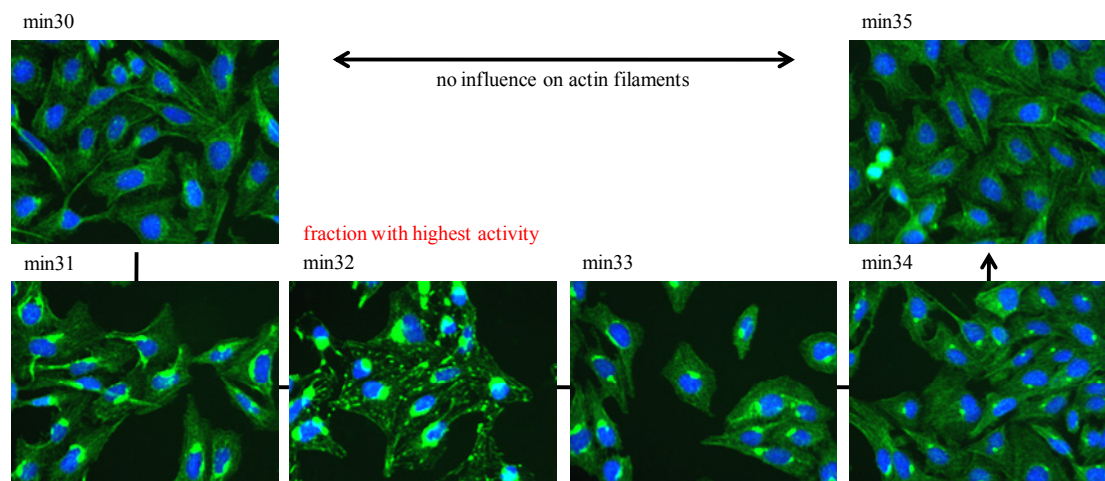


Figure 3-35: Bioactivity in secondary RP-HPLC fractions of silica gel fraction G.

Silica gel fraction G was separated by RP-HPLC and samples were subjected to HCS on actin filaments using U-2 OS cells. Cells were immunostained on β -actin (pseudocolor green) and nuclei were stained with Hoechst33342 (pseudocolor blue). Actin-targeting compounds eluted between min31 and min34.

Encouraged by the discovery of new chondramides, HR-MS data of crude extracts were extensively evaluated and the analysis was guided by the hypothesis that novel derivatives could exist which might be highly variable in terms of substitution of the peptide part and/or altered in the polyketide part of the molecule. Indeed, additional 24 different derivatives could be detected based on the combined evaluation of HR-MS, isotope pattern and tandem-MS fragmentation.

Briefly summarized, novel chondramide scaffolds include analogs that are phosphorylated or glycosylated at the aryl group on C7', halogenated (chlorine or bromine) at C6' and/or at C5'' of tryptophan, and/or altered in the polyketide moiety by incorporation of a different starter unit.

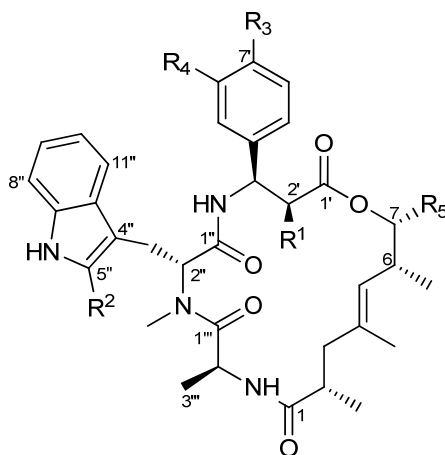


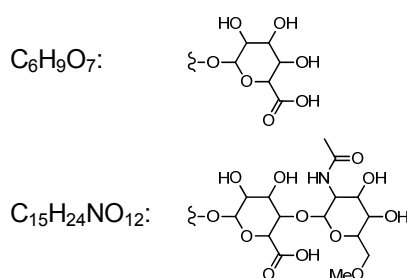
Figure 3-36: Chondramide core structure.

Table 3-5: Chondramides produced by *Chondromyces sp.* SBCm007.

Derivative ^[a]	R ¹	R ²	R ³	R ⁴	R ⁵
Chondramide A*	OMe	H	OH	H	Me
Chondramide B*	OMe	Cl	OH	H	Me
Chondramide C*	H	H	OH	H	Me
Chondramide D†*	H	Cl	OH	H	Me
Chondramide A3	OMe	H	OH	Cl	Me
Chondramide A4	OMe	Cl	OH	Cl	Me
Chondramide A6	OMe	Cl	P	H	Me
Chondramide A8	OMe	Cl	P	Cl	Me
Chondramide A9	OMe	H	C ₆ H ₉ O ₇ ^[b]	Cl	Me
Chondramide A10	OMe	Cl	C ₆ H ₉ O ₇ ^[b]	Cl	Me
Chondramide A3 (linear)†	OMe	H	OH	Cl	Me
Chondramide A10 Variant†	OMe	Cl	C ₁₅ H ₂₄ NO ₁₂ ^[b]	Cl	Me
Bromo-Chondramide A3	OMe	H	OH	Br	Me
Bromo-Chondramide C3	H	H	OH	Br	Me
Propionyl-Chondramide C1	H	H	OH	H	Et
Propionyl-Bromo-Chondramide C3	H	H	OH	Br	Et
Chondramide E2†	OH	Cl	OH	H	Me
Chondramide E4	OH	Cl	OH	Cl	Me

[a] The chondramide scaffold is given in Figure 3-36. Listed are derivatives, which were purified from SBCm007 extracts and were confirmed by NMR. *Known chondramides; †no biological evaluation.

[b] Planar structure of the carbohydrate moieties:



3.2.5 DETERMINATION OF GI₅₀ VALUES OF CHONDRAMIDES

The biological activity of the newly discovered chondramides was compared to the already described chondramide derivatives A~C. The growth inhibitory potential was assessed in tetrazolium salt-based assays (MTT) after 5 d treatment of cells with the compounds in serial dilution (Table 3-6). For the evaluation, a small panel of cancer cell lines (U-2 OS, HCT-116,

KB-3.1, and the MDR cell line KB-V.1), wildtype fibroblast cell lines (L-929 and MRC5), and primary cells (HUVEC) were used.

Table 3-6: GI₅₀ values^[a] [nM] of chondramides.

Chondramide derivative ^[b]	Cell Line ^[c]						
	HCT-116	U-2 OS	KB-3.1	KB-V.1	L-929	MRC5	HUVEC
A	48.9	27.1	50.5	38.0	90.9	63.8	43.7
B	30.1	20.8	40.7	56.4	80.8	20.9	30.7
C	33.7	25.6	36.8	85.8	87.3	26.1	34.0
A3	28.6	46.7	63.5	85.7	72.8	38.0	50.5
A4	44.4	26.4	56.8	83.1	67.6	12.7	52.5
A6	60.9	51.6	49.3	23.1	44.6	25.9	67.7
A8	49.3	33.2	13.4	58.1	56.2	7.6	24.1
A9	n.a.	n.a.	n.a.	w.a.	w.a.	w.a.	n.a.
A10	n.a.	n.a.	w.a.	w.a.	w.a.	n.a.	n.a.
Br-Chondr. A3	42.9	37.7	74.5	11.2	69.4	44.5	23.7
Br-Chondr. C3	17.7	4.8	46.8	23.8	14.0	57.7	44.4
Prop.-Chondr. C1	42.1	15.1	56.3	22.7	30.0	71.9	54.6
Prop.-Br-Chondr. C3	17.2	9.0	38.0	31.9	23.0	129.8	50.2
E4	378.8	351.9	627.2	251.5	554.8	479.7	207.4

[a] Compounds were tested in serial dilution for 5 d on various cell lines and viability was assessed in an MTT assay. GI₅₀ values were determined by sigmoidal curve fitting and calculated as the average of two independent measurements. n.a.: not active up to 10 μM; w.a.: weak activity in the range of 5-10 μM. [b] For chemical structures see Figure 3-36 and Table 3-5. Chondr.: Chondramide; Prop.: Propionyl. [c] HCT-116: human colon carcinoma; U-2 OS: human osteosarcoma; KB-3.1: human cervical carcinoma; KB-V.1: human cervical carcinoma (MDR); L-929: mouse subcutaneous connective tissue fibroblasts; MRC5: human lung fibroblasts; HUVEC: human umbilical vein endothelial cells.

Already described chondramides A~C exhibited GI₅₀ values in the mid nanomolar range on all tested cell lines without any apparent specificity for certain cell lines. Newly discovered chondramides A3, A4, A6, and A8 were likewise active suggesting that neither chlorination at C6' nor phosphorylation on C7' of the aryl moiety has a great impact on overall potency. Contrary, glycosylation at C7' is not tolerated and for chondramides A9 and A10 GI₅₀ values could not be determined in the assay's concentration range. Also chondramide E4, bearing a chlorine at C6' and a hydroxyl at C2' instead of a methoxy group or hydrogen, was approximately by one order of magnitude less active than chondramide reference compounds (A~C). Brominated chondramides were, in general, active in the low nanomolar range but interestingly, bromo-chondramide C3 and its propionyl analog displayed a slightly higher

potency on cancer cell lines and a less toxic effect on human non-cancerous cells compared to chondramides A~C.

In addition to GI_{50} determination, the actin-targeting mechanism was confirmed for all tested derivatives in human U-2 OS osteosarcoma cells as exemplarily shown for propionyl-chondramide C3 and bromo-chondramide C3 (Figure 3-37).

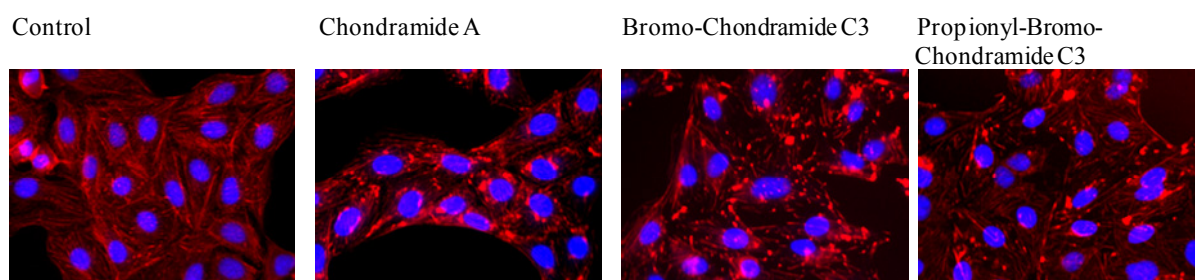


Figure 3-37: Actin polymerization induced by novel chondramides.

Human U-2 OS osteosarcoma cells were either left untreated or treated for 4 h with chondramides at a final concentration of 100 nM. Actin was labeled with Acti-Stain555-phalloidin (pseudocolor red) and nuclei were stained with Hoechst33342 (pseudocolor blue).

3.2.5 *IN VITRO* ACTIN POLYMERIZATION

Since the GI_{50} values for some of the new derivative were significantly different to those determined for chondramides A~C, all compounds were evaluated in a cell-free system on actin polymerization. Especially glycosylated chondramides A9 and A10, which lost potency by at least three orders of magnitude (GI_{50} values $>10 \mu\text{M}$), might eventually exhibit higher *in vitro* potency than suggested by the cell-based assay. For better comparability compounds were grouped as follows: chondramides with GI_{50} values $>100 \text{ nM}$ (Figure 3-38), brominated derivatives (Figure 3-39), and other chondramides with mid nanomolar activity (Figure 3-40).

The studies were performed using pyrene-labeled rabbit muscle actin^[224] at a concentration of $5 \mu\text{M}$ under non-polymerizing (low salt) conditions. In a pre-evaluation study with reference compounds chondramide A~C it was found that a final concentration of $20 \mu\text{M}$ of the polymerization inducers gave best results, thus, every chondramide derivative was tested under these conditions and fluorescence of pyrene-actin was followed over 85 min at 37°C .

For chondramides A and B saturation was observed after approximately 30 min and also chondramides C potently induces actin polymerization *in vitro*. As indicated by the cell-based growth inhibition studies, the glycosylated chondramide A9 does not exhibit any actin-polymerizing effect under the tested conditions. Nevertheless, glycosylated chondramide A10

shows a slow increase in G-actin polymerization, which is significantly less pronounced than observed for reference compounds chondramides A~C. Chondramide E4 was by one order of magnitude less potent compared to chondramides A~C with regards to its GI₅₀ values, a fact, which might also partly be explained by its decreased ability to polymerize actin.

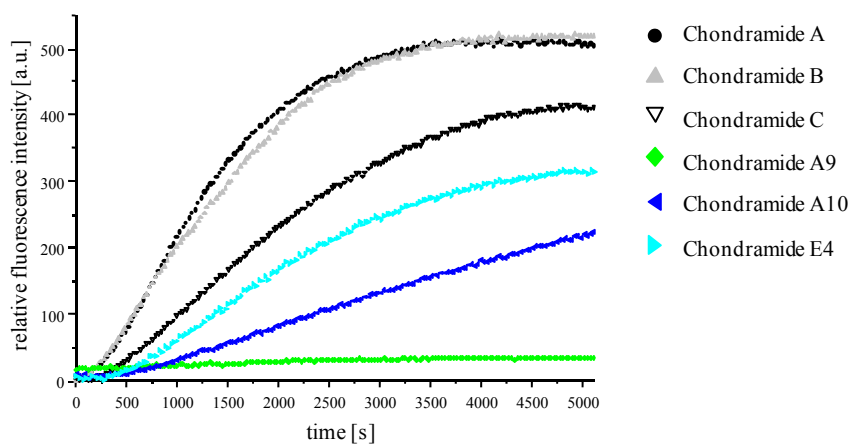


Figure 3-38: Induction of G-actin polymerization by chondramides with reduced cytostatic potency.

Chondramides were applied at a final concentration of 20 μM and fluorescence intensity of pyrene-actin (5 μM) was measured at 37°C for 85 min, every 30 s, at an emission wavelength of 405 nm (excitation at 360 nm). Curves represent the average of two independent experiments.

Brominated chondramide C3 derivatives, which were, by tendency, the most active derivatives in terms of cancer cell inhibition, were only poorly active in actin polymerization studies. However, it is also noticeable that bromo-chondramide A3, the least potent amongst the brominated analogs, quickly polymerizes G-actin, with similar efficacy as chondramides A and B. Furthermore, chondramides A3, A6, A8, and propionyl-chondramide C1, although having GI₅₀ values comparable to chondramides A~C, show a significantly reduced actin-polymerizing effect, merely chondramide A4 is similarly potent in the cell-free system. Table 3-7 summarizes the relative effects on G-actin polymerization.

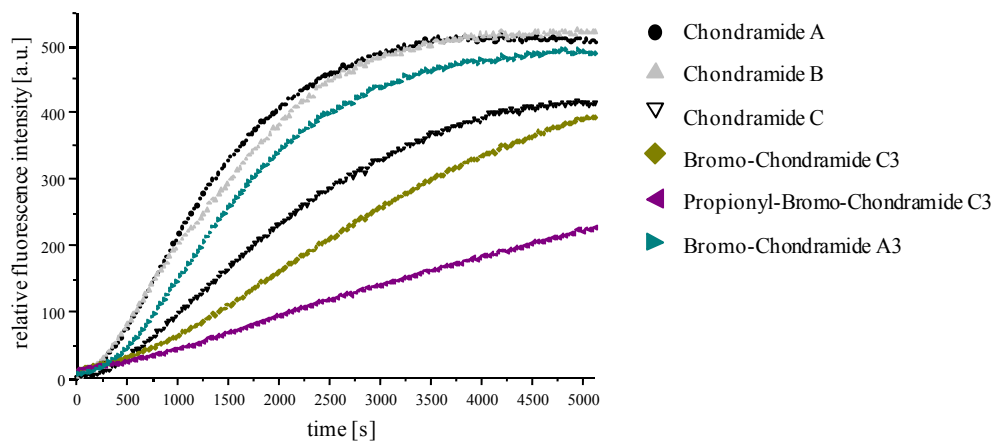


Figure 3-39: Induction of G-actin polymerization by brominated chondramides.

Chondramides were applied at a final concentration of 20 μM and fluorescence intensity of pyrene-actin (5 μM) was measured at 37°C for 85 min, every 30 s, at an emission wavelength of 405 nm (excitation at 360 nm). Curves represent the average of two independent experiments.

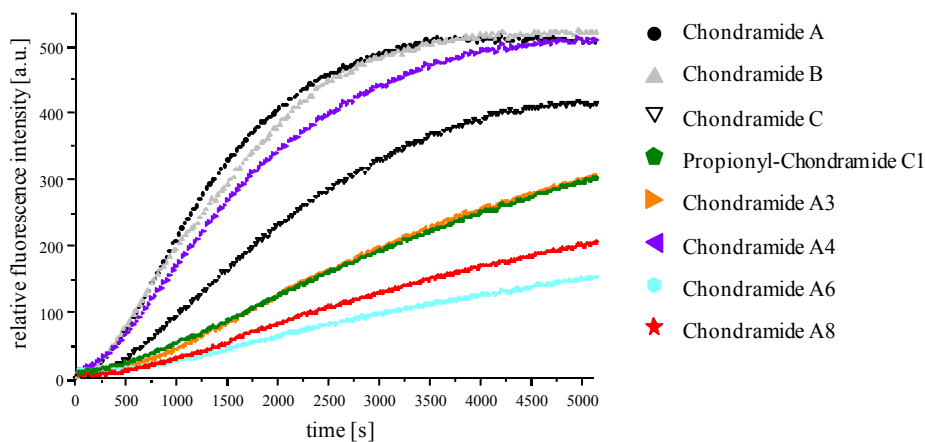


Figure 3-40: Induction of G-actin polymerization by several chondramide derivatives.

Chondramides were applied at a final concentration of 20 μM and fluorescence intensity of pyrene-actin (5 μM) was measured at 37°C for 85 min, every 30 s, at an emission wavelength of 405 nm (excitation at 360 nm). Curves represent the average of two independent experiments.

Table 3-7: Summarized values for G-actin polymerization.

Compound	relative slope [RFU per min]^[a]
Chondramide A	14.7 ± 0.20
Chondramide B	11.8 ± 0.14
Chondramide C	8.3 ± 0.08
Chondramide A3	4.5 ± 0.08
Chondramide A4	12.0 ± 0.10
Chondramide A6	1.9 ± 0.06
Chondramide A8	2.7 ± 0.06
Chondramide A9	0.2 ± 0.04
Chondramide A10	2.9 ± 0.05
Bromo-Chondramide A3	13.2 ± 0.08
Bromo-Chondramide C3	5.1 ± 0.07
Propionyl-Chondramide C1	3.9 ± 0.06
Propionyl-Bromo-Chondramide C3	2.8 ± 0.06
Chondramide E4	6.2 ± 0.12

[a] Corresponding curves are displayed in Figures 3-38, 3-39, and 3-40. The slope ± SD (increase of relative fluorescence units per minute) was calculated for each sample in the linear range of the curve.

DISCUSSION

4.1 PRETUBULYSIN AS POTENTIAL NOVEL LEAD STRUCTURE

This section deals with results from the biological evaluation of pretubulysin. Structure-activity relationships of several synthetic derivatives, apoptotic mechanisms induced by pretubulysin and its putative application as molecular probe in studies on microtubule assembly are discussed in detail. Due to only a minor loss in activity of pretubulysin compared to two intensely studied parent compounds (tubulysins A and D) and since the typical supply issue encountered with natural products can be circumvented, pretubulysin might emerge as novel lead structure in tumor therapy.

4.1.1 STRUCTURE-ACTIVITY RELATIONSHIP OF TUBULYSINS AND PRETUBULYSINS

Within the myxobacteria tubulysins are frequently produced but restricted to the suborder Cystobacterineae. Thus, these compounds were found in strains of the genera *Angiococcus*, *Archangium*, *Cystobacter*, and *Stigmatella*. Nine tubulysin derivatives were initially described from myxobacterial strains *Archangium gephyra* Ar 315 and *Angiococcus disciformis* An d48 (Figure 4-1). Tubulysins were found by bioactivity-guided isolation because of a superior cytotoxicity of the respective myxobacterial extracts on mouse L-929 fibroblast cells. Isolated derivatives were completely inactive against bacteria and yeast but exhibited moderate activity against some filamentous fungi. However, GI₅₀ values determined on several cell lines were in the low picomolar to low nanomolar range and by this, tubulysins surpass the growth inhibition potential of other antimetabolites, such as epothilones, vinblastine, and taxol, by a factor of 20-1000.^[192, 225]

The antiproliferative potential of tubulysins correlates well with their lipophilicity so that tubuphenylalanine derivatives, being rather lipophilic, are generally by one order of magnitude more potent than corresponding tubutyrosine analogs. The 11-acyloxy side chain on Tuv seems to play only a minor role although within the two groups (Tup and Tut derivatives) analogs with a 3-methylbutyryl side chain (tubulysins D and A) are the most active and analogs with an acetyl side chain (tubulysins H and I) are the least active. Interestingly, *in vitro* tubulin polymerization inhibition was approximately constant with all derivatives leading to the conclusion that preferential cellular uptake of more lipophilic tubulysins, in part, explains their greater potency in cell-based assays on growth inhibition.^[225] Similar results were obtained in a recent study on several tubulysin analogs, which were obtained from mixtures of natural Tut type tubulysins via TFA-mediated

formation of an *N*-acyliminium ion within the Tuv segment. Upon treatment of this intermediate species with either alcohols, thiols, or nitriles the respective *N*-acyl-*N,O*-acetals, *N*-acyl-*N,S*-thioacetals, or *N,N'*-diacyl-aminals were formed and derivatives with varying alkyl side chain at the *N,O*- or *N,S*-acetals exhibited very similar GI₅₀ values on human cancer cells that were all in the low nanomolar range.^[226]

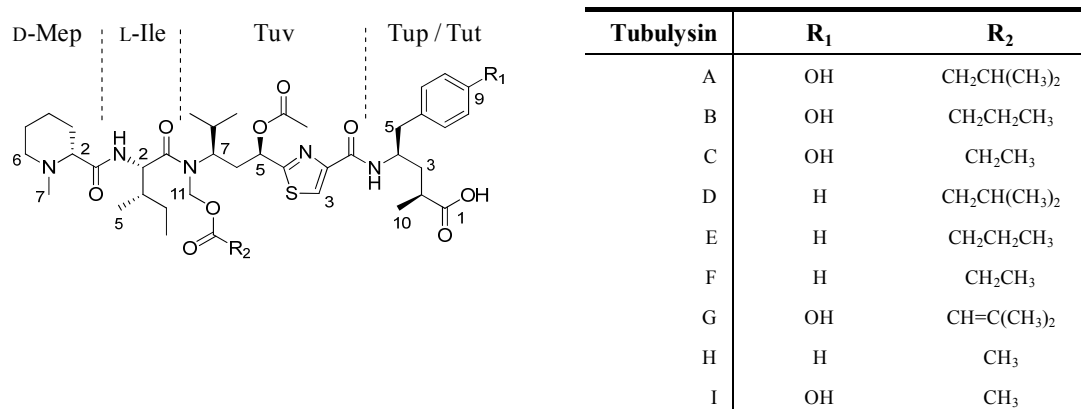


Figure 4-1: Natural tubulysins isolated from myxobacterial strains.

Archangium gephyra produces tubulysin A (2-4 mg/L) and as minor components tubulysins B, C, G, and I with a *p*-hydroxyphenyl residue (Tut). *Angiococcus disciformis* produces phenyl analogs (Tup) D, E, F, and H (all ca. 0.5 mg/L).

Because of tubulysins' distinct structure and high potency, these compounds have attracted considerable synthetic interest. Total synthesis efforts towards tubulysins revealed the introduction of the acid and base labile *N,O*-acetal functionality present on the Tuv fragment in a cluster of other sterically demanding groups, such as the *O*-acetate group at Tuv-C5, and stereochemical requirements of the *C*-terminal γ -amino acid as most challenging.^[196, 227] Several reports on the synthesis of tubulysin fragments have been published^[228, 229, 230], whereas introduction of the labile *N,O*-acetal at the Tuv amino group was not achieved until 2006, when Peltier *et al.*^[201] published the first total synthesis of tubulysin D with an 13% overall yield over 16 synthetic steps. Another series of tubulysins (tubulysins U-Z) without the *N,O*-acetal ester fragment, was the subject of several synthetic studies. Tubulysin U, which lacks the *N,O*-acetal functionality, and tubulysin V, which additionally bears a hydroxyl instead of an acetate at Tuv-C5, can be prepared by total synthesis in reasonable quantities.^[231, 232, 233] Evaluation of their antiproliferative activity revealed that these derivatives are less active by several orders of magnitude (in the low to high nanomolar range) compared to other natural tubulysins. However, syntheses around tubulysins U and V

enabled important SAR insights. Tubulysin U is by two orders of magnitude more active than tubulysin V revealing the great impact of the acetylated Tuv segment. It was also found that the absolute stereochemistry of the Tuv-C5 functional group is important since *epi*-tubulysin V (a stereoisomer of tubulysin V) is by factor of 30 to 45 less potent than the natural variant.^[234] Other stereoisomers of Tuv in tubulysin D (*5-epi*-, *7-epi*-, and *5,7-di-epi*-tubulysin D) basically revealed a similar relationship. Inverted configuration at either Tuv-C5 or Tuv-C7 lead to a decreased potency (mid nanomolar range), whereas *5,7-di-epi*-tubulysin D was essentially inactive.^[235] On the contrary, a Tut-C2 epimer of tubulysin B exhibited equal potency to the corresponding natural tubulysin.^[236] In addition, growth inhibitory studies with tubulysin V variants that all bear a ketone group at Tuv-C5 and an acyclic *N*-Mep, displayed the importance of the stereogenic α -methyl group in Tup; the desmethyl variant was active in the high nanomolar range, whereas the dimethyl and methyl variants were essentially inactive with GI₅₀ values in the mid micromolar range or even not active up to 50 μ M, respectively.^[234] Complementary to tubulysin U and V derivatives with a secondary amine in the Tuv segment, Wipf and Wang^[237] synthesized a desacetoxytubulysin with a simple *N*-methyl group in 20 steps and 2.1% overall yield. This replacement was not essential for the antiproliferative activity resulting in GI₅₀ values in the low nanomolar range, comparable to the tubulin-binder vinblastine. Replacement of *N*-Mep by *N*-methylsarcosine, however, significantly lowered potency by approximately two orders of magnitude. Similar to the reported *epi*-tubulysin V, the natural (*R*)-configuration of the acetate on Tuv-C5 in the desacetoxy variant is preferred with regards to *in vitro* tubulin assembly inhibition but exhibits nearly equal potency in cell-based studies than its diastereomer.^[238] In desmethyl and dimethyl Tup derivatives of tubulysin (secondary amine instead of *N,O*-acetal and Tuv-C5 keto group) the role of the *N*-terminus was probed. Replacing the natural *N*-Me-D-Pip in either a Tup-C2 desmethyl or dimethyl variant by *N*-Me-D-Pro reduced the antiproliferative activity approximately by factor 10, whereas dimethyl analogs were generally more potent. However, the natural D-configuration and the *N*-methyl group on either Mep or MePro appeared to be essential for biological activity.^[239, 240]

In summary, as exemplified by comprehensive SAR studies on tubulysin D analogs by the Ellman group^[241, 242], various modifications can be introduced on the C-terminus of tubulysins with only modest loss in antiproliferative activity. By retaining only the phenethyl or γ -carboxy group of the Tup fragment, derivatives were still active in the low nanomolar range. Interestingly, also an *N*-methyl analog and the truncated tripeptide lacking Tup were considerably active. Thus, this site seems to be appropriate for further modifications or the

attachment of functionality, such as fluorophors or targeted antibodies. Contrary, modifications of the *N*-terminus seemed to be only tolerated, in terms of potent antiproliferative activity of derivatives, when a basic tertiary amine is still present. Variants with a simple *N*-acetyl group or completely lacking Mep lost activity by three orders of magnitude. Furthermore, neither the *O*-acetyl group of Tuv nor the *N,O*-acetal side chain were significantly influencing biological activity.^[241]

Figure 4.2 summarizes the aforementioned basic SAR conclusions with tubulysin A as the core structure.

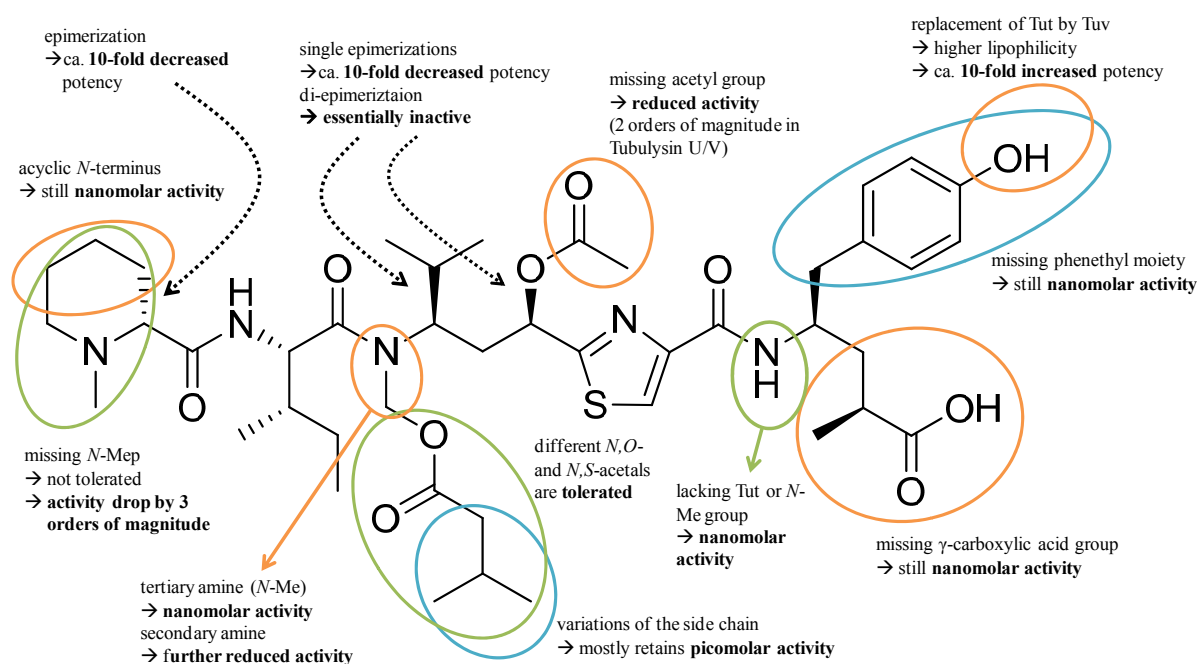


Figure 4-2: Structure-activity relationships of tubulysins.

Tubulysin A, which is displayed as the core structure, exhibits antiproliferative activity in the mid picomolar range on various cancer cell lines. Several studies on either natural tubulysins or synthetic derivatives accounted for important SAR conclusions. A highly simplified overall conclusion is that variations of the *N,O*-acetal of Tuv and simplifications of the *C*-terminal amino acid are very well tolerated, whereas variation of the *N*-terminal Mep has a much higher impact.

In addition to great achievements in the course of synthetical surveys, the biosynthesis of tubulysins was the subject of several comprehensive studies. The biosynthetic gene cluster for tubulysin synthesis was first identified in *A. disciformis* An d48 by transposon mutagenesis and molecular analysis revealed that the secondary metabolites are assembled by a multienzyme PKS/NRPS hybrid system that consists of five NRPS modules and two PKS

modules. In this study of the biosynthetic machinery, a precursor of tubulysin was postulated for the first time; this precursor is released from the last module in the assembly line, the type I PKS TubF. The enzyme-free precursor, referred to as ‘pretubulysin’, would then undergo oxidation and acylation reactions to form the natural product (cf. Figure 1-13). However, no candidate gene encoding the respective enzymes for oxidation and acylation could be identified and confirmed.^[243] The gene cluster also contains a cyclodeaminase-encoding gene, *tubZ*, which is putatively involved in the formation of the starter unit pipercolic acid. The gene was inactivated in strain An d48 to probe its function, and it was expected that tubulysin production would be completely abolished. Astonishingly, tubulysin production in an An d48-*tubZ*⁻ mutant strain was only reduced to approximately 3% of the wild-type level. Furthermore, the proposed pretubulysin could be detected in substantial amounts in the mutant strain and, after reanalysis, in minute amounts in the wild-type strain. Despite growing *A. disciformis* on a larger scale, pretubulysin could not be isolated in sufficient amounts for further development. Therefore, the total synthesis of pretubulysin was initiated, and the biosynthetic hypothesis was finally proven by comparing synthetic and naturally occurring pretubulysin via mass spectrometry and NMR.^[202] The biological characterization of pretubulysin, which can be obtained synthetically in gram-scale quantities, was the subject of this thesis.^[203, 244] Having a practical chemical synthesis in hands, other even more simplified pretubulysin analogs were prepared and their biological activity was evaluated using a panel of different cell lines. In initial growth inhibition experiments, it turned out that pretubulysin was active in a low to sub-nanomolar range against various cell lines from different origin and tissue, including colon, hepatocellular, and cervical carcinoma, and exhibits a mean GI₅₀ value of ca. 1.6 nM on cancer cell lines. Thus, based on GI₅₀ values, pretubulysin is, on average, only a factor of 10 or 100 less active than naturally occurring tubulysin A (mean GI₅₀ of 0.17 nM) and tubulysin D (mean GI₅₀ of 0.02 nM), respectively. Furthermore, a significant antiproliferative activity on Pgp-overexpressing MDR cell lines (here: KB-V.1) was found for pretubulysin, as already reported for the natural parent compounds^[192] (Table 3-2). Antiproliferative testing in mouse L-929 cells of a series of pretubulysin derivatives with shorter chain at the C-terminus and reference compounds (Figure 3-1 and Table 3-1a) again revealed that tubulysins D and A exhibit GI₅₀ values in the picomolar range, whereas pretubulysin was approximately 20-fold less active (5.8 nM). However, activity was nearly abolished in all other analogs. Pretubulysin analog I in which the propionate group of Tup was missing (9.6 μM) or analog II in which the C-terminal amino acid was missing completely (14.2 μM) were by three orders of magnitude less potent than pretubulysin.

Contrary, for tubulysin D derivatives that resemble pretubulysin analog I and II a nanomolar activity was detected^[241]. However, it has to be taken into account that the natural tubulysin D is already by two orders of magnitude more potent than pretubulysin with a GI₅₀ value of 20 pM in L-929 cells. Interestingly, the MepIleMe'Val' derivative in which Val is replaced by the C2-prolonged homolog (γ -amino acid; pretubulysin analog III) exhibited slightly increased activity relative to analog II (MepIleTuv), with a GI₅₀ value of 6.5 μ M against L-929 mouse cells. This finding is particularly striking since analog III completely lacks the two aromatic rings of pretubulysin. This compound was therefore tested on three cancer cell lines (Table 3-2) and GI₅₀ values were determined to be in the micromolar range. By tendency, human HL-60 promyelocytic leukemia cells were the most sensitive towards pretubulysin analog III treatment (GI₅₀ of 1.25 μ M), which is accordance to the results from other tubulysins and pretubulysins. However, single Mep, MepIle, and MepIleMeVal building blocks did not inhibit L-929 cells at concentrations up to 25 μ M.

Other pretubulysin derivatives with variations of the *N*- and *C*-terminus, thiazole ring of Tuv, and of aliphatic side chains on Ile-C2 and the tertiary amine of Tuv were evaluated in growth inhibition experiments using human U-2 OS osteosarcoma cells (Figure 3-2 and Table 3-1b). As determined with other cell lines, pretubulysin is active in the low nanomolar range (GI₅₀ of 0.84 nM). On the *C*-terminus of the molecule different variations were probed. The 2-desmethyl variant was still active in a low nanomolar range (4.93 nM). Thus, potency was reduced approximately by factor 10, as additionally determined in a larger panel of various cell lines (Table 3-2). However, a dehydrogenation of C2-C3 in Tup was shown to have a much higher impact. 2,3-didehydro-pretubulysin, either as free acid or ethyl ester, exhibited GI₅₀ values in the high nanomolar range, which depicts a lowered potency compared to pretubulysin by at least three orders of magnitude. Other variations of the *C*-terminal amino acid (pretubulysins with propargylamide or *n*-butylamide functionalities instead of the γ -carboxylic acid functional group in Tup) led to GI₅₀ values in the mid nanomolar range, i.e. 50- to 100-fold reduced potency. It has been reported that variations of *N*-Mep generally have a higher impact on the molecule's potency than variations of the *C*-terminal amino acid. Indeed, *N*-methylsarcosine-pretubulysin was essentially inactive (GI₅₀ of 4.7 μ M) and its potency is comparable to the aforementioned MepIleTuv (analog II) or MepIleMe'Val' (analog III) derivatives that completely lack *N*-terminal Tup. Likewise, the methylproline derivative is by two orders of magnitude less potent than pretubulysin (GI₅₀ of 164 nM) and a pipercolic acid variant lacking the *N*-methyl group is even by three orders of magnitude less active (GI₅₀ of 1.1 μ M). Next, the influence of the thiazole ring in pretubulysin was assessed

and it turned out that substitution by either a phenyl or triazole functionality is not tolerated very well. Respective free carboxylic acid or methyl ester analogs were active in the high nanomolar to low micromolar range. Phenyl-pretubulysin exhibited a GI_{50} value of 119 nM on U-2 OS cells and triazole-pretubulysin was even 5-fold less active (644 nM). Corresponding methyl ester analogs further reduced potency approximately by factor 5. Solely a replacement of the thiazole by an oxazole ring did not impact potency (GI_{50} of 1.55 nM) and the corresponding methyl ester was also still active in the low nanomolar range (10.0 nM). Upon testing of oxazole-pretubulysin in a larger panel of cell lines it could be shown that this derivative is equally potent to pretubulysin. Another series of pretubulysins was available that varied in the alkylation pattern of the tertiary amine in Tuv or the Ile-C2. Replacing the *N*-Me group by either an allyl or ethyl group did not influence pretubulysin's potency and GI_{50} values were still in the low nanomolar range (1.5 nM and 0.9 nM, respectively). This is in accordance to SAR conclusions from natural tubulysins bearing an *N,O*-acetal group, whereas it was found that variations of this position are mostly very well tolerated with regards to full bioactivity. On the other hand, the influence of aliphatic groups on Ile-C2 seems to be mostly controlled by the sterical demand of these groups. The 2-isopropyl variant has comparable antiproliferative potency than pretubulysin that bears a 2-*sec*-butyl group instead. However, a 2-isopropyl variant loses activity by approximately one order of magnitude (GI_{50} of 46 nM) and Ile-C2-benzyl-pretubulysin was inactive up to a concentration of 5 μ M.

By tendency, SAR conclusions from pretubulysin testing (Figure 4-3) resemble those from previously reported studies on natural tubulysins (cf. Figure 4-2). In brief, variation of the C-terminus (on the γ -carboxy side chain of Tut) was somewhat tolerated with only a minor loss in activity, whereas *N*-terminal Mep appeared to be crucial for a nanomolar activity. Solely substitution of Mep with MePro was tolerated to some extent. The thiazole ring of Tuv might be replaced by an oxazole without impacting pretubulysin's potency, but phenyl and triazole are disadvantageous. Regarding aliphatic side chains, variations of the tertiary amine in Tuv and Ile-C2 substitution are tolerated, whereas bulky groups at the latter position significantly reduce potency. In addition, with systematically shortened analogs (starting from the C-terminus) potency was significantly reduced by three order of magnitude and single MepIleMeVal building blocks were inactive up to 25 μ M. Nevertheless, some of the variations appeared to have a greater impact with regards to biological activity than reported for e.g. tubulysin D, which might, in part, be explained by pretubulysin's *per se* 100-fold reduced potency compared to tubulysin D.

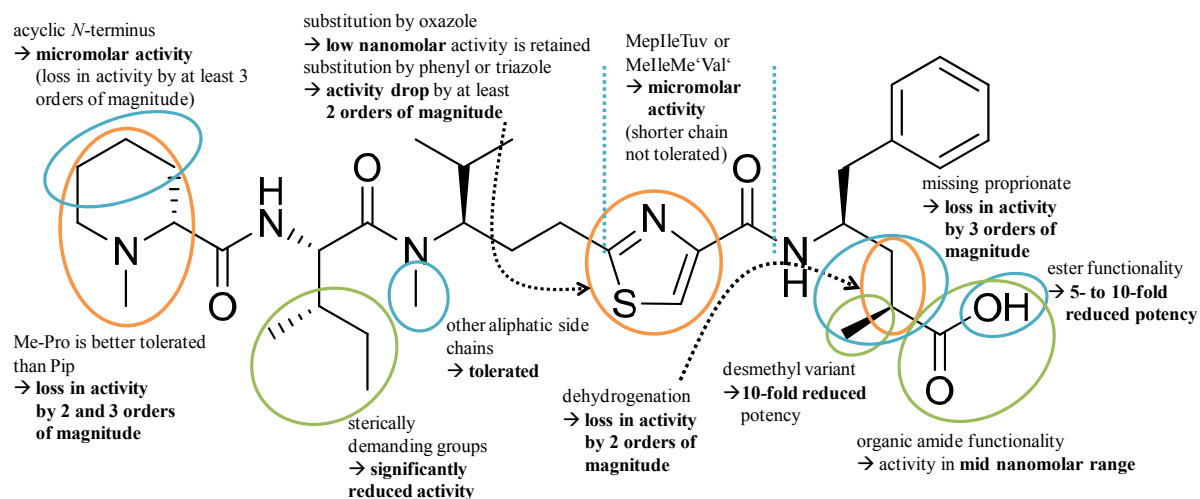


Figure 4-3: Structure-activity relationships of pretubulysins.

Pretubulysin, which shows antiproliferative activity in the low nanomolar range, is displayed as the core structure. Determination of the growth inhibitory potential of several synthetic derivatives allowed for important SAR conclusions. In addition to reported results from tubulysins, the role of the thiazole ring of Tuv was assessed in pretubulysin.

A way to assess SAR of NPs is not only via total synthesis and chemical derivatization but may also include screening for natural derivatives. In the case of tubulysins, a multitude of further natural tubulysin derivatives has been discovered in *A. disciformis* An d48 and *Cystobacter sp.* SBCb004 producer strains by using elaborate HPLC-MS analyses. It was found that many steps in the biosynthetic pathway do not go to completion and especially post-assembly reactions appeared to be relatively inefficient.^[245] In addition to these naturally produced derivatives, the ca. 40 kb core biosynthetic tubulysin gene cluster lacking acyl transfer and oxidation functions was recently reconstituted, and heterologous expression was achieved in two different host systems. This result paves the way for the production of another generation of bioactive tubulysin metabolites by genetic manipulations.^[246]

4.1.2 PRETUBULYSIN LEADS TO MITOTIC ARREST AND APOPTOSIS INDUCTION

Tubulysins are active on a wide variety of cancer cell lines from different origins and tissues, including lung, colon, cervix, ovarian, prostate, breast, and leukemia cancer lines, as determined in the NCI-60 test panel. Moreover, potency of tubulysins on Pgp-overexpressing MDR cell lines (e.g. KB-V.1 and HCT-15) remains extraordinary high and equals the activity on corresponding non-MDR cell lines (e.g. KB3.1 and HCT-116).^[192, 196, 199] Emerging multidrug resistance of cancer cells is common with many antimitotic agents but nevertheless, chemotherapeutics of this class are particularly successful in clinical applications. The MDR

phenotype may also include overexpression of other efflux pumps (e.g. MDR-1), upregulation of key players in apoptosis (e.g. antiapoptotic Bcl-2), post-translational modifications, and the expression of different tubulin phenotypes.^[167] Thus, there is an increasing demand for novel microtubule inhibitors in order to circumvent already established resistance.

In pre-clinical MoA studies with tubulysin A it was found that the NP has salient antimetabolic and antiangiogenic properties, which may translate into clinically useful anticancer features.^[199, 220] The tubulysin-induced depolymerization of microtubules was assessed on a biochemical and cellular level, revealing that tubulysin noncompetitively inhibits vinblastine binding to microtubules and also to a minor extent inhibited colchicine binding, which suggested a binding mode for tubulysin at the peptide site^[247], in close proximity to the vinca site of the *Vinca* domain on β -tubulin. As a consequence of irreversible microtubule depolymerization, eukaryotic cells accumulated in G₂/M phase of the cell cycle, which ultimately led to the induction of apoptosis, as specified by caspase-3 activation, nuclear fragmentation, and DNA laddering.^[220] Furthermore, cord formation and chemotaxis assays with primary cells (HUVEC) suggest a strong antiangiogenic effect of tubulysin A.^[199] Angiogenesis describes the formation of new small blood vessels *in vivo*, which plays a role in the growth of solid tumors^[248] and antiangiogenic properties have also been found for other antimetabolic agents, such as the microtubule-stabilizer paclitaxel, and have been linked to the cytostatic effect, which is mediated by the initiation of the intrinsic (mitochondrial) apoptosis pathway.^[249] In a current study, it could be shown that pretubulysin exhibits antiangiogenic properties at a similar level than tubulysin A and additionally, led to a dramatic reduction of tumor growth and vascular density without any obvious toxicity in an ectopic murine xenograft model with hepatocellular HUH7 carcinoma cells.^[204] Other pre-clinical *in vivo* data of tubulysins was likewise encouraging, although toxic side effects delayed further development. In order to improve the therapeutic index of highly cytotoxic tubulysins, several targeting strategies, such as ligand-coupling (targeting folate receptors)^[250], delivery via nanoparticles^[251], and peptide dendrimers^[252] have been applied.

Here, some of the underlying mechanisms of pretubulysin's cytostatic activity were evaluated and a summary is given in Figure 4-4, which displays a schematic overview of the induced cellular and molecular changes that were found in the course of this study.

In growth inhibition experiments, pretubulysin exhibited GI₅₀ values in the low nanomolar range on various cultured mammalian cells, and thus, was only 10- to 100-fold less active than the parent compounds tubulysins A and D, respectively. Additionally, pretubulysin was able to inhibit growth of the Pgp-overexpressing MDR cell line KB-V.1, as it was already

described for natural tubulysins^[192] (Table 3-2). As pretubulysin was most likely acting on the same target than tubulysins, its influence on the microtubule architecture was probed (Figure 3-11). While at high dosages of pretubulysin (50 nM) a complete disruption of microtubules, i.e. depolymerization, was observed in human U-2 OS osteosarcoma cells following 24 h treatment, at a lower dosage microtubules were not directly disrupted in their overall structure but abnormally accumulated around the nuclear periphery.

In fact, it has been shown for the microtubule destabilizer vinblastine, that a stabilizing effect can be observed at low concentrations by its ability to suppress dynamic mechanisms at the high-affinity binding sites at the end of microtubules.^[253] The same effect might explain the abnormal accumulation of interphase microtubules in pretubulysin-treated cells, which resembles a local stabilization. In addition, an HCS experiment (Figure 3-20) revealed that this phenomenon also occurred when U-2 OS cells were treated for 24 h with other microtubule-destabilizing agents (tubulysins A and D, disorazol A). Following segmentation of the nuclear and cytoplasmic area (Figure 3-17), the standard deviation of tubulin fluorescence was calculated within the latter segment, which is an indicative parameter of microtubule disruption. At concentrations near the respective GI₅₀ value of the antimetabolites, an increase in microtubule fluorescence SD was observed that upon image data dereplication turned out to be caused by an initial stabilizing effect. This peak value was followed by a decline in tubulin fluorescence SD, which is indicative for a depolymerization of microtubules. A second peak was observed with tubulysins A and D that reflects rounded-up, late apoptotic cells for which automated analysis and calculation of decisive parameters partially fails. Interestingly, cells treated with the microtubule stabilizer epothilone B led to similar results, although values for tubulin fluorescence SD were generally higher and a maximum value was achieved not until more-than-10-fold higher concentrations than the compound's GI₅₀ value, reflecting maximal stabilization of microtubules. At higher concentrations cells died, which is represented by lower SD values.

In addition to the described cell-based studies, it could be demonstrated in *in vitro* experiments that pretubulysin is able to inhibit the polymerization of tubulin protein and induce depolymerization of built-up microtubules, in a manner similar to that of tubulysin A (Figure 3-22 and 3-23). The absorbance of microtubule protein at 350 nm was measured over time and addition of either 1 μ M tubulysin A or 1 μ M pretubulysin led to an approximately 50% reduction in tubulin polymerization. This result is in accordance to previous studies where it was reported that, although GI₅₀ values on mammalian cell cultures differ by up to three orders of magnitude, the *in vitro* potency of natural tubulysins is barely affected.^[225]

Furthermore, inhibition of tubulin polymerization by pretubulysin was dose-dependent; at a concentration of 3.4 μM only ca. 25% polymerization was observed and electron micrographs of samples that were incubated with 5 μM pretubulysin revealed that microtubules are fully destroyed. However, higher concentrations of pretubulysin needed to be applied to depolymerize already built-up microtubules. Using a concentration of 1.5 μM , still 80% of intact microtubules were present, and even with 3.8 μM pretubulysin the post-assembly addition did not lead to a full depolymerization also reflected by electron micrographs of samples incubated with 5 μM of the drug. These results imply that pretubulysin rather binds to tubulin protein subunits than to filamentous tubulin and thus, sequestration of tubulin prevents microtubule assembly.

As expected for a microtubule-destabilizing drug, abnormal multipolar spindles were observed in pretubulysin-treated cell populations (Figure 3-11). Since the dynamic nature of microtubules is a prerequisite for cellular division and chromosome segregation during mitosis pretubulysin and tubulysin A were evaluated in cell cycle studies (Figure 3-8 and 3-10; Table 3-3 and 3-4). The mitotic spindle is attached to the two opposing centrosomes, with the minus-ends of the microtubules attaching to the poles, and the plus-ends extending away from them.^[254] Microtubule-targeting drugs generally function by repressing the highly dynamic processes during and prior to chromosome segregation, thus, inhibiting metaphase/anaphase transition, blocking mitosis, and ultimately inducing apoptosis.^[167] Tubulysin A exhibited GI_{50} values of 0.23 nM and 0.14 nM, and GI_{50} values determined for pretubulysin were 5.81 nM and 0.96 nM on mouse L-929 fibroblasts and human HepG2 hepatocellular carcinoma cells, respectively (Table 3-2). By this, pretubulysin was approximately by one order of magnitude less potent than the natural parent compound. By tendency, a similar difference in potency was observed in cell cycle studies. Treatment of L-929 cells for 24 h with either 12 nM tubulysin A or 150 nM pretubulysin resulted in the accumulation of ca. 45% of all viable cells in the G_2/M phase. In untreated control samples, only ca. 25% of cells were in G_2/M . However, already lower concentrations (2 nM for tubulysin A and 30 nM for pretubulysin) were sufficient to observe a slight increase of the G_2/M population (30-40% of viable cells) without a significant effect on the G_1 population. In a cell cycle experiment with HepG2 cells equal concentrations of both antimetabolites were applied (50, 100, and 200 nM) and cells were treated for 24 h. In the control population, ca. 20% of viable cells were in the G_2/M phase and 50% were in G_1 phase. At the lowest concentration of tubulysin already a significant accumulation of cells in the G_2/M phase was observed (> 70%) and the relative number only slightly increased with increasing

concentrations. When HepG2 cells were treated with 50 nM pretubulysin the G₂/M population increased to ca. 45% and simultaneously the portion of cells in G₁ decreased to 40%. At the two higher concentrations similar effects than with 50 nM tubulysin were observed, with ca. 70% of viable cells in G₂/M and 15% in G₁. In conclusion, pretubulysin is a potent antimetabolic agent, whereas treated cells are halted in the G₂/M phase of the cell cycle efficiently at concentrations around 100 nM after 24 h.

In general HCS studies on morphological alterations it was found that all antimetabolic agents in the test panel (tubulysins A and D, pretubulysin, disorazol A, and epothilone B) led to significantly enlarged cells and nuclei following 24 h treatment at concentrations near the respective GI₅₀ values (Figure 3-18 and 3-19). In the case of pretubulysin, the cytoplasmic and nuclear area was increased by nearly 30% at concentrations between 50 nM and 500 nM. Furthermore, detailed analysis of pretubulysin-treated cells, but also cells treated with the other drugs, revealed nuclear fragmentation (multiple micronuclei) and cells with condensed chromatin, both being typical hallmarks of apoptosis. In addition, cells were probed on phospho-histone γ H2A.X (Figure 3-21), which is widely used as a marker for DSBs because H2A.X is phosphorylated on serine residue 139 within seconds after the induction of DSBs.^[255] As a result, no direct DSB induction by the antimetabolic compounds at sublethal concentrations was detected, instead, large γ H2A.X foci were exclusively associated with already fragmented nuclei leading to the assumption that enhanced phosphorylation is probably triggered by downstream apoptotic signaling as a consequence of DNA fragmentation. It is quite possible that the aforementioned effects on nuclei are the consequence of the so-called ‘mitotic catastrophe’, a type of cell death which results from deficient cell cycle checkpoints and cellular damage^[256] and in particular, is observed with microtubule-targeting agents.^[257] Complementary to these macroscopic effects on nuclei, it was found that pretubulysin and its 2-desmethyl variant induce DNA laddering as determined by agarose gel electrophoresis (Figure 3-13). In human HL-60 promyelocytic leukemia cells, that were treated for 24 h or 48 h with both drugs at a final concentration of 30 nM or 75 nM, a typical DNA ladder was observed, as it was already found for tubulysin A-treated KB-3.1 cells^[220]. Both, nuclear fragmentation and DNA laddering are specific hallmarks of late apoptosis (programmed cell death) and were likewise observed for other antimetotics, such as paclitaxel.^[258, 259] Indeed, following 48 h treatment approximately 40-50% of human L3.6pl pancreatic cancer cells were found to be apoptotic due to treatment with either 10 nM tubulysin A or 10 nM pretubulysin (Figure 3-12). However, the inhibition of effector caspases did not necessarily protect the cells against cell death (Figure 3-14). When cells were co-

incubated with the broad-spectrum caspase inhibitor Q-VD-OPh the amount of late apoptotic cells with already permeabilized membrane decreased from initially 40-50% to only approximately 25% and by this, pretubulysin-induced apoptosis is only partly caspase-dependent. This caspase-independent 'apoptosis-like' cell death was also found to be induced by other microtubule-targeting compounds, such as paclitaxel, epothilone B, or combretastatin-A4.^[260, 261, 262] It might be speculated that these processes are of lysosomal origin involving the release of proteolytic enzymes in the cytosol that may either act directly on key cellular substrates or in concert with caspases.^[263]

Nevertheless, an involvement of mitochondria could clearly be confirmed for several microtubule-destabilizing agents of myxobacterial origin, as these all induced an increase of mitochondrial outer membrane permeability (MOMP) and thus, a loss of mitochondrial membrane potential (MMP) (Figure 3-15). Following loss of MMP, cytochrome-*c* is released from mitochondria, which interacts with Apaf-1 (apoptotic protease activating factor) and procaspase 9, which in turn, activates the caspase cascade, and finally, DNA is fragmented, whereas these effects are mainly modulated by proteins of the Bcl-2 family. However, also caspase-independent apoptotic signaling cascades can be triggered via mitochondria, for instance by the release of AIF (apoptosis-inducing factor), which translocates to the nucleus and induces DNA fragmentation through interaction with other factors.^[264]

In this study, one of the key players of the intrinsic (mitochondrial) apoptosis pathway was found to be modulated by treatment of cells with either 10 nM tubulysin A or 10 nM pretubulysin (Figure 3-16). Transiently enhanced levels of phosphorylated Bcl-2 (pBcl-2) in human L3.6pl pancreatic cancer cells were already observed after 8 h treatment, and highest levels were detected either after 24 h or 8 h treatment for tubulysin A and pretubulysin, respectively. Although the specific signaling events that are commonly induced by antimetabolites, which lead to inactivation, i.e. phosphorylation, of antiapoptotic Bcl-2, are only fairly understood, it is evident that phosphorylation is accomplished by cellular mechanisms involving different kinases, such as JNK and ERK1/2.^[265] However, Bcl-2 prevents apoptosis by abrogating cytochrome-*c* release and the subsequent activation of caspases.^[266] As a proof of principle, it could be shown that treatment of L3.6pl cells with either tubulysin A or pretubulysin (Figure 3-16) led to cleavage of PARP, which is a substrate of caspase-3 and functions in DNA damage detection and repair.^[267] Cleaved PARP was already detectable after 24 h and the effect was even more pronounced following 48 h treatment with either drug. In summary, it could be demonstrated that pretubulysin shares common characteristic to other antimetabolite agents and in particular, acts in similar manner as its parent compound

tubulysin A. Following an initial formation of abnormal spindle pole structures and cell cycle arrest, apoptosis is triggered at least in part via the intrinsic (mitochondrial) pathway, which culminates in fragmented DNA and cell death (Figure 4-4).

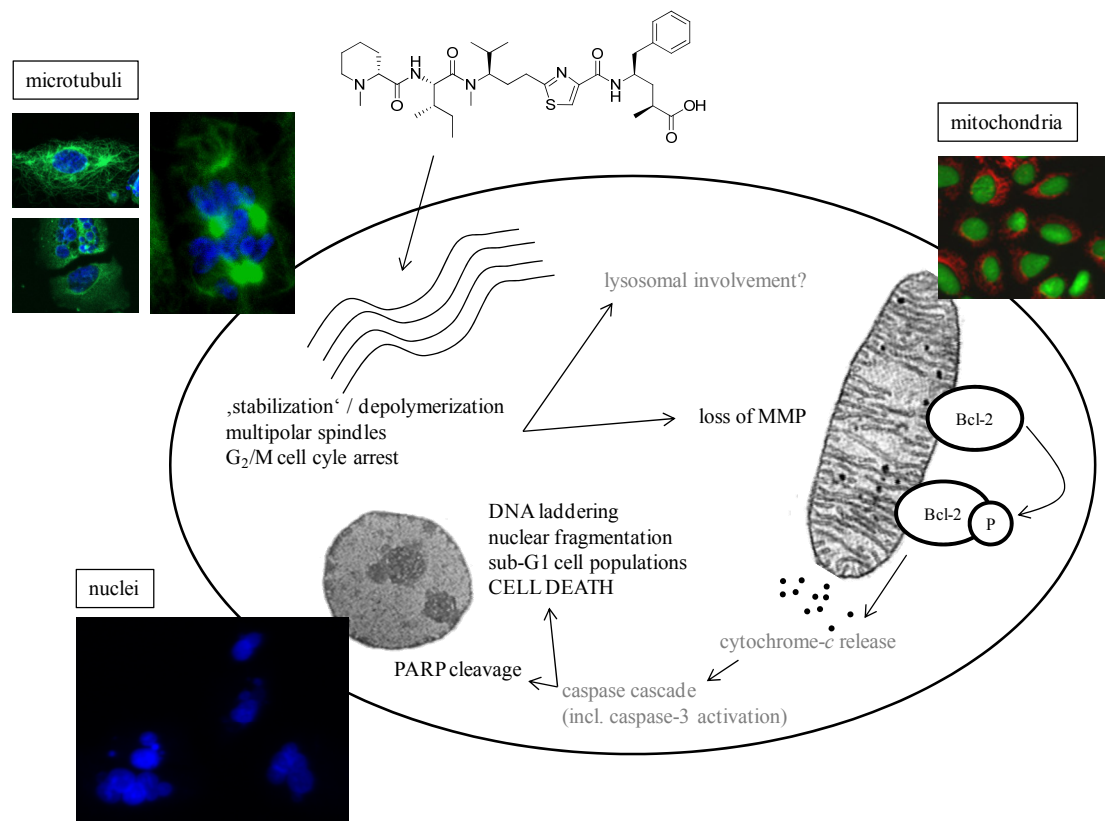


Figure 4-4: Schematic representation of cellular events triggered by pretubulysin.

Due to pretubulysin's primary action on microtubules cells are arrested at the metaphase/anaphase transition and as part of the 'mitotic catastrophe' the mitochondrial apoptosis pathway is initiated as displayed by a loss of MMP. Following phosphorylation of antiapoptotic Bcl-2, cytochrome-*c* is released from mitochondria that triggers the caspase cascade activation and finally, nuclear damage and cell death. Events displayed in grey were not directly studied in the course of this thesis.

4.1.3 SMALL PRECURSOR MOLECULES DESTABILIZE MICROTUBULES

As determined by NMR structural analyses on the tubulin-bound conformation of tubulysin A in aqueous solution, the thiazole ring of Tuv (via the nitrogen atom) and the aromatic ring of Tut form a basal platform upon which the *N,O*-acetal side chain of Tuv packs to form a hydrophobic core. The *O*-acetyl group on Tuv-C5 and the remaining backbone towards *N*-Mep protrude from this region. Based on these results, authors concluded that the hydrophobic skeleton described by the thiazole ring, the Val side chain of Tuv, the Ile side chain, and a tertiary amine on the *N*-terminus are essential for full bioactivity, whereas *N*-

Mep, the γ -carboxy group of Tut, and the *N,O*-acetal functionality are dispensable.^[268] These conclusions are basically in accordance to previous SAR data based on biological activity (cf. chapter 4.1.1). Furthermore, pretubulysin's high potency is even more definite since most important determinants of biological activity, in terms of tubulin-binding, are still present in this simplified precursor of tubulysin.

Here, it was found that a pretubulysin precursor (analog III), which lacks the aromatic rings of Tup and Tuv, still exhibits a considerable biological activity in cell-based studies with GI_{50} values in the low nanomolar range on several cell lines (Table 3-2). However, it was not clear whether this is due to a rather nonspecific cytotoxic effect. In HCS studies (Figures 3-18 to 3-21) it was then found that pretubulysin analog III induces all typical morphological changes in human U-2 OS cells, which were also found with tubulysins A and D and pretubulysin, and generally, these are typical effects observed with microtubule-destabilizing agents. Most importantly, following 24 h treatment, a destabilizing effect of microtubules was observed at concentrations as low as 5 μ M, which is specified in the HCS assay by an increased value of the standard deviation of microtubule fluorescence due to a higher density of microtubules around the nuclear periphery. At 10-fold higher concentrations (50 μ M) even a complete depolymerization of microtubules was observed, which clearly reflects a similar MoA than for the other tubulysins in the assay. By tendency, all compounds induced microtubule depolymerization at concentrations near their respective GI_{50} value and full depolymerization was achieved at 10-fold higher concentrations (Figure 3-20). Furthermore, typical hallmarks of apoptosis of antimetabolic drugs were observed in HCS assays in cells treated with pretubulysin analog III, i.e. significant enlargement of cells (Figure 3-18) and nuclei (Figure 3-19), and nuclear fragmentation. Both morphological changes are often associated with a preceding G_2/M cell cycle arrest. In human HL-60 promyelocytic leukemia cells, which were most sensitive towards pretubulysin treatment, a nearly complete G_2/M cell cycle arrest was observed after 48 h treatment with 10 μ M pretubulysin analog III. The G_1 population decreased from 49% to 16%, and simultaneously, the G_2/M population increased from 23% to 71% (Figure 3-9). However, when tubulysin A, pretubulysin, and pretubulysin analog III were directly compared in cell cycle studies with human HepG2 hepatocellular cells (Figure 3-10 and Table 3-4), it was found that that effective concentrations are reflective of previously determined GI_{50} values. Tubulysin A (GI_{50} on HepG2: 0.14 nM) concentrations as low as 50 nM led to a significantly increased G_2/M population (> 70% of the total population) already after 24 h treatment, whereas a comparable effect with pretubulysin (GI_{50} on HepG2: 0.96 nM) was only achieved when the assay concentration was 4-fold higher (200 nM). The

GI₅₀ value of pretubulysin analog III was determined to be 2.4 μ M on HepG2 cells, which displays a by three orders of magnitude reduced potency compared to full-length pretubulysin. Thus, in cell cycle studies, HepG2 cells were treated for 24 h with 0.5-20 μ M pretubulysin analog III. Compared to the control cell population, already at the lowest concentration applied an increase of the G₂/M population by ca. 5% was observed. At an assay concentration of 5 μ M, nearly 40% of all viable cells accumulated in G₂/M phase. However, at higher drug concentrations, the percentage of viable cells in G₂/M further increased to up to 60%, in parallel with an emerging sub-G₁ population, which most likely reflects late apoptotic cells in which the DNA has already been degraded. This effect is a common hallmark for late apoptosis and is often linked to the typical DNA ladder observed in agarose gel electrophoresis of isolated chromosomal DNA.^[269] As characterized by a clearly induced G₂/M accumulation of viable cells, the small pretubulysin precursor (analog III), which is also able to destabilize microtubules, as observed in HCS experiments, in turn, leads to mitotic arrest in HepG2 cells. Nevertheless, the effect seems to be more nonspecific than that of pretubulysin itself, a difference that is reflected by a higher toxicity that is likely due to the greater than 100-fold-higher concentrations required to observe any effect on the cell cycle.

The overall loss of potency with pretubulysin analog III by about three orders of magnitude compared to pretubulysin, the findings from cell cycle studies, and generally, missing decisive structural features (pretubulysin analog III lacks the complete C-terminal Tup and the triazole moiety of Tuv), are already indicative for a less efficient binding to tubulin protein. Natural tubulysins and pretubulysin exhibit only minor differences when it comes to inhibition of *in vitro* tubulin polymerization^[203, 225], although potency varies by up to two orders of magnitude in cell-based growth inhibition experiments. However, it was found that 20 μ M pretubulysin analog III are required to reduce tubulin polymerization (10 μ M tubulin protein) to about 30% of the untreated control (Figure 3-24). In the same experiment, 2 μ M pretubulysin were sufficient to yield a similar effect. Corresponding electron micrographs revealed that treatment with either 2 μ M pretubulysin or 25 μ M pretubulysin analog III cause similar effects with respect to microtubule disruption, as depicted by shortened microtubules and the perturbed tubular structure relative to the control (Figure 3-22 and 3-24). The activity of the shorter chain analog was approximately 10-fold reduced in the cell-free system and thus, it is likely that not only cellular uptake or reduced metabolic stability causes the loss of growth inhibition activity but also that binding affinity to purified tubulin is reduced, a conclusion which would be in accordance to NMR structural analyses of tubulin-bound tubulysin A.^[268]

Even though the potency of the small pretubulysin precursor (analog III), which consists of only two out of the four original amino acids, was significantly reduced in all accomplished assays, the precursor molecule still exhibits a similar MoA than the parent compound pretubulysin, which is mainly characterized by microtubule disruption and an induction of mitotic arrest. These results suggest that pretubulysin might be further simplified and modified easily and attachment of various functional groups on the C-terminus appears manageable. Some reports on other further simplified and functionalized pretubulysins^[270, 271, 272] have already been published and future synthetic approaches might aid in obtaining greater insight in the MoA of this compound family and allow the ‘fine-tuning’ of the target binding, toxicity, and tumor specificity properties of pretubulysin.

4.1.4 PRETUBULYSINS AS MOLECULAR PROBES

Fluorophor-coupled conjugates of tubulin binding agents, such as BODIPY-vinblastine and BODIPY FL-paclitaxel are already employed mainly in *in vitro* studies with isolated tubulin but also in live cell studies, for instance as tools to determine transport functions of ABC drug transporters.^[273] Incubation of living cells with the BODIPY conjugate of the microtubule destabilizer vinblastine results in a rather uniform fluorescence that is accumulated in the cytoplasmic region.^[274] However, the bis-acetylated form of a paclitaxel (microtubule stabilizer) fluorophor conjugate was successfully applied to visualize distinct microtubules^[275], which might be attributed to the fact that paclitaxel directly binds to polymeric tubulin rather than to monomeric subunits.

Here, a triazole-pretubulysin was prepared that is functionalized by a coumarin 460 group, which was directly coupled via an aliphatic linker to the triazole moiety and by this, replaces Tup. The corresponding pretubulysin precursor (analog II, MepIleTuv) exhibited a GI₅₀ value of 14.2 μ M in mouse L-929 fibroblasts. However, the coumarin-coupled triazole analog was approximately by factor 10 more potent than the single MepIleTuv building block with GI₅₀ values in the low micromolar range. Nevertheless, this implies a reduced potency by 2-3 orders of magnitude compared to the original pretubulysin.

It was shown that the tool compound is able to completely destroy the microtubule architecture following 48 h treatment in a manner highly similar to pretubulysin (Figure 3-5). When assessing the cellular distribution of triazole-pretubulysin coumarin in live cell imaging studies (Figure 3-6) no localization could be observed up to 30 min of treatment. This might be attributed to a strong background fluorescence of the compound in the cell culture medium and unbound pretubulysin inside the cells, which significantly hampers image data analysis.

However, throughout the 30 min - 12 h experiment fluorescence was detected organized as small vesicles distributed within the cells and at later time points these vesicles were somewhat preferably found around the periphery of nuclei. Interestingly, similar results were obtained with a fluorophor-coupled tubulysin A construct (personal communication Dr. F. Sasse). Unfortunately, the used tool compound is incompatible with common fixation techniques so that no direct co-localization with microtubules could be assessed using immunostaining for α -tubulin. This issue might be circumvented by using tubulin-GFP fusion constructs for labeling of microtubules in living cells. However, post-immunostaining of microtubules revealed the typical phenotype with enlarged cells and a higher density of microtubules around the nuclear periphery, which is characteristic for a starting depolymerization effect. In order to determine the exact localization of the detected fluorescent vesicles, acridine orange (AO) staining of vital cells was applied (Figure 3-7). When accumulated in acidic lysosomes, this dye exhibits a characteristic orange to red fluorescence (λ_{max} ca. 630 nm) and thus, emission maxima of coumarin (λ_{max} ca. 450 nm) and AO are sufficiently separated. Surprisingly, an exact co-localization of the triazole-pretubulysin tool compound and lysosomes was observed. Since lysosomal trafficking is mediated via interplay of microtubules, myosin, and actin^[276] the appearance of a larger fraction of fluorescent spots around nuclei might, in part, be explained indirectly by a higher density of microtubules around the nuclear periphery in treated cells. This is also in accordance to the finding that depolymerization of microtubules affects the positioning of endosomal and lysosomal compartments.^[277, 278] Interestingly, accumulation in acidic vesicles (endosomes, lysosomes, vesicles of the Golgi compartments) has also been described for a variety of other drugs (mostly lipophilic weak bases) as part of a detoxification mechanism of the cell or lysosomal trapping is a desired and essential property of a compound, as for instance with some antimalarial drugs that target parasite lysosomes.^[279] However, in case of triazole-pretubulysin coumarin the lysosomal uptake might be favored due to the weak basic amine functionalities. Inside lysosomes the compound might become protonated and therefore trapped within the acidic compartment. Nevertheless, a certain amount of the overall compound load must contribute to microtubule depolymerization by binding to tubulin. Since this is most probably due to binding to monomeric subunits, local concentrations might be too low to be detectable by fluorescence microscopy in the presence of accumulated dye in lysosomes. In principle, it might also be possible that the tool compound very early in the process and irreversibly affects microtubule architecture and later on, is mostly accumulated in the acidic compartments. This would be in accordance to experiments with pretubulysin

and tubulysin A, which both inhibit the long term survival of pancreatic cancer cells over a 6 d period after a rather short stimulation with the drugs (Figure 3-3). At nanomolar concentrations, both compounds were able to reduce the number of cancer cell colonies by at least 50%. However, the drawn conclusions are at this stage rather speculative and further efforts have to be undertaken to reveal pretubulysin's cellular localization and details of its MoA.

In an independent study, a second generation of pretubulysin tool compounds has been prepared. The pretubulysin core structure was functionalized by a benzophenone moiety, which replaces the phenyl group of Tut, and an additional propargylamine coupled to the C-terminus. In target analysis studies, cells were labeled *in situ* by UV-induced cross-linking of the probe (via benzophenone) with respective binding partners and after cell lysis, a biotin tag was introduced by click chemistry via the alkyne group of the tool compound enabling enrichment and MS analysis of respective binding partners. Thus, it could be shown for the first time that pretubulysin exhibits a remarkably high affinity for β -tubulin. Interestingly, a similar approach was applied for fluorescence imaging studies, where it could be shown by co-staining of α -tubulin that the used tool compound disturbs microtubule structures. However, the covalently-linked fluorescent tool compound was also found to appear as little spots that were associated with microtubules, which only remotely resembled the structures observed in studies with triazole-pretubulysin coumarin, and authors concluded that these are monomeric tubulin units.^[272]

In summary, functionalized pretubulysins appear to be valuable tools for the elucidation of binding partners and cellular processes induced by this compound class. Future studies may focus on further optimization of the molecules in terms of maintaining original potency, elucidation of the exact localization and dynamics within cells, and tool compounds may also be applied for in-depth SAR studies by functionalization of various pretubulysin derivatives.

4.2 NEW CHONDRAMIDES WITH ALTERED ACTIVITY PROFILE

Standardized crude extracts from myxobacteria were screened in the course of this thesis on their biological activity in whole cell viability assays with regards to antibacterial, antifungal, and cytotoxic properties. In a case study with *Chondromyces sp.* SBCm007, it was found that crude extracts were highly cytotoxic and furthermore, induced characteristic morphological changes in cultured mammalian cells. Thus, bioactivity-guided isolation was moved from classical approaches to high-content screening on defined targets. Dereplication using a targeted MS profiling approach^[79] highlighted the presence of the actin-targeting cyclic depsipeptides chondramides A~D^[194] that, in part, explained the strong cytotoxicity of the crude material. However, a multitude of novel chondramides derivatives was discovered by combining elaborate fermentation, screening, and HR-MS techniques. In particular, biological profiling of purified compounds revealed some brominated analogs as invaluable in terms of their higher potency on cancer cell lines and an altered affinity in actin polymerization studies compared to already described chondramides A~D.

4.2.1 HIGH-CONTENT SCREENING IS APPLICABLE FOR CRUDE EXTRACTS

With the advent of HCS it was expected that this technology might greatly facilitate the early drug discovery process and subsequent SAR - and toxicity studies. Due to the implementation of HTS in the R&D pipeline, primary screening has already been improved in terms of productivity. However, higher quality leads are most probably discovered in sophisticated, more focused and multiparametric whole cell screens using fluorescence as a read-out. Numerous probes have been developed that are commonly either based on labeling certain cellular components, indicating environmental signal transduction events, or intrinsic labeling of target molecules in living cells.^[280] The advantages and disadvantages of both, HCS and HTS, are obvious when it comes to screening of large combinatorial or NP-based libraries. In the course of further miniaturization of assays and achievements in liquid handling and automation processes, HTS allows for very fast screening of large compound libraries, however, success rates with regards to marketing of new drugs did not meet expectations. Functional HCS assays, on the other hand, have the potential to yield more relevant hits, but cell culture techniques are generally time-consuming and difficult to handle at a scale required for HCS of large libraries.^[281]

Compared to the screening of pure compound libraries, application of HTS and HCS for crude extract bioactivity-guided isolation is even more challenging. Due to the inherent complexity of extracts, a significant interference with the assay read-outs is probable, which anticipates a

straight forward isolation of NCEs.^[1] On the other hand, following traditional approaches (whole cell growth inhibition screens) highly active compounds present in the extracts might mask other interesting bioactive metabolites.^[105]

In the course of the presented study it was found that a morphological ‘pre-screening’ of cells treated with cytotoxic crude extracts is essential as part of the decision-making process whether a sample is subjected to HCS. Early on in the bioactivity-guided isolation process extracts that induce specific morphological changes, which are indicative for a cytostatic effect, are prioritized over those that cause unspecific toxicity or precipitate. Bioactivities due to already known secondary metabolites can then be distinguished from those induced by NCEs in an initial HCS experiment by applying focused screens on the established cellular targets and putative other apoptotic events (Figure 4-5).

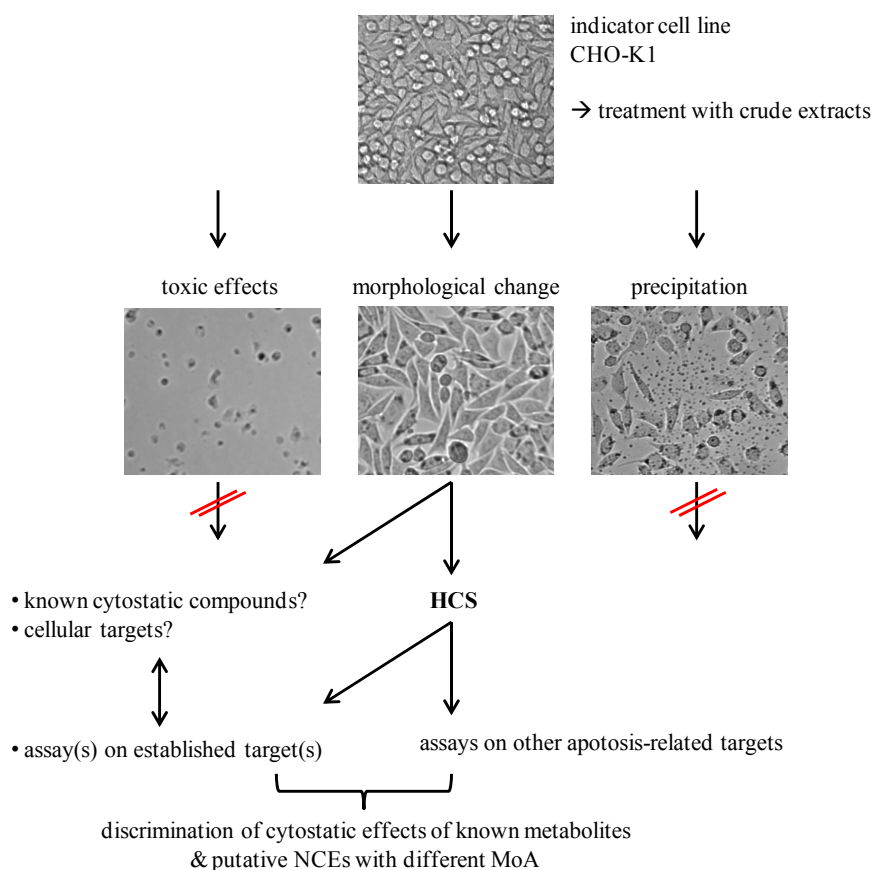


Figure 4-5: Integration of HCS in bioactivity-guided isolation of NPs from crude extracts.

Crude extracts that induce distinct effects in cultured mammalian cell are suitable for being further processed via HCS. The technology can thereby aid to distinguish cellular events that are caused by already described cytostatic NPs and novel NPs with different MoA.

Here, crude extracts of *Chondromyces sp.* SBCm007 were found to be highly active in terms of cytotoxicity and furthermore, treated cells were enlarged and contained up to four nuclei per cell (Figure 3-25 and 3-26). In principle, these effects could have been attributed to the actin-targeting chondramides A~D produced by strain SBCm007 (Figure 3-27). Nevertheless, it was expected that other biological activities might be masked by the presence of the cyclic depsipetides and thus, the crude extract was subjected to further profiling in HCS experiments. Indeed, it could be demonstrated that besides a pronounced actin polymerization typically observed with chondramides, LMP (lysosomal membrane permeabilization) was induced upon treatment of U-2 OS cells with the crude material. The latter effect could not be attributed to the known chondramides (Figures 3-28 and 3-29).

Following conventional bioactivity-guided isolation, the cytotoxicity of primary fractions was assessed in a tetrazolium salt-based viability assay (Figure 3-33). These results displayed again the strong cytostatic activity of chondramides being mainly present in two out of thirteen fractions. Without having the preliminary data from HCS profiling further processing of the crude extract would have probably been aborted since the viability assay failed to detect pronounced activities in ‘non-chondramide’ fractions. However, in the following, HCS revealed the superiority of image-based screening over conventional cytotoxicity screening. Applying the above mentioned primary fractions in HCS experiments on either lysosomal integrity (Figure 3-31) or actin filament disruption (Figure 3-32) revealed additional bioactive fractions. LMP was expected to be caused by novel metabolites but actin polymerization and an increase of lysosomal pH were not ideally separated in terms of active silica gel fractions. The crude material was also fractionated using SEC and in fact, distinct fractions that induce LMP were obtained (Figure 3-30). Although the effects on lysosomes were highly reproducible and distinct in the course of the screening campaign until the first fractionation step, LMP induction was not observed anymore in samples from secondary fractionation of a SEC fraction by RP-HPLC. Nevertheless, bioactivity was detected in HPLC fractions from a primary silica gel fraction (Figure 3-32). Unfortunately, NPs that act by inducing LMP could not be isolated in the course of this study, a shortcoming which can be attributed to very low abundance of the compounds; due to this, even the definition of target masses could not be accomplished for some fractions. Efforts to optimize cultivation conditions for the production of these metabolites by strain SBCm007 are currently ongoing. Encouragingly, it could be demonstrated recently in an independent study that the secondary metabolite profile observed from strain SBCm007 can be successfully diversified by means of gaseous composition variation in fermentation processes.^[282]

Interestingly, actin polymerization activity was found throughout all primary fractions, even in those where the MTT viability assay failed to detect any toxicity (Figure 3-34). Following the general procedure already applied in bioactivity-guided studies on LMP induction, primary fractions were further separated by RP-HPLC, tested in HCS on actin polymerization and indeed, the effect on actin filaments could be attributed to distinct HPLC fractions containing masses (and corresponding fragmentation patterns) other than those of described chondramides. However, upon purification and full structural elucidation by NMR of the first putatively novel NPs, it turned out that strain SBCm007 produces new structural variants of the chondramide family (Figure 3-36 and Table 3-5). For instance, chondramide A10 was found to be glycosylated at C7' and additionally bears a chlorine at C6' of the aryl moiety. Despite being present only in minute amounts in the crude extracts compared to known chondramides, its potency was reduced by at least three orders of magnitude ($GI_{50} > 10 \mu\text{M}$). Nevertheless, chondramide A10 was highlighted by HCS assays from HPLC fractions due to its specific effects on actin filaments. This finding demonstrates the usefulness and applicability of the HCS screening approach for the rapid identification of low-abundance bioactive natural products.

Encouraged by the discovery of some structural variants of chondramides, HR-MS data of crude extracts and fractions was screened again, assuming that novel chondramides might be highly variable in terms of structural features. In addition, supplementation of the culture broth with different halogens (e.g. replacement of NaCl by KBr) led to the production of new 'non-natural' C6'-brominated chondramides. In summary, application of HCS for bioactivity-guided isolation of NPs produced by *Chondromyces sp.* led to the discovery of altogether 35 new chondramides variants. Furthermore, 11 of these new NP variants were characterized in terms of their bioactivity and results were invaluable for initial SAR conclusions. By combining HCS with sensitive analytical techniques for compound identification and structure elucidation, and elaborate production optimization to improve the yield of newly identified target compounds, it might be possible that significant numbers of novel scaffolds can be isolated from myxobacteria and other natural product sources that have been missed by previously applied conventional bioactivity-guided isolation approaches.

4.2.2 STRUCTURE-ACTIVITY RELATIONSHIP OF CHONDRAMIDES

Highly cytotoxic chondramides A~D were originally isolated from terrestrial strains of the species *Chondromyces crocatus*, and strain Cm c5 was found to be the most efficient producer so far (several mg per liter). On average, chondramides exhibited GI_{50} values in the low- to

mid nanomolar range on several mammalian cell lines and interestingly, also inhibited the growth of the Pgp-overexpressing MDR cell line KB-V.1.^[194, 283] Similar to the structurally related jaspamide/jasplakinolide^[206, 207] isolated from *Jaspis* sponge, chondramides target the actin cytoskeleton of mammalian cells and induce a hyperpolymerization of filaments, which culminates in the formation of large actin lumps, inhibition of cytokinesis, and cell death. Furthermore, both compound families share a common binding site on F-actin, similar to that of the mushroom toxin phalloidin, as observed in competition experiments.^[208, 209]

As mentioned previously, tubulin-targeting drugs are an integral part of the pharmacopoeia for cancer treatment, but also actin has been thought to be a valid target. However, no actin-targeting drug is currently in clinical use.^[168, 167] Jasplakinolide and chondramides have been considered for further preclinical evaluation although having a rather low therapeutic index, especially pulmonary hemorrhage induced by jasplakinolide hampered its clinical development.^[284] Encouragingly, these NPs, unlike phalloidin, are cell-permeable and might prove to be excellent probes in studies on actin dynamics.^[212] These considerations, in turn, fostered several synthesis studies and two independent reports on the total synthesis of chondramide C were published more than ten years after the discovery of the cyclodepsipeptides.^[285, 211] The synthesis studies enabled the configurational assignment of all stereogenic centers and additionally, accounted for important SAR insights. It was found that the stereochemistry at the C6-C7 region in the polyketide segment significantly impacts chondramide's activity (efficacy was attenuated by 10- to 100-fold with two of the three additionally prepared diastereomers) presumably by populating an unfavorable conformation of the tripeptide part of the molecule.^[285] This proposal was further substantiated by findings from ligand-ligand similarity studies of chondramide C and phalloidin in polymeric actin, made up of three independent actin subunits. In addition, interactions of the Trp side chain and the hydroxyl group of Tyr in the phalloidin cavity of actin were found.^[211] Total synthesis of chondramide A, which contains 3-amino-2-methoxy-3-aryl propanoic acid instead of β -tyrosine, confirmed the configuration at C2' to be (2*S*,3*S*).^[286] With modified synthetic analogs of this derivative it could be demonstrated that the aryl group is essential for activity but can be modified at the *para*-position by a variety of rather small substituents, such as a methyl group, fluorine, or a nitrile group. The biological activity of these derivatives was more or less comparable to natural chondramides, merely a C7' phenyl analog and an amide derivative forfeit potency by 1-2 orders of magnitude, respectively^[287], and substitution of the phenolic OH with other even bulkier groups was actually less tolerated.^[288] Probing the influence on biological potency of other structural features of the chondramides scaffold it

was found that in general, the C6-C7 configuration, *N*-methylation of the tryptophan α -amino group, and the olefin geometry at C4-C5 have a ‘fine-tuning’ function although being essential for retaining full biological potency. Solely the stereochemical arrangement at C2 had a great impact, as indicated by significantly reduced activity of (2*R*)-configured analogs compared to corresponding (2*S*)-isomers.^[288] Figure 4.6 summarizes the aforementioned basic SAR conclusions with natural chondramide B as the core structure.

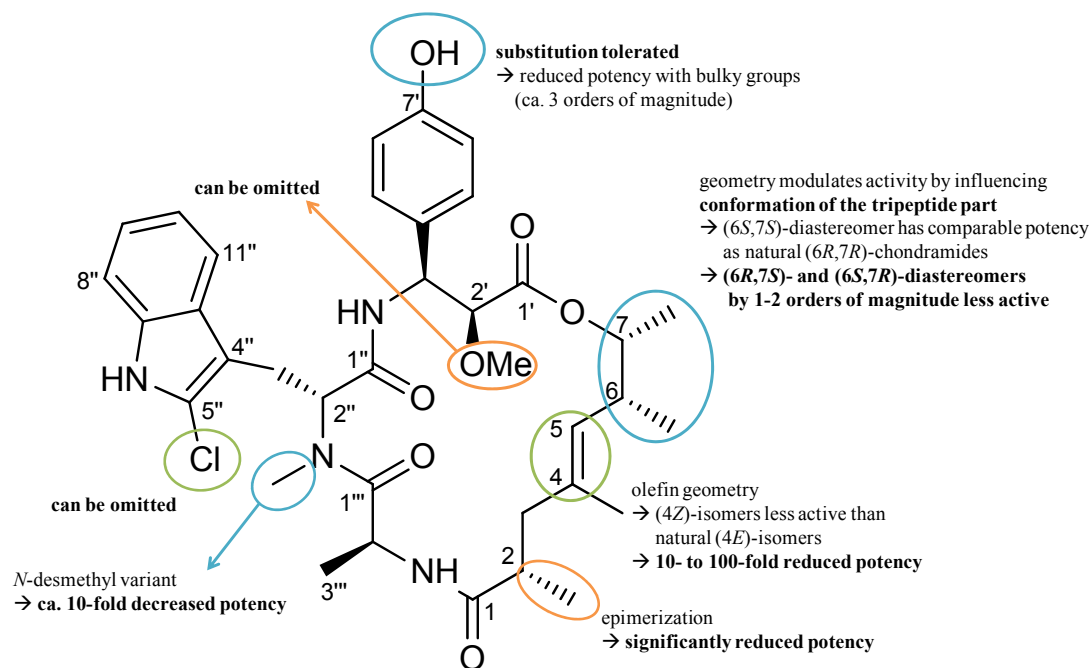


Figure 4-6: Structure-activity relationships of synthetic chondramides.

Chondramides A~D are active in the low- to mid nanomolar range on cultured mammalian cells. With natural derivatives neither the chlorination at C5'' of Trp nor the methoxylation at C2' significantly influences the biological activity of chondramides.

Analysis of the biosynthetic machinery in strain Cm c5 revealed a PKS/NRPS gene cluster for the assembly of chondramides, which are comprised of three amino acids (Ala, *N*-MeTrp, and β -tyrosine or α -methoxy- β -tyrosine) and a polyketide chain. In addition to the expected genes for PKS and NRPS, a rare tyrosine aminomutase (CmdF) and a previously unknown tryptophan-2-halogenase (CmdE) were found to be encoded by the cluster and on the basis of structural similarity to jaspamide/jasplakinolide it was proposed that an unusual (*R*)- β -tyrosine moiety is incorporated.^[289] In further biosynthesis studies this expectation was confirmed and it could also be demonstrated *in vitro* that the aminomutase CmdF directly converts L- α -tyrosine into β -tyrosine with (*R*)- β -tyrosine as the kinetically preferred product.^[290] The structural diversity of new chondramides derivatives from strain SBCm007 discovered in the

course of this thesis is most probably caused by a subset of enzymes absent from the original producer strain *C. crocatus* Cm c5. Halogenation at C6' and glycosylation or phosphorylation at C7' of the aryl moiety, hydroxylation of C2', and an ethyl group at C7 of the polyketide segment are not present in originally described chondramides A~D. However, the described variations are incorporated independently from each other, except for the carbohydrate group at C7', which can solely be found in combination with a halogenation at C6'; no glycosylated derivative without halogen at this position could be detected.

The presumed actin-polymerizing activity was found with all purified novel chondramides (Figure 3-37 displays exemplary images of cells treated with medium concentrations of chondramides), and the effects resembled those described for jasplakinolide^[291]. Upon treatment with rather low concentrations actin lumps were observed in the perinuclear region and at higher dosage, actin was nearly completely depleted from the central region of the cells, which exhibited an altered morphology in terms of cell shape and thick actin aggregates were found predominantly at the cell margins.

GI₅₀ values of chondramides were assessed in an MTT viability assay on a small panel of cell lines and human primary cells (Table 3-6). Except for the above mentioned glycosylated derivatives and chondramide E4, all chondramides were found to be active in the low- to mid nanomolar range, which is in accordance to previously reported values for reference compounds chondramides A~D.^[194, 209] In general, chondramides exhibited no certain specificity with respect to origin and tissue of the tested cell lines; most derivatives were active in the two-digit nanomolar range on cancer cell lines, including the MDR cell line KB-V.1, non-cancerous cell lines, and HUVEC. A direct comparison of activity and substitution pattern reveals that bulky groups coupled to the hydroxyl moiety of the aryl residue, such as a carbohydrate moiety, generally weaken the activity in cell-based studies, a finding also supported by results from other groups.^[287, 288] This relationship might be partially explained by the lower permeability of the eukaryotic cell membrane for more polar compounds. Nevertheless, a phosphate group seems to be tolerated. When comparing chondramide A6 (phosphorylated) with chondramide B, and chondramide A8 (phosphorylated, C6'-chlorinated) with chondramide A4, average GI₅₀ values are all in the range of 35 to 50 nM. On the other hand, derivatives with a carbohydrate residue (chondramides A9 and A10) were significantly less active in terms of growth inhibition and GI₅₀ values were not determinable in the assay's concentration range but are expected to be greater than 5 μM. Another structural feature which was not evaluated in previous SAR studies on synthetic chondramides is a hydroxylation at C2'. With regards to chondramides

A~D, which either bear a hydrogen or methoxy group at this position, C2' substitution does not seem to impact potency. However, a hydroxyl group, as found in chondramide E4, significantly lowers activity by approximately one order of magnitude (GI_{50} values in the high nanomolar to low micromolar range).

Most interestingly, brominated chondramide C3 analogs were clearly more active on cancer cell lines than on human non-cancerous cells and aside from that were generally more potent than all other tested derivatives. On average, the C6'-brominated analogs of chondramide C either bearing a methyl group at C7 of the polyketide backbone or an ethyl group (eventually derived by incorporation of a prolonged starter unit; propionyl-CoA instead of acetyl-CoA) were by factor two less toxic for human non-cancerous and primary cells than for human cancer cell lines. In comparison, chondramide C exhibits average GI_{50} values of 45 nM and 30 nM on cancer cells and non-cancerous/primary cells, respectively. By this, the two most important derivatizations, in terms of shifting growth inhibitory activity towards cancer cell lines, seem to be the substitution at C6' (halogen) and C7 (ethyl group). Figure 4-7 summarizes the SAR conclusions based on GI_{50} values.

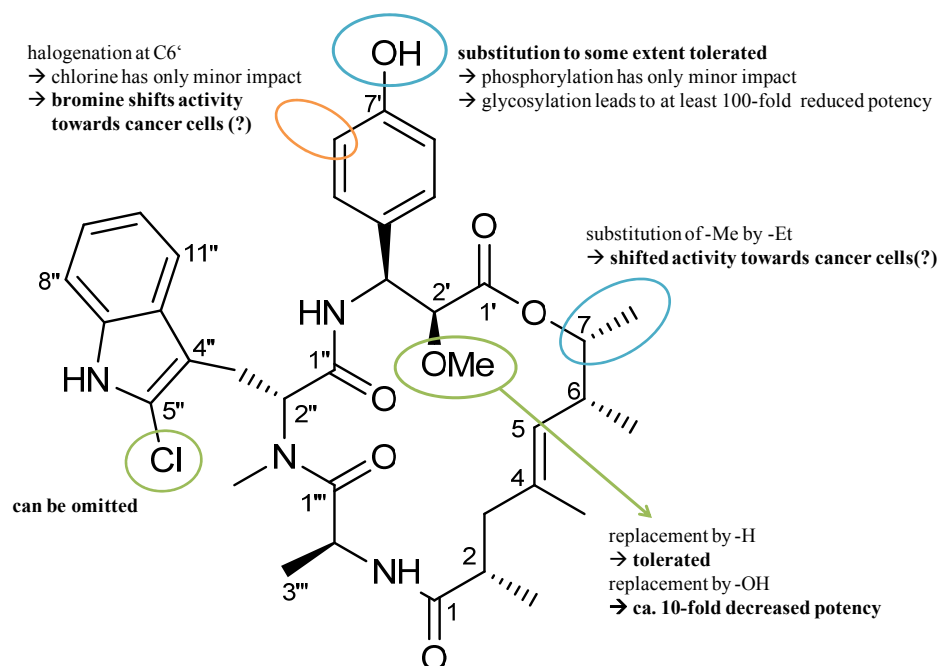


Figure 4-7: Structure-activity relationships of novel chondramides based on GI_{50} values.

Novel chondramides isolated from strain SBCm007 were active in the low- to mid nanomolar range. Only a carbohydrate moiety at C6' and hydroxylation of C2' negatively impact potency. Interestingly, an ethyl residue at C7 and bromine at C6' seemed to shift specificity of chondramides towards cancer cell lines.

4.2.3 BIOLOGICAL AND BIOCHEMICAL DATA SUGGEST A PUTATIVE OFF-TARGET

Based on the results from growth inhibition experiments (Table 3-6) it was assumed that the *in vitro* actin polymerization potency of chondramides might also differ significantly. Thus, compounds were grouped according to their respective GI₅₀ values and activity patterns and actin polymerization was assessed. For this purpose, fluorescence of a 5 μM pyrene-labeled actin preparation, incubated with 20 μM chondramide, in non-polymerizing buffer (low salt conditions) was measured over time (Figure 3-38, 3-39, and 3-40; Table 3-7).

It has already been proposed that chondramides, as well as the related jaspamide/jasplakinolide family share a common binding site on F-actin, similar to that of phalloidin.^[208, 209] These compounds bind to actin filaments much more tightly than to actin monomer and shift the equilibrium (treadmilling) to favor filament formation over dissociation by lowering the critical concentration due to a decreased rate constant for subunit dissociation from the minus-end.^[291, 292] This is also in accordance to live cell imaging studies using synthetic chondramide- and jasplakinolide probes, which were coupled to a BODIPY fluorophore. The dye-coupled depsipetides led to considerably weaker labeling of cytosolic G-actin and highly dynamic actin structure (e.g. lamellipodia) than of static long-lived filament populations (e.g. stress fibers and arcs).^[212] In addition, spontaneous hypernucleation of G-actin as a result of bundling of very short actin filaments and subsequent actin polymerization are typically observed with the above mentioned actin-targeting drugs.^[291] Here, it was assumed that spontaneous actin polymerization *in vitro* is either proportional to the determined cytostatic activity or might be influenced by cellular uptake of unequally substituted chondramides.

The first test set comprised novel chondramides with GI₅₀ values greater than 200 nM. Indeed, polymerization of G-actin was slowed down in comparison to chondramides A~C. As already indicated by GI₅₀ values, chondramide E4 (C2'-hydroxyl) was the most active among these novel derivatives but exhibited an approximately 2-fold slower increase of pyrene-actin fluorescence compared to the reference compounds. For the glycosylated derivatives it seems likely that halogenation on the tryptophan residue (C5''-Cl) can partly restore the ability to polymerize actin when directly comparing chondramides A9 and A10. The former does not exhibit any actin-polymerizing activity *in vitro*, whereas with the latter analog polymerization steadily increased. A similar relationship is observed for chondramides A3 and A4, where additional chlorination at C5'' increased the polymerization rate even more drastically. Interestingly, chondramide A3 (C6'-Cl) and chondramide B (C5''-Cl) differed significantly in their potency of inducing G-actin polymerization; the C6'-Cl analog was approximately by

factor three less active. However, this is not in accordance to determined GI_{50} values, which were highly comparable for both compounds. Also phosphorylated analogs A6 and A8 did not induce fast G-actin polymerization as suggested by their growth inhibitory potential. With average GI_{50} values of ca. 40 nM these derivatives were nearly as active as reference chondramides A~C. However, *in vitro* polymerization potency was approximately 5-fold reduced. This result may indicate that phosphorylated chondramides are taken up by living cells but the phosphate ester might be cleaved by intra- or extracellular phosphatases, which in turn, counteracts a hindered binding to actin as indicated by observations in the *in vitro* system.

As mentioned above, a shifted growth inhibitory activity towards human cancer cells seemed to be mainly determined by C6'-bromine and C7-ethyl groups, as found in propionyl-bromo-chondramide C3. Strikingly, this goes along with a ca. 5-fold weaker *in vitro* activity in actin polymerization studies compared to chondramide C.

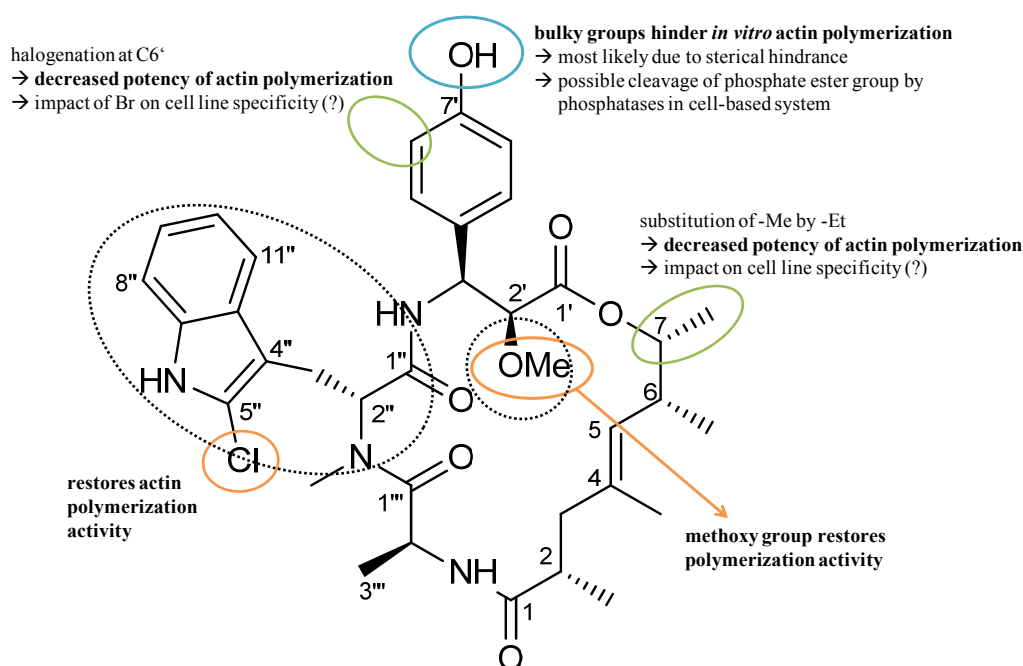


Figure 4-8: Overview of structure-activity relationships of novel chondramides.

Novel chondramides isolated from strain SBCm007 were evaluated in cell-based and *in vitro* assays. Taken together, the results suggested a putative off-target. The affinity to this target appears to be mainly determined by the substitution pattern at C6' and C7. Future synthetic approaches might aid to reveal off-target effects by lowering chondramide's affinity to actin, putatively realized by replacement of tryptophan for another amino acid and omitting the C2' methoxy group (highlighted by dashed circles).

Similar observations are made for derivatives where only bromine or an ethyl group is present (propionyl-chondramide C1 and bromo-chondramide C3), indicating that these substituents might disturb the affinity to actin or rather increase the affinity to a second putative target. The existence of this second target is even more probable since *in vitro* activity on actin can be restored to highest levels when the methoxy moiety is present in a brominated analog as shown for bromo-chondramide A3, indicating that induction of actin polymerization is actually not hindered by the halogen substituent. Interestingly, chondramide A3, which is the chlorinated analog of bromo-chondramide A3, seems to be less affine to G-actin than its counterpart. Unfortunately, no propionyl-chondramide C3 could be isolated to verify these findings.

Figure 4-8 opposes SAR conclusions from cell-based studies to SAR from *in vitro* experiments and highlights possible modification sites for future off-target finding studies. In conclusion, substitution of tryptophan in the peptide backbone for another amino acid might lower the molecule's affinity to actin and increase thereby availability of chondramides for other putative off-targets. Likewise, absence of the methoxy group at C2' might aid to further weaken the affinity for actin. Based on a scaffold with C6'-bromination and C7-ethylation it should be possible to synthesize, with the already established and/or modified routes, molecules suitable for further SAR studies and subsequently evaluate both, target-related and off-target effects. Nevertheless, at this point, it remains to be proven whether chondramides really target other biomolecules than actin.

4.2.4 DIVERSITY OF NATURAL PRODUCT SCAFFOLDS

It is assumed that organisms, which are able to retain chemical diversity at low cost, are evolutionary favored^[9]. With regard to this, it is not surprising that the host strain SBCm007 further increases the small number of related chondramide derivatives by acquisition of a subset of additional enzymes that are not directly associated with the original biosynthetic gene cluster. By this, diversity in terms of chemical and physical properties of the compounds is increased with minimal additional energetic effort. In addition to chemical diversity *per se*, NPs are optimized in terms of possible protein interactions^[25, 26] and considering three-dimensional structure similarities of proteins, NPs are generally able to interact with a plethora of cellular targets that often leads to the modulation of various signaling pathways.^[26, 27] Based on the aforementioned considerations, it seems to be rather unlikely that chondramides do not have a second or even multiple targets. Thus, it might be concluded that chondramides in general interact with putative off-targets to a certain extent, a

speculation which is strengthened by decisive structural elements of the newly discovered derivatives, which may indeed lead to higher affinity to alternative protein targets.

These phenomena are also common to other drugs and regarded as beneficial since, e.g., an emerging multidrug resistance of many cancers is observed with current therapeutic approaches. Especially the application of targeted therapies, in contrast to conventional chemotherapy, which acts on all dividing cells, fostered a higher rate of resistance development. With the approval of new generation anticancer drugs, such as sorafenib, inhibition of several signaling pathways will eventually develop as state-of-the-art treatment or at least as promising alternative to conventional strategies^[293]. Besides the desired targeting of several target proteins by the same compound, off-target cytotoxicity has often hampered the development of NPs into clinically useful agents. For instance the plant-derived non-alkaloid toxin lignan podophyllotoxin acts by inhibiting tubulin polymerization but has severe toxic side effects. The further development of this drug then led to the discovery of a second target molecule, topoisomerase II, and the semisynthetic podophyllotoxin analog etoposide was developed for clinical use as topoisomerase II inhibitor.^[294]

In the case of the newly discovered chondramide derivatives both scenarios are conceivable: chondramides having a common second target, which remained so far undiscovered and/or the future synthesis of analogs that have improved properties with regards to exclusively targeting physiologically relevant proteins other than actin in cancer cells.

SUMMARY AND CONCLUSIONS

Natural products remain the most productive source of novel lead structures for a variety of therapeutical applications. In the last decades, the fascinating order of Myxococcales (myxobacteria) has emerged as a highly valuable source of NPs as these bacteria produce a variety of secondary metabolites with unique structures that often exhibit a new mode-of-action. Numerous myxobacterial metabolites have cytotoxic or cytostatic properties and six distinct compound classes have been described to directly target the eukaryotic cytoskeleton. In the course of this study, myxobacterial compounds of two different classes were investigated by means of cell biological and *in vitro* methods. The antimitotic tubulysin precursor pretubulysin and some of its derivatives were biologically evaluated. In addition, high-content screening was implemented for the bioactivity-guided isolation of NPs from myxobacterial origin. This, in turn, resulted in the discovery of novel derivatives of actin-targeting chondramides that were further characterized.

5.1 PRETUBULYSINS

Pretubulysin is a natural product that is found in several strains of myxobacteria in only minute amounts. It represents the first enzyme-free intermediate in the biosynthesis of tubulysins that undergoes post-assembly acylation and oxidation reactions. In the course of this study it could be demonstrated that pretubulysin inhibits the growth of cultured mammalian cells, as do tubulysins, which are already in advanced preclinical development as anticancer and antiangiogenic agents. The MoA of this highly potent compound class has been described and involves the depolymerization of microtubules, thereby inducing mitotic arrest. By total synthesis of pretubulysin, the supply issues with the naturally occurring derivatives can be circumvented and in contrast to tubulysin, pretubulysin is synthetically accessible in gram-scale quantities.

Encouragingly, it was found that the simplified precursor of tubulysin is nearly equally potent to the parent compound as demonstrated by growth inhibition studies using a panel of cell lines from different origin and tissue. The testing of several other pretubulysin derivatives, which were either direct synthetic precursors or altered in the substitution pattern at various positions of the linear tetrapeptide, revealed important SAR insights, which were partly not covered in studies on tubulysins so far. As a result, tested derivatives were less potent than pretubulysin itself or merely equally active. Nevertheless, it was found that also highly simplified molecules, such as pretubulysin analog III that consists only of two out of the four original amino acids, still exhibit a certain cytotoxicity in the micromolar range on mammalian

cell lines. Analyzing the antimetabolic potential of pretubulysins in comparison to well-studied myxobacterial secondary metabolites that target microtubules (tubulysins, disorazol, and epothilone) it was found that all tested microtubule destabilizers show a highly comparable MoA by means of tubulin-related effects. Interestingly, although the activity of pretubulysin analog III was reduced by approximately three orders of magnitude compared to pretubulysin in growth inhibition experiments, this compound still can bind to tubulin *in vitro* and cause microtubule depolymerization in cell-based assays. However, these effects appeared to be more toxic than observed for pretubulysin itself as revealed by flow cytometric measurements.

In more detailed studies it turned out that pretubulysin induces apoptosis in part via the intrinsic (mitochondrial) pathway as a result of mitotic block as depicted by a G₂/M cell cycle arrest, and is also able to inhibit the long-term survival of cancer cells. Similarly to results from *in vitro* experiments, pretubulysin was comparably active to its parent compound tubulysin. Consequently, pretubulysin appears to be an ideal candidate for future development in preclinical trials and is a very promising early lead structure in cancer therapy as it exhibits common characteristics of other already established antimetabolic compounds. In addition, SAR studies revealed possible modification sites of the core pretubulysin structure, which, in turn, might aid to develop improved pretubulysins and functionalized molecules for future in-depth preclinical evaluations. First attempts were already promising, as coumarin-tagged triazole-pretubulysin was still active in the low micromolar range and in addition, did not lose its ability to depolymerize microtubules. However, results from live cell imaging studies cannot be definitely construed at this stage. With a synthetic route in hand, pretubulysin can be easily modified by means of further simplification and the attachment of various other functional groups. Future synthetic approaches will thereby aid in obtaining greater insight into the MoA of this compound family and will allow the ‘fine-tuning’ of the target-binding, toxicity, and tumor specificity properties of pretubulysin.

5.2 CHONDRAMIDES

Several bottlenecks in traditional bioactivity-guided isolation hamper the successful discovery of new chemical entities with potent bioactivity from natural sources. One issue is the presence of already described bioactive metabolites in e.g. bacterial extracts that might mask activities of other interesting NPs. By implementing high-content screening for bioactivity-guided isolation with a focus on cytostatic compounds it was expected that the deconvolution of various observations, in terms of activity, might be greatly facilitated.

In the course of this study, extracts and fractions of *Chondromyces sp.* SBCm007 were subjected to in-depth HCS studies. Mainly two distinct biological effects were found: the polymerization of actin and a loss of lysosomal integrity. Compounds that induce the latter effect could not be isolated in the course of this work as these metabolites were produced in minute amounts only. Current work focuses on the production optimization with respect to these NPs.

However, dereplication of LC-MS data against our in-house database revealed the presence of chondramides A~D in SBCm007 extracts and this could further be confirmed by means of cytotoxicity as depicted by conventional viability screening using mammalian cell lines. These cyclic depsipeptides are described to target actin filaments with a similar binding mode to the mushroom toxin phalloidin. Astonishingly, in HCS experiments, actin polymerization was found throughout all prepared fractions, also in the 'non-chondramide' samples for which viability screening failed to detect any pronounced activity. Thus, by the application of focused HC screens, over 30 novel chondramide derivatives were discovered from *Chondromyces sp.* SBCm007, some of which were present in minute amounts only. In addition, supplementation of the culture broth with potassium bromide afforded the production of brominated analogs.

The initial biological profiling of 11 new derivatives in comparison to reference compounds (chondramides A~C) lead to important SAR conclusions. In particular, bromo-chondramide C3 and propionyl-bromo-chondramide C3 were the most active in cell-based studies, with GI₅₀ values on human cancer cell lines in the low nanomolar range. Furthermore, these bromo-chondramides are in average by factor 2-4 less cytotoxic for non-cancerous human cells in comparison to average values on cancer cell lines. However, for these two compounds activity could not be exclusively explained by a strong actin polymerizing effect, as observed for instance with chondramides A and B in *in vitro* experiments. In fact, *in vitro* actin polymerization using brominated analogs showed an apparently different progression than observed for chondramides A~C as bromo-chondramides were much less active in the cell-free system. For these reasons, a second cancer cell target for chondramides, other than actin, was proposed. This cellular target currently remains undiscovered and should be the subject of future investigations.

In summary, HCS is highlighted as a valuable tool for bioactivity-guided isolation of NPs from crude bacterial extracts. Given the fact that the growth inhibitory activity on cancer cell lines of newly discovered bromo-chondramide C3 and propionyl-bromo-chondramide C3 outcompetes that of described chondramides and that these derivatives were less potent on

non-cancerous human cells and less active in *in vitro* actin polymerization experiments, evidence for a putative off-target for this exciting class of NPs is provided. The results of the presented study can also aid the further SAR-guided development of chondramides either as molecular probes or pharmaceutical agents.

BIBLIOGRAPHY

- [1] J. W.-H. Li and J. C. Vederas, "Drug Discovery and Natural Products: End of an Era or an Endless Frontier?," *Science*, vol. 161, pp. 161-165, 2009.
- [2] D. D. Baker, M. Chu, U. Oza and V. Rajgarhia, "The value of natural products for future pharmaceutical discovery," *Nat. Prod. Rep.*, vol. 24, pp. 1225-1244, 2007.
- [3] A. L. Demain and A. Fang, "The Natural Functions of Secondary Metabolites," in *Advances in Biochemical Engineering/Biotechnology*, vol. 69, Berlin, Springer Verlag, 2000, pp. 1-39.
- [4] M. J. Kiristis and M. R. Parsek, "Does *Pseudomonas aeruginosa* use intercellular signalling to build biofilm communities?," *Cell. Microbiol.*, vol. 8, pp. 1841-1849, 2006.
- [5] D. A. Hogan and R. Kolter, "Pseudomonas-Candida Interactions: An Ecological Role for Virulence Factors," *Science*, vol. 296, pp. 2229-2232, 2002.
- [6] D. A. Hogan, A. Vik and R. Kolter, "A *Pseudomonas aeruginosa* quorum-sensing molecule influences *Candida albicans* morphology," *Mol. Microbiol.*, vol. 54, pp. 1212-1223, 2004.
- [7] P. D. Straight and R. Kolter, "Interspecies Chemical Communication and Bacterial Development," *Annu. Rev. Microbiol.*, vol. 63, pp. 99-118, 2009.
- [8] C. G. Jones and R. D. Firn, "On the Evolution of Plant Secondary Chemical Diversity," *Phil. Trans. R. Soc. Lond. B*, vol. 333, pp. 273-280, 1991.
- [9] R. D. Firn and C. G. Jones, "Natural products - a simple model to explain chemical diversity," *Nat. Prod. Rep.*, vol. 20, pp. 382-391, 2003.
- [10] R. Yuan and Y. Lin, "Traditional Chinese medicine: an approach to scientific proof and clinical validation," *Pharmacol. Ther.*, vol. 86, pp. 191-198, 2000.
- [11] F. E. Koehn and G. T. Carter, "The Evolving Role of Natural Products in Drug Discovery," *Nat. Rev. Drug Discov.*, vol. 4, pp. 206-220, 2005.
- [12] A. L. Harvey, "Natural products in drug discovery," *Drug Disc. Tod.*, vol. 13, pp. 894-901, 2008.
- [13] D. J. Newman and G. M. Cragg, "Natural Products as Sources of New Drugs over the Last 25 Years," *J. Nat. Prod.*, vol. 70, pp. 461-477, 2007.
- [14] M. C. Wani, H. L. Taylor, M. E. Wall, P. Coggon and A. T. McPhail, "Plant antitumor agents. VI. The isolation and structure of taxol, a novel antileukemic and antitumor agent from *Taxus brevifolia*," *J. Am. Chem. Soc.*, vol. 93, pp. 2325-2327, 1971.
- [15] W. P. McGuire, E. K. Rowinsky, N. B. Rosenshein, F. C. Grumbine, D. S. Ettinger, D. K. Armstrong and R. C. Donehower, "Taxol: a unique antineoplastic agent with significant activity in advanced ovarian epithelial neoplasms," *Ann. Intern. Med.*, vol. 111, pp. 273-279, 1989.

- [16] J. J. Manfredi and S. B. Horwitz, "Taxol: An Antimitotic Agent With a New Mechanism of Action," *Pharmac. Ther.*, vol. 25, pp. 83-125, 1984.
- [17] G. M. Cragg, S. A. Schepartz, M. Suffness and M. R. Grever, "The Taxol Supply Crisis. New NCI Policies for Handling the Large-Scale Production of Novel Natural Product Anticancer and Anti-HIV Agents," *J. Nat. Prod.*, vol. 56, pp. 1657-1668, 1993.
- [18] K. C. Nicolaou, W.-M. Dai and R. K. Guy, "Chemistry and Biology of Taxol," *Angew. Chem. Int. Ed. Engl.*, vol. 33, pp. 15-44, 1994.
- [19] D. G. I. Kingston, "Modern Natural Products Drug Discovery and Its Relevance to Biodiversity Conservation," *J. Nat. Prod.*, vol. 74, pp. 496-511, 2011.
- [20] K. C. Nicolaou, Z. Yang, J. J. Liu, H. Ueno, P. G. Nantermet, R. K. Guy, C. F. Claiborne, J. Renaud, E. A. Couladouros, K. Paulvannan and E. J. Sorensen, "Total synthesis of taxol," *Nature*, vol. 367, pp. 630-634, 1994.
- [21] L. Wessjohann, "The First Total Syntheses of Taxol," *Angew. Chem. Int. Ed. Engl.*, vol. 33, pp. 959-961, 1994.
- [22] L. A. Wessjohan, "Synthesis of natural-product-based compound libraries," *Curr. Opin. Chem. Biol.*, vol. 4, pp. 303-309, 2000.
- [23] D. J. Newman and G. M. Cragg, "Natural Products As Sources of New Drugs over the 30 Years from 1981 to 2010," *J. Nat. Prod.*, vol. 75, pp. 311-335, 2012.
- [24] M. S. Butler, "Natural products to drugs: natural product-derived compounds in clinical trials," *Nat. Prod. Rep.*, vol. 25, pp. 475-516, 2008.
- [25] L. Holm and C. Sander, "Mapping the Protein Universe," *Science*, vol. 273, pp. 595-602, 1996.
- [26] E. Kellenberger, A. Hofmann and R. J. Quinn, "Similar interactions of natural products with biosynthetic enzymes and therapeutic target could explain why nature produces such a large proportion of existing drugs," *Nat. Prod. Rep.*, vol. 28, pp. 1483-1492, 2011.
- [27] J. Clardy and C. Walsh, "Lessons from natural molecules," *Nature*, vol. 432, pp. 829-837, 2004.
- [28] G. T. Carter, "Natural products and Pharma 2011: Strategic changes spur new opportunities," *Nat. Prod. Rep.*, vol. 28, pp. 1783-1789, 2011.
- [29] I. Kola and J. Landis, "Can the pharmaceutical industry reduce attrition rates?," *Nat. Rev. Drug Discov.*, vol. 3, pp. 711-715, 2004.
- [30] S. Faivre, S. Djelloul and E. Raymond, "New Paradigms in Anticancer Therapy: Targeting Multiple Signaling Pathways With Kinase Inhibitors," *Semin. Oncol.*, vol. 33, pp. 407-420, 2006.
- [31] J. Zhang, P. L. Yang and N. S. Gray, "Targeting cancer with small molecule kinase inhibitors," *Nat. Rev. Canc.*, vol. 9, pp. 28-39, 2009.
- [32] C. T. Walsh, "Polyketide and Nonribosomal Peptide Antibiotics: Modularity and Versatility," *Science*, vol. 303, pp. 1805-1810, 2004.

-
- [33] M. M. Wagenaar, "Pre-fractionated microbial samples - the second generation natural products library at Wyeth," *Molecules*, vol. 13, pp. 1406-1426, 2008.
- [34] F. E. Koehn and G. T. Carter, "Rediscovering natural products as a source of new drugs," *Discov. Med.*, vol. 5, pp. 159-164, 2005.
- [35] F. W. Sertürner, "Darstellung der reinen Mohnsäure (Opiumsäure) nebst einer chemischen Untersuchung des Opiums mit vorzüglicher Hinsicht auf einen darin neu entdeckten Stoff und dahin gehörigen Bemerkungen," *Tromsdorffs Journal der Pharmazie*, vol. 14, pp. 47-93, 1806.
- [36] G. R. Hamilton and T. F. Baskett, "In the arms of Morpheus: the development of morphine for postoperative pain relief," *Can. J. Anaest.*, vol. 47, pp. 367-374, 2000.
- [37] J. Bérdy, "Bioactive Microbial Metabolites," *J. Antibiot.*, vol. 58, pp. 1-26, 2005.
- [38] B. L. Ligon, "Penicillin: its discovery and early development," *Semin. Pediatr. Infect. Dis.*, vol. 15, pp. 52-57, 2004.
- [39] J. Davies, "Where have all the antibiotics gone?," *Can. J. Infect. Dis. Med. Microbiol.*, vol. 17, pp. 287-290, 2006.
- [40] M. G. Watve, R. Tickoo, M. M. Jog and B. D. Bhole, "How many antibiotics are produced by the genus *Streptomyces*?," *Arch. Microbiol.*, vol. 176, pp. 386-390, 2001.
- [41] R. H. Baltz, "Renaissance in antibacterial discovery from actinomycetes," *Curr. Opin. Pharmacol.*, vol. 8, pp. 557-563, 2008.
- [42] R. H. Baltz, "Antimicrobials from Actinomycetes: Back to the Future," *Microbe*, vol. 2, pp. 125-131, 2007.
- [43] W. Fenical and P. R. Jensen, "Developing a new resource for drug discovery: marine actinomycete bacteria," *Nat. Chem. Biol.*, vol. 2, pp. 666-673, 2006.
- [44] R. H. Felting, G. O. Buchanan, T. J. Mincer, C. A. Kauffman, P. R. Jensen and W. Fenical, "Salinosporamide A: A Highly Cytotoxic Proteasome Inhibitor from a Novel Microbial Source, a Marine Bacterium of the New Genus *Salinospora*," *Angew. Chem. Int. Ed.*, vol. 42, pp. 355-357, 2003.
- [45] K. S. Lam, G. K. Lloyd, S. T. C. Neuteboom, M. A. Palladino, K. M. Sethna, M. A. Spear and B. C. Potts, "From Natural Product to Clinical Trials: NPI-0052 (Salinosporamide A), a Marine Actinomycete-Derived Anticancer Agent," in *Natural Product Chemistry for Drug Discovery*, Royal Society of Chemistry, 2010, pp. 355-373.
- [46] S. B. Zotchev, "Marine actinomycetes as an emerging resource for the drug development pipelines," *J. Biotechnol.*, vol. 158, pp. 168-175, 2012.
- [47] E. M. Fox and B. J. Howlett, "Secondary metabolism: regulation and role in fungal biology," *Curr. Opin. Microbiol.*, vol. 11, pp. 481-487, 2008.
- [48] A. A. Brakhage and V. Schroeckh, "Fungal secondary metabolites - Strategies to activate silent gene clusters," *Fung. Genet. Biol.*, vol. 48, pp. 15-22, 2011.

- [49] D. L. Hawksworth, "The fungal dimension of biodiversity: magnitude, significance, and conservation," *Mycol. Res.*, vol. 95, pp. 641-655, 1991.
- [50] D. L. Hawksworth, "The magnitude of fungal diversity: the 1.5 million species estimate revisited," *Mycol. Res.*, vol. 105, pp. 1422-1432, 2001.
- [51] T. A. Richards, M. D. M. Jones, G. Leonard and D. Bass, "Marine Fungi: Their Ecology and Molecular Diversity," *Annu. Rev. Mar. Sci.*, vol. 4, pp. 495-522, 2012.
- [52] B. Schulz, C. Boyle, S. Draeger, A.-K. Römmert and K. Krohn, "Endophytic fungi: a source of novel biologically active secondary metabolites," *Mycol. Res.*, vol. 106, pp. 996-1004, 2002.
- [53] S. E. Hartley and A. C. Gange, "Impacts of Plant Symbiotic Fungi on Insect Herbivores: Mutualism in a Multitrophic Context," *Annu. Rev. Entomol.*, vol. 54, pp. 323-342, 2009.
- [54] H. W. Zhang, Y. C. Song and R. X. Tan, "Biology and chemistry of endophytes," *Nat. Prod. Rep.*, vol. 23, pp. 753-771, 2006.
- [55] M. Wink, "Plant secondary metabolism: diversity, function and its evolution," *Nat. Prod. Commun.*, vol. 3, pp. 1205-1216, 2008.
- [56] T. Iizuka, Y. Jojima, R. Fudou and S. Yamanaka, "Isolation of myxobacteria from the marine environment," *FEMS Microbiol. Lett.*, vol. 169, pp. 317-322, 1998.
- [57] R. A. Sanford, J. R. Cole and J. M. Tiedje, "Characterization and description of *Anaeromyxobacter dehalogenans* gen. nov., sp. nov., an aryl-halo-respiring facultative anaerobic myxobacterium," *Appl. Environ. Microbiol.*, vol. 68, pp. 893-900, 2002.
- [58] W. Dawid, C. A. Gallikowski and P. Hirsch, "Psychrophilic myxobacteria from Antarctic soils," *Polarforschung*, vol. 58, pp. 271-278, 1988.
- [59] H. Reichenbach, "The ecology of the myxobacteria," *Environ. Microbiol.*, vol. 1, pp. 15-21, 1999.
- [60] W. Dawid, "Biology and global distribution of myxobacteria in soils," *FEMS Microbiol. Rev.*, vol. 24, pp. 403-427, 2000.
- [61] H. Reichenbach, "Myxobacteria, producers of novel bioactive substances," *J. Ind. Microbiol. Biotechnol.*, vol. 27, pp. 149-156, 2001.
- [62] G. J. Velicer and M. Vos, "Sociobiology of Myxobacteria," *Annu. Rev. Microbiol.*, vol. 63, pp. 599-623, 2009.
- [63] D. Kaiser, "Coupling Cell Movement to Multicellular Development in Myxobacteria," *Nat. Rev. Microbiol.*, vol. 1, pp. 46-64, 2003.
- [64] J. E. Berleman and J. R. Kirby, "Deciphering the hunting strategy of a bacterial wolfpack," *FEMS Microbiol. Rev.*, vol. 33, pp. 942-957, 2009.
- [65] B. Nan, J. Chen, J. C. Neu, R. M. Berry, G. Oster and D. R. Zusman, "Myxobacteria gliding motility requires cytoskeleton rotation powered by proton motive force," *Proc. Natl. Acad. Sci. USA*, vol. 108, pp. 2498-2503, 2011.

- [66] J. Hodgkin and D. Kaiser, "Genetics of gliding motility in *Myxococcus xanthus* (Myxobacterales): genes controlling movement of single cells," *Mol. Gen. Genet.*, vol. 171, pp. 177-191, 1979.
- [67] Y. N. Li, H. Sun, X. Y. Ma, A. Lu, R. Lux, D. Zusman and W. Shi, "Extracellular polysaccharides mediate pilus retraction during social motility of *Myxococcus xanthus*," *Proc. Natl. Acad. Sci. USA*, vol. 100, pp. 5443-5448, 2003.
- [68] R. Yu and D. Kaiser, "Gliding motility and polarized slime secretion," *Mol. Microbiol.*, vol. 63, pp. 454-467, 2007.
- [69] T. Mignot, J. W. Shaevitz, P. L. Hartzell and D. R. Zusman, "Evidence that focal adhesion complexes power bacterial gliding motility," *Science*, vol. 315, pp. 853-856, 2007.
- [70] J. Diez, J. P. Martinez, J. Mestres, F. Sasse, R. Frank and A. Meyerhans, "Myxobacteria: natural pharmaceutical factories," *Microb. Cell Fact.*, vol. 11, p. 52 [Epub ahead of print], 2012.
- [71] B. S. Goldman, W. C. Nierman, D. Kaiser, S. C. Slater, A. S. Durkin, J. A. Eisen, C. M. Ronning, W. B. Barbazuk, M. Blanchard, C. Field, C. Halling, G. Hinkle, O. Iartchuk, H. S. Kim, C. Mackenzie, R. Madupu, N. Miller, A. Shvartsbeyn, S. A. Sullivan, M. Vaudin, R. Wiegand and H. B. Kaplan, "Evolution of sensory complexity recorded in a myxobacterial genome," *PNAS*, vol. 103, pp. 15200-15205, 2006.
- [72] B. E. Laue and R. E. Gill, "Use of a phase variation-specific promoter of *Myxococcus xanthus* in a strategy for isolating a phase-locked mutant," *J. Bacteriol.*, vol. 176, pp. 5341-5349, 1994.
- [73] B. E. Laue and R. E. Gill, "Using a phase-locked mutant of *Myxococcus xanthus* to study the role of phase variation in development," *J. Bacteriol.*, vol. 177, pp. 4089-4096, 1995.
- [74] P. Meiser, H. B. Bode and R. Müller, "The unique DKxanthene secondary metabolite family from the myxobacterium *Myxococcus xanthus* is required for developmental sporulation," *PNAS*, vol. 103, pp. 19128-19133, 2006.
- [75] S. C. Wenzel and R. Müller, "The biosynthetic potential of myxobacteria and their impact in drug discovery," *Curr. Opin. Drug. Discov. Devel.*, vol. 12, pp. 220-230, 2009.
- [76] K. J. Weissman and R. Müller, "Myxobacterial secondary metabolites: bioactivities and modes-of-action," *Nat. Prod. Rep.*, vol. 27, pp. 1276-1295, 2010.
- [77] K. J. Weissman and R. Müller, "A brief tour of myxobacterial secondary metabolism," *Bioorg. Med. Chem.*, vol. 17, pp. 2121-2136, 2009.
- [78] K. Gerth, S. Pradella, O. Perlova, S. Beyer and R. Müller, "Myxobacteria: proficient producers of novel natural products with various biological activities - past and future biotechnological aspects with the focus on the genus *Sorangium*," *J. Biotechnol.*, vol. 106, pp. 233-253, 2003.
- [79] R. O. Garcia, D. Krug and R. Müller, "Chapter 3. Discovering natural products from myxobacteria with emphasis on rare producer strains in combination with improved analytical methods," *Methods Enzymol.*, vol. 458, pp. 59-91, 2009.
- [80] M. Nett and G. M. König, "The chemistry of gliding bacteria," *Nat. Prod. Rep.*, vol. 24, pp. 1245-1261, 2007.

- [81] B. Kunze, T. Kemmer, G. Höfle and H. Reichenbach, "Stigmatellin, a new antibiotic from *Stigmatella aurantiaca* (myxobacterales). I. Production, physico-chemical and biological properties," *J. Antibiot. (Tokyo)*, vol. 37, pp. 454-461, 1984.
- [82] G. von Jagow and T. Ohnishi, "The chromone inhibitor stigmatellin - binding to the ubiquinol oxidation center at the C-side of the mitochondrial membrane," *FEBS Lett.*, vol. 185, pp. 311-315, 1985.
- [83] F. Sasse, H. Steinmetz, G. Höfle and H. Reichenbach, "Archazolids, new cytotoxic macrolactones from *Archangium gephyra* (Myxobacteria). Production, isolation, physico-chemical and biological properties," *J. Antibiot. (Tokyo)*, vol. 56, pp. 520-525, 2003.
- [84] M. Huss, F. Sasse, B. Kunze, R. Jansen, H. Steinmetz, G. Ingenhorst, A. Zeeck and H. Wieczorek, "Archazolid and apicularen: novel specific V-ATPase inhibitors," *BMC Biochem.*, vol. 4, p. 6:13, 2005.
- [85] M. Huss and H. Wieczorek, "Inhibitors of V-ATPases: old and new players," *J. Exp. Biol.*, vol. 212, pp. 341-346, 2009.
- [86] M. Pérez-Sayáns, J. M. Somoza-Martín, F. Barros-Angueira, J. M. Rey and A. García-García, "V-ATPase inhibitors and implication in cancer treatment," *Cancer Treat. Rev.*, vol. 35, pp. 707-713, 2009.
- [87] S. M. Ringel, R. C. Greenough, S. Roemer, D. Connor, A. L. Gutt, B. Blair, G. Kanter and M. von Strandtmann, "Ambruticin (W7783), a new antifungal antibiotic," *J. Antibiot. (Tokyo)*, vol. 30, pp. 371-375, 1977.
- [88] S. M. Ringel, "In Vitro and In Vivo Studies of Ambruticin (W7783): New Class of Antifungal Agents," *Antimicrob. Agents Chemother.*, vol. 12, pp. 762-769, 1978.
- [89] L. Vetcher, H. G. Menzella, T. Kudo, T. Motoyama and L. Katz, "The antifungal polyketide ambruticin targets the HOG pathway," *Antimicrob. Agents Chemother.*, vol. 51, pp. 3734-3736, 2007.
- [90] K. Gerth, N. Bedorf, H. Irschik, G. Höfle and H. Reichenbach, "The soraphens: a family of novel antifungal compounds from *Sorangium cellulosum* (Myxobacteria). I. Soraphen A1 alpha: fermentation, isolation, biological properties," *J. Antibiot. (Tokyo)*, vol. 47, pp. 23-31, 1994.
- [91] H. F. Vahlensieck, L. Pridzun, H. Reichenbach and A. Hinnen, "Identification of the yeast ACC1 gene product (acetyl-CoA carboxylase) as the target of the polyketide fungicide soraphen A," *Curr. Genet.*, vol. 25, pp. 95-100, 1994.
- [92] D. B. Jump, M. Torres-Gonzales and L. K. Olson, "Soraphen A, an inhibitor of acetyl CoA carboxylase activity, interferes with fatty acid elongation," *Biochem. Pharmacol.*, vol. 81, pp. 649-660, 2011.
- [93] A. M. Olsen, B. L. Eisenberg, N. B. Kuemmerle, A. J. Flanagan, P. M. Morganelli, P. S. Lombardo, J. V. Swinnen and W. B. Kinlaw, "Fatty acid synthesis is a therapeutic target in human liposarcoma," *Int. J. Oncol.*, vol. 36, pp. 1309-1314, 2010.
- [94] D. M. Bollag, P. A. McQueney, J. Zhu, O. Hensens, L. Koupal, J. Liesch, M. Goetz, E. Lazarides and C. M. Woods, "Epothilones, a new class of microtubule-stabilizing agents with a taxol-like mechanism of action," *Cancer Res.*, vol. 55, pp. 2325-2333, 1995.

- [95] K. Gerth, N. Bedorf, G. Höfle, H. Irschik and H. Reichenbach, "Epothilons A and B: Antifungal and Cytotoxic Compounds from *Sorangium cellulosum* (Myxobacteria). Production, Physico-chemical and Biological Properties," *J. Antibiot. (Tokyo)*, vol. 49, pp. 560-563, 1996.
- [96] A. Conlin, M. Fournier, C. Hudis, S. Kar and P. Kirkpatrick, "Ixabepilone," *Nat. Rev. Drug Discov.*, vol. 6, pp. 953-954, 2007.
- [97] M. Herrmann, B. Böhlendorf, H. Irschik, H. Reichenbach and G. Höfle, "Maracin and Maracen: New Types of Ethynyl Vinyl Ether and alpha-Chloro Divinyl Ether Antibiotics from *Sorangium cellulosum* with Specific Activity Against Mycobacteria," *Angew. Chem. Int. Ed.*, vol. 37, pp. 1253-1255, 1998.
- [98] S. C. Wenzel and R. Müller, "The impact of genomics on the exploitation of the myxobacterial secondary metabolome," *Nat. Prod. Rep.*, vol. 26, pp. 1385-1407, 2009.
- [99] B. S. Goldman, W. C. Nierman, D. Kaiser, S. C. Slater, A. S. Durkin, J. A. Eisen, C. M. Ronning, W. B. Barbazuk, M. Blanchard, C. Field, C. Halling, G. Hinkle, O. Iartchuk, H. S. Kim, C. Mackenzie, R. Madupu, N. Miller, A. Shvartsbeyn, S. A. Sullivan, M. Vaudin, R. Wiegand and H. B. Kaplan, "Evolution of sensory complexity recorded in a myxobacterial genome," *PNAS*, vol. 103, pp. 15200-15205, 2006.
- [100] S. Schneiker, O. Perlova, O. Kaiser, K. Gerth, A. Alici, M. O. Altmeyer, D. Bartels, T. Bekel, S. Beyer, E. Bode, H. B. Bode, C. J. Bolten, J. V. Choudhuri, S. Doss, Y. E. Elnakady, B. Frank, L. Gaigalat, A. Goesmann, C. Groeger, F. Gross, L. Jelsbak, L. Jelsbak, J. Kalinowski, C. Kegler, T. Knauber, S. Konietzny, M. Kopp, L. Krause, D. Krug, B. Linke, T. Mahmud, R. Martinez-Arias, A. C. McHardy, M. Merai, F. Meyer, S. Mormann, J. Munoz-Dorado, J. Perez, S. Pradella, S. Rachid, G. Raddatz, F. Rosenau, C. Rückert, F. Sasse, M. Scharfe, S. C. Schuster, G. Suen, A. Treuner-Lange, G. J. Velicer, F.-J. Vorhölter, K. J. Weissman, R. D. Welch, S. C. Wenzel, D. E. Withworth, S. Wilhelm, C. Wittmann, H. Blöcker, A. Pühler and R. Müller, "Complete genome sequence of the myxobacterium *Sorangium cellulosum*," *Nat. Biotechnol.*, vol. 25, pp. 1281-1289, 2007.
- [101] H. B. Bode and R. Müller, "Analysis of myxobacterial secondary metabolism goes molecular," *J. Ind. Microbiol. Biotechnol.*, vol. 33, pp. 577-588, 2006.
- [102] S. D. Bentley, K. F. Chater, A.-M. Cerdeno-Tárraga, G. L. Challis, N. R. Thomson, K. D. James, D. E. Harris, M. A. Quail, H. Kieser, D. Harper, A. Bateman, S. Brown, G. Chandra, C. W. Chen, M. Collins, A. Cronin, A. Fraser, A. Goble, J. Hidalgo, T. Hornsby, S. Howarth, C.-H. Huang, T. Kieser, L. Larke, L. Murphy, K. Oliver, S. O'Neil, E. Rabinowitsch, M.-A. Rajandream, K. Rutherford, S. Rutter, K. Seeger, D. Saunders, S. Sharp, R. Squares, S. Squares, K. Taylor, T. Warren, A. Wietzorrek, J. Woodward, B. G. Barrell, J. Parkhill and D. A. Hopwood, "Complete genome sequence of the model actinomycete *Streptomyces coelicolor* A3(2)," *Nature*, vol. 417, pp. 141-147, 2002.
- [103] S. C. Wenzel and R. Müller, "Myxobacterial natural product assembly lines. fascinating examples of curious biochemistry," *Nat. Prod. Rep.*, vol. 24, pp. 1211-1224, 2007.
- [104] N. S. Cortina, D. Krug, A. Plaza, O. Revermann and R. Müller, "Myxoprincomide: A Natural Product from *Myxococcus xanthus* Discovered by Comprehensive Analysis of the Secondary Metabolome," *Angew. Chem. Int. Ed.*, vol. 51, pp. 811-816, 2012.
- [105] B. Wilkinson and J. Micklefield, "Mining and engineering natural-product biosynthetic pathways," *Nat. Chem. Biol.*, vol. 3, pp. 379-386, 2007.

- [106] J. Stach, "Antimicrobials: treasures from the ocean," *Microbiol. Today*, vol. 37, pp. 104-109, 2010.
- [107] Z. E. Wilson and M. A. Brimble, "Molecules derived from the extremes of life," *Nat. Prod. Rep.*, vol. 26, pp. 44-71, 2009.
- [108] S. Qin, K. Xing, J.-H. Jiang, L.-H. Xu and W.-J. Li, "Biodiversity, bioactive natural products and biotechnological potential of plant-associated endophytic actinobacteria," *Appl. Microbiol. Biotechnol.*, vol. 89, pp. 457-473, 2011.
- [109] D. Skropeta, "Deep-sea natural products," *Nat. Prod. Rep.*, vol. 25, pp. 1131-1166, 2008.
- [110] D. G. I. Kingston, "Modern Natural Products Drug Discovery and Its Relevance to Biodiversity Conservation," *J. Nat. Prod.*, vol. 74, pp. 496-511, 2011.
- [111] A. Harvey, "Strategies for discovering drugs from previously unexplored natural products," *Drug Discov. Today*, vol. 5, pp. 294-300, 2000.
- [112] A. A. Stierle, D. B. Stierle and T. Girtsman, "Caspase-1 Inhibitors from an Extremophilic Fungus That Target Specific Leukemia Cell Lines," *J. Nat. Prod.*, vol. 75, pp. 344-350, 2012.
- [113] B. Bister, D. Bischoff, M. Ströbele, J. Riedlinger, A. Reicke, F. Wolter, A. T. Bull, H. Zähler, H.-P. Fiedler and R. D. Süßmuth, "Abyssomicin C - A Polycyclic Antibiotic from a Marine *Verrucospora* Strain as an Inhibitor of the p-Aminobenzoic Acid/Tetrahydrofolate Biosynthesis Pathway," *Angew. Chem. Int. Ed.*, vol. 43, pp. 2574-2576, 2004.
- [114] J. S. Freundlich, M. Lalgondar, J.-R. Wei, S. Swanson, E. J. Sorensen, E. J. Rubin and J. C. Sacchettini, "The Abyssomicin C family as in vitro inhibitors of *Mycobacterium tuberculosis*," *Tuberculosis*, vol. 90, pp. 298-300, 2010.
- [115] S. Kusari, S. Zühlke and M. Spiteller, "An Endophytic Fungus from *Camptotheca acuminata* That Produces Camptothecin and Analogues," *J. Nat. Prod.*, vol. 72, pp. 2-7, 2009.
- [116] E. L. Ghisalberti, "Detection and Isolation of Bioactive Natural Products," in *Bioactive Natural Products: Detection, Isolation, and Structural Determination*, 2nd ed., CRC Press, 2007, pp. 11-76.
- [117] L. M. Mayr and P. Fuerst, "The Future of High-Throughput Screening," *J. Biomol. Screen.*, vol. 13, pp. 443-448, 2008.
- [118] K. Young, H. Jayasuriya, J. G. Ondeyka, K. Herath, C. Zhang, S. Kodali, A. Galgoci, R. Painter, V. Brown-Driver, R. Yamamoto, L. L. Silver, Y. Zheng, J. I. Ventura, J. Sigmund, S. Ha, A. Basilio, F. Vicente, J. R. Tormo, F. Pelaez, P. Youngman, D. Cully, J. F. Barrett, D. Schmatz, S. B. Singh and J. Wang, "Discovery of FabH/FabF Inhibitors from Natural Products," *Antimicrob. Agents Chemother.*, vol. 50, pp. 519-526, 2006.
- [119] J. Wang, S. M. Soisson, K. Young, W. Shoop, S. Kodali, A. Galgoci, R. Painter, G. Parthasarathy, Y. S. Tang, R. Cummings, S. Ha, K. Dorso, M. Motyl, H. Jayasuriya, J. Ondeyka, K. Herath, C. Zhang, L. Hernandez, J. Allocco, A. Basilio, J. R. Tormo, O. Genilloud, F. Vicente, F. Pelaez, L. Colwell, S. H. Lee, B. Michael, T. Felcetto, C. Gill, L. L. Silver, J. D. Hermes, K. Bartizal, J. Barrett, D. Schmatz, J. W. Becker, D. Cully and S. B. Singh, "Platensimycin is a selective FabF inhibitor with potent antibiotic properties," *Nature*, vol. 441, pp. 358-361, 2006.

- [120] H. Jayasuriya, K. B. Herath, C. Zhang, D. L. Zink, A. Basilio, O. Genilloud, M. T. Diez, F. Vicente, I. Gonzalez, O. Salazar, F. Pelaez, R. Cummings, S. Ha, J. Wang and S. B. Singh, "Isolation and Structure of Platenicin: A FabH and FabF Dual Inhibitor with Potent Broad-Spectrum Antibiotic Activity," *Angew. Chem. Int. Ed.*, vol. 46, pp. 4684-4688, 2007.
- [121] N. Kato, S. Takahashi, T. Nogawa, T. Saito and H. Osada, "Construction of a microbial natural product library for chemical biology studies," *Curr. Opin. Chem. Biol.*, vol. 16, pp. 101-108, 2012.
- [122] D. Camp, R. A. Davis, M. Campitelli, J. Ebdon and R. J. Quinn, "Drug-like Properties: Guiding Principles for the Design of Natural Product Libraries," *J. Nat. Prod.*, vol. 75, pp. 72-81, 2012.
- [123] T. A. Johnson, J. Sohn, W. D. Inman, S. A. Estee, S. T. Loveridge, H. C. Vervoort, K. Tenney, J. Liu, K. K.-H. Ang, J. Ratnam, W. M. Bray, N. C. Gassner, Y. Y. Shen, R. S. Lokey, J. H. McKerrow, K. Boundy-Mills, A. Nukanto, A. Kanti, H. Julistiono, L. B. S. Kardono, L. F. Bjeldanes and P. Crews, "Natural Product Libraries to Accelerate the High-Throughput Discovery of Therapeutic Leads," *J. Nat. Prod.*, vol. 74, pp. 2545-2555, 2011.
- [124] T. S. Bugni, B. Richards, L. Bhoite, D. Cimborá, M. K. Harper and C. M. Ireland, "Marine Natural Product Libraries for High-Throughput Screening and Rapid Drug Discovery," *J. Nat. Prod.*, vol. 71, pp. 1095-1098, 2008.
- [125] S. Fox, S. Farr-Jones, A. Boggs, H. Wang Nicely, R. Khoury and M. Biros, "High-Throughput Screening: Update on Practices and Success," *J. Biomol. Screen.*, vol. 11, pp. 864-869, 2006.
- [126] F. Zanella, J. B. Lorens and W. Link, "High content screening: seeing is believing," *Trends Biotechnol.*, vol. 28, pp. 237-245, 2010.
- [127] K. A. Giuliano, J. R. Haskins and D. L. Taylor, "Advances in High Content Screening for Drug Discovery," *Assay Drug Devel. Technol.*, vol. 1, pp. 565-577, 2003.
- [128] S. A. Haney, P. LaPan, J. Pan and J. Zhang, "High-content screening moves to the front of the line," *Drug Disc. Today*, vol. 11, pp. 889-894, 2006.
- [129] W. Link, J. Oyarzabai, B. G. Serelde, M. I. Albarran, O. Rabal, A. Cebriá, P. Alfonso, J. Fominaya, O. Renner, S. Peregrina, D. Soilán, P. A. Ceballos, A.-I. Hernández, M. Lorenzo, P. Pevarello, T. G. Granda, G. Kurz, A. Carnero and J. R. Bischoff, "Chemical Interrogation of FOXO3a Nuclear Translocation Identifies Potent and Selective Inhibitors of Phosphoinositide 3-Kinases," *J. Biol. Chem.*, vol. 284, pp. 28392-28400, 2009.
- [130] Y.-J. Kwon, W. Lee, A. Genovesio and N. Emans, "A High-Content Subtractive Screen for Selecting Small Molecules Affecting Internalization of GPCRs," *J. Biomol. Screen.*, vol. 17, pp. 379-385, 2012.
- [131] V. Starkuviene, U. Liebel, J. C. Simpson, H. Erfle, A. Poustka, S. Wiemann and R. Pepperkok, "High-Content Screening Microscopy Identifies Novel Proteins With a Putative Role in Secretory Membrane Traffic," *Genome Res.*, vol. 14, pp. 1948-1956, 2004.
- [132] J. Wang, X. Zhou, P. L. Bradley, S. F. Chang, N. Perrimon and S. T. Wong, "Cellular phenotype recognition for high-content RNA interference genome-wide screening," *J. Biomol. Screen.*, vol. 13, pp. 29-39, 2008.

- [133] M. T. Donato, L. Tolosa, N. Jiménez, J. V. Castell and M. J. Gómez-Lechón, "High-Content Imaging Technology for the Evaluation of drug-Induced Steatosis Using a Multiparametric Cell-Based Assay," *J. Biomol. Screen.*, vol. 17, pp. 394-400, 2012.
- [134] D. L. Towne, E. E. Nicholl, K. M. Comess, S. C. Galasinski, P. J. Hajduk and V. C. Abraham, "Development of a High-Content Screening Assay Panel to Accelerate Mechanism of Action Studies for Oncology Research," *J. Biomol. Screen.*, p. [Epub ahead of print], 2012.
- [135] G. T. Bass, K. A. Ryall, A. Katikapalli, B. E. Taylor, S. T. Dang, S. T. Acton and J. J. Saucerman, "Automated image analysis identifies signaling pathways regulating distinct signatures of cardiac myocyte hypertrophy," *J. Mol. Cell. Cardiol.*, vol. 52, pp. 923-930, 2012.
- [136] P. D. Andrews, M. Becroft, A. Aspegren, J. Gilmour, M. J. James, S. McRae, R. Kime, R. W. Allcock, A. Abraham, Z. Jiang, R. Strehl, J. C. Mountford, G. Milligan, M. D. Houslay, D. R. Adams and J. A. Frearson, "High-content screening of feeder-free human embryonic stem cells to identify pro-survival small molecules," *Biochem. J.*, vol. 432, pp. 21-33, 2010.
- [137] P. Brodin and T. Christophe, "High-content screening in infectious diseases," *Curr. Opin. Chem. Biol.*, vol. 15, pp. 534-539, 2011.
- [138] A. Vogt, A. Cholewinski, X. Shen, S. G. Nelson, J. S. Lazo, M. Tsang and N. A. Hukriede, "Automated Image-Based Phenotypic Analysis in Zebrafish Embryos," *Dev. Dyn.*, vol. 238, pp. 656-663, 2009.
- [139] N. A. Jensen, K. Gerth, T. Grotjohann, D. Kapp, M. Keck and K. Niehaus, "Establishment of a high content assay for the identification and characterisation of bioactivities in crude bacterial extracts that interfere with the eukaryotic cell cycle," *J. Biotechnol.*, vol. 140, pp. 124-134, 2009.
- [140] S. Cervantes, P. E. Stout, J. Prudhomme, S. Engel, M. Bruton, M. Cervantes, D. Carter, Y. Tae-Chang, M. E. Hay, W. Aalbersberg, J. Kubanek and K. G. Le Roch, "High content live cell imaging for the discovery of new antimalarial marine natural products," *BMC Infect. Dis.*, vol. 12:1, 2011.
- [141] A. Koul, E. Arnoult, N. Lounis, J. Guillemont and K. Andries, "The challenge of new drug discovery for tuberculosis," *Nature*, vol. 469, pp. 483-490, 2011.
- [142] G. M. Cragg, P. G. Grothaus and D. J. Newman, "Impact of Natural Products on Developing New Anti-Cancer Agents," *Chem. Rev.*, vol. 109, pp. 3012-3043, 2009.
- [143] N. Triller, P. Korosec, I. Kern, M. Kosnik and A. Debeljak, "Multidrug resistance in small cell lung cancer: expression of P-glycoprotein, multidrug resistance protein 1 and lung resistance protein in chemo-naive patients and in relapsed disease," *Lung Cancer*, vol. 54, pp. 235-240, 2006.
- [144] P. Neuhaus, J. Klupp and J. M. Langrehr, "mTOR Inhibitors: An Overview," *Liver Transplantation*, vol. 7, pp. 473-484, 2001.
- [145] A. W. Alberts, "Lovastatin and Simvastatin - Inhibitors of HMG CoA Reductase and Cholesterol Biosynthesis," *Cardiology*, vol. 77, pp. 14-21, 1990.
- [146] A. L. Dourmishev, L. A. Dourmishev and R. A. Schwartz, "Ivermectin: pharmacology and application in dermatology," *Int. J. Dermatol.*, vol. 44, pp. 981-988, 2005.

- [147] C. Triplitt and E. Chiquette, "Exenatide: from the Gila monster to the pharmacy," *J. Am. Pharm. Assoc.* (2003), vol. 46, pp. 44-52 quiz 53-54, 2006.
- [148] G. M. Cragg and D. J. Newman, "Plants as source of anti-cancer agents," *J. Ethnopharmacol.*, vol. 100, pp. 72-79, 2005.
- [149] M. Gordaliza, P. A. García, J. M. Miguel del Corral, M. A. Castro and M. A. Gómez-Zurita, "Podophyllotoxin: distribution, sources, applications and new cytotoxic derivatives," *Toxicon*, vol. 44, pp. 441-459, 2004.
- [150] K. R. Hande, "Etoposide: four decades of development of a topoisomerase II inhibitor," *Eur. J. Cancer*, vol. 34, pp. 1514-1521, 1998.
- [151] T. Sandmann and M. Boutros, "Screens, maps & networks: from genome sequences to personalized medicine," *Curr. Opin. Genet. Dev.*, vol. 22, pp. 36-44, 2012.
- [152] K. Hastak, E. Alli and J. M. Ford, "Synergistic Chemosensitivity of Triple-Negative Breast Cancer Cell Lines to Poly(ADP-Ribose) Polymerase Inhibition, Gemcitabine, and Cisplatin," *Cancer Res.*, vol. 70, pp. 7970-7980, 2010.
- [153] G. D'Onoforio, F. Tramontano, A. S. Dorio, A. Muzi, V. Maselli, D. Fulgione, G. Graziani, M. Malanga and P. Quesada, "Poly(ADP-ribose) polymerase signaling of topoisomerase 1-dependent DNA damage in carcinoma cells," *Biochem. Pharmacol.*, vol. 81, pp. 194-202, 2011.
- [154] K. Aziz, S. Nowsheen, G. Pantelias, G. Iliakis, V. G. Gorgoulis and A. G. Georgakilas, "Targeting DNA damage and repair: Embracing the pharmacological era of successful cancer therapy," *Pharmacol. Ther.*, vol. 133, pp. 334-350, 2012.
- [155] D. Fabbro, S. Ruetz, E. Buchdunger, S. W. Cowan-Jacob, G. Fendrich, J. Liebetanz, J. Mestan, T. O'Reilly, P. Traxler, B. Chaudhuri, H. Fretz, J. Zimmermann, T. Meyer, G. Caravatti, P. Furet and P. W. Manley, "Protein kinases as targets for anticancer agents: from inhibitors to useful drugs," *Pharmacol Ther.*, vol. 93, pp. 79-98, 2002.
- [156] S. M. Wilhelm, C. Carter, L. Tang, D. Wilkie, A. McNabola, H. Rong, C. Chen, X. Zhang, P. Vincent, M. McHugh, Y. Cao, J. Shujath, S. Gawlak, D. Eveleigh, B. Rowley, L. Liu, L. Adnane, M. Lynch, D. Auclair, I. Taylor, R. Gedrich, A. Voznesensky, B. Riedl, L. E. Post, G. Bollag and P. A. Trail, "BAY 43-9006 Exhibits Broad Spectrum Oral Antitumor Activity and Targets the RAF/MEK/ERK Pathway and Receptor Tyrosine Kinases Involved in Tumor Progression and Angiogenesis," *Cancer Res.*, vol. 64, pp. 7099-7109, 2004.
- [157] C. Dumontet and M. A. Jordan, "Microtubule-binding agents: a dynamic field of cancer therapeutics," *Nat. Rev. Drug Discov.*, vol. 9, pp. 790-803, 2010.
- [158] J. Sterz, I. von Metzler, J.-C. Hahne, B. Lamottke, J. Rademacher, U. Heider, E. Terpos and O. Sezer, "The potential of proteasome inhibitors in cancer therapy," *Expert Opin. Investig. Drugs*, vol. 17, pp. 879-895, 2008.
- [159] B. Sitohy, J. A. Nagy and H. F. Dvorak, "Anti-VEGF/VEGFR Therapy for Cancer: Reassessing the Target," *Cancer Res.*, vol. 72, pp. 1909-1914, 2012.

- [160] A. Giaccia, B. G. Siim and R. S. Johnson, "HIF-1 as Target for Drug Development," *Nat. Rev. Drug Discov.*, vol. 2, pp. 803-811, 2003.
- [161] L. Ducry and B. Stump, "Antibody-Drug Conjugates: Linking Cytotoxic Payloads to Monoclonal Antibodies," *Bioconjugate Chem.*, vol. 21, pp. 5-13, 2010.
- [162] J. A. Francisco, C. G. Cerveny, D. L. Meyer, B. J. Mixan, K. Klussman, D. F. Chace, S. X. Rejniak, K. A. Gordon, R. DeBlanc, B. E. Toki, C.-L. Law, S. O. Doronina, C. B. Siegall, P. D. Senter and A. F. Wahl, "cAC10-vcMMAE, an ant-CD30-monomethyl auristatin E conjugate with potent and selective antitumor activity," *Blood*, vol. 102, pp. 1458-1465, 2003.
- [163] K. F. Tse, M. Jeffers, V. A. Pollack, D. A. McCabe, M. L. Shadish, N. V. Khramtsov, C. S. Hackett, S. G. Shenoy, B. Kuang, F. L. Boldog, J. R. MacDougall, L. Rastelli, J. Herrmann, M. Gallo, G. Gazit-Bornstein, P. D. Senter, D. L. Meyer, H. S. Lichenstein and W. J. LaRochelle, "CR011, a Fully Human Monoclonal Antibody-Auristatin E Conjugate, for the Treatment of Melanoma," *Clin. Cancer Res.*, vol. 12, pp. 1373-1382, 2006.
- [164] B. Alberts, A. Johnson, J. Lewis, M. Raff, K. Roberts and P. Walter, "The Self-Assembly and Dynamic Structure of Cytoskeletal Filaments," in *Molecular Biology of the Cell*, 4th ed., New York, Garland Science, 2002.
- [165] M. Stewart, "Intermediate filament structure and assembly," *Curr. Opin. Cell Biol.*, vol. 5, pp. 3-11, 1993.
- [166] R. D. Goldman, M. M. Cleland, S. N. P. Murthy, S. Mahammad and E. R. Kuczmarski, "Inroads into the structure and function of intermediate filament networks," *J. Struct. Biol.*, vol. 177, pp. 14-23, 2012.
- [167] M. A. Jordan and L. Wilson, "Microtubules as Target for Anticancer Drugs," *Nat. Rev. Cancer*, vol. 4, pp. 253-265, 2004.
- [168] G. Fenteany and S. Zhu, "Small-Molecule Inhibitors of Actin Dynamics and Cell Motility," *Curr. Top. Med. Chem.*, vol. 3, pp. 593-616, 2003.
- [169] M. A. Jordan and L. Wilson, "Microtubules and actin filaments: dynamic targets for cancer chemotherapy," *Curr. Opin. Cell Biol.*, vol. 10, pp. 123-130, 1998.
- [170] A. Desai and T. J. Mitchison, "Microtubule polymerization dynamics," *Annu. Rev. Cell. Dev. Biol.*, vol. 13, pp. 83-117, 1997.
- [171] J. C. Gatlin and K. Bloom, "Microtubule motors in eukaryotic spindle assembly and maintenance," *Semin. Cell. Dev. Biol.*, vol. 21, pp. 248-254, 2010.
- [172] C. L. Asbury, "XMAP215: a tip tracker that really moves," *Cell*, vol. 132, pp. 19-20, 2008.
- [173] G. J. Brouhard, J. H. Stear, T. L. Noetzel, J. Al-Bassam, K. Kinoshita, S. C. Harrison, J. Howard and A. A. Hyman, "XMAP215 is a processive microtubule polymerase," *Cell*, vol. 132, pp. 79-88, 2008.
- [174] J. Helenius, G. Brouhard, Y. Kalaidzidis, S. Diez and J. Howard, "The depolymerizing kinesin MCAK uses lattice diffusion to rapidly target microtubule ends," *Nature*, vol. 441, pp. 115-119, 2006.

- [175] B. Alberts, A. Johnson, J. Lewis, M. Raff, K. Roberts and P. Walter, "How Cells Regulate Their Cytoskeletal Filaments," in *Molecular Biology of the Cell*, 4th ed., New York, Garland Science, 2002.
- [176] H. de Forges, A. Bouissou and F. Perez, "Interplay between microtubule dynamics and intracellular organization," *Int. J. Biochem. Cell Biol.*, vol. 44, pp. 266-274, 2012.
- [177] J. Howard and A. A. Hyman, "Microtubule polymerases and depolymerases," *Curr. Opin. Cell Biol.*, vol. 19, pp. 31-35, 2007.
- [178] O. Esue, Y. Tseng and D. Wirtz, " α -Actinin and Filamin Cooperatively Enhance the Stiffness of Actin Filament Networks," *PLoS ONE*, vol. 4(2): e4411, 2009.
- [179] R. C. May, "The Arp2/3 complex: a central regulator of the actin cytoskeleton," *Cell. Mol. Life Sci.*, vol. 58, pp. 1607-1626, 2001.
- [180] S. J. Winder, "Structural insights into actin-binding, branching and bundling proteins," *Curr. Opin. Cell Biol.*, vol. 15, pp. 14-22, 2003.
- [181] E. G. Yarmola, S. Parikh and M. R. Bubb, "Formation and Implications of a Ternary Complex of Profilin, Thymosin b4, and Actin," *J. Biol. Chem.*, vol. 276, pp. 45555-45563, 2001.
- [182] C.-A. Schoenenberger, H. G. Mannherz and B. M. Jokusch, "Actin: From structural plasticity to functional diversity," *Eur. J. Cell Biol.*, vol. 90, pp. 797-804, 2011.
- [183] C. Husson, F.-X. Cantrelle, P. Roblin, D. Didry, K. H. D. Le, J. Perez, E. Guittet, C. Van Heijenoort, L. Renault and M.-F. Carlier, "Multifunctionality of the beta-thymosin/WH2 module: actin sequestration, actin filament growth, nucleation, and severing," *Ann. N.Y. Acad. Sci.*, vol. 1194, pp. 44-52, 2010.
- [184] H. Q. Sun, M. Yamamoto, M. Mejillano and H. L. Yin, "Gelsolin, a Multifunctional Actin Regulatory Protein," *J. Biol. Chem.*, vol. 274, pp. 33179-33182, 1999.
- [185] R. Dominguez and K. C. Holmes, "Actin Structure and Function," *Annu. Rev. Biophys.*, vol. 40, pp. 169-186, 2011.
- [186] B. Kunze, F. Sasse, H. Wiczorek and M. Huss, "Cruentaren A, a highly cytotoxic benzolactone from Myxobacteria is a novel selective inhibitor of mitochondrial F1-ATPases," *FEBS Lett.*, vol. 581, pp. 3523-3527, 2007.
- [187] H. Irschik, W. Trowitzsch-Kienast, K. Gerth, G. Höfle and H. Reichenbach, "Saframycin Mx1, a new natural saframycin isolated from a myxobacterium," *J. Antibiot. (Tokyo)*, vol. 41, pp. 993-998, 1988.
- [188] F. Sasse, H. Steinmetz, G. Höfle and H. Reichenbach, "Gephyronic acid, a novel inhibitor of eukaryotic protein synthesis from *Archangium gephyra* (myxobacteria). Production, isolation, physico-chemical and biological properties, and mechanism of action," *J. Antibiot. (Tokyo)*, vol. 48, pp. 21-25, 1995.
- [189] I. Nিকেleit, S. Zender, F. Sasse, R. Geffers, G. Brandes, I. Sørensen, H. Steinmetz, S. Kubicka, T. Carlomagno, D. Menche, I. Gütgemann, J. Buer, A. Gossler, M. P. Manns, M. Kalesse, R. Frank and N. P. Malek, "Argyirin A reveals a critical role for the tumor suppressor protein p27(kip1) in mediating antitumor activities in response to proteasome inhibition," *Cancer Cell*, vol. 14, pp. 23-35, 2008.

- [190] M. Köster, S. Lykke-Andersen, Y. A. Elnakady, K. Gerth, P. Washausen, G. Höfle, F. Sasse, J. Kjems and H. Hauser, "Ratjadones inhibit nuclear export by blocking CRM1/exportin 1," *Exp. Cell Res.*, vol. 286, pp. 321-331, 2003.
- [191] R. Jansen, H. Irschik, H. Reichenbach, V. Wray and G. Höfle, "Antibiotics from Gliding Bacteria, LIX. Disorazoles, Highly Cytotoxic Metabolites from the Sorangicin-Producing Bacterium *Sorangium cellulosum*, Strain So ce12," *Liebigs Ann. Chem.*, pp. 759-773, 1994.
- [192] F. Sasse, H. Steinmetz, J. Heil, G. Höfle and H. Reichenbach, "Tubulysins, new cytostatic peptides from myxobacteria acting on microtubuli. Production, isolation, physico-chemical and biological properties," *J. Antibiot. (Tokyo)*, vol. 53, pp. 879-885, 2000.
- [193] H. Irschik, R. Jansen, K. Gerth, G. Höfle and H. Reichenbach, "Chivosazol A, a new inhibitor of eukaryotic organisms isolated from myxobacteria," *J. Antibiot. (Tokyo)*, vol. 48, pp. 962-966, 1995.
- [194] B. Kunze, R. Jansen, F. Sasse, G. Höfle and H. Reichenbach, "Chondramides A approximately D, new antifungal and cytostatic depsipeptides from *Chondromyces crocatus* (myxobacteria). Production, physico-chemical and biological properties," *J. Antibiot. (Tokyo)*, vol. 48, pp. 1262-1266, 1995.
- [195] F. Sasse, H. Steinmetz, G. Höfle and H. Reichenbach, "Rhizopodin, a new compound from *Myxococcus stipitatus* (myxobacteria) causes formation of rhizopodia-like structures in animal cell cultures. Production, isolation, physico-chemical and biological properties," *J. Antibiot. (Tokyo)*, vol. 46, pp. 741-748, 1993.
- [196] A. Dömling and W. Richter, "Myxobacterial epothilones and tubulysins as promising anticancer agents," *Mol. Divers.*, vol. 9, pp. 141-147, 2005.
- [197] C. D. Hopkins and P. Wipf, "Isolation, biology and chemistry of the disorazoles: new anticancer macrodiolides," *Nat. Prod. Rep.*, vol. 26, pp. 585-601, 2009.
- [198] J. J. Lee and S. M. Swain, "Development of Novel Chemotherapeutic Agents to Evade the Mechanisms of Multidrug Resistance (MDR)," *Semin. Oncol.*, vol. 32, pp. 22-26, 2005.
- [199] G. Kaur, M. Hollingshead, S. Holbeck, V. Schauner-Vukasinovic, R. F. Camalier, A. Dömling and S. Agarwal, "Biological evaluation of tubulysin A: a potential anticancer and antiangiogenic natural product," *Biochem. J.*, vol. 396, pp. 235-242, 2006.
- [200] D. Neri, G. Fossati and M. Zanda, "Efforts towards the total synthesis of tubulysins: new hopes for a more effective targeted drug delivery to tumors," *Chem. Med. Chem.*, vol. 1, pp. 175-180, 2006.
- [201] H. M. Peltier, J. P. McMahon, A. W. Patterson and J. A. Ellman, "The total synthesis of tubulysin D," *J. Am. Chem. Soc.*, vol. 128, pp. 16018-16019, 2006.
- [202] A. Ullrich, Y. Chai, D. Pistorius, Y. A. Elnakady, J. Herrmann, K. J. Weissman, U. Kazmaier and R. Müller, "Pretubulysin, a potent and chemically accessible tubulysin precursor from *Angiococcus disciformis*," *Angew. Chem. Int. Ed. Engl.*, vol. 48, pp. 4422-4425, 2009.
- [203] J. Herrmann, Y. A. Elnakady, R. M. Wiedmann, A. Ullrich, M. Rohde, U. Kazmaier, A. M. Vollmar and R. Müller, "Pretubulysin: from hypothetical biosynthetic intermediate to potential lead in tumor therapy," *PLoS ONE*, vol. 7(5):e37416, 2012.

- [204] S. Rath, J. Liebl, R. Fürst, A. Ullrich, J. L. Burkhart, U. Kazmaier, J. Herrmann, R. Müller, M. Günther, L. Schreiner, E. Wagner, A. M. Vollmar and S. Zahler, "Anti-angiogenic effects of the tubulysin precursor pretubulysin and of simplified pretubulysin derivatives," *Br. J. Pharmacol.*, vol. [Epub ahead of print], 2012.
- [205] E. G. Guenther, K. W. Paulini, B. Aicher, S. Baasner, P. Schmidt, M. Teifel, O. Schaefer, C. Grundker and S. Fister, *Targeting Disorazol Z to LHRH-receptor positive tumors by the cytotoxic conjugate AEZS-125*, poster presented at the American Association for Cancer Research (AACR) Annual Meeting, 2008.
- [206] P. Crews, L. V. Manes and M. Boehler, "Jasplakinolide, a cyclodepsipeptide from the marine sponge, Jaspis SP.," *Tetrahedron Lett.*, vol. 27, pp. 2797-2800, 1986.
- [207] T. M. Zabriskie, J. A. Klocke, C. M. Ireland, A. H. Marcus, T. F. Molinski, D. J. Faulkner, C. Xu and J. Clardy, "Jaspamide, a modified peptide from a Jaspis sponge, with insecticidal and antifungal activity," *J. Am. Chem. Soc.*, vol. 108, pp. 3123-3124, 1986.
- [208] M. R. Bubb, A. M. J. Senderowicz, E. A. Sausville, L. K. Duncan and E. D. Korn, "Jasplakinolide, a Cytotoxic Natural Product, Induces Actin Polymerization and Competitively Inhibits the Binding of Phalloidin to F-actin," *J. Biol. Chem.*, vol. 269, pp. 14869-14871, 1994.
- [209] F. Sasse, B. Kunze, T. M. A. Gronewold and H. Reichenbach, "The Chondramides: Cytostatic Agents From Myxobacteria Acting on the Actin Cytoskeleton," *J. Nat. Cancer Inst.*, vol. 90, pp. 1559-1563, 1998.
- [210] T. Oda, K. Namba and Y. Maéda, "Position and Orientation of Phalloidin in F-Actin Determined by X-Ray Fiber Diffraction Analysis," *Biophys. J.*, vol. 88, pp. 2727-2736, 2005.
- [211] H. Waldmann, T.-S. Hu, S. Renner, S. Menninger, R. Tannert, T. Oda and H.-D. Arndt, "Total Synthesis of Chondramide C and Its Binding Mode to F-Actin," *Angew. Chem. Int. Ed.*, vol. 47, pp. 6473-6477, 2008.
- [212] L.-G. Milroy, S. Rizzo, A. Calderon, B. Ellinger, S. Erdmann, J. Mondry, P. Verveer, P. Bastiaens, H. Waldmann, L. Dehmelt and H.-D. Arndt, "Selective chemical imaging of static actin in live cells," *J. Am. Chem. Soc.*, vol. 134, pp. 8480-8486, 2012.
- [213] C. J. Bruns, M. T. Harbison, H. Kuniyasu, I. Eue and I. J. Fidler, "In Vivo Selection and Characterization of Metastatic Variants from Human Pancreatic Adenocarcinoma by Using Orthotopic Implantation in Nude Mice," *Neoplasia*, vol. 1, pp. 50-62, 1999.
- [214] T. Mosmann, "Rapid Colorimetric Assay for Cellular Growth and Survival: Application to Proliferation and Cytotoxicity Assays," *J. Immunol. Meth.*, vol. 65, pp. 55-63, 1983.
- [215] I. Nicoletti, G. Migliorati, M. C. Pagliacci, F. Grignani and C. Riccardi, "A rapid and simple method for measuring thymocyte apoptosis by propidium iodide staining and flow cytometry," *J. Immunol. Meth.*, vol. 139, pp. 271-279, 1991.
- [216] U. K. Laemmli, "Cleavage of Structural Proteins during the Assembly of the Head of Bacteriophage T4," *Nature*, vol. 227, pp. 680-685, 1970.
- [217] J. Gong, F. Traganos and Z. Darzynkiewicz, "A selective procedure for DNA extraction from apoptotic cells applicable for gel electrophoresis and flow cytometry," *Anal. Biochem.*, vol. 218, pp. 314-319, 1994.

- [218] R. D. Sloboda, W. L. Dentler and J. L. Rosenbaum, "Microtubule-associated proteins and the stimulation of tubulin assembly in vitro," *Biochemistry*, vol. 15, pp. 4497-4505, 1976.
- [219] F. Gaskin, C. R. Cantor and M. L. Shelanski, "Turbidimetric studies of the in vitro assembly and disassembly of porcine neurotubules," *J. Mol. Biol.*, vol. 89, pp. 737-755, 1974.
- [220] M. W. Khalil, F. Sasse, H. Lünsdorf, Y. A. Elnakady and H. Reichenbach, "Mechanism of action of tubulysin, an antimetabolic peptide from myxobacteria," *ChemBioChem*, vol. 7, pp. 678-683, 2006.
- [221] S. C. Wenzel and R. Müller, "Naturstoffbiotechnologie des Myxobakteriums *Chondromyces crocatus*," *Biospektrum*, vol. 17, pp. 580-582, 2011.
- [222] P. Boya and G. Kroemer, "Lysosomal membrane permeabilization in cell death," *Oncogene*, vol. 27, pp. 6434-6451, 2008.
- [223] F. Antunes, E. Cadenas and U. T. Brunk, "Apoptosis induced by exposure to a low steady-state concentration of H₂O₂ is a consequence of lysosomal rupture," *Biochem. J.*, vol. 356, pp. 549-555, 2001.
- [224] J. A. Cooper, S. B. Walker and T. D. Pollard, "Pyrene actin: documentation of the validity of a sensitive assay for actin polymerization," *J. Muscle Res. Cell Motil.*, vol. 4, pp. 253-262, 1983.
- [225] H. Steinmetz, N. Glaser, E. Herdtweck, F. Sasse, H. Reichenbach and G. Höfle, "Isolation, Crystal and Solution Structure Determination, and Biosynthesis of Tubulysins - Powerful Inhibitors of Tubulin Polymerization from Myxobacteria," *Angew. Chem. Int. Ed.*, vol. 43, pp. 4888-4892, 2004.
- [226] I. R. Vlahov, Y. Wang, M. Vetzal, S. Hahn, P. J. Kleindl, J. A. Reddy and C. P. Leamon, "Acid mediated formation of an N-acyliminium ion from tubulysins: A new methodology for the synthesis of natural tubulysin and their analogs," *Bioorg. Med. Chem. Lett.*, vol. 21, pp. 6778-6781, 2011.
- [227] F. Sasse and D. Menche, "Success in tubulysin D synthesis," *Nat. Chem. Biol.*, vol. 3, pp. 87-89, 2007.
- [228] G. Höfle, N. Glaser, T. Leibold, U. Karama, F. Sasse and H. Steinmetz, "Semisynthesis and degradation of the tubulin inhibitors epothilone and tubulysin," *Pure Appl. Chem.*, vol. 75, pp. 167-178, 2003.
- [229] G. K. Friestad, J.-C. Marié and A. M. Deveau, "Stereoselective Mn-Mediated Coupling of Functionalized Iodides and Hydrazones: A Synthetic Entry to the Tubulysin gamma-Amino Acids," *Org. Lett.*, vol. 6, pp. 3249-3252, 2004.
- [230] P. Wipf, T. Takada and M. J. Rishel, "Synthesis of the Tubovaline-Tubuphenylalanine (Tuv-Tup) Fragment of Tubulysin," *Org. Lett.*, vol. 6, pp. 4057-4060, 2004.
- [231] A. Dömling, B. Beck, U. Eichelberger, S. Sakamuri, S. Menon, Q.-Z. Chen, Y. Lu and L. A. Wessjohann, "Total Synthesis of Tubulysin U and V," *Angew. Chem. Int. Ed.*, vol. 45, pp. 7235-7239, 2006.
- [232] M. Sani, G. Fossati, F. Huguenot and M. Zanda, "Total Synthesis of Tubulysin U and V," *Angew. Chem. Int. Ed.*, vol. 46, pp. 3526-3529, 2007.
- [233] T. Shibue, T. Hirai, I. Okamoto, N. Morita, H. Masu, I. Azumaya and O. Tamura, "Total Syntheses of Tubulysins," *Chem. Eur. J.*, vol. 16, pp. 11678-11688, 2010.

- [234] R. Balasubramanian, B. Raghavan, A. Begaye, D. L. Sackett and R. A. Fecik, "Total Synthesis and Biological Evaluation of Tubulysin U, Tubulysin V, and Their Analogues," *J. Med. Chem.*, vol. 52, pp. 238-240, 2009.
- [235] T. Shibue, I. Okamoto, N. Morita, H. Morita, Y. Hirasawa, T. Hosoya and O. Tamura, "Synthesis and biological evaluation of tubulysin D analogs related to stereoisomers of tubovaline," *Bioorg. Med. Chem. Lett.*, vol. 21, pp. 431-434, 2011.
- [236] O. Pando, S. Dörner, R. Preusentanz, A. Denkert, A. Porzel, W. Richter and L. Wessjohann, "First Total Synthesis of Tubulysin B," *Org. Lett.*, vol. 11, pp. 5567-5569, 2009.
- [237] P. Wipf and Z. Wang, "Total Synthesis of N14-Desacetoxytubulysin H," *Org. Lett.*, vol. 9, pp. 1605-1607, 2007.
- [238] Z. Wang, P. A. McPherson, B. S. Raccor, R. Balachandran, G. Zhu, B. W. Day, A. Vogt and P. Wipf, "Structure-activity and High-content Imaging Analyses of Novel Tubulysins," *Chem. Biol. Drug Des.*, vol. 70, pp. 75-86, 2007.
- [239] B. Raghavan, R. Balasubramanian, J. C. Steele, D. L. Sackett and R. A. Fecik, "Cytotoxic Simplified Tubulysin Analogues," *J. Med. Chem.*, vol. 51, pp. 1530-1533, 2008.
- [240] R. Balasubramanian, B. Raghavan, J. C. Steele, D. L. Sackett and R. A. Fecik, "Tubulysin analogs incorporating desmethyl and dimethyl tubuphenylalanine derivatives," *Bioorg. Med. Chem. Lett.*, vol. 18, pp. 2996-2999, 2008.
- [241] A. W. Patterson, H. M. Peltier, F. Sasse and J. A. Ellman, "Design, Synthesis and Biological Properties of Highly Potent Tubulysin D Analogues," *Chem. Eur. J.*, vol. 13, pp. 9534-9541, 2007.
- [242] A. W. Patterson, H. M. Peltier and J. A. Ellman, "Expedient Synthesis of N-Methyl Tubulysin Analogues with High Cytotoxicity," *J. Org. Chem.*, vol. 73, pp. 4362-4369, 2008.
- [243] A. Sandmann, F. Sasse and R. Müller, "Identification and Analysis of the Core Biosynthetic Machinery of Tubulysin, a Potent Cytotoxin with Potential Anticancer Activity," *Chem. Biol.*, vol. 11, pp. 1071-1079, 2004.
- [244] A. Ullrich, J. Herrmann, R. Müller and U. Kazmaier, "Synthesis and Biological Evaluation of Pretubulysin and Derivatives," *Eur. J. Org. Chem.*, pp. 6367-6378, 2009.
- [245] Y. Chai, D. Pistorius, A. Ullrich, K. J. Weissman, U. Kazmaier and R. Müller, "Discovery of 23 Natural Tubulysins from *Angiococcus disciformis* An d48 and *Cystobacter* SBCb004," *Chem. Biol.*, vol. 17, pp. 296-309, 2010.
- [246] Y. Chai, S. Shan, K. J. Weissman, S. Hu, Y. Zhang and R. Müller, "Heterologous Expression and Genetic Engineering of the Tubulysin Biosynthetic Gene Cluster Using Red/ET Recombineering and Inactivation Mutagenesis," *Chem. Biol.*, vol. 19, pp. 361-371, 2012.
- [247] R. Bai, G. R. Pettit and E. Hamel, "Binding of Dolastatin 10 to Tubulin at a Distinct Site for Peptide Antimitotics Agents Near the Exchangeable Nucleotide and Vinca Alkaloid Sites," *J. Biol. Chem.*, vol. 265, pp. 17141-17149, 1990.

- [248] T. Tonini, F. Rossi and P. P. Claudio, "Molecular basis of angiogenesis and cancer," *Oncogene*, vol. 22, pp. 6549-6556, 2003.
- [249] E. Pasquier, M. Carré, B. Pourroy, L. Camoin, O. Rebai, C. Briand and D. Braguer, "Antiangiogenic activity of paclitaxel is associated with its cytostatic effect, mediated by the initiation but not completion of a mitochondrial apoptotic signaling pathway," *Mol. Cancer Ther.*, vol. 3, pp. 1301-1310, 2004.
- [250] C. P. Leamon, J. A. Reddy, M. Vetzal, R. Dorton, E. Westrick, N. Parker, Y. Wang and I. Vlahov, "Folate Targeting Enables Durable and Specific Antitumor Responses from a Therapeutically Null Tubulysin B Analogue," *Cancer Res.*, vol. 68, pp. 9839-9844, 2008.
- [251] T. Schluess, P. Gunawan, L. Ma, G. S. Jensen, J. Durringer, S. Hinton, W. Richter and J. Hwang, "Polymeric Tubulysin-Peptide Nanoparticles with Potent Antitumor Activity," *Clin. Cancer Res.*, vol. 15, pp. 181-189, 2009.
- [252] W. C. 3. Floyd, G. K. Datta, S. Imamura, H. M. Kieler-Ferguson, K. Jerger, A. W. Patterson, M. E. Fox, F. C. Szoka, J. M. Fréchet and J. A. Ellman, "Chemotherapeutic evaluation of a synthetic tubulysin analogue-dendrimer conjugate in c26 tumor bearing mice," *ChemMedChem*, vol. 6, pp. 49-53, 2011.
- [253] M. A. Jordan, "Mechanism of action of antitumor drugs that interact with microtubules and tubulin," *Curr. Med. Chem. Anticancer Agents*, vol. 2, pp. 1-17, 2002.
- [254] S. Honore, E. Pasquier and D. Braguer, "Understanding microtubule dynamics for improved cancer therapy," *Cell. Mol. Life Sci.*, vol. 62, pp. 3039-3056, 2005.
- [255] E. P. Rogakou, W. Nieves-Neira, C. Boon, Y. Pommier and W. M. Bonner, "Initiation of DNA Fragmentation during Apoptosis Induces Phosphorylation of H2AX Histone at Serine 139," *J. Biol. Chem.*, vol. 275, pp. 9390-9395, 2000.
- [256] M. Castedo, J.-L. Perfettini, T. Roumier, K. Andreau, R. Medema and G. Kroemer, "Cell death by mitotic catastrophe: a molecular definition," *Oncogene*, vol. 23, pp. 2825-2837, 2004.
- [257] I. B. Roninson, E. V. Broude and B. D. Chang, "If not apoptosis, then what? Treatment-induced senescence and mitotic catastrophe in tumor cells," *Drug Resist. Updat.*, vol. 4, pp. 303-312, 2001.
- [258] A. H. Wyllie, "Glucocorticoid-induced thymocyte apoptosis is associated with endogenous endonuclease activation," *Nature*, vol. 284, pp. 555-556, 1980.
- [259] K. Bhalla, A. M. Ibrado, E. Tourkina, C. Tang, M. E. Mahoney and Y. Huang, "Taxol induces internucleosomal DNA fragmentation associated with programmed cell death in human myeloid leukemia cells," *Leukemia*, vol. 7, pp. 563-568, 1993.
- [260] C. Huisman, C. G. Ferreira, L. E. Bröker, J. A. Rodriguez, E. F. Smit, P. E. Postmus, F. A. E. Kruijff and G. Giaccone, "Paclitaxel Triggers Cell Death Primarily via Caspase-independent Routes in the Non-Small Cell Lung Cancer Cell Line NCI-H460," *Clin. Cancer Res.*, vol. 8, pp. 596-606, 2002.
- [261] S. M. Nabha, R. M. Mohammad, M. H. Dandashi, B. Coupaye-Gerard, A. Aboukameel, G. R. Pettit and A. M. Al-Katib, "Combretastatin-A4 Prodrug Induces Mitotic Catastrophe in Chronic Lymphocytic Leukemia Cell Line Independent of Caspase Activation and Poly(ADP-ribose) Polymerase Cleavage," *Clin. Cancer Res.*, vol. 8, pp. 2735-2741, 2002.

- [262] L. E. Bröker, C. Huisman, C. G. Ferreira, J. A. Rodriguez, F. A. E. Kruyt and G. Giaccone, "Late Activation of Apoptotic Pathways Plays a Negligible Role in Mediating the Cytotoxic Effects of Discodermolide and Epothilone B in Non-Small Lung Cancer Cells," *Cancer Res.*, vol. 62, pp. 4081-4088, 2002.
- [263] M. E. Guicciardi, M. Leist and G. J. Gores, "Lysosomes in cell death," *Oncogene*, vol. 23, pp. 2881-2890, 2004.
- [264] E. C. C. Cheung, N. Joza, N. A. E. Steenaart, K. A. McClellan, M. Neuspiel, S. McNamara, J. G. MacLaurin, P. Rippstein, D. S. Park, G. C. Shore, H. M. McBride, J. M. Penninger and R. S. Slack, "Dissociating the dual roles of apoptosis-inducing factor in maintaining mitochondrial structure and apoptosis," *EMBO J.*, vol. 25, pp. 4061-4073, 2006.
- [265] M. V. Blagosklonny, "Unwinding the loop of Bcl-2 phosphorylation," *Leukemia*, vol. 15, pp. 869-874, 2001.
- [266] M. S. Ola, M. Nawaz and H. Ahsan, "Role of Bcl-2 family proteins and caspases in the regulation of apoptosis," *Mol. Cell. Biochem.*, vol. 351, pp. 41-58, 2011.
- [267] L. Virág and C. Szabó, "The therapeutic potential of poly(ADP-ribose) polymerase inhibitors," *Pharmacol. Rev.*, vol. 54, pp. 375-429, 2002.
- [268] K. Kubicek, S. K. Grimm, J. Orts, F. Sasse and T. Carlomagno, "The Tubulin-Bound Structure of the Antimitotic Drug Tubulysin," *Angew. Chem. Int. Ed.*, vol. 49, pp. 4809-4812, 2010.
- [269] J. Muppidi, M. Porter and R. M. Siegel, "Measurement of Apoptosis and Other Forms of Cell Death," *Curr. Protoc. Immunol.*, vol. 59, pp. 3.17.1-3.17.36, 2004.
- [270] J. L. Burkhart, R. Müller and U. Kazmaier, "Syntheses and Evaluation of Simplified Pretubulysin Analogues," *Eur. J. Org. Chem.*, pp. 3050-3059, 2011.
- [271] J. L. Burkhart and U. Kazmaier, "A straightforward click-approach towards pretubulysin-analogues," *RCS Advances*, vol. 2, pp. 3785-3790, 2012.
- [272] J. Eirich, J. L. Burkhart, A. Ullrich, G. C. Rudolf, A. M. Vollmar, S. Zahler, U. Kazmaier and S. A. Sieber, "Pretubulysin derived probes as novel tools for monitoring the microtubule network via activity-based protein profiling and fluorescence microscopy," *Mol. BioSyst.*, vol. 8, pp. 2067-2075, 2012.
- [273] T. Litman, M. Brangi, E. Hudson, P. Fetsch, A. Abati, D. D. Ross, K. Miyake, J. H. Resau and S. E. Bates, "The multidrug-resistant phenotype associated with overexpression of the new ABC half-transporter, MXR (ABCG2)," *J. Cell Sci.*, vol. 113, pp. 2011-2021, 2000.
- [274] Z. Yang, D. Wu, T. Bui and R. J. Y. Ho, "A Novel Human Multidrug Resistance Gene MDR1 Variant G571A (G191R) Modulates Cancer Drug Resistance and Efflux Transport," *J. Pharmacol. Exp. Ther.*, vol. 327, pp. 474-481, 2008.
- [275] G. B. Alsop, W. Chen, M. Foss, K. F. Tseng and D. Zhang, "Redistribution of actin during assembly and reassembly of the contractile ring in grasshopper spermatocytes," *PLoS One*, vol. 4(3):e4892, 2009.
- [276] M. N. Cordonnier, D. Dauzonne, D. Louvard and E. Coudrier, "Actin filaments and myosin I alpha cooperate with microtubules for the movement of lysosomes," *Mol. Biol. Cell*, vol. 12, pp. 4013-4029, 2001.

- [277] D. J. Stephens, "Functional coupling of microtubules to membranes - implications for membrane structure and dynamics," *J. Cell Sci.*, vol. 125, pp. 1-10, 2012.
- [278] R. Matteoni and T. E. Kreis, "Translocation and Clustering of Endosomes and Lysosomes Depends on Microtubules," *J. Cell Biol.*, vol. 105, pp. 1253-1265, 1987.
- [279] J. Kornhuber, A. W. Henkel, T. W. Groemer, S. Städtler, O. Welzel, P. Tripal, A. Rotter, S. Bleich and S. Trapp, "Lipophilic cationic drugs increase the permeability of lysosomal membranes in a cell culture system," *J. Cell. Physiol.*, vol. 224, pp. 152-164, 2010.
- [280] K. A. Giuliano, R. L. DeBiasio, R. T. Dunlay, A. Gough, J. M. Volosky, J. Zock, G. N. Pavlakis and D. L. Taylor, "High-Content Screening: A New Approach to Easing Key Bottlenecks in the Drug Discovery Process," *J. Biomol. Screen.*, vol. 2, pp. 249-259, 1997.
- [281] A. Dove, "Screening for content - the evolution of high throughput," *Nat. Biotechnol.*, vol. 21, pp. 859-864, 2003.
- [282] S. Hüttel and R. Müller, "Methods to optimize myxobacterial fermentations using off-gas analysis," *Microb. Cell Fact.*, vol. 11:59, 2012.
- [283] R. Jansen, B. Kunze, H. Reichenbach and G. Höfle, "Chondramides A-D, new cytostatic and antifungal cyclodepsipeptides from *Chondromyces crocatus* (myxobacteria): isolation and structure elucidation," *Liebigs Ann.*, vol. 1996, pp. 285-290, 1996.
- [284] J. E. Schindler-Horvat, D. G. Fairchild, C. Hassler, J. E. Tomaszewski, S. J. Donohue and C. A. Tyson, "Toxicity of jasplakinolide (NSC 613009) in rats and dogs," *Proc. Am. Assoc. Cancer Res.*, vol. 39, p. 597, 1998.
- [285] U. Eggert, R. Diestel, F. Sasse, R. Jansen, B. Kunze and M. Kalesse, "Chondramide C: Synthesis, Configurational Assignment, and Structure-Activity Relationship Studies," *Angew. Chem. Int. Ed.*, vol. 47, pp. 6478-6482, 2008.
- [286] A. Schmauder, L. D. Sibley and M. E. Maier, "Total Synthesis and Configurational Assignment of Chondramide A," *Chem. Eur. J.*, vol. 16, pp. 4328-4336, 2010.
- [287] A. Zhdanko, A. Schmauder, C. I. Ma, L. D. Sibley, D. Sept, F. Sasse and M. E. Maier, "Synthesis of Chondramide A Analogues with Modified beta-Tyrosine and Their Biological Evaluation," *Chem. Eur. J.*, vol. 17, pp. 13349-13357, 2011.
- [288] R. Tannert, L.-G. Milroy, B. Ellinger, T.-S. Hu, H.-D. Arndt and H. Waldmann, "Synthesis and Structure-Activity Correlation of Natural-Product Inspired Cyclodepsipeptides Stabilizing F-Actin," *J. Am. Chem. Soc.*, vol. 132, pp. 3063-3077, 2010.
- [289] S. Rachid, D. Krug, B. Kunze, I. Kochems, M. Scharfe, T. M. Zabriskie, H. Blöcker and R. Müller, "Molecular and Biochemical Studies of Chondramide Formation - Highly Cytotoxic Natural Products from *Chondromyces crocatus* Cm c5," *Chem. Biol.*, vol. 14, pp. 667-681, 2006.
- [290] S. Rachid, D. Krug, K. J. Weissman and R. Müller, "Biosynthesis of (R)-beta-Tyrosine and Its Incorporation into the Highly Cytotoxic Chondramides Produced by *Chondromyces crocatus*," *J. Biol. Chem.*, vol. 282, pp. 21810-21817, 2007.

- [291] M. R. Bubb, I. Spector, B. B. Beyer and K. M. Fosen, "Effects of Jasplakinolide on the Kinetics of Actin Polymerization," *J. Biol. Chem.*, vol. 275, pp. 5163-5170, 2000.
- [292] J. A. Cooper, "Effects of Cytochalasin and Phalloidin on Actin," *J. Biol. Chem.*, vol. 105, pp. 1473-1478, 1987.
- [293] A. Petrelli and S. Giordano, "From single- to multi-target drugs in cancer therapy: when aspecificity becomes an advantage," *Curr. Med. Chem.*, vol. 15, pp. 422-432, 2008.
- [294] S. Desbène and S. Giorgi-Renault, "Drugs that inhibit tubulin polymerization: the particular case of podophyllotoxin and analogues," *Curr. Med. Chem. Anticancer Agents*, vol. 2, pp. 71-90, 2002.

APPENDIX

7.1 ABBREVIATIONS

ABP	actin-binding protein
ACC	acetyl CoA carboxylase
ADC	antibody-drug conjugate
ADP	adenosine diphosphate
AIF	apoptosis inducing factor
AO	acridine orange
Apaf-1	apoptotic protease activating factor 1
ARP	actin-related protein
ATP	adenosine triphosphate
a.u.	arbitrary units
Bcl-2/pBcl-2	B cell lymphoma 2/phosphorylated B cell lymphoma 2
bFGF	basic fibroblast growth factor (recombinant human)
BODIPY FL	boron-dipyrromethene fluorescein-like fluorescence
BPC	base peak chromatogram
γ H2A.X	phosphorylated histone H2A.X
γ -TuRC	γ -tubulin ring complex
CD	cluster of differentiation
CDK	cyclin-dependent kinase
cf.	confer
CF	cystic fibrosis
Ctrl.	control
Da	Dalton
dd	double-distilled
DMEM	Dulbecco's modified eagle medium
DMSO	dimethyl sulfoxide
DNA	deoxyribonucleic acid
dNTP	deoxynucleoside triphosphate
DSB	DNA double-strand break
ECGS	endothelial cell growth supplement (bovine hypothalamic extract)
EDTA	ethylene diamine tetraacetic acid
e.g.	<i>exempli gratia</i>
EGF	epidermal growth factor (recombinant human)
EGTA	ethylene glycol tetraacetic acid
EPS	exopolysaccharide
ERK1/2	extracellular signal-regulated kinases 1/2
F-actin	filamentous (or polymeric) actin
FBS	fetal bovine serum
FCM	flow cytometric measurement
FCS	fetal calf serum
G-actin	globular (or monomeric) actin
GDP	guanosine diphosphate
GFP	green-fluorescent protein
GI ₅₀	half maximal growth inhibitory concentration
GLP-1	glucagon-like peptide-1
GTP	guanosine triphosphate
HCS	high-content screening
HIF-1	hypoxia-inducible factor-1
HMG-CoA	3-hydroxy-3-methyl-glutaryl-coenzyme A
HPLC	high-performance liquid chromatography
HR-MS	high-resolution mass spectrometry
HTS	high-throughput screening

HU	hydroxyurea
IC ₅₀	half maximal inhibitory concentration
i.e.	<i>id est</i>
IF	intermediate filament <u>or</u> immunofluorescence
IgG (H+L)	immunoglobulin G (heavy and light chains)
Ile	isoleucin
JNK	<i>c</i> -Jun <i>N</i> -terminal kinase
LC	liquid chromatography
LHRH	luteinizing hormone-releasing hormone
LMP	lysosomal membrane permeabilization
mAb	monoclonal antibody
MAP	microtubule-associated protein
Mb	mega base pairs
MCAK	mitotic centromere-associated kinesin (kinesin-like protein KIF2C)
MDR	multidrug resistant
MDR-TB	multidrug resistant tuberculosis
MEM	minimum essential medium eagle
Mep	<i>N</i> -methylpipercolic acid
Me ^o Val ^o	methylvaline derivative in which Val is replaced by the C2-prolonged homolog (γ -amino acid)
MMP	mitochondrial membrane potential
MoA	mode-of-action
MOMP	mitochondrial outer membrane permeability
MRP	multidrug resistant protein
MRSA	methicillin-resistant <i>Staphylococcus aureus</i>
MS	mass spectrometry
Mtb	<i>Mycobacterium tuberculosis</i>
MTOC	microtubule-organizing center
mTOR	mammalian target of rapamycin
MTT	3-(4,5-dimethylthiazol-2-yl)-2,5-diphenyltetrazolium bromide
NCE	new chemical entity
NCS	newborn calf serum
n.d.	not determined
NEAA	non-essential amino acids
NMR	nuclear magnetic resonance
NP	natural product
NRP	non-ribosomal peptide
NRPS	non-ribosomal peptide synthetase
o/n	overnight
PARP	poly(ADP-ribose) polymerase
PBS	phosphate-buffered saline
PCB	phosphate-citrate buffer
P-gp	P-glycoprotein
PI	propidium iodide
Pip	piperic acid
PIP ₂	polyphosphoinositide 4,5-bisphosphate
PIPES	piperazine- <i>N,N'</i> -bis(2-ethanesulfonic acid)
PK	polyketide
PKS	polyketide synthase
Q-VD-OPh	quinolyl-valyl-O-methylaspartyl-[-2, 6-difluorophenoxy]-methyl ketone
R&D	research and discovery
RFU	relative fluorescence units
RNA	ribonucleic acid
ROI	region-of-interest
RPMI	Roswell Park Memorial Institute medium
RTK	receptor tyrosine kinase

SAR	structure-activity relationship
SD	standard deviation
SEC	size-exclusion chromatography
SEM	standard error of the mean
TCM	traditional Chinese medicine
TEM	transmission electron microscopy
TFA	trifluoro acetic acid
TMRM	tetramethyl rhodamine methyl ester
Tup	tubuphenylalanine
Tut	tubutyrosine
Tuv	tubuvaline
Val	valine
V-ATPase	vacuolar-type H ⁺ -adenosine triphosphatase
v/v	volume-to-volume
WT	wildtype
w/v	weight-in-volume
XDR-TB	extensively drug-resistant tuberculosis
XMAP215	microtubule-associated protein 215 kDa

7.2 PUBLICATIONS

7.2.1 ORIGINAL PUBLICATIONS

Jennifer Herrmann*, Stephan Hüttel*, and Rolf Müller (2012): **Discovery of New Chondramide Derivatives with Improved Bioactivity in Extracts of Chondromyces sp. SBCm007.** *in preparation*, *these authors contributed equally.

Qiaoli Zhao, Maen Zeino, Tolga Eichhorn, Jennifer Herrmann, Rolf Müller, and Thomas Efferth (2012): **Molecular docking studies of myxobacterial disorazoles and tubulysins to tubulin.** *J. Biosci. Med.*, accepted.

Diana Wischang, Madlen Radlow, Heiko Schulz, Hans Vilter, Lutz Viehweger, Matthias O. Altmeyer, Carsten Kegler, Jennifer Herrmann, Rolf Müller, Fanny Gaillard, Ludovic Delage, Catherine Leblanc, and Jens Hartung (2012): **Molecular Cloning, Structure, and Reactivity of the Second Bromoperoxidase from Ascophyllum nodosum.** *Bioorg. Chem.* (June 2012), doi:10.1016/j.bioorg.2012.05.003

Christian A. Ruge, Ulrich F. Schäfer, Jennifer Herrmann, Julian Kirch, Olga Cañadas, Mercedes Echaide, Jesús Pérez-Gil, Cristina Casals, Rolf Müller, and Claus-Michael Lehr (2012): **The Interplay of Lung Surfactant Proteins and Lipids Assimilates the Macrophage Clearance of Nanoparticles.** *PLoS ONE* 7:e40775. Epub 2012 Jul 10.

Sebastian Rath, Johanna Liebl, Robert Fürst, Angelika Ullrich, Jens L. Burkhardt, Uli Kazmaier, Jennifer Herrmann, Rolf Müller, Michael Günther, Laura Schreiner, Ernst Wagner, Angelika M. Vollmar, and Stefan Zahler (2012): **Anti-angiogenic effects of the tubulysin precursor pretubulysin and of simplified pretubulysin derivatives.** *Br. J. Pharmacol.* doi: 10.1111/j.1476-5381.2012.02037.x. [Epub ahead of print]

Jennifer Herrmann, Yasser A. Elnakady, Romina M. Wiedmann, Angelika Ullrich, Manfred Rohde, Uli Kazmaier, Angelika M. Vollmar, and Rolf Müller (2012). **Pretubulysin: From Hypothetical Biosynthetic Intermediate to Potential Lead in Tumor Therapy.** *PLoS ONE* 7: e37416. Epub 2012 May 17.

Anna Proschak, Katharina Schulz, Jennifer Herrmann, Andrea J. Dowling, Alexander O. Brachmann, Richard ffrench-Constant, Rolf Müller, and Helge B. Bode (2011). **Cytotoxic Fatty Acid Amines from Xenorhabdus**. *ChemBioChem* 12: 2011-2015.

Shwan Rachid, Liujie Huo, Jennifer Herrmann, Marc Stadler, Bärbel Köpcke, Jens Bitzer, and Rolf Müller (2011). **Mining the Cinnabaramide Biosynthetic Pathway to Generate Novel Proteasome Inhibitors**. *ChemBioChem* 12: 922-931.

Angelika Ullrich, Jennifer Herrmann, Rolf Müller, and Uli Kazmaier (2009). **Synthesis and Biological Evaluation of Pretubulysins and Derivatives**. *Eur. J. Org. Chem.* 2009: 6367-6378.

Angelika Ullrich, Yi Chai, Dominik Pistorius, Yasser A. Elnakady, Jennifer Herrmann, Kira J. Weissman, Uli Kazmaier, and Rolf Müller (2009). **Pretubulysin, a Potent and Chemically Accessible Tubulysin Precursor from Angiococcus disciformis**. *Angew. Chem. Int. Ed.* 48: 4422-4425.

Martin Bindl, Ludovic Jean, Jennifer Herrmann, Rolf Müller, and Alois Fürstner (2009). **Preparation, Modification, and Evaluation of Cruentaren A and Analogues**. *Chem. Eur. J.* 15: 12310-12319.

Takashi Nagano, Jiří Pospíšil, Guillaume Chollet, Saskia Schulthoff, Volker Hickmann, Emilie Moulin, Jennifer Herrmann, Rolf Müller, and Alois Fürstner (2009). **Total Synthesis and Biological Evaluation of the Cytotoxic Resin Glycosides Ipomoeassin A-F and Analogues**. *Chem. Eur. J.* 15: 9697-9706.

7.2.2 CONFERENCE CONTRIBUTIONS

Jennifer Herrmann, Yasser A. Elnakady, Romina M. Wiedmann, Angelika Ullrich, Manfred Rohde, Uli Kazmaier, Angelika M. Vollmar, and Rolf Müller (July 2012): Oral presentation – **Comparative bioactivity studies on pretubulysin and other antimitotics from myxobacteria**. International conference: *Natural Anticancer Drugs*, Olomouc, Czech Republic.

Jennifer Herrmann*, Stephan Hüttel*, and Rolf Müller (June 2012): Poster presentation – **More than 30 Years of Natural Product Isolation from Myxobacteria – What’s Next?** International symposium: *2nd international HIPS Symposium*, Saarbrücken, Germany, *these authors contributed equally.

Jennifer Herrmann, Angela G. Kling, and Rolf Müller (April 2012): Poster presentation – **A Screening Approach for the Identification of Anti-Infective Compounds that Target the Adherence of *Staphylococcus aureus* to Mammalian Host Cells**. International conference: *Gordon Research Conference New Antibacterial Discovery & Development*; Lucca, Italy.

Jennifer Herrmann*, Alberto Plaza*, Ronald O. Garcia, Kirsten Harmrolfs, Ritesh Raju, Klaus Gerth, Heinrich Steinmetz, and Rolf Müller (September 2011): Poster presentation – **Fast Discovery of New Antimicrobials from Myxobacteria**. International workshop: *Biology of bacteria producing natural products*, Bonn, Germany, *these authors contributed equally.

Jennifer Herrmann, Ronald Garcia, Alberto Plaza, Angela G. Kling, and Rolf Müller (June 2011): Poster presentation – **Fast Discovery of Antimicrobials from Myxobacteria**. International symposium: *1st international HIPS Symposium*, Saarbrücken, Germany.

Jennifer Herrmann and Rolf Müller (September 2010): Oral presentation – **Biological Screen for the Identification of Novel Natural Products from Myxobacteria**. International workshop: *Biology of bacteria producing natural products*, Tübingen, Germany.

Stephan Hüttel, Jennifer Herrmann, and Rolf Müller (September 2010): Poster presentation – **Fermentation Strategy and Downstream Processing of *Chondromyces* for Identification of Novel Bioactive Substances**. International workshop: *Biology of bacteria producing natural products*, Tübingen, Germany.

7.3 DANKSAGUNG

Mein besonderer Dank gilt Prof. Dr. Rolf Müller für die Überlassung der sehr interessanten und herausfordernden Themen in einer inspirierenden wissenschaftlichen Umgebung, seine stetige Unterstützung und Diskussionsbereitschaft, sowie für sein mir entgegen gebrachtes Vertrauen.

Herzlich bedanken möchte ich mich des Weiteren bei Prof. Dr. Uli Kazmaier für die Übernahme des Koreferates sowie für die sehr gute und ergiebige Kooperation in einer Reihe von Projekten.

Ein ganz herzliches Dankeschön an Assist. Prof. Dr. Yasser A. Elnakady für die sehr schöne Anfangszeit meiner Promotion, die mich nicht nur wissenschaftlich inspiriert hat, sondern mich auch menschlich prägte.

An dieser Stelle möchte ich mich nochmals bei allen Kooperationspartnern bedanken, durch die ich viel dazu gelernt habe und deren Unterstützung ich sehr wert schätze! Insbesondere geht mein Dank an Dr. Angelika Ullrich und Dr. Jens L. Burkhart für zahlreiche Synthesen, Dr. Romina M. Wiedmann, Prof. Dr. Angelika M. Vollmar und Prof. Dr. Manfred Rohde für ihre Mitarbeit am Prätubulysin-Projekt und Stephan Hüttel für die stets gute Zusammenarbeit.

Herzlich bedanken möchte ich mich außerdem bei Eva Luxenburger und Thomas Hoffmann für MS-Messungen, Dr. Ritesh Raju für das Korrekturlesen von Teilen dieser Arbeit, Dr. Florenz Sasse für seine stetige Diskussionsbereitschaft und Freundlichkeit, Angie Kling und Viktoria Schmitt für die schöne und sehr lustige Zeit und natürlich bei der gesamten Myxoarbeitsgruppe inklusive der Kollegen in Braunschweig für die gute Atmosphäre und Zusammenarbeit im Labor.

Ein ganz großes Danke an meine Freunde, besonders an Sina Janietz, und Susi und Stephan Fuchs. Für ihre Freundschaft. Ebenfalls ein von Herzen kommendes Dankeschön an Stephan Hüttel. Dafür dass er an meiner Seite ist.

Nicht zuletzt danke ich meinen Eltern und meinem Bruder für ihre stetige Unterstützung, ihren Rat und dafür mir immer ein Halt zu sein!

7.4 CURRICULUM VITAE

Jennifer Herrmann

Diplom-Chemikerin

*05.08.1982 in Siegen, Deutschland

Schulausbildung

08/1988-07/1992 Grundschule Friedewald, Deutschland

08/1992-06/2001 Freiherr-vom-Stein Gymnasium Betzdorf-Kirchen/Sieg, Deutschland

Hochschulstudium

10/2001-07/2007 Studium der Chemie an der Technischen Universität Kaiserslautern, Deutschland

04/2004 Vordiplomprüfung

03/2005-07/2005 Forschungspraktikum in Organischer Chemie im Rahmen des ERASMUS Programmes an der Universität Murcia, Spanien

09/2005-12/2005 Praktikum bei Bayer CropScience (R&D, Discovery, Biology, Bereich HTS) in Monheim, Deutschland

09/2006 Diplomprüfung

10/2006-07/2007 Diplomarbeit unter der Leitung von Prof. Dr. T. Kietzmann am Institut für Biochemie, Technische Universität Kaiserslautern, Deutschland

09/2007-11/2007 *Visiting Scholar* im Rahmen des LEONARDO Programmes bei Drug Discovery Ltd. (Prof. Dr. Alan Harvey) in Glasgow, Schottland

12/2007 Beginn der Promotion unter der Leitung von Prof. Dr. Rolf Müller am Institut für Pharmazeutische Biotechnologie, Universität des Saarlandes, Saarbrücken, Deutschland